ISSN 1880-8468

Technical Report of
International Development Engineering

国際開発工学研究報告

TRIDE-2023-01 March 31, 2023

# Abstracts of Master Theses Presented from September 2016 to March 2019

Department of International Development Engineering,
Graduate School of Science and Engineering,
Tokyo Institute of Technology
**http://www.ide.titech.ac.jp/TR**

# Preface

This technical report consists of the abstracts of Master theses presented in the Department of International Development Engineering, Tokyo Institute of Technology, on August 2, 2016, October 19, 2016, February 14, 2017, Augusut 1, 2017, February 15, 2018, and February 14, 2019.

**Technical Report of International Development Engineering**
**TRIDE-2023-01**

**Table of Contents**

# ACCELERATED COMPOSTING BY INOCULATION OF ACID DEGRADING MICROORGANISM

Student Number: 14M51687 Name: Hapsari PUSPITALOKA Supervisor: Kiyohiko NAKASAKI

酸分解微生物の接種による高速コンポスト化

In this study, the effect of inoculating thermophilic acid degrading bacteria in composting was investigated in order to accelerate the composting by overcoming the low pH problem. Base on the detailed analyses of the previous work of accelerated composting by *Pichia kudriavzevii* RB1, three candidates of thermophilic bacteria which has potential to degrade organic acids were found, namely *Bacillus coagulans, Geobacillus thermantarcticus and Bacillus subterraneus.* From this three candidates, one of the bacteria *Bacillus coagulans* IP1 was successfully isolated. Solid culture fermentation of IP1 exhibited that IP1 degraded acetic acid, also they produced acetic acid. IP1 was also found to be able to degrade the organic acids in the composting. To conclude, it was suggested that inoculation of IP1 can accelerate the composting during thermophilic condition by the vigorous organic acid degradation.

## 1. Introduction

Composting is one of best method to recycle the municipal solid waste due to its eco-compatibility and easy operational procedures. Food waste is a fraction of the organic waste which can be recycled as compost for the agricultural purpose [1]. One of the common problems in food waste composting is the low pH [2]. Accumulation of organic acids in the food waste prior to composting has contributed to the acidic condition of the raw material. Furthermore, the organic acids concentration increases during the initial phase of composting, with the degradation of organic matter [2,3]. The low pH condition of raw material can lead to the failure of composting.

A Previous study found that by the inoculation of *Pichia kudriavzevii* RB1 (a mesophilic yeast) into the raw material and temperature controlling, the composting can be accelerated [4]. RB1 was active and degrade organic acid in mesophilic condition. However, with the temperature rise, RB1 died off. Interestingly, degradation of organic acid was observed at the later thermophilic period, although RB1 is absent. Therefore, it could be hypothesized there were other bacteria can degrade the organic acid in the composting and this bacteria can tolerate to thermophilic and acidic condition. In this study, the aim is to find out the acid degrading bacteria which can tolerate to thermophilic condition and investigate the effect of inoculating the isolated acid degrading bacteria in the food waste composting, in order to accelerate the composting of acidified food waste.

## 2. Material and methods

### 2.1 Proliferation of acid degrading microorganism in accelerated composting

This research investigated a composting run (Run 3A) from previous study with inoculation of RB1 and controlling temperature (at 40 °C for 1 day) [4]. The rabbit food and rice (ratio 7:3) with the additional of organic acids were used as a representative model of food waste. This experiment was conducted in bench scale reactor (300 mm x 400 mm).

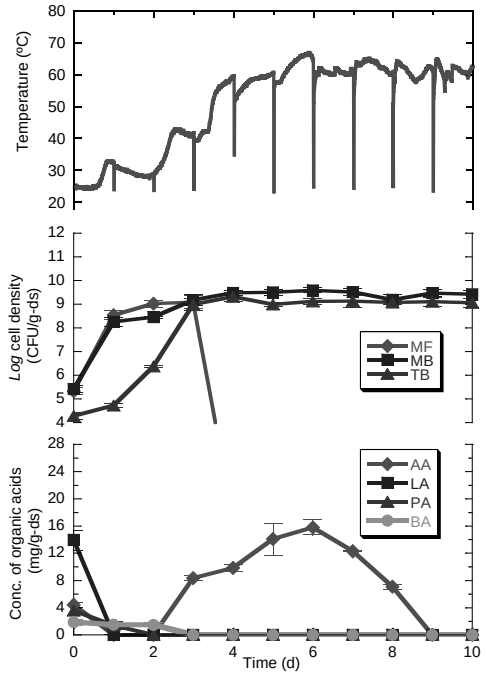


Fig. 1 Time course of temperature, cell density and organic acids concentration in Run 3A [4]. In *Log* cell density graph MF, MB and TB representative mesophilic fungi, mesophilic bacteria and thermophilic bacteria, respectively. In conc. of organic acids graphs AA, LA, PA and BA representative acetic acid, lactic acid, propionic acid and butyric acid, respectively.

The detailed analyses of accelerated composting was started by observed the physicochemical factor of composting. Fig. 1 shows the time course of temperature, cell density and organic acids concentration from previous study. When the temperature reached to 40 ºC by self-heating it was maintained for one day. After that, the temperature increased until 60 ºC and RB1 was not detected during this period. Meanwhile, the concentration of acetic acid started to increase from day 2 and reached its peak on day 6. The concentration of acetic acid was then decreased and diminished on day 10, though RB1 died off during this period. Therefore, we suggest that there were bacteria which actively degraded the organic acids during the thermophilic stage of composting. PCR-DGGE analyses of accelerated composting by *Pichia kudriavzevii* RB1 was then observed in this study. The analyses was started by DNA extraction of the compost samples. PCR amplification targeting the 16S rRNA gene region was then conducted using the extracted DNA as template. Afterwards, PCR product was subjected to Denaturing Gradient Gel Electrophoresis (DGGE). Using the DGGE image as a reference, the bands of interest were excised from the gel and DNA sequence was determined. The sequencing results was then compared to the 16s rRNA genes available in GenBank databases.

### 2.2 The ability of *Bacillus coagulans* IP1 in degrading organic acids in solid culture fermentation

A thermophilic bacteria was isolated from Run 3A compost sample (day 10), namely as *Bacillus coagulans* IP1. The ability of this bacteria in degrading organic acids were tested in solid culture fermentation experiments. The experiments were carried out in a mini-reactor comprised of a Pyrex glass cylinder (diameter: 45 mm, depth: 100 mm). The mini reactor consisted 15 gram of the mixture of rabbit food and sawdust (as bulking agent). Prior to the inoculation of IP1, the solid substrate was sterilized by autoclaving, then add with filter sterilized of acetic acid with the concentration of 3 mg/g-ds and inoculum of IP1. Throughout the cultivation period, the reactor was shaken daily, the aeration rate was fixed at 5.5 mL/min and moisture content was maintained around 60%. A 10 L polyvinyl fluoride plastic bag was used for collection the exhaust gas. The plastic bag was changed once daily, and $CO_2$ concentration in the exhaust gas was measured using Kitagawa gas detector tubes. The solid culture was cultivated with temperature at 50 °C until three days. The compost samples were measured for pH, concentration of organic acids and cell density of IP1.

### 2.3 Effect of inoculating *Bacillus coagulans* IP1 towards thermophilic composting

The mini reactor which was used in this experiments similar to the solid culture fermentation experiment (Section 2.2). About 15 gram of rabbit food, rice (ratio 7:3), seeding material (Alles G™) and saw dust (the bulking agent) were mixed, the mixture of rabbit food and rice was represent a simulated food waste in the composting experiment. Four kinds of organic acids (acetic acid, lactic acid, propionic acid and butyric acid) were added to raw compost mixture. The moisture content of mixed composting material was maintained around 60% throughout the experiment. Two experiment runs were conducted, namely Run 5A and 5B. Run 5A was inoculated with IP1, meanwhile in Run 5B (control) the composting was started without the inoculation of IP1. For both Run 5A and 5B, the incubator was kept at 50 °C throughout the composting process (10 days). The composting materials in mini reactor were mixed daily. The compost samples were measured for pH, concentration of organic acids and cell density of thermophilic bacteria.

## 3. Results & Discussions

### 3.1 Proliferation of acid degrading microorganism in accelerated composting

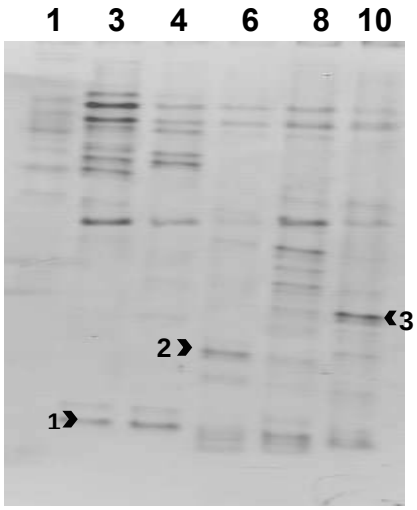


Fig. 2 The dynamic changes of bacterial community in DGGE patterns in Run 3A. The number over each lane shows the age in days after the start of composting. These bands represented by number were excised and sequenced.

Fig. 2 shows the dynamic changes of bacterial community in DGGE patterns in Run 3A. From the DGGE image results, three bands were suggested have ability in degrading the organic acids during thermophilic condition. Band 1, band 2 and band 3 appeared on or after 3 days of composting, whereas during this period the temperature of composting started to increase to 60 ºC. The concentration of acetic acid at this period increased from day 3 to day 6 then decreased after reached its peak on day 6. The sequence of band 2 and band 3 were closely related to *Bacillus subterraneus* and *Geobacillus thermantarcticus*. Interestingly, the sequence band 1 which was closely related to *Bacillus coagulans* might have ability to produce as well as to degrade the acetic acid since this bacteria appeared during the period when acetic acid concentration increased and decreased.

### 3.2 The ability of *Bacillus coagulans* IP1 in degrading organic acids in solid culture fermentation

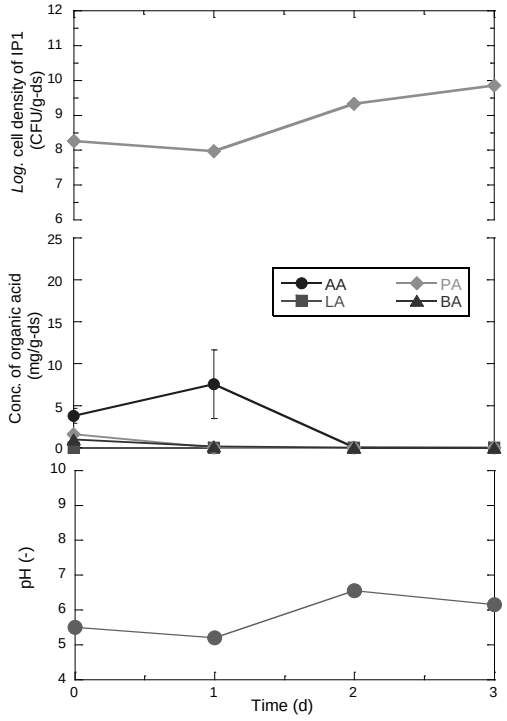


Fig.3 The concentration of cell density, organic acids concentration and pH in solid culture fermentation of IP1. In conc. of organic acids graphs AA, LA, PA and BA representative acetic acid, lactic acid, propionic acid and butyric acid, respectively.

Fig.3 shows the concentration of cell density, organic acids concentration and pH in solid culture fermentation of IP1. There was increment in cell density of IP1 during three days solid culture fermentation. The figure shows that in the initial stage of fermentation the concentration of acetic acid, propionic acid and butyric acid were around 3.7 mg/g-ds, 1.58 mg/g-ds and 0.96 mg/g-ds, respectively. Meanwhile, lactic acid was not detected in the initial condition of culture fermentation. After one day of fermentation, the concentration of acetic acid increased until 7.5 mg/g-ds. Moreover, pH after one day fermentation also decreased from pH 5.5 to 5.2. From this results it seems that the IP1 could produce the acetic acid. However, after 2 days of fermentation, the organic acids including the acetic acid were totally degraded. The pH also increased to almost neutral condition at the end of fermentation. In conclusion, the IP1 has ability to produce the acetic acid and degrade the organic acids. Therefore, the IP1 has the potential to be used as inoculum in composting in order to overcome the acidic condition in food waste composting.

### 3.3 Effect of inoculating *Bacillus coagulans* IP1 towards thermophilic composting

Fig. 4 shows time course of $CO_2$ evolution rate, organic acids concentration, pH and concentration of cell density of thermophilic bacteria in Run 5A and 5B. The $CO_2$ evolution rate in Run 5A (with IP1 inoculation) kept increase until reached its peak value at 16.1 x $10^{-3}$ mol/day on day 4 of composting. Afterwards, the $CO_2$ evolution rate in Run 5A decreased until the end of composting process. In Run 5B (without IP1 inoculation), there were increment of $CO_2$ evolution rate until day 4 of composting. However, the increment of $CO_2$ evolution rate in Run 5B was only until 0.7 x $10^{-3}$ mol/day. For the concentration of organic acids in Run 5A, the acetic acid increased at day 1 of composting yet all the organic acids were totally degraded at day 2 of composting. Meanwhile, the organic acids for the control run (Run 5B) were not totally degraded. Especially for the concentration of acetic acid, it became higher until reached to 18.85 mg/g-ds. Furthermore, the pH for Run 5A increased after 2 days of composting time, and finally the pH reached to pH 8.7 at the end of composting time. On the contrary, the pH in Run 5B could not elevate to neutral condition. From the results above, it was concluded that the composting in Run 5A succeeded while Run 5B failed. The successful of Run 5A was marked by rapid of organic matter degradation during the composting and the pH reached until alkaline condition at the end of composting. In Run 5A, IP1 can degrade the accumulation of organic acids in the composting. Thus, the condition in composting become neutral and other microorganisms can grow. Finally, the composting was accelerated. In contrary, the composting failed in Run 5B because the organic acids cannot be degraded thus it inhibited the activity of

microorganism. As the results, the microorganisms cannot degrade the organic matter in the composting. Hence, the acidic condition in Run 5B still remain until the end of composting.

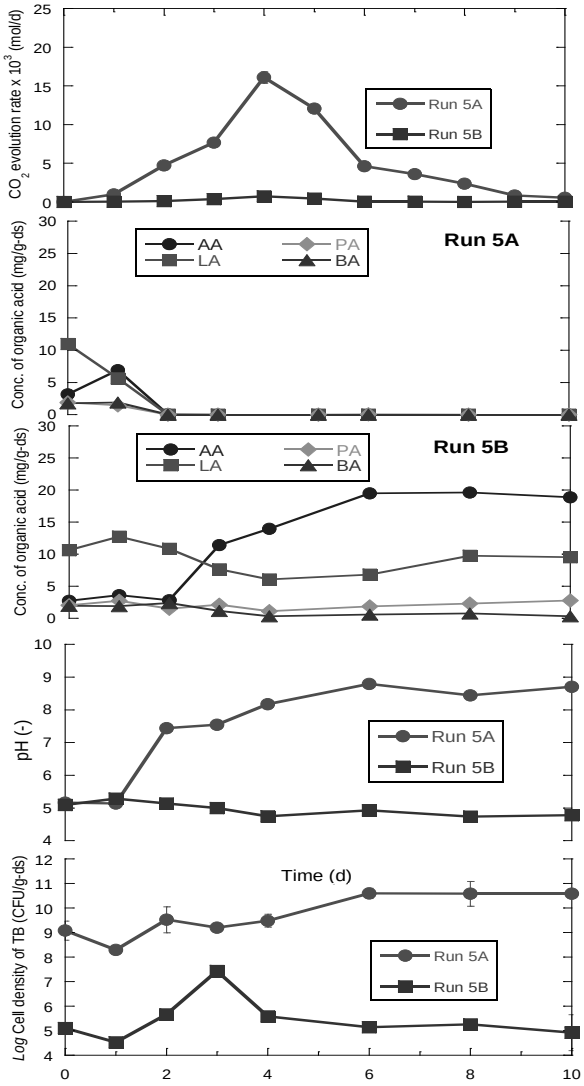


Fig.4 Time course of $CO_2$ evolution rate, organic acids concentration, pH and concentration of cell density of thermophilic bacteria in Run 5A and 5B. In concentration of organic acids graphs AA, LA, PA and BA representative acetic acid, lactic acid, propionic acid and butyric acid, respectively.

The cell density of thermophilic bacteria in Run 5A decreased until around $10^8$ CFU/g-ds on the first day of composting. It might be due to the fact there were increment of organic acids concentration in composting which negatively affected to the growth of thermophilic bacteria. However, after two days of composting the cell density of thermophilic bacteria increased and it achieved to $10^{10.6}$ CFU/g-ds at the end of composting. In Run 5B, the cell density of thermophilic bacteria started with $10^5$ CFU/g-ds, then it decreased to $10^{4.5}$ CFU/g-ds and increased on day 3 of composting until $10^7$ CFU/g-ds. In Run 5B, composting failed because the high concentration of organic acids inhibited the activity of microorganisms to degrade the organic matter of the raw material. Meanwhile, the organic acids in Run 5A were degraded after two days of composting thus the degradation of organic matter was not inhibited. Therefore, the composting in Run 5A succeeded. From the results above it can be concluded, by inoculating IP1 in the thermophilic composting at 50 ºC throughout the composting could enhance the proliferation other thermophilic bacteria. The IP1 could degrade the high concentration of organic acids in the initial stage of composting and has made the environment of composting become favorable to other microorganisms to grow and thus the organic matter was vigorously degraded.

## 4. Conclusions

Base on detailed analyses of accelerated compost, it was suggested three bands of DGGE gel related to the thermophilic bacteria might have ability to degrade the acetic acids in the composting. The sequence band were closely related to *Bacillus coagulans, Geobacillus thermantarcticus* and *Bacillus subterraneus*. One of the bacteria namely as *Bacillus coagulans* IP1 was found able to degrade the organic acids in solid culture fermentation at thermophilic condition. Furthermore, the inoculation of IP1 into the raw material of composting has decreased the organic acids concentration in composting and elevated the pH, thus it can proliferate other thermophilic bacteria and accelerate the thermophilic composting.

## References


[1] K. Nakasaki, S. Araya, H. Mimoto, Inoculation of Pichia kudriavzevii RB1 degrades the organic acids present in raw compost material and accelerates composting, Bioresour. Technol. 144 (2013)

[2] C. Sundberg, S. Smars, H. Jonsson, Low pH as an inhibiting factor in the transition from mesophilic to thermophilic phase in composting, Bioresour. Technol. 95 (2004) 145–150.

[3] K. Nakasaki, Y. Sasaki, H. Kubota, Effects of pH control on composting of garbage, Waste, Manag. Res. 11 (1993) 117–125.

[4] H. Hirai, Acceleration of the composting by inoculating strain RB1 and controlling composting temperature, Tokyo Institute of Technology, 2015.

# EFFECT OF LAND USE ON CRIME TYPES IN DHAKA, BANGLADESH

Student Number: 14M51658 Name: Mashroof Hossain Supervisor: Shinya HANAOKA

The research takes Uttara, Dhaka, the Northern zone of the capital city of Bangladesh, as the study area and aims at finding solutions to its high crime rate and low resource to countervail it. For that, it collects crime records for the year 2013-2014 and uses GIS to evaluate its association with various land use, e.g., residential area, commercial area, educational institutes, mosques, open space and highways. Notable findings suggest that drug related crimes are positively related to mosques and commercial areas; murders take place near mosques but away from highways, grievously hurt takes place closer to mosques and negatively related to open space and residential areas; robbery takes place near mosques, and theft takes place near mosques and highways.

## 1. Background

Crime is a very severe problem in Bangladesh and according to Bangladesh Police website, total number of crimes has crossed the total of 150 thousand every single year since 2007. In Bangladesh, Police is the federal agency solely responsible for law enforcement and crime prevention. There are major resource constraints prevailing in the law enforcement sector that are clearly visible. Police to people ratio in Bangladesh is around 96:100,000 which is the lowest in the region and just one-third of the proposed UN ratio[1] (300:100000). The existing law through which police department operates goes back to 1861, and there has been very little change since then. The possibility of sudden, revolutionary change in the existing bureaucratic system is small. Under these circumstances, it is imperative to investigate if the situation can be improved through alternative measures.

Existing literature suggests that there is a relationship between crime pattern and land use. Greenberg et.al[2] stated that the differences in physical characteristics of various neighborhoods significantly affect their crime scenario. The role of commercial land use mix in crime has been investigated in some literature. The role of urban circumstances in occurrence of crime is also well discussed. Spatial patterns of crime and shortest path distance from an area to some facilities as a factor to be exposed to crime has also been investigated. Some studies found significant relationship between violent assault, murder and land use. This research takes Uttara, the Northern part of Dhaka city as study area and investigates if certain types of crimes have association with certain land-use or special arrangement of the road network. In order to do so, the study

- collects historical crime data and investigates its patterns,
- identifies various land use and road network attributes and develops a logistic regression based model to investigate the underlying relationships between these variables and crime types.

## 2. Study Area and the Data

Uttara is one of the eight crime divisions in Dhaka, Bangladesh. It is one of the newest parts of the city and was initially designed to be a model residential town. However, due to unplanned land use, it is now house to numerous educational institutions, mosques, community center, street markets, and commercial areas along with empty plots coexisting with residential settlements. Being at the outskirt of the city, it connected to highways as well as semi-urban slums within close proximity. The study area covers an area of 36.91 square kilometers with a population of 179,907. There are 180 police officers responsible for the law and order situation of Uttara.

Detailed crime data for two years (2013 - 2014) have been collected from First Information Report (FIR) books of Uttara East and Uttara West Police stations. The data contained information on crime types (theft, robbery, drug, grievous hurt and murder), location, time, time for police to arrive along with a brief description of the crime. The other data, i.e., land use data, was collected by identifying various landmarks, e.g., commercial areas, educational institutes, mosques, community centers, open spaces and residential areas, and geocoding them using GPS. Apart from that, GIS map of Uttara along with its road network was collected.

## 3. Methodology

The study uses ArcGIS to digitize the crime locations along with various land uses – commercial area,

residential area, schools and open spaces. Then, the study area is divided into three different mesh sizes – 50 m X 50 m, 100 m X 100 m and 150 m X 150 m. Afterwards, each cell of the mesh was assigned an appropriate land use. The attributes of each cell was also updated with crime types, i.e., if a crime of certain type took place in that particular cell. Figure 1 represents the land use and mosque locations on GIS map for 50m X 50 m mesh.

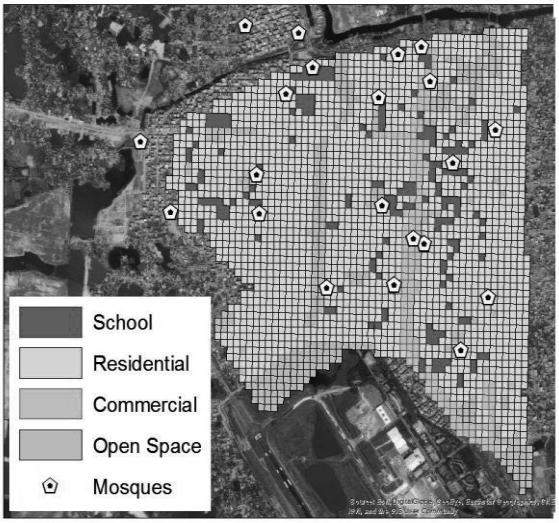


Figure 1: Land Use and location of mosques

Next, for each cell, shortest route distances from its centroid to the closest mosque and the Dhaka-Mymensingh highway was calculated. Finally, logistic regression based models were constructed for each of the five aforementioned crime types where presence of crime was marked as '1' and its absence as '0' for each cell. The independent variables for each cell were the dichotomous dummy variables representing commercial area (DUMMY_COMMERCIAL), dichotomous dummy variable representing residential area (DUMMY_RESIDENTIAL), dichotomous dummy variable representing open space (DUMMY_OPENSPACE), dichotomous dummy variable representing educational institutes (DUMMY_SCHOOL), continuous distance variable from the centroid of the cell to nearest mosque (MOSQUE_DISTANCE) and continuous distance variable from the centroid of the cell to Dhaka - Mymensingh highway (HIGHWAY_DISTANCE). DUMMY_SCHOOL is considered as the base variable. Apart from logistic regression that tested the likelihood of different crime types, Poisson regression was also used in the end to examine the crime count data in each cell.

**4. Analysis and Results**

Figure 2 presents the number of different types of crimes taking place in Uttara between 2013 and 2014.

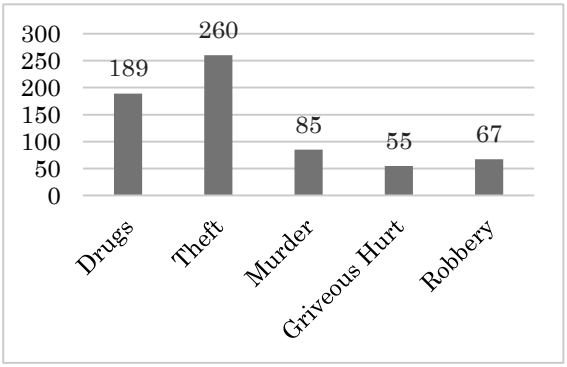


Figure 2: Frequency of crime in Uttara

Among the five types of crimes, drug is unique for the study area. Uttara is the entry point of the capital city, which makes it a preferred place for criminals in bringing drugs and distributing it throughout the city. As a category, different types of thefts (car theft, fraudulent activity etc. all put under theft category) show the highest frequency. Uttara is also a densely populated area with a high number of both residents and businesses, which gives the thieves a fairly high number of possible victims to choose from. There are 85 murders in two years, which is very high compared to the population density and overall murder rate. However, given the urban-commercial nature of Uttara this is not unusual. The number of grievous hurt crimes and robberies seem to be low compared to the other areas. Well-planned and neatly structured residential sectors with collapsible gates might lead to this.

From the results of logistic regression (Table1) we can get a very clear picture of the crime pattern and its relation with land use. The table shows the results found for all five crime categories for 50X50 mesh. The patterns of continuous and dummy variables reveal how each separate type of crimes takes place in different pattern. For theft, areas near to mosque and highway more vulnerable compared to far areas. This result is intuitively meaningful because highway gives a better chance of escape for a thief. However, in case of mosque this is significant because Bangladesh is a Muslim oriented country, it is surprising that theft takes place closer to mosque areas. The reason behind this might be that criminals' take advantage of the myth of safety where in reality security measures near mosques are less than other areas.

Table 1: Results of the Logistic Regression for 50x50m

| | | Estimate | Odds Ratio | p-value |
|---|---|---|---|---|
| Theft | INTERCEPT | -0.967*** | 0.380 | 0.000 |
| | DUMMY_RESIDENTIAL | -0.764*** | 0.465 | 0.000 |
| | DUMMY_COMMERCIAL | 0.209 | 1.232 | 0.488 |
| | DUMMY_OPENSPACE | -2.574*** | 0.076 | 0.000 |
| | HIGHWAY_DISTANCE | -5.348** | 0.004 | 0.003 |
| | MOSQUE_DISTANCE | -1.183** | 0.306 | 0.001 |
| Robbery | INTERCEPT | -2.914*** | 0.054 | 0.000 |
| | DUMMY_RESIDENTIAL | 0.141 | 1.151 | 0.792 |
| | DUMMY_COMMERCIAL | 0.674 | 1.962 | 0.305 |
| | DUMMY_OPENSPACE | -0.344 | 0.708 | 0.658 |
| | HIGHWAY_DISTANCE | -4.213 | 0.014 | 0.198 |
| | MOSQUE_DISTANCE | -1.967** | 0.139 | 0.007 |
| Drug | INTERCEPT | -1.727*** | 0.177 | 0.000 |
| | DUMMY_RESIDENTIAL | -0.451 | 0.636 | 0.126 |
| | DUMMY_COMMERCIAL | 1.086** | 2.962 | 0.002 |
| | DUMMY_OPENSPACE | -0.481 | 0.618 | 0.248 |
| | HIGHWAY_DISTANCE | -2.736 | 0.064 | 0.176 |
| | MOSQUE_DISTANCE | -1.577*** | 0.206 | 0.000 |
| Grievous Hurt | INTERCEPT | -2.484*** | 0.083 | 0.000 |
| | DUMMY_RESIDENTIAL | -1.193** | 0.303 | 0.001 |
| | DUMMY_COMMERCIAL | 0.109 | 1.115 | 0.838 |
| | DUMMY_OPENSPACE | -1.443* | 0.236 | 0.030 |
| | HIGHWAY_DISTANCE | 4.257 | 70.59 | 0.117 |
| | MOSQUE_DISTANCE | -1.947** | 0.142 | 0.006 |
| Murder | INTERCEPT | -2.850*** | 0.057 | 0.000 |
| | DUMMY_RESIDENTIAL | -0.407 | 0.665 | 0.273 |
| | DUMMY_COMMERCIAL | 0.779 | 2.179 | 0.117 |
| | DUMMY_OPENSPACE | -2.419* | 0.089 | 0.022 |
| | HIGHWAY_DISTANCE | 4.313 | 74.6@ | 0.060 |
| | MOSQUE_DISTANCE | -1.457** | 0.232 | 0.007 |

(***0.1%, **1%,*5%,@10% Significance level)

In case of robbery we can see that areas closer to mosques are more prone to robberies. In case of drug crimes we also find that mosque areas are very highly prone to drug crimes.

Table 2: Results for overall crime in all three mesh size

| Mesh | | Estimate | Odds Ratio | P-Value |
|---|---|---|---|---|
| 50M | INTERCEPT | -0.341 | 0.711 | 0.084. |
| | DUMMY_RESIDENTIAL | -0.560** | 0.571 | 0.001 |
| | DUMMY_COMMERCIAL | 0.742** | 2.100 | 0.002 |
| | DUMMY_OPENSPACE | -1.303*** | 0.271 | 0.000 |
| | HIGHWAY_DISTANCE | -1.680 | 0.186 | 0.153 |
| | MOSQUE_DISTANCE | -1.592*** | 0.203 | 0.000 |
| 100M | INTERCEPT | 1.098*** | 2.998 | 0.000 |
| | DUMMY_RESIDENTIAL | -0.507* | 0.602 | 0.027 |
| | DUMMY_COMMERCIAL | 0.949* | 2.583 | 0.029 |
| | DUMMY_OPENSPACE | -1.908*** | 0.148 | 0.000 |
| | HIGHWAY_DISTANCE | -0.031 | 0.969 | 0.850 |
| | MOSQUE_DISTANCE | -1.700*** | 0.182 | 0.000 |
| 150Mr | INTERCEPT | 2.708*** | 14.999 | 0.000 |
| | DUMMY_RESIDENTIAL | -1.265* | 0.282 | 0.012 |
| | DUMMY_COMMERCIAL | -0.396 | 0.673 | 0.593 |
| | DUMMY_OPENSPACE | -2.457*** | 0.086 | 0.000 |
| | HIGHWAY_DISTANCE | 0.186 | 1.204 | 0.497 |
| | MOSQUE_DISTANCE | -2.113*** | 0.121 | 0.000 |

(***0.1%, **1%,*5% Significance level)

We can also see that drug crimes happen more in commercial areas compared to school areas, which makes sense intuitively. In case of grievous hurts, mosque area is again very prone to this crime, whereas open spaces and residential areas are less prone to such crimes compared to school areas. In case of murder we can see that murder is more prone to mosque areas and less prone near highways. Open spaces are less prone to murder compared to school areas.

Apart from specific crime results, logistic regression was also used to find out the overall crime scenario (any of the five crimes taking place). In all three mesh sizes, mosque areas were found crime prone (table 2).

Poisson regression was applied to the count data for five crime categories on each cell of all three mesh sizes which brought out similar results. For example, expected number of drug occurrences decreased with an increase of distance from the mosque. A representative result for drug crime (50 meter mesh) is showed below.

| Drug | Estimate | Exp.(Estimate) |
|---|---|---|
| INTERCEPT | -1.210*** | 0.298 |
| DUMMY_RESIDENTIAL | -0.503* | 0.605 |
| DUMMY_COMMERCIAL | -0.960* | 0.383 |
| DUMMY_OPENSPACE | -0.853* | 0.426 |
| HIGHWAY_DISTANCE | -6.008** | 0.002 |
| MOSQUE_DISTANCE | -0.989* | 0.372 |

Table 3: Poisson Regression on Drug (50m)

(***0.1%, **1%,*5%, Significance level)

However, results for dummy (commercial) in Poisson regression shows opposite direction from the result of logistic regression. In logistic regression, predicted likelihood of drug crime is higher in commercial area compared to schools (base) but in Poisson regression predicted number of drug crimes is lower in commercial area (compared to base). As dummy variables are compared against base variable, the estimate signs can be completely opposite depending on how the occurrences are spread in the area. If few occurrences are spread in more cells, likelihood of crime will be higher in the dummy. On the other hand, when frequency is considered, higher number of densely occurred crime in the base will predict lower number of occurrence in the dummy. This explains the opposite signs in commercial dummy in two different regressions.

In figure 3, predicted probabilities of all four types of land use have been plotted against distance from mosque in case of overall crime. The plot shows that all four land types show decreasing crime probability with an increase of distance from mosque, making the mosque area more crime prone. Since mosques are spread throughout Uttara irrespective of specific business districts (figure-1), this supports our findings that crimes happen more nearby mosque areas.

In smaller mesh sizes commercial areas are more crime infested compared to other areas. This changes with 150m mesh size; school areas become the most crime prone. This happens because smaller mesh size helps to locate the crimes more accurately at a finer resolution. Larger mesh size, with a coarser resolution, aggregates multiple crimes in one cell and thereby compromises the locational accuracy of the crime points. As a common approach in spatial analysis to evaluate any result at multiple spatial resolutions, three different mesh sizes were chosen. This was done to avoid Modifiable Areal Unit Problem (MAUP). We can see that in most of the cases our findings remain same.

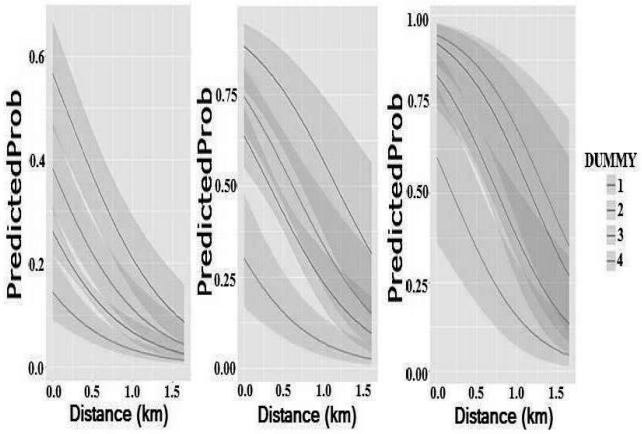


Figure 3: Predicted Probabilities VS mosque distance in 50m, 100m and 150m mesh (from left to right)

Note: Dummy1-4 representing school, residential, commercial and open space areas consecutively

## 5. Conclusion

The most significant finding from this study is the vulnerability of areas near mosques. This finding contradicts the common belief that mosque areas are safer due to the religious beliefs of majority population. Local police administrations often do not emphasize mosque areas for security. An important policy implication for police administration can be dispatching more resources (police patrol, guards etc.) near mosque areas to improve safety and security. Drug is the most notorious crime in Uttara and we find evidence that commercial areas are highly prone to it. If a special anti-drug drive is taken, commercial areas should be the main target for the police to secure. In this way, every specific crime can be studied and necessary measures can be taken. If similar method is used in another police jurisdiction, we produce customized strategies that would help Police in Bangladesh to fight crime more efficiently.

**Reference:**

1. United Nations Office on Drugs, & Crime. (2005). Crime and Development in Africa. United Nations Publications. 67-87.

2. Greenberg, Stephanie W., William M. Rohe, and Jay R. Williams. (1982) "Safety in urban neighborhoods: A comparison of physical characteristics and informal territorial control in high and low crime neighborhoods." *Population and Environment* 5.3: 141-165.

# COMPETITIVE DYNAMICS AMONG CROSS REGIONAL HUB PORTS FOR THE CONTAINER TRANSSHIPMENTS: CASE STUDY FOR THE PORT OF COLOMBO

Student Number: 15M51756 Name: Chathumi Kavirathna Supervisor: Shinya HANAOKA

Hub port competition has complicated with numerous decisions making criteria and multiple liner network structures while accelerating beyond the regional boundaries. Despite location advantages, the port of Colombo has serious exposure in losing market share due to competitive hub ports located in surrounding regions established to cater transhipment market. The study aims to analyse the transhipment hub role of port of Colombo for both "Hub and Spoke" and "Relay" networks considering competition with Ports of Singapore, Kelang and TanjungPelepas. The hub port selection criteria categorized under Monetary, Time, Location, Operational and Liner related categories are analysed by shipping lines while evaluating the performances of competitive hub ports. The Port Performance Index is generated and generalized cost approach is used for assessing the port choice behaviour via estimating the transhipment market share of hub ports while discussing potential implications of liner shipping industry with several scenarios analysis.

## 1. Introduction

Involvement of multiple players with strategic alliances and enlargement of vessel's size accelerated the hub port competition beyond the regional boundaries (Veldman, and Buckmann, 2003). Meanwhile multiple network structures and numerous decision making criteria have intensified the complexity of hub port section decision. Transhipment refers to the shipment of goods/containers to an intermediate destination before being taken to the final destination while transhipment hub port facilitates the efficient logistic platform to carry out transhipment operation between vessels. According to Ducruet and Notteboom (2012, p.2), 'A container on average was handled 3.5 times between the first port of loading and the last port of discharge in 2008" which indicates the significance of transhipment operation. Further the overlapping origin/destination markets which are being served simultaneously by cross regional multiple hub ports created many alternative choices for shipping lines.Even though there is no scarcity of studies related to port choice or port competition analysis, none of the previous studies focused on cross regional hub ports considering different types of liner service networks alone with range of decision making criteria. Thus current study fulfils the research gap by analysing the hub port competition through hub port choice behaviour for both hub and spoke and relay networks while considering range of qualitative and quantitative criteria rather than conventional approach of port competition analysis.

Hub and Spoke network is characterized by service optimization effort with both mainlines and feeder services operated in an integrated manner to realize the transportation between ultimate origin and destination ports regardless of the infrastructure constrains associated with minor ports while enabling transhipment between mainline vessels and feeder vessels. Secondly Relay network is designed to optimize the network configuration by integrating multiple mainline services to enhance the geographical coverage while undertaking transhipment between two mainline vessels with different port of calling's patterns.

The port of Colombo is strategically located with East-West main sea route for being developed as a transhipment hub port. But currently the port has serious exposure in losing market share due to lack of competitiveness compared to other competitive hub ports located in surrounding regions. Further transhipment status of port of Colombo is highly vulnerable due to serious dependency on Indian sub-continent feeder market as development of Indian port infrastructures could eventually reduce the transhipment volume handled in port of Colombo. Further majority of transhipment cargo handled in port of Colombo is related to hub and spoke network while currently port doesn`t play an important role in terms of relay networks. Therefore, the study is designed to achieve four different research objectives as follows,

1. To develop a contextualized framework of the factors influencing on the hub ports selections from the practical viewpoints of decision makers
2. To identify significant criteria for the hub port's selection by shipping lines for both "Hub and Spoke" and "Relay" networks separately
3. To analyse the competition among Port of Colombo and other competitive hub ports to act as the transhipment hub for different maritime markets
4. To identify future role of port of Colombo as a transhipment hub in the region

Thus study focuses on Port of Colombo located in South Asian region while Port of Singapore, TanjungPelapas and Kelang located in Southeast Asian region are considered as competitive hub ports. Competition is analysed for nine feeder ports in two feeder markets related to hub and spoke network individually and relay network separately.

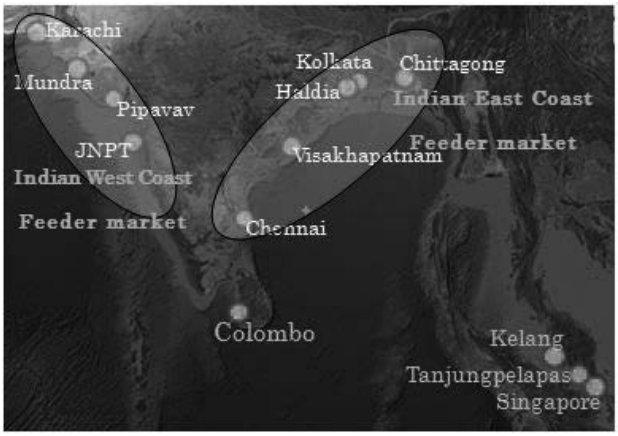


**Figure 1-1: Locations of ports considered in study**

## 2. Methodology

Qualitative analysis based on grounded theory approach is applied for achieving first research objective with the data collected through interview survey. Rest of the objectives are achieved using sequential mathematical modeling approach based on generalized cost model and logit model as indicated in Figure 2-1. Initially hub port selection criteria identified through literature reviews and interviews are grouped in to Monetary, Time, Location, Operational and Liner Related categories while the significance of criteria and the performances of hub ports related to non-quantitative criteria are evaluated based on questionnaire survey conducted with sample set of shipping lines with thirteen respondents.

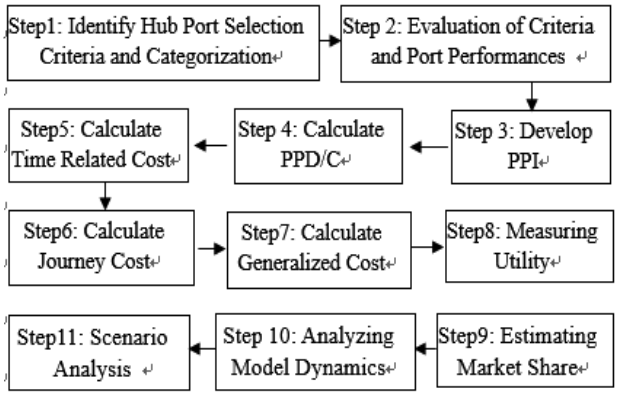


**Figure 2-1: Methodology flow for achieving Objective 2, 3 and 4**

Port Performance Index (PPI) is developed for each hub ports considering non quantitative criteria in terms of hub and spoke and relay network separately as follows.

$$PPI\ (A) = LEI\ (A)\ +\ OEI\ (A)\ +\ LREI(A) \tag{1}$$

$$LEI(A) = \left[\sum_{i=1}^{i=n} AAS(A, LE) * ASS(LE)\right]/n \tag{2}$$

$$OEI(A) = \left[\sum_{i=1}^{i=n} AAS(A, OE) * ASS(OE)\right]/n \tag{3}$$

$$LREI(A) = \left[\sum_{i=1}^{i=n} AAS(A, LRF) * ASS(LRF)\right]/n \tag{4}$$

LEI(A) , OFI(A) and LRFI(A) indicate the "Location Efficiency Index", "Operational Efficiency Index" and "Liner Related Efficiency Index" of Port A respectively. AAS and ASS refer to the "Average Appreciation Score" and "Average Significance Score" while "n" indicates the numbers of criteria under each category. Next in order to calculate the monetary values of non-quantitative criteria, "Port Performance Discount/Cost" (PPD/C) is calculated using equation (5). The positive and negative PPD/C indicate discounts and cost respectively.

$$\begin{aligned} PP[D/C]\ (A)\ =\ & PC(A) * LEI(A)/ASS(PC) + PC(A) \\ & * OEI(A)/ASS(PC)\ + PC(A) \\ & * LREI(A)/ASS(PC) \end{aligned} \tag{5}$$

As the next step, the time related cost is calculated using following equations. VTT, WT, DT represent the Vessel Turn Around Time, Waiting Time, Deviation Time of Hub port and JT (A-X) represents the Journey time in feeder link between hub port and feeder port. 'i (Average)' reflects the average value of $i^{th}$ time related criteria among four hub ports.

$$\begin{aligned} TC(A) = & [VOT(VTT) * VTT(A)] + [VOT(WT) * WT(A)] \\ & + [VOT(JT) * Ni * JT\ (A-X)] + [VOT(L \\ & * DT\ (A)] \end{aligned} \tag{6}$$

$$VOT(i, A) =\ [PC\ (A) * (ASS(i)\ /\ ASS(PC))]/i(Average) \tag{7}$$

As the next step, the calculation of Journey cost (JC) is done using equations (8) and (9) as mentioned below.

$$\begin{aligned} JC(A) = & [Ni * Distance(A-X) * Unit\ Distance\ Value(FC)] \\ & + [Distance(Deviation) \\ & * Unit\ Distance\ Value(DC) \end{aligned} \tag{8}$$

$$\begin{aligned} & Unit\ Distance\ Value(i) \\ & =\ [PC\ (A) * (ASS(i)\ /\ ASS(PC))]/i\ (Average) \end{aligned} \tag{9}$$

Distance (A-X), Distance (Deviation) represent the distance of feeder link and deviation distance from East West trunk sea route respectively. For the equations of both time and journey cost, Ni is a dummy variable which Ni=1 for hub and spoke and Ni=0 for relay. After calculating all cost values, Generalized cost (GC) related to hub port choices are measured with following GC function.

$$\begin{aligned} GC\ (A) =\ & PC\ (A) + Mi * JC(A) + Mi * TC\ (A) \\ & -\ PP[D/C]\ (A) \end{aligned} \tag{10}$$

PC represents the "Port Monetary Cost" and Mi is a dummy variable which Mi=1 for hub and spoke, Mi=2 for relay. Then calculated GC is converted in to utility with following approach as proposed by Koi Yu (2006), which GC(Min) and Utility (A) represent the GC of best performing port and utility of hub port A respectively.

$$Utility(A) = \frac{1}{\frac{GC\ (A)}{GC(Min)}} \tag{11}$$

Next logit model approach is used to estimate the market share (EMS) of hub ports with equation (12) using the utility values calculated from previous steps.

$$EMS(A) = \frac{e^{U(A)}}{\sum_{i=1}^{i=k} e^{U(i)}} \tag{12}$$

After estimating market share, model market share is compared with predicted market share from alternative approach based on simple linear regression. Further model dynamics are analysed to understand the relationship between each components of GC functions. Finally four practical scenarios are analysed considering various potential implication of liner shipping industry.

## 3. Analysis and Findings

The contextual framework is developed as the result of first research objective while identifying five main influences and various sub influences for the hub port selection decision from the practical aspect as illustrated in Figure 3-1. Then as the results of the questionnaire survey, ASS is calculated for both networks separately as mentioned in Table 3-1. According to that, related to majority of criteria, Hub and Spoke network obtains high ASS than relay network even though "Berth availability" is considered as the most significant criteria for both networks.

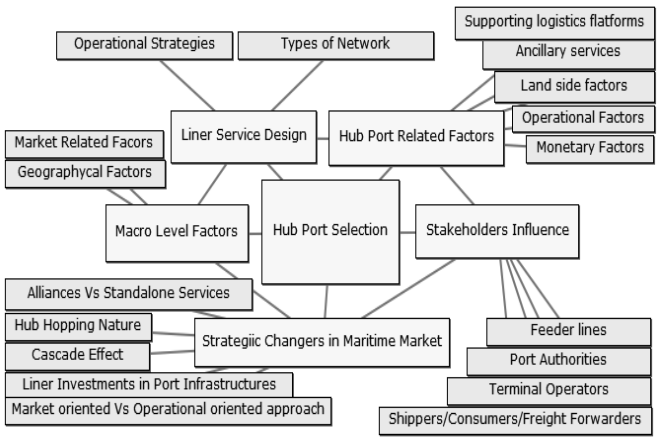


**Figure 3-1: Contextualized framework of factors on hub ports**

Criteria "Hub port Accessibility", "Frequency of Delays", "Efficiency of Husbandry Services" and "Availability of Dedicated/Own Terminal" obtained higher ASS for relay case than hub and spoke case while "Port Superstructures", "Port's Flexibility" and "Financial Clearance Capability" are obtained equal ASS for both networks.

**Table 3-1: ASS of Hub port Selection Criteria**

| Criteria | Hub and Spoke | Relay |
|---|---|---|
| Cost for deviation from main sea route | 4.462 | 4.308 |
| Port Cost | 4.462 | 4.308 |
| Cost in Feeder link | 4.692 | N/A |
| Deviation Time | 4.692 | 4.308 |
| Vessel Turnaround Time | 4.769 | 4.538 |
| Waiting Time | 4.462 | 4.308 |
| Time in Feeder link | 4.769 | N/A |
| Location with other hub ports | 4.000 | 3.846 |
| Hub port Accessibility | 4.231 | 4.385 |
| Location with feeder Markets | 4.154 | N/A |
| Port Capacity (TEUs) | 4.308 | 4.231 |
| Berth Availability | 5.000 | 4.846 |
| Frequency of Delays | 4.692 | 4.769 |
| Records of damages | 3.692 | 3.615 |
| Policies and Regulations | 4.000 | 3.846 |
| Port Infrastructures | 4.154 | 4.077 |
| Port Superstructures | 3.923 | 3.923 |
| IT and Advanced Technology | 4.000 | 3.692 |
| Logistics Facilities | 4.077 | 3.615 |
| Efficiency of Navigational Services | 4.308 | 4.077 |
| Efficiency of Husbandry Services | 3.000 | 3.154 |
| Professional employees | 4.000 | 3.923 |
| Marketing efforts | 3.231 | 3.000 |
| Port 's Flexibility | 4.154 | 4.154 |
| Financial Clearance Capability | 3.615 | 3.615 |
| Frequency of ship`s visits | 3.923 | 3.846 |
| No of Services Calling at port | 3.923 | 3.923 |
| Availability of Dedicated/Own Terminal | 3.077 | 3.231 |
| Personal Contacts | 3.231 | 3.154 |
| Special Preferences on shipping lines | 3.231 | 3.000 |
| Availability of customers/ Captive Cargo | 3.769 | 3.615 |
| Availability of Feeder Services | 3.769 | N/A |
| Opinion/ Preferences of Shipper/forwarders | 3.615 | 3.538 |
| Location of Hub Port with their services | 3.692 | 3.615 |

PPI is developed for two feeder markets in hub and spoke network and relay network separately as indicated in Figure 3-2. SIG, CMB, PKG and TPP indicate Singapore, Colombo, Kelang and TanjungPelepas ports respectively

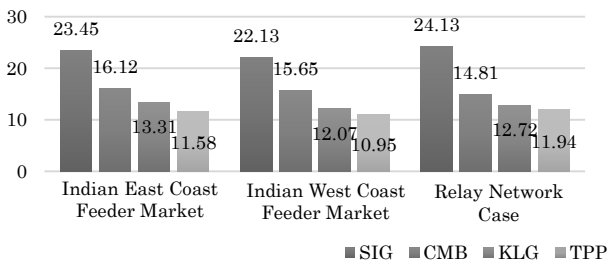


**Figure 3-2: PPI of competitive hub ports**

It is important to mention that CMB has lesser PPI for relay case than hub and poke case while all other three hub ports have higher PPI for relay case than hub and spoke case. Further SIG has the highest while TPP has the lowest PPI for all three cases.

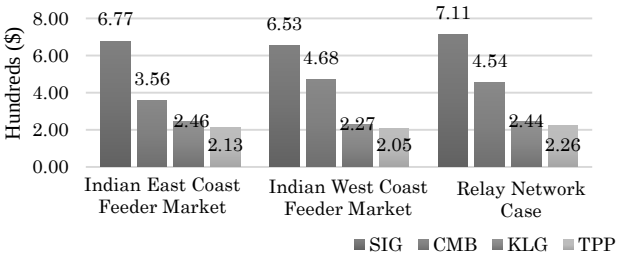


**Figure 3-3: PP D/C of competitive hub ports**

Further monetary values of non-quantitative criteria are calculated as PPD/C and results are indicated in Figure 3-3. Next market shares are calculated for all nine feeder ports related to hub and spoke case as mentioned in Figure 3-4 which indicates dominant market share of SIG.

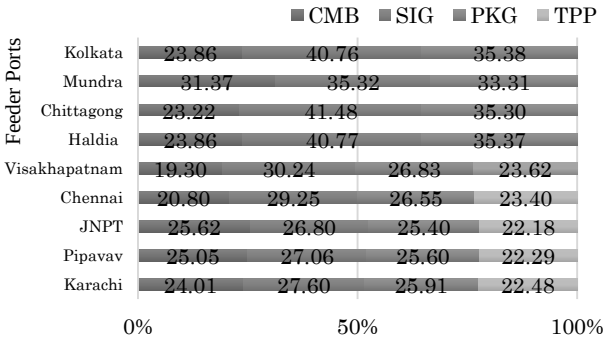


**Figure 3-4: Estimated market share for Hub and Spoke Case**

Besides that market share related to relay network case are calculated for each hub ports as mentioned in Figure 3-5 which indicates least market share for CMB.

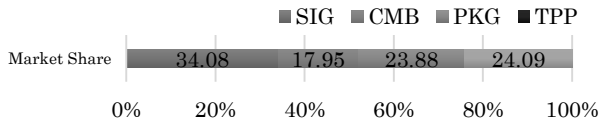


**Figure 3-5: Estimated market share for Relay Case**

Next estimated model market share is compared with predicted market share from regression model. For the prediction, the "No of Vessels deployed in services" is used as the explanatory variable as it derived the best fitting model to estimate the transhipment volumes. Then estimated model market share and predicted market share from regression method is compared and two examples of results related CMB and SIG ports are illustrated in following figures. .

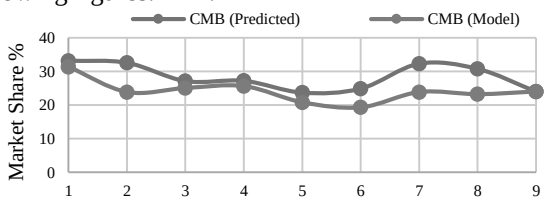


1-Mundra, 2-Kolkata, 3-Pipavav, 4–JNPT, 5–Chennai, 6 –Vishakhapatnam, 7 –Haldia, 8 –Chittagong, 9-Karachi

**Figure 3-6: Model VS Predicted market shares of CMB**

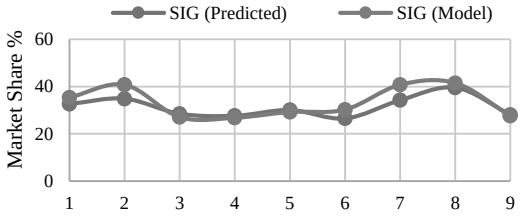


1-Mundra, 2-Kolkata, 3-Pipavav, 4–JNPT, 5–Chennai, 6 –Vishakhapatnam, 7 –Haldia, 8 –Chittagong, 9-Karachi

**Figure 3-7: Model VS Predicted market shares of SIG**

As the next step, four different scenarios focusing on "Price change effect", "Colombo port expansion project impact", "Best performing port effect" and "SINGA project impact" respectively named as scenario 1- 4 are analysed for achieving forth research objective and results are indicated in following figures.

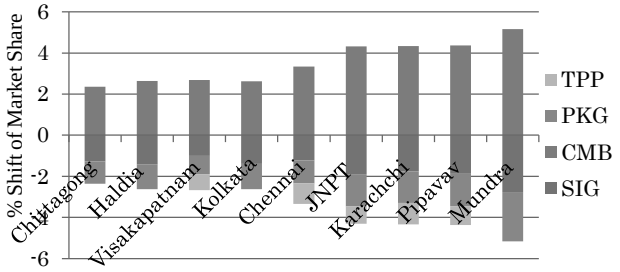


**Figure 3-8: Positive/Negative shifts of Market share from Scenario-1**

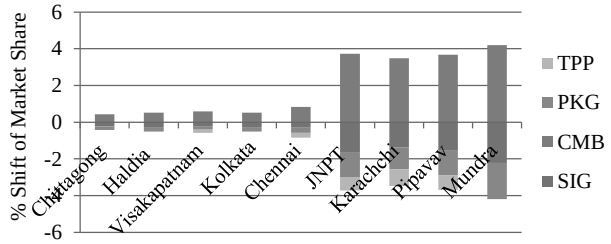


**Figure 3-9: Positive/Negative shifts of Market share from Scenario-2**

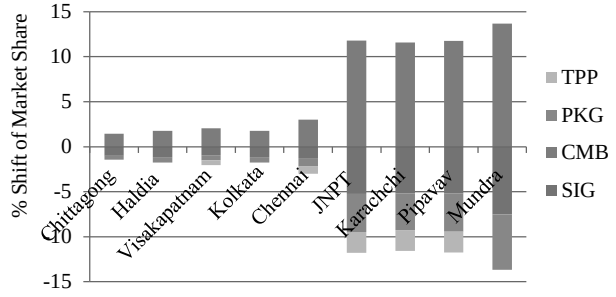


**Figure 3-10: Positive/Negative shifts of Market share from Scenario-3**

First three scenarios has been analysed based on CMB while Scenario 4 is based on SIG. According to the results of scenario analysis, first two scenarios show comparatively lesser market share gain than 3rd scenario while there is significantly higher impacts related to feeder ports located in Indian West coast feeder market than Indian East coast feeder market. Further SIG has the highest negative shift while TPP has the least negative shift from all three scenarios. Then results of Scenario 4 is illustrated in Figure 3-11 indicating the significant market share gain of SIG as the results of SINGA project while highest negative impact is showed by PKG.

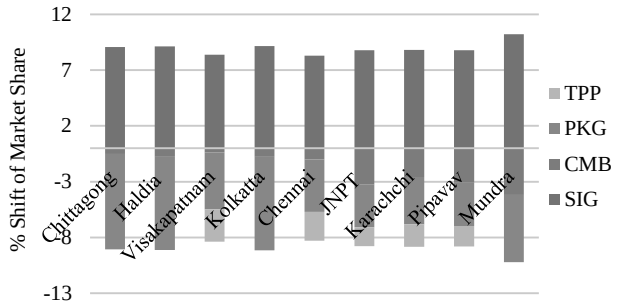


**Figure 3-11: Positive/Negative shifts of Market share from Scenario - 4**

Next Figure 3-12 illustrates the positive and negative shifts of market share related to scenario analysis in Relay network case which indicates clear difference between first three scenario and forth scenario. Further related to first three scenarios, highest negative shifts is observed from SIG while PKG and TPP has nearly equal negative shift of market share. As indicated CMB has the least negative impact from SINGA project development in SIG.

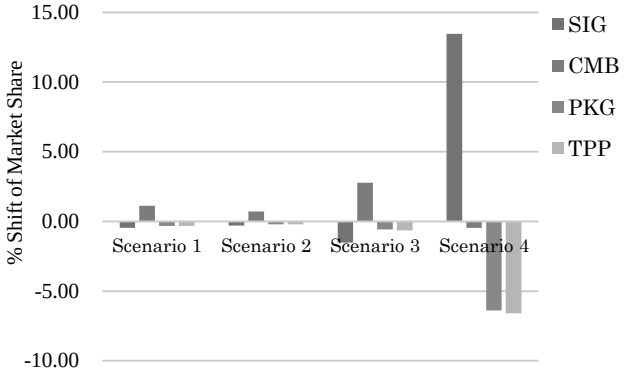


**Figure 3-12: Positive /Negative shifts of market Share of Scenario in Relay case**

## 4. Conclusion

The study develops a mathematical modelling approach to evaluate the competition among four competitive hub ports, Colombo, Singapore, Kelang and TanjungPelepas considering "Hub and Spoke" and "Relay" networks separately. Further significant decision making criteria are identified for the selection of transhipment hub port while the results indicate a visible differences in significance of selection criteria between two networks. Dominant performance of Singapore port is highlighted for all markets while performances of other three hub ports are varied based on different markets. Recommendations are made for the Port of Colombo based on the analysis of current competition and several future scenarios.

## References

Ducruet, C. and Notteboom, T. (2012) 'Developing Liner Service Networks in Container Shipping, Maritime Logistics: A complete guide to effective shipping and port management', pp. 77-100.

Koi-Yu, A. (2006) 'Theory and structure of port competition', University of Oxford.

Veldman, S.J .and Buckmann, E. H. (2003) 'A Model on Container Port Competition: An Application for the West European Container Hub-Ports', Maritime Economics and Logistics, 2003, 5, pp.3–22.

# Impact of high-speed rail entry on airport choice behavior in China

Student Number: 15M18210 Name: Jiawen JIANG Supervisor: Shinya HANAOKA

# 中国の高速鉄道の開通が空港選択行動に与える影響

姜佳文

本研究は、都市間が高速鉄道で繋がっている上海＝南京(301km)及び成都＝重慶(350km)路線を対象に選好意識調査を行い、非集計選択モデルを用いて、国際線利用時における対象地域の人々の空港とアクセス交通機関の選択要因を明らかにした。分析の結果、航空運賃、アクセス費用、アクセス時間、公共交通の運行頻度、アクセス時の乗換回数、路線距離ダミーが有意な変数となった。また、回答間の誤差を考慮した MXML と MXNL モデルの推定結果が優れており、高速鉄道のアクセス交通機関選択率が最も高い結果となった。

## 1. Introduction

China has the world's longest high speed rail (HSR) network as 20,000km by Sep.2016, and the number is going to reach 45,000km by 2030.

In short to middle-haul domestic routes, HSR had taken over the market of air transport and coach , however, the impact of HSR's feeder effect on international routes at China's airports have not been discussed. Terpstra (2015) mentions that HSR connection between two airports will increase both of their catchment area, and as the catchment area increases, competition between airports will be enhanced. However, it lies in the assumption that HSR is used as airport access mode. Despite the fact that even the average price on the routes with higher speed (For example: Guangzhou-Wuhan, Zhengzhou-Xi'an) is less than half of those in Japan and Europe, HSR price is still expensive compared to other airport access mode. Furthermore, while the share of transfer passengers has been shown as an important determinant for the scope of cooperation, according to report by CAMIC (2010) only one fourth of Chinese passengers showed an interest in HSR service. Considering facts discussed above, potential of HSR's feeder effect is still vague.

This research sets two objectives as follows:

(1) To identify significant factors in passenger's airport and access mode choice behavior in China.

(2) To identify whether HSR is chosen as airport access mode by international flight passengers in China.

As far as our knowledge, there is no study on HSR's feeder effect on international travel from China.

When impact of HSR on airport choice behavior is clarified in this study, the concept of multiple airport region in China will be stretched as the service hinterland that is accessible via ground transport mode within one and two hours of each international airport expands. This provides insights for alleviating congestion at major international hub airports as they can divert traffic to other airports by HSR. Furthermore, new roles can be assigned to each airport in the stretched multi-airport region. Figure 1 is the illustration of the change of roles after concept of multiple airport region is stretched. Airport A and B are two international airports, yellow and grey arrows represent domestic and international flights, separately.

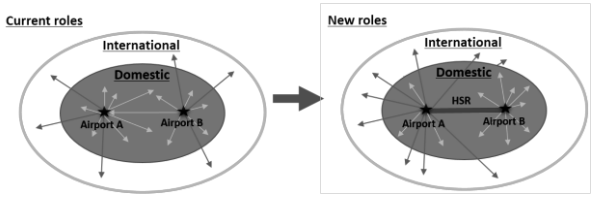


Figure 1 Illustration of airport's role change under different scale of multi-airport region.

As in airport A, slots that are previously used for domestic flights can be used for international flights instead, which will enhance connectivity of the multi-airport region, as well as its competitiveness among world hub airports.

## 2. Methodology

Discrete choice model is widely used in marketing and transportation field since the model analysis are usually based on the random utility maximization framework. It is used in order to measure the significance of factors of goods or services by observing respondents' choice behavior when choosing their favorite alternative among choice sets.

Index the number of respondents as $n$ = 1,2,3,…N and the number of alternatives as $i$ = 1,2,3,…I. The utility of respondent n for alternative $i$ is:

$$U_{ni} = \varepsilon_{ni} + \beta_i X_{ni} = \varepsilon_{ni} + V_{ni} \qquad (1)$$

Where as, $U_{ni}$ is the utility of alternative $i$ as perceived by respondent $n$, $V_{ni}$ represents characteristics of alternative $I$ and respondent $n$, $X_{ni}$ is a vector of parameters to be estimated and $\varepsilon_{ni}$ is a random unobserved component of utility, which is independent and identically distributed (i.i.d). The rest of this chapter introduces choice model conducted in this study, all the models are estimated using Biogeme (Bierlaire, 2013)

### 2.1 Multinomial Logit Model (MNL)

MNL model is the simplest and most popular practical discrete choice model. It is based on the assumption that the random components $\epsilon_{ni}$ are independently and identically distributed. With this assumption the choice probabilities are:

$$P_{ni} = \frac{\exp(V_{ni})}{\sum_{j \in I} \exp(V_{nj})} \qquad (2)$$

Despite the fact that the MNL model is the most commonly used model in transport research field, MNL model has the property of independence from irrelevant alternatives (IIA). The advantage of IIA property is that it makes the subset of the full choice set available for model estimation when the total number of alternatives in a choice set is large. The disadvantage, however, if some alternatives are "correlated", MNL calculates choice probabilities inconsistent with our intuition.

## 2.2 Nested Logit Model (NL)

NL model relaxed the i.i.d. assumption in MNL when alternatives are not independent, in which similar alternatives are grouped together (the group is called nest) and each alternative belongs to exactly one nest. A structural parameter (also can be called as nest parameter or scale parameter) is assigned to each nest to measure the degree of independence between alternatives in the respective nest. Assuming a nest of two levels, with $M$ number of lower nests. Scale parameter of upper and lower nest are μ and ϑ respectively. Choice probability of individual $n$ choosing alternative $i$ among $A_g$ alternatives in nest $g$ is shown as below:

$$P_{ni} = P[g] * P[i \mid g] = \frac{\exp(\frac{\mu}{\theta} \ln \sum_{a \in A_g} \frac{V_a}{\theta})}{\sum \exp(\frac{\mu}{\theta} \ln \sum_{k \in A_j} \frac{V_k}{\theta})} * \frac{\exp(\frac{V_i}{\theta})}{\sum_{l \in A_g} \exp(\frac{V_l}{\theta})} \quad (3)$$

Ratio of structure parameters (upper and lower nest) can be estimated together with utility parameters, with a value being in the range of [0,1] to hold the hypothesis of random utility maximization.

## 2.3 Cross Nested Logit Model (CNL)

CNL can be seen as an extension of the NL model. Its model structure allows to simulate multiple correlations between alternatives hypothesizing partially overlapping groups. CNL was conducted because the choice process in designed SP scenarios is two dimensional. Therefore, we assume if a respondent's current airport-access mode combination becomes unavailable, he or she will be more likely to switch to another option that keeps one of the dimensions of choice constant, rather than changing both airport and access mode. That's why we aimed to allow for correlation along both dimensions of choice. However, estimation result turns out that decision making of respondents in this study do not correspond with this model structure.

## 2.4 Mixed Logit Model (ML)

ML model was developed to relax the MNL assumption that the error term is independently and identically distributed across individual alternatives. It is highly flexible because it can approximate any random utility model. In this study, mixed logit model in MNL, NL and CNL structure was conducted. By change the distribution of parameters and error terms, ML models all for random taste variation, unrestricted substitution patterns and correlation in unobserved factors over time. Choice probabilities of ML model is defined in Train (1997). Probability of individual n choosing alternative $i$ is shown as below:

$$P_{ni} = \int L_{ni}(\theta) f(\theta) d\theta \quad (4)$$

$L_{ni}(\theta)$ is the probability that individual $n$ chooses alternative $i$. $f(\theta)$ is the density function of parameter $\theta$, which is known as mixing distribution. In this study, multiple observations were acquired from each respondent. Therefore, panel effect was added to the utility function, in the consideration of accounting for intra-respondent homogeneity of tastes.

# 3. SP Survey

## 3.1 Survey OD Selection

Nanjing ~ Shanghai and Chengdu ~ Chongqing are selected as target route. Details of the two routes are given in Table 1. Five origin cities are selected based on criteria below: (1) Located in between airports on target route; (2) Presence of HSR station; (3) Residents are able to access both airport by coach, HSR and private car; (4) significant distance difference to either airport on the target route.

Table 1 Details of Target Routes

| Route | Designed Speed (km/h) | Distance (km) | Service Launch Year | En-route time |
|---|---|---|---|---|
| Nanjing~ Shanghai | 250 | 301 | 2011 | 2h4min |
| Chengdu~ Chongqing | 200 | 350 | 2012 | 1h49min |

For destination, Seoul and Singapore were selected as short and middle haul destination for their high popularity among Chinese travelers and high monthly frequency of direct service from all target airports.

## 3.2 Survey Design

The designed survey is consisted of three parts. Part one asks about personal information and trip experience of respondents, such as gender, age, occupation, average monthly income, ownership of private car in the household, number of domestic and international round trip by air in 2016 and most frequent trip purpose among international trips. In part two, respondents will be asked about details of the last international trip under their most frequent trip purpose. Questions include trip destination, number of accompanies, departure airport (last domestic departure airport if that was a transit flight), access mode to the airport and choose three important factor for choosing this departure flight then rank them in order.

Part three starts with questions on the departure and arrival time in respondent's last international trip under their most frequent trip purpose. Then respondents are asked to imagine they live in a city without airport, and they are planning whether to go for an international trip to Seoul and Singapore. Respondents are required to make airport and access mode choice based on given situation in different scenarios that follow. Scenarios are different in terms of whether it is a departure or arrival flight, haul length, presence of accompany, number of

baggage, flight schedule, airfare, total access time, access cost, number of transit from starting point to airport and additional waiting time if respondent miss the designated bus or train. Information on two airports (Airport A and Airport B) is provided, therefore respondent can choose which airport for departure or arrival, access mode to that airport, or give up the trip if they are not satisfied with the provided scenario. Airports name is unlabeled because revealed airport name might introduce biases if respondents don't have experience of both airports and simply choose the airport that they are more familiar with.

Access mode attributes include access time, access cost, service interval of coach, HSR and private car, as well as total number of transit from start point to airport. Base information of each mode is acquired from widely used map and ticket booking website Gaode.map and ctrip.com.

Schedule delay is the time difference between desired and actual departure and arrival time, which is commonly used as an alternative for flight frequency. We assume the departure and arrival time of the last trip of each respondent is their desired flight schedule. Departure or arrival time might be two hours earlier, two hours later than, or the same with desired flight time in different scenarios. Base airfare from the same airline (China Eastern) is collected from ctrip.com.

To lessen the burden of respondents while preserving orthogonality between each scenario, Ngene (©2014ChoiceMetrics) is used as a tool for orthogonal design. After a thorough correlation and logic check, eventually 12 designs with HSR alternative and 8 designs without HSR alternative are selected. Figure 2 is the scenario example.

SP survey was conducted through Internet during Dec.29, 2016 ~ Jan. 3rd, 2017, 569 effective samples were gathered during survey period. To ensure the reliability of survey result, we selected respondents resident in the target area who experienced at least one international travel in 2016.

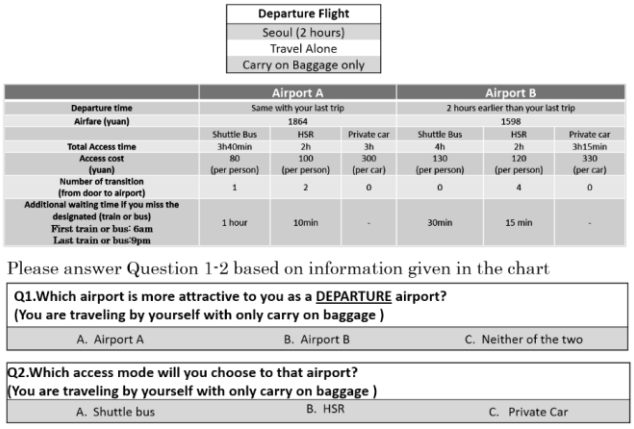


Figure 2 Scenario Example in SP Survey

## 4. Model Estimation

All models were calibrated using both continuous and dummy variables. Continuous variables include airfare, access cost, access time, interval of public transport service, number of transit and income. Dummy variables are trip haul length (set to 1.0 for short haul trip), and number of accompanies (set to 1.0 when the scenario is under the condition of travelling with someone else).

Estimation result on MNL, NL, MXML, MXNL and MXCNL model for observation type (O), adjusted rho-square ( $\hat{\rho}^2$ ), coefficient of parameter (β), nest parameter (μ) and diagnostic are summarized in Table 2. Abbreviations are concluded in the bracket after the table.

Table 2 Summary of Model Estimation Results

| | No | O | $\hat{\rho}^2$ | $\beta$ | $\mu$ | D |
|---|---|---|---|---|---|---|
| MNL | 1 | $W_t$ | 0.053 | ○ | - | ○ |
| | 2 | $W_o$ | 0.091 | × | | |
| | 3 | $W_c$ | 0.061 | ○ | | |
| NL(A) | 4 | $W_c$ | 0.064 | ○ | ○(W) | Δ |
| NL(M) | 5 | $W_c$ | 0.063 | × | ○ | Δ |
| MXML | 6 | $W_t$ | 0.150 | ○ | - | ○ |
| | 7 | $W_o$ | 0.146 | × | | |
| | **8** | **$W_c$** | **0.148** | ○ | | |
| | 9 | $W_c$ &B | 0.167 | × | | |
| | 10 | $W_c$ &N | 0.140 | ○ | | |
| MXNL (A) | **11** | **$W_c$** | **0.153** | ○ | ○(W) | ○ |
| MXNL (M) | 12 | $W_c$ | 0.168 | ○ | × | ○ |
| MXNL (A) | 13 | $W_c$ &B | - | - | - | × |
| | 14 | $W_c$ &N | 0.143 | ○ | ○(W) | ○ |
| MXCNL | 15 | $W_c$ &F | 0.162 | ○ | × | Δ |
| | 16 | $W_c$ &F&B | - | - | - | × |
| | 17 | $W_c$ &F&N | 0.162 | ○ | × | Δ |
| | 18 | $W_c$ &F&C | 0.163 | ○ | × | ○ |

($W_t$ : Choice data with HSR alternative [2276 samples]
$W_o$ : Choice data without HSR alternative [1138 samples]
$W_c$: Combined choice data with and without HSR alternatives
B: Choice data made under business trip purpose [714 samples]
N: Choice data made under non-business trip purpose [2700 samples]
F: Allocation parameters are fixed to a value
C: Constraints are added to nest parameters
○: Satisfying level,
Δ: Not satisfying but acceptable level
×: Rejected)

Significant improvement in adjusted rho-square can be observed in Model 6 ~ Model 18 because panel effect was taken into consideration, which accounts for intra-respondent homogeneity of tastes since multiple observations were acquired from each respondent. Models that are estimated only on choice data in scenario without HSR alternative are rejected due to low significance level of $\beta$ which results from the lack of scenario pattern in the choice set. Discussions mainly focus on models that are estimated using a combination of choice data with and without HSR alternatives, so that marginal utilities of variables for scenarios without HSR alternative can be correctly estimated and discussed. A scale parameter for choice data with HSR alternative was estimated, which is inversely proportional to the variance of the error term.

Among all 569 respondents, only less than 120 were familiar with international business trip, therefore, convergence in Model 9, Model 13 and Model 16 were hardly reached because of the small sample size. Model 12, in which access mode is on the upper nest, was rejected

because the ratio of nest parameters indicates the structure failed to hold the hypothesis of random utility maximization. MXCNL structure was rejected because in Model 15 ~ Model 18, all nest parameters were smaller than 1.0, implying decision making of survey respondents do not fit the model structure. Therefore, in the following part, we will discuss on Model 8 and Model 11. Details are given in Table 3.

Table 3 Estimation Results of Model 8 and Model 11

| Models | | MXML-8 | | MXNL(A)-11 | |
|---|---|---|---|---|---|
| | | $\beta$ | $t$-value | $\beta$ | $t$-value |
| Airfare | | -0.164 | -9.69** | -0.171 | -7.28** |
| Access Cost | | -0.203 | -4.17** | -0.193 | -4.21** |
| Access Time | | -0.111 | -3.88** | -0.0775 | -2.96** |
| Interval of PT | | -0.0763 | -4.19** | -0.0544 | -3.5** |
| No. of Transit | | -0.0805 | -4.83** | -0.0524 | -3.82** |
| Haul Length | | 0.35 | 2.42** | 0.28 | 1.88* |
| No. of Accompany | | 0.0738 | 0.52 | 0.03 | 0.2 |
| Income | | -0.0141 | -0.76 | -0.0103 | -0.57 |
| ASC (Ap2) | | -0.517 | -6.52** | -0.835 | -5.93** |
| ASC (Car) | | -0.554 | -4.89** | -0.416 | -3.22** |
| ASC (HSR) | | -0.232 | -2.71** | -0.172 | -2.47** |
| ASC (No) | | -4.72 | -10.84** | -4.68 | -8.28** |
| Nest Parameter | | | | | |
| Ap1 | $W_t$ | - | | 2.45 | 6.21** |
| | $W_o$ | | | 0.702 | 6.41** |
| Ap2 | $W_t$ | | | 1.27 | 8.00** |
| | $W_o$ | | | 0.495 | 7.38** |
| Scale Parameter | | 1.56 | 3.36** | 1.44 | 2.32** |
| $\hat{\rho}^2$ | | 0.148 | | 0.153 | |

(*: 5% significance level **: 1% significance level)

Results show that negative marginal utilities for increases in airfare, access cost, access time, interval of public transport service, number of transit in both models are at 1% significance level. Haul length is significant at 5% level in Model 8 and 1% level in Model 11, the positive sign can be interpreted as respondents have higher utility when taking short haul trip. Number of accompanies and income were insignificant in both models. Airport and mode alternative specific constants (ASC) were introduced to represent the part of individual utility that is not captured by proposed variables but well perceived in the respondent's mind. Due to how logit model works, it is not possible to specify an ASC for every alternative, ASCs for airport 1 and coach are fixed to zero as reference. As other ASCs are estimated relative to the fixed ASC, there is no loss of generality by doing so. For access mode, we can see that all else being equal, coach (the base) has the highest utility and the lowest utility is obtained for car in both models. Regarding the fact that in both models the scale parameter for choices with HSR alternative exceeds 1.0, it can be indicated that a somewhat reduced error variance for responses in those scenarios.

In Model 11, nest parameter on the upper nest is fixed to be 1.0 in order to estimate the nest parameters on the lower part. For both airports, the ratios of nest parameters in scenarios without HSR alternative are greater than 1.0, which indicates the structure failed to hold the hypothesis of random utility maximization. This result can be interpreted as in scenarios without HSR alternative respondents do not decide departure or arrival airport in the 1st place. Improvement in $\hat{\rho}^2$ can be observed in Model 11 because correlation between unobserved utilities of airports in scenarios with HSR alternative are captured.

Access mode share of Model 11 calculated using logit model is shown in Figure 3. We can see that coach has the largest share when without HSR alternative and HSR dominants over coach and private car. There are more respondents switched from coach to HSR than that of private car, and the share of respondents that are not satisfied with provided scenario remains the same.

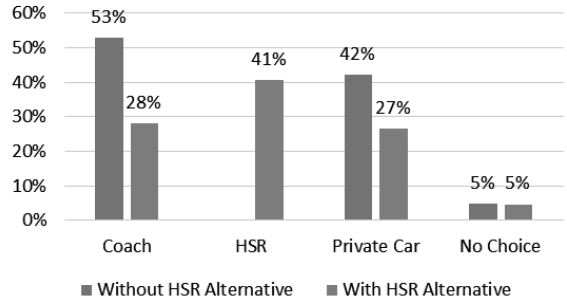


Figure 3 Access Mode Share of Model 11

## 5. Conclusion

In this study, to clarify impact of HSR entry on airport and access mode choice behavior in China, SP survey was conducted on two target routes. MNL, NL, CNL, ML are estimated, major findings are: (1) Airfare, access cost, access time, interval between public transport service, number of transit in public access mode as well as the length of international flight were significant in respondent's airport and access mode choice; (2) Mode share of HSR dominants over coach and private car; (3) MXNL model with panel effect outperformed other models for its consideration of intra-respondent homogeneity of tastes.

## Reference

[1] Mid-Longterm Railway Development Plan (2016), National Development and Reform Commission (NDRC).
[2] Domestic Passenger Characteristics Report (2010), Civil Aviation Management Institute of China (CAMIC)
[3] Terpstra. I and Lijesen. M. (2015), The impact of high speed rail on airport competition, Tijdschrift voor Economische en Sociale Geografie, 106, (3), 263-275
[4] Johnson, D., Hess, S. and Matthews, B.(2014), Understanding air travelers' trade-offs between connecting flights and surface access characteristics, Journal of Air Transport Management, 34, 70-77.

# INFLUENCE OF DEFECTS ON STEEL CORROSION OF REINFORCED CONCRETE EXPOSED TO MARINE ENVIRONMENT FOR LONG-TERM

Student ID: 15M18173 Name: Daisuke MIZUSHIRI Supervisor: Mitsuyasu IWANAMI

長期間海洋環境に暴露された鉄筋コンクリートの鉄筋腐食に及ぼす初期欠陥の影響

水尻　大輔

本研究では、既存の研究例がほとんどない長期間実海洋環境に暴露された欠陥を有する鉄筋コンクリート供試体を用いて、打継目やひび割れといった初期欠陥が海洋環境下で鉄筋腐食に及ぼす影響を明らかにすることを目的とした。実験結果から、初期ひび割れを有する海水練りの供試体では、初期ひび割れ幅が大きいと腐食による鉄筋の質量減少率が大きくなる傾向が確認された。打継目を有する供試体では、打継ぎ材料を用いた供試体では、レイタンスの除去により腐食による鉄筋の質量減少率が増加していた。また、実験結果および既往の研究結果を用いて、実環境下における鉄筋腐食の経時変化や腐食速度の経験式の妥当性について検討を行った。

## 1. Introduction

There are many reinforced concrete (RC) structures under marine environment in Japan because Japan is an island country and surrounded by the ocean. Then deterioration of RC structures by chloride attack is one of the major social problems.

Chloride attack causes corrosion of steel bar in concrete, which deteriorate the durability of RC. Deterioration factors go into concrete through defects, such as crack and construction joint. Influence of defects on the durability of concrete have been investigated by laboratory tests.

However there are few studies on corrosion of steel in concrete exposed to real marine environment. Therefore in this study, the following objectives have been set.

1. To clarify the influence of crack and construction joint on steel corrosion in the marine environment
2. To examine the process of steel corrosion under the real environment and the validity of empirical equations of corrosion rate

## 2. Experimental Overview

### 2.1. Specimens and Exposure Condition

Two types of concrete specimens after long-term exposure to marine environment were used in this study.

One was prism concrete specimens with a steel bar made in 1981, and shown in Table 1 (a). These specimens were made with flexural cracks at the center by loading as initial cracks. The initial crack width was 0.1, 0.2 and 0.3 mm. They were exposed to a seawater tank which emulates dry and wet cycles by 6 hours for 32 years.

The other was cylinder concrete specimens made in 1973, and shown in Table 1 (b). These specimens were made with 3 steel bars and construction joint. Three steel bars of 9 mm diameter and 18 cm length were set at cover depths of 2, 4 and 7cm. Seven types of joint treatments were conducted on the construction joint. Those specimens were submerged in the same seawater tank continuously for 40 years.

Table 1 Types of Specimens

(a) RC with Initial Crack

| Size (mm) | Cover (mm) | Mixing Water | Water Cement Ratio (%) | Initial Crack Width (mm) | Name |
|---|---|---|---|---|---|
| 100×100×600 | 20 | W | 55 | 0.2 | W20_55_0.2 |
| | | | 65 | | W20_65_0.2 |
| | | S | 55 | 0.2 | S20_55_0.2 |
| | | | 65 | | S20_55_0.2 |
| | 40 | W | 55 | 0.1 | W40_55_0.1 |
| | | | | 0.2 | W40_55_0.2 |
| | | | | 0.3 | W40_55_0.3 |
| | | | 65 | 0.2 | W40_65_0.2 |
| | | S | 45 | 0.2 | S40_45_0.2 |
| | | | 55 | 0.1 | S40_55_0.1 |
| | | | | 0.2 | S40_55_0.2 |
| | | | | 0.3 | S40_55_0.3 |
| | | | 65 | 0.2 | S40_65_0.2 |
| 150×150×600 | 70 | W | 55 | 0.2 | W70_55_0.2 |
| | | | 65 | | W70_65_0.2 |
| | | S | 55 | | S70_55_0.2 |
| | | | 65 | | S70_65_0.2 |

W: Tap Water S: Sea water

(b) RC with Construction Joint

| No. | Joint Treatment | |
|---|---|---|
| | Removal of Laitance | Joint Material |
| A | Not Removed | Nothing |
| B | | Mortar |
| C | | Epoxy Resin |
| D | Removed | Nothing |
| E | | Mortar |
| F | | Epoxy Resin |
| G | | Latex Paste |

### 2.2. Experimental Methods

**(1) Corrosion Current Density**

Polarization resistance was measured by using a corrosion monitor. It was measured at 3 points in specimens (the center and both edges). Then, corrosion current density was given by Eq. (1).

$$I_{corr} = \frac{K}{R_{ct} \times S} \quad \text{Eq. (1)}$$

Where $I_{corr}$ is the corrosion current density and K is a constant (0.0209 V). $R_{ct}$ and S are polarization resistance and surface area of a steel bar respectively.

**(2) Corrosion Area Ratio**

Steel bars in specimens were removed after measurement of corrosion current density. Corroded points on the steel surface were sketched on a film wrapped around the steel bar. Corrosion area sketched on the film was calculated by an image analysis software.

**(3) Mass Loss Ratio and Corrosion Amount**

After measuring of corrosion area ratio, steel bars were soaked in 10% diammonium hydrogen citrate solution for two

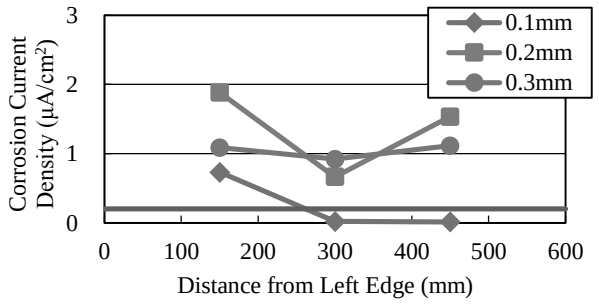


(a) Tap Water, Cover: 4cm, W/C: 55%

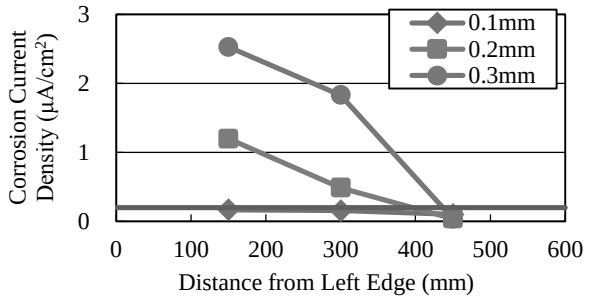


(b) Sea Water, Cover: 4cm, W/C: 55%

Fig.1 Corrosion Current Density of Specimens with Initial Crack

days to remove rust on steel bars. A mass of the steel bar after removing rust was measured.

### 3. Steel Corrosion of RC with Initial Crack Exposed for 32 years

**(1) Corrosion Current Density**

Fig.1 shows one of the results of corrosion current density of prism specimens. When the corrosion current density is higher than 0.2 μA/cm$^2$ (Red line in Fig.1), the steel in concrete is corroded according to evaluation method of CEB. In the case of tap water mixing, there is not a clear tendency by difference in initial crack width in results of corrosion current density. On the other hand, specimens mixed with sea water showed that corrosion current density was larger as increase in initial crack width. Differences in corrosion current density by initial crack did not show a clear trend between the center (30cm) and the edge of specimen (15cm, 45cm).

**(2) Corrosion Area Ratio**

Results of corrosion area ratio are shown in Table 2. Steel corrosion occurred on the whole of steel surface because corrosion area ratio was 100% or near 100%. But corrosion area ratio of S40_45_0.2 was 49.0%, which was the smallest value of all. It was a half of values of other specimens. In the case of S40_55, corrosion current density became larger as initial crack width became larger. The tendency of S40_55 was not confirmed in W40_55.

**(3) Mass Loss Ratio and Corrosion Amount**

Mass loss ratio of W70_65_0.2 was the largest, which was 25.9% from Table 2. When initial crack width increased from 0.1mm to 0.3mm for W/C 55% specimens, mass loss ratio increased by 0.4% in the case of tap water mixing. The value of specimens mixed with sea water also increased by 1.3%. Therefore mass loss ratio showed a tendency to increase as increase in initial crack width.

As well as mass loss, corrosion amount of W70_65_0.2 was the largest, which was 483.0mg/cm$^2$. The same tendency as the mass loss ratio relative to initial crack width was confirmed on the corrosion amount.

Table 2 Results of Measurement for Specimens with initial Crack

| Name | Corrosion Current Density (μA/cm$^2$) | Corrosion Area Ratio (%) | Mass Loss Ratio (%) | Corrosion Amount (mg/cm$^2$) |
|---|---|---|---|---|
| W20_55_0.2 | 2.84 | 100.0 | 10.8 | 262.0 |
| W20_65_0.2 | 2.49 | 100.0 | 12.0 | 293.3 |
| S20_55_0.2 | 2.29 | 96.9 | 12.7 | 308.5 |
| S20_55_0.2 | 0.66 | 100.0 | 12.1 | 295.3 |
| W40_55_0.1 | 0.25 | 100.0 | 8.4 | 203.7 |
| W40_55_0.2 | 1.36 | 93.0 | 8.3 | 203.2 |
| W40_55_0.3 | 1.04 | 100.0 | 8.8 | 214.7 |
| W40_65_0.2 | 2.03 | 100.0 | 7.7 | 187.8 |
| S40_45_0.2 | 0.11 | 100.0 | 5.2 | 125.6 |
| S40_55_0.1 | 0.14 | 100.0 | 8.1 | 196.4 |
| S40_55_0.2 | 0.58 | 49.0 | 8.3 | 201.8 |
| S40_55_0.3 | 1.46 | 93.6 | 9.4 | 229.2 |
| S40_65_0.2 | 2.42 | 97.1 | 7.8 | 190.3 |
| W70_55_0.2 | 0.05 | 99.8 | 20.9 | 333.3 |
| W70_65_0.2 | 1.40 | 98.9 | 25.9 | 483.0 |
| S70_55_0.2 | 0.07 | 81.7 | 9.0 | 220.4 |
| S70_65_0.2 | 0.34 | - | - | - |

Table 3 Results of Corrosion Current Density for Specimens with Construction Joint

| No. | Corrosion Current Density (μA/cm$^2$) | | | | | | | | |
|---|---|---|---|---|---|---|---|---|---|
| | Cover:20mm | | | Cover: 40mm | | | Cover: 70mm | | |
| | 60 mm | 150 mm | 240 mm | 60 mm | 150 mm | 240 mm | 60 mm | 150 mm | 240 mm |
| A | 0.21 | 0.85 | 0.77 | 0.18 | 0.48 | 0.54 | 0.33 | 0.43 | 0.45 |
| B | 0.10 | 0.93 | 1.63 | 0.09 | 0.16 | 0.77 | 0.18 | 0.16 | 0.16 |
| C | 1.02 | 0.18 | 1.72 | 0.14 | 2.08 | 1.11 | 0.19 | 0.21 | 0.13 |
| D | 0.18 | 0.26 | 0.57 | 0.24 | 1.04 | 0.96 | 0.14 | 1.11 | 0.22 |
| E | 0.99 | 0.44 | 0.51 | 1.54 | 1.78 | 1.88 | 0.58 | 0.29 | 0.44 |
| F | 0.51 | 0.68 | 0.57 | 0.35 | 1.32 | 0.37 | 0.19 | 1.79 | 1.33 |
| G | 0.81 | 4.17 | 1.88 | 0.57 | 0.99 | 1.26 | 0.38 | 0.52 | 0.91 |

### 4. Steel Corrosion of RC with Construction Joint Exposed to 40 years

**(1) Corrosion Current Density**

Corrosion current density at construction joint (150mm) was generally higher than that at the edge of specimen (60mm, 240mm) in case of A, D and F type as shown in Table 3.

Corrosion current density did not have a big difference by removing laitance. Also, a clear tendency was not observed in different joint materials after exposure to submerged zone for 40 years.

**(2) Corrosion Area Ratio**

Fig.2 shows corrosion area ratio of specimens with construction joint. Corrosion area ratio was 100% or near 100%, and steel corrosion occurred on the whole of steel surface. A difference in corrosion area ratio by joint treatment and cover was small at 40 years after exposure to submerged zone.

**(3) Mass Loss Ratio and Corrosion Amount**

Result of mass loss ratio is shown in Fig.3. In the cases without removing laitance, mass loss ratio of B and C type decreased by 0.1-2.1% and 2.0-3.6% than A type, respectively. In the other cases with removing laitance, mass loss ratio of E, F, G type increased by 0.5-2.8% than D type, which was the opposite tendency.

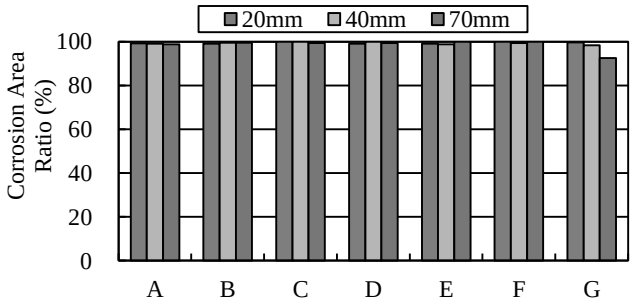

Fig.2 Corrosion Area Ratio of specimens with Construction Joint

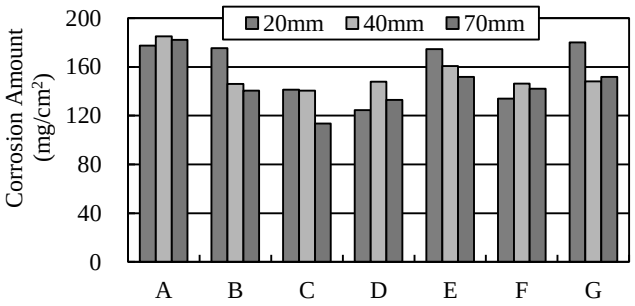

Fig.4 Corrosion Amount of Specimens with Construction Joint

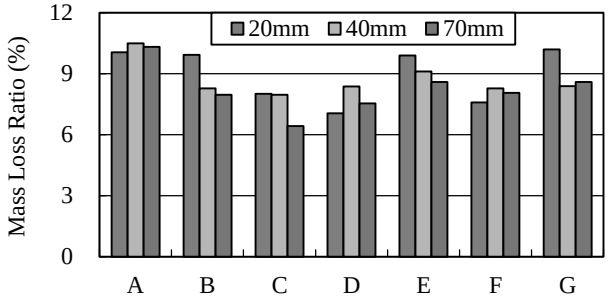

Fig.3 Mass Loss Ratio of Specimens with Construction Joint

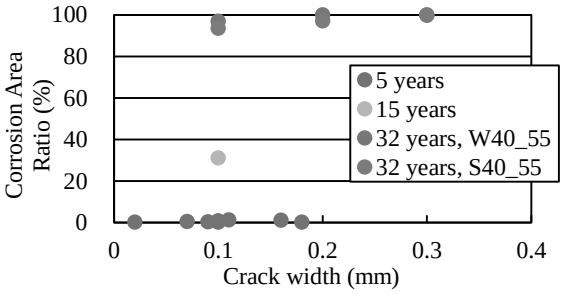

Fig.5 Time History of Corrosion Area Ratio of Specimens with Initial Crack

Mass loss Ratio of D type decreased by 2.1-3.0% compared with A type, which is an effect of removing laitance. When the joint materials were used, a clear difference by removing laitance was not observed.

Result of corrosion amount is shown in Fig. 4. Corrosion amount of A type is the highest value, which was 177.4, 185.2, and 182.2 mg/cm$^2$ at 20, 40, and 70 mm of cover, respectively. Differences by joint treatment were the same trend as result of mass loss ratio.

## 5. Time history of Steel Corrosion of RC with Initial Defects Exposed to Marine Environment

Examination of the process of steel corrosion under the real environment was conducted by use of experimental and previous results in this chapter.

### 5.1. RC with Initial Crack Exposed to Tidal Zone for Long-Term

Previous Studies have investigated steel corrosion of RC with initial crack exposed to tidal zone for 5 and 15 years[1), 2)]. Fig.5 shows corrosion area ratio after 5, 15 and 32 years' exposure to tidal zone. Corrosion area ratio was about 1% at 5 years' exposure, but it increased about 30% after 15 years. After that, corrosion area ratio after 32 years became 100%. Steel corrosion occurred on undersurface of the steel around the initial crack after 5 years. Corrosion was confirmed on the steel surface other than initial crack at 15 years. Also, corrosion area was large around initial crack unless autogenous healing was observed at 15 years.

Therefore, the following is considered. Steel corrosion starts from around initial crack during the first 5 years' exposure. It develops on steel surface other than initial crack in the next 10 years, the whole steel bar is corroded by 32 years.

### 5.2. RC with Construction Joint Exposed to Submerged Zone for Long-Term

Previous Studies have investigated steel corrosion of RC with construction joint exposed to submerged zone for 1.5, 5, and 10 years[3), 4)]. Fig.6 shows corrosion area ratio of 20mm of cover after 5, 15, and 32 years' exposure to submerged zone. Corrosion area ratio of A and F type were 0.2% and 0.6% respectively at 1.5 years' exposure. After 5 and 10 years, corrosion area ratio of all types increased up to about 1-11%. Steel bars in specimens exposed for 40 years were corroded on the whole of steel surface. Therefore steel corrosion developed during 30 years after the first 10 years. These tendencies were also observed in the cases of 40 and 70 mm cover.

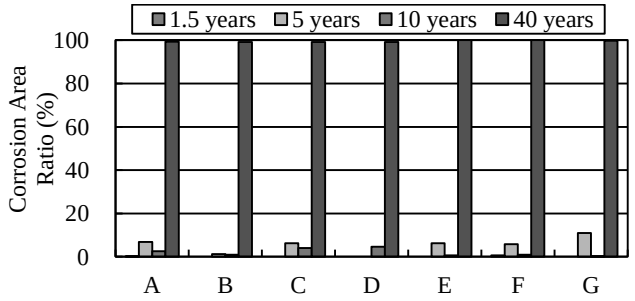

Fig.6 Time History of Corrosion Area Ratio of Specimens with Construction Joint

## 6. Consideration of Empirical Equations and Experimental Results

### 6.1. Empirical Equations in Previous Studies

Some empirical equations were suggested in previous studies so far. Then, experimental results were compared with two following empirical equations with regard to the corrosion amount.

(1) Empirical Equation 1

・W/C: 50~55%

$$q_{50\text{-}55}=0.092\cdot\exp\left\{(0.0423\cdot(W/C)-1.5091)\cdot Cl^-\right\}\cdot\frac{1}{\sqrt{c}} \quad \text{Eq. (2)}$$

・W/C: 55~65%

$$q_{55\text{-}65}=0.092\cdot\exp\{(-0.0003\cdot(W/C)+0.8390)\cdot Cl^-\}\cdot\frac{1}{\sqrt{c}} \quad \text{Eq. (3)}$$

$$q=\frac{\Delta W_r}{t};\ q_s=\frac{\Delta W}{(S/100)\cdot t}=\frac{W_0}{100\cdot(S/100)}\cdot q$$
$$=\frac{(d/10)\cdot(1000\rho)}{400}\cdot q=1.95\cdot d\cdot q \quad \text{Eq. (4)}$$

Where, $q_s$ : Corrosion Rate (mg/cm$^2$/year), q:Corrosion Rate (%/year), $Cl^-$ : Chloride Ion Concentration (kg/m$^3$), W/C : Water Cement Ratio (%), c : Cover (mm), d : Diameter of a Steel Bar(mm), ρ : Density of Steel (=7.8)(mg/mm$^3$), L : Length of a Steel Bar (mm), $W_0$ : Mass of a Steel Bar ($=\pi(d/2)2L\rho$)(mg), S : Steel Surface ($=\pi dL$)(mm$^2$), ΔW : Mass Loss (mg), $\Delta W_r$ : Mass Loss Ratio ($=\Delta W/W_0\times100$) (%), t : Period (year)

(2) Empirical Equation 2

$$V_{3tn}=\frac{0.78}{\sqrt{c}}(7.70\cdot Cl_{tn}+0.503(W/C)-40.6 \quad \text{Eq. (5)}$$

Where, c: Cover (mm), $Cl_{tn}$: Chloride Ion Concentration (kg/m$^3$), W/C: Water Cement Ratio (%)

Chloride ion concentration of specimens was assumed as 15.0 kg/m$^3$ from the previous studies[4].

### 6.2. Comparison of Empirical Equation and Experimental Results

Calculation results of specimen with initial crack were shown in Table 4. Corrosion rate given from empirical equation 1 was much higher than that of experimental results. The values given from empirical equation 2 were close to the experimental results. Those were 0.4-1.6 times as large as the experimental results.

Table 5 is calculation results of specimen with construction joint. Corrosion rate given from empirical equation 1 was much higher than that of experimental results as well as the calculation results of specimens with initial crack. Corrosion rate given from empirical equation 2 was 1.9-3.3 times as large as that of experimental results.

In two empirical equations, empirical equation 1 describes that corrosion rate increase exponentially. On the other hand, Corrosion rate increased linearly in empirical equation 2. Chloride ion concentration used in this calculation was as large as 15.0kg/m$^3$ because the specimens were exposed to marine environment for long-term. Then, calculation results became excessively higher in empirical equation 1 due to chloride ion concentration in the exponent part. Therefore empirical equation 2 may by good for the case of high chloride ion concentration

Chloride ion concentration and water cement ratio are used as parameters in the above empirical equations. However, the amount or permeability of oxygen are not considered in the equations even though oxygen is also one of important factors on steel corrosion. It may be necessary to consider a high chloride ion concentration and the influence of exposure condition like amount of oxygen when corrosion rate is considered after long-term exposure

Table 4 Calculation Results of Specimen with Initial Crack Exposed to Tidal Zone

| Cover (mm) | Mixing Water | Water Cement Ratio (%) | Initial Crack Width (mm) | Experimental Results (mg/cm$^2$/year) | Empirical Equation 1 (mg/cm$^2$/year) | Empirical Equation 2 (mg/cm$^2$/year) |
|---|---|---|---|---|---|---|
| 20 | W | 55 | 0.2 | 8.19 | 110188 | 13.1 |
| | | 65 | | 9.17 | 113714 | |
| | S | 55 | 0.2 | 9.64 | 110188 | |
| | | 65 | | 9.23 | 113714 | |
| 40 | W | 55 | 0.1 | 6.37 | 77915 | 9.3 |
| | | | 0.2 | 6.35 | | |
| | | | 0.3 | 6.71 | | |
| | | 65 | 0.2 | 5.87 | 80408 | |
| | S | 55 | 0.1 | 6.14 | 77915 | |
| | | | 0.2 | 6.30 | | |
| | | | 0.3 | 7.16 | | |
| | | 65 | 0.2 | 5.95 | 80408 | |
| 70 | W | 55 | 0.2 | 13.70 | 58898 | 7.0 |
| | | 65 | | 18.94 | 60783 | |
| | S | 55 | | 5.47 | 58898 | |
| | | 65 | | - | 60783 | |

W: Tap Water S: Sea water

Table 5 Calculation Results of Specimens with Construction Joint Exposed to Submerged Zone

| Cover (mm) | Water Cement Ratio (%) | Experimental Results (mg/cm$^2$/year) | Empirical Equation 1 (mg/cm$^2$/year) | Empirical Equation 2 (mg/cm$^2$/year) |
|---|---|---|---|---|
| 20 | 50 | 4.0 | 4617 | 13.1 |
| 40 | | 3.8 | 3265 | 9.3 |
| 70 | | 3.6 | 2468 | 7.0 |

## 7. Conclusions

- Corrosion area ratio, mass loss ratio and corrosion amount increased as increase in initial crack width in specimens mixed with sea water with initial crack
- Without laitance removal, mass loss ratio for samples with joint covered with mortar and epoxy resin (B, C type) decrease by 0.1-3.6% than not covered sample A. With laitance removal, mass loss ratio of E, F and G type increased by 0.5-2.8% than D type, which was the opposite tendency.
- Steel corrosion of specimen with initial crack developed after 5 years' exposure. Steel corrosion of specimen with construction joint developed during 30 years after 10 years' exposure
- Calculation results became higher in empirical equation 1 due to chloride ion concentration in the exponent part. Empirical equation 2 may by good for the case of high chloride ion concentration

### References


1) H. SEKI, N. OTSUKI, Y. HORII: Corrosion of Reinforcing Bars due to Concrete Mixed with Sea Water and Residual Crack (Five Years' Test), TECHNICAL NOTE OF THE PORT HARBOUR RESEARCH INSTITUTE, No. 237, pp.3-25, 1976.6

2) T. U. Mohammed, N. Otsuki, H. Hamada : Corrosion of Steel Bars in Cracked Concrete under Marine Environment, Journal of Materials in Civil Engineering , No. 15, pp.460-469, 2003.10

3) S. NAGATAKI, N. OTSUKI, M. HISADA: Influence of Joints and Cracks on Macro-Cell Corrosion in Reinforced Concrete, Proceeding of the 4th International Conference on Structural Failure, Durability and Retrofitting, pp.327-334, 1993

4) F. UKISHIMA: Experimental investigation on Corrosion of Steel Bars in Concrete with Horizontal Construction Joint under marine environment, a doctoral thesis, Tokyo Institute of Technology, 2008

# STUDY ON CEMENT-FREE CONCRETE USING FLY ASH

Student Number: 15M18121　Name: Hikaru TANAKA　Supervisor: Hirofumi HINODE, Keisuke MATSUKAWA

# フライアッシュ使用セメントフリーコンクリートに関する研究

田中　光

本研究では，セメント使用量の削減と廃棄物の有効利用の観点から，セメントの代わりにフライアッシュと水酸化カルシウムを混合した粉体を使用し，練り混ぜ水として水道水の他に海水やアルカリ溶液を用いてコンクリートを作製することを検討した．結果として，練り混ぜ水にケイ酸ナトリウムと水酸化ナトリウム水溶液を用いることで，材齢 28 日において 2.7MPa の強度が得られ，外観上通常のコンクリートと遜色ない硬化体を作製することができた．

## 1　Introduction

### 1.1　Background

Concrete, which is usually made from cement, is one of the most common structural materials. It is used for buildings, dams, roads, and many other infrastructures. Nowadays, the cement usage in the world is increasing with the rapid development such as in China and India. It leads to an environmental problem because the production of cement is energy-intensive and emits a great deal of $CO_2$. On the other hand, the fly ash discharged from coal fired power plants is also increasing. The amount of discharged fly ash is already beyond the utilization capacity because coal fired power plants owe a part of the electricity supply which is originally assigned to nuclear power plant. Therefore, from the environmental viewpoint, the cement usage in concrete should be decreased and the recycling of fly ash should be further promoted.

### 1.2　Existing methods

There are two major methods which can decrease the cement usage and increase the fly ash utilization. One is fly ash concrete, and the other is geopolymer concrete. As shown in Fig. 1, fly ash concrete can reduce the cement usage by 5-30 wt% and geopolymer concrete can be made without using cement. Instead of the use of cement, geopolymer concrete needs alkaline solution as an activating solution.

### 1.3　Objectives

The general objective of this research is to make cement-free concrete by utilizing coal fly ash. In order to achieve this objective, the specific objectives are as follows:

1) To propose new mixtures which can be alternatives to cement concrete and check their feasibility in terms of strength and workability.

2) To conduct analysis study in the hardening mechanism in the proposed mixtures.

### 1.4　Flow of the study

The flow of the study is shown in Fig. 2. The investigation on the proposed mixtures conducted in two ways. One is to check the feasibility by making concretes and measure their strength. The other is to investigate the mechanism of hardening in the proposed mixtures by some test analyses.

## 2　Materials

### 2.1　Specifications

The fly ash used in this experiment is classified as “class F” by ASTM C618 which contains CaO less than 10 wt%. Chemicals are all regent grade. The chemical composition of the artificial seawater is in accordance with ASTM D 1141-98.

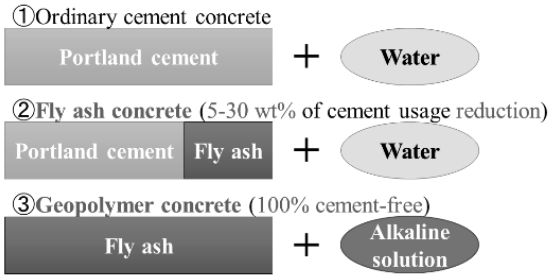


**Figure 1　Comparison of Existing Methods**

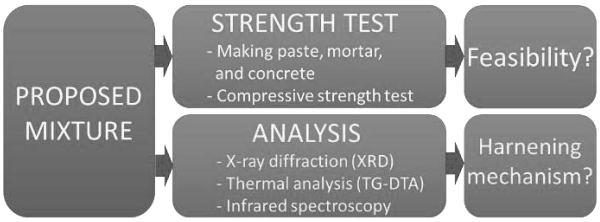


**Figure 2　Flow of Study**

**Table 1　Mix Proportions**

| Lot. | Binder Composition（wt%） | | | | Mixing Water | Sodium Silicate（g/L） | NaOH (mol/L) |
|---|---|---|---|---|---|---|---|
| | Cement（OPC） | Fly Ash（FA） | Slag（BFS） | $Ca(OH)_2$ | | | |
| OPC | 100 | 0 | 0 | 0 | Tap | 0 | 0 |
| FA70_SW | 30 | 70 | 0 | 0 | Sea | 0 | 0 |
| GP | 0 | 88 | 12 | 0 | Tap | 130 | 0.5 |
| CH | 0 | 70 | 0 | 30 | Tap | 0 | 0 |
| CH_SW | 0 | 70 | 0 | 30 | Sea | 0 | 0 |
| CH_NS | 0 | 70 | 0 | 30 | Tap | 130 | 0 |
| CH_NS_NH | 0 | 70 | 0 | 30 | Tap | 130 | 0.5 |

## 2.2 Mixtures

The mix proportions used in this study are listed in Table 1. OPC, FA70_SW, and GP means ordinary Portland cement, fly ash concrete mixed with seawater with the fly ash replacement ratio of 70 wt%, and geopolymer, respectively. The other mixtures are newly proposed in this study. The common binder components of the new mixtures are fly ash and $Ca(OH)_2$, of which mass ratio is 7:3. CH, CH_SW, CH_NS, and CH_NS_NH means the binder is mixed with tap water, seawater, sodium silicate (NS) solution, and sodium silicate and NaOH (NH) solution, respectively.

## 2.3 Preparation of specimens

Paste specimens were made of water and binder. The water-binder ratio (W/B) is 0.5. Mortar specimens were made of water, binder, and sand. The mass ratio between binder and sand is 1:2. The W/B is 0.5. Concrete specimens were made of water, binder, sand, and gravel. The ratio of sand to aggregates (sand and gravel) is 44 wt%. The W/B was 0.5 for OPC, FA70_SW and GP, and 0.6 for CH_SW and CH_NS_NH. All specimens were cured in air for 7 days. Afterwards, specimens were demolded and cured under tap water until the testing day.

# 3 Experimental Methods

## 3.1 Compressive strength

For the paste test, 40x40x40 mm cube specimens were prepared and testing age were 7, 28, and 91-day. For the mortar test, ϕ50x100 mm cylinder specimens were prepared and testing age were 7 and 28-day. For the concrete test, ϕ100x200 mm cylinder specimens were prepared and testing age were 7 and 28-day.

## 3.2 X-ray diffraction (XRD) analysis

Samples for analysis were taken from the paste cube specimen after 28-day strength test. Type of x-ray is Cu Kα and measured range is 2θ=5-60°.

## 3.3 Thermal analysis (TG-DTA)

Samples for thermogravimetry-differential thermal analysis were taken from the paste cube specimen after 7 and 28-day strength test. The reference material used was γ-alumina, and the sample was analyzed under air. Analyzed temperature was RT-900°C. Heating rate was 10°C/min.

Calcium silicate hydrate (C-S-H) is one of the major products of hydration of CaO-based cementitious materials. Especially in the reaction between fly ash (amorphous-$SiO_2$) and $Ca(OH)_2$ , that is called pozzolanic reaction, C-S-H is produced by the reaction described as formula (1).

$$a\text{-}SiO_2 + Ca(OH)_2 + H_2O \rightarrow C\text{-}S\text{-}H \quad (1)$$

Thus, the amount of C-S-H reflects the intensity of pozzolanic reaction for proposed mixtures (FA + $Ca(OH)_2$). In this study, the amount of C-S-H was estimated by the procedure shown in Fig. 3. The initial content of Ca is only $Ca(OH)_2$ (16.2 wt% as Ca). After the reaction, $Ca(OH)_2$ changes into three calcium compounds, $Ca(OH)_2$, $CaCO_3$, and C-S-H. The content of $Ca(OH)_2$ and $CaCO_3$ can be measured with TG-DTA, so the content of C-S-H can be calculated. In order to compare the amounts of the three different calcium compounds, the weights of all of the calcium compounds were converted into the weight ratios of Ca to the total weights. Therefore, the total Ca content of $Ca(OH)_2$, $CaCO_3$, and C-S-H is 16.2 wt% (i.e. initial Ca content).

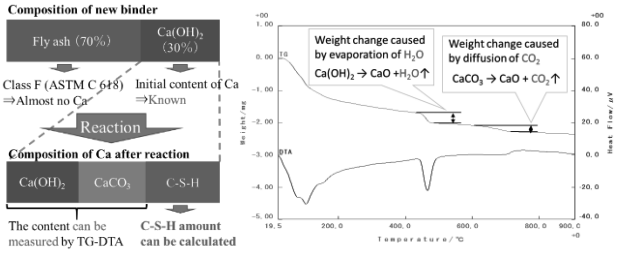


**Figure 3 Estimation of C-S-H by TG-DTA**

## 3.4 Infrared spectroscopy (FTIR)

Samples for Fourier-transform infrared spectroscopy were taken from the paste cube specimen after 28-day strength test. Measured range is 400-4000 $cm^{-1}$. Scan speed is 2 mm/sec. Cumulated number is 16 times.

# 4 Results and Discussion

## 4.1 Strength and feasibility

### 4.1.1 Compressive strength

The results of strength test are shown in Table 2. The tendency of the strength development of mortar and concrete were almost the same as paste. The 28-day strength and 91-day strength were almost the same for all samples. Thus, by taking the paste samples as representative, the strength development between the 7 and 28-day was compared in Fig. 4. "xO.O" in the figure means the strength ratio of 28-day to 7-day and that of OPC was x1.8. The acceleration of pozzolanic reaction by seawater was indicated in the previous study [1]. In this research, the acceleration was confirmed in the comparison of CH and CH_SW. Compared with OPC, FA70_SW, and GP, the strength ratios of 28-day to 7-day samples for the proposed mixtures were larger. As there is no cement hydration in the new mixtures and strength development in this period is known to be attributed to pozzolanic reaction for fly ash concrete, the main hardening reaction of proposed mixture is considered to be pozzolanic reaction.

**Table 2 Results of Compressive Strength Test**

| Lot. | Compressive Strength (MPa) | | | | | | |
|---|---|---|---|---|---|---|---|
| | PASTE | | | MORTAR | | CONCRETE | |
| | 7-day | 28-day | 91-day | 7-day | 28-day | 7-day | 28-day |
| OPC | 27.7 | 50.3 | 47.9 | 21.1 | 35.7 | 26.5 | 37.2 |
| FA70_SW | 5.8 | 10.0 | 9.6 | 2.8 | 6.2 | 3.1 | 6.1 |
| GP | 3.9 | 5.1 | 5.2 | 1.9 | 3.4 | 1.9 | 3.6 |
| CH | 0.2 | 0.7 | - | - | - | - | - |
| CH_SW | 0.7 | 2.1 | 2.1 | 0.3 | 1.0 | 0 | 1.1 |
| CH_NS | 1.6 | 4.8 | 4.8 | - | - | - | - |
| CH_NS_NH | 1.8 | 4.2 | 4.3 | 0.8 | 3.2 | 0.6 | 2.7 |

**Table 3 Slump Test**

| | OPC | FA70_SW | GP | CH_SW | CH_NS_NH |
|---|---|---|---|---|---|
| W/B | 0.5 | 0.5 | 0.5 | 0.6 | 0.6 |
| Slump (cm) | 13 | 6 | 14 | 9 | 8 |

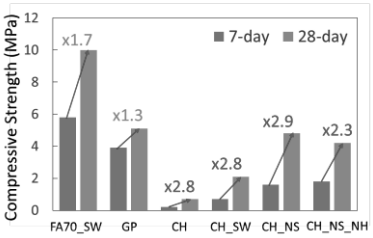


**Figure 4 28-day/7-day Compressive Strength**

### 4.1.2 Feasibility

The results of slump test (JIS A 1101) are shown in Table 3. For the proposed mixtures, sufficient slumps were obtained by increasing the water content up to 0.6 in W/B ratio. Fig. 5 shows the appearance of concrete. The appearance of CH_NS_NH was as good as OPC concrete. The compressive strength of the concrete as shown in Table 2 are of strength level sufficient for the ground improvement [2]. In terms of workability, strength, and appearance, the proposed mixtures are considered feasible.

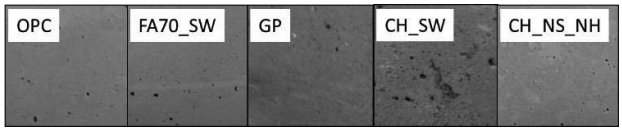


**Figure 5 Appearance of Concrete (28-day)**

## 4.2 X-ray diffraction (XRD)

The results of XRD analysis are shown in Fig. 6. The word "powder" means binder which is not mixed with mixing solution. The raw fly ash consists of quartz, mullite, and amorphous-$SiO_2$ ("FA powder" in (a)). Regarding GP (b), there is no significant change by mixing with solutions. For the proposed mixtures (c), the peak around 2θ=11-12° appeared after the reaction, which is considered to be calcium aluminate hydrate [3]. Regarding the proposed mixtures, the broad peak around 2θ=20-45° shifted upward by the mixing. The reason of this shift is thought that the amount of amorphous increased by the generation of C-S-H substances.

## 4.3 Thermal analysis (TG-DTA)

Compositions of calcium compounds in the samples and their comparison are shown in Fig. 8. The tendency of C-S-H content at age 7-day is similar to that of the strength on the same age. Thus the reason of strength development is considered to be C-S-H generation. Comparing the C-S-H content of CH and CH_SW with that of CH_NS and CH_NS_NH, the latter is larger. The clear difference between the former and the latter is the alkaline solution. Using alkaline solution, it is considered that fly ash dissolution is accelerated and the pozzolanic reaction was promoted. Graph (c) shows the comparison of C-S-H content between 7-day and 28-day. Addition of alkali (NS or NH) leads to smaller C-S-H content ratio of 28-day to 7-day. That means addition of alkali accelerates the reaction in early age.

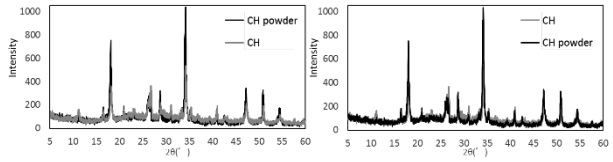


**Figure 7 Pozzolanic Reaction (XRD)**

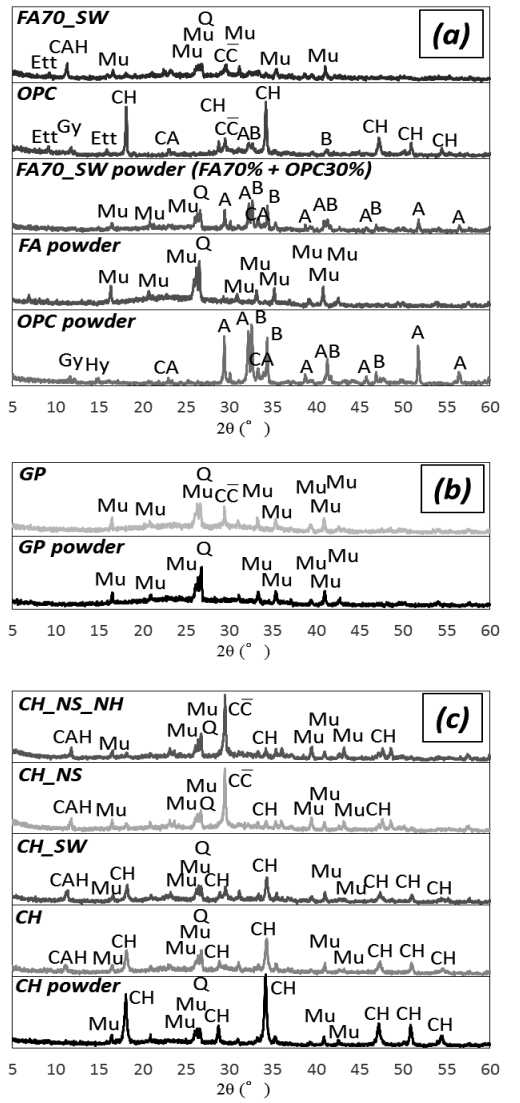


A: alite($3CaO \cdot SiO_2$)
B: belite($2CaO \cdot SiO_2$)
CA: aluminate($3CaO \cdot Al_2O_3$)
CF: ferrite($4CaO \cdot Al_2O_3 \cdot Fe_2O_3$)
CAH: calcium aluminate hydrate($4CaO \cdot Al_2O_3 \cdot 13H_2O$)
Ett: ettringite($3CaO \cdot Al_2O_3 \cdot 3CaSO_4 \cdot 32H_2O$)
Gy: gypsum($CaSO_4 \cdot 2H_2O$)
Hy: bassanite($CaSO_4 \cdot 0.5H_2O$)

Q: quartz
Mu: mullite
CH: $Ca(OH)_2$
$\overline{CC}$: $CaCO_3$

**Figure 6 Results of XRD analysis**

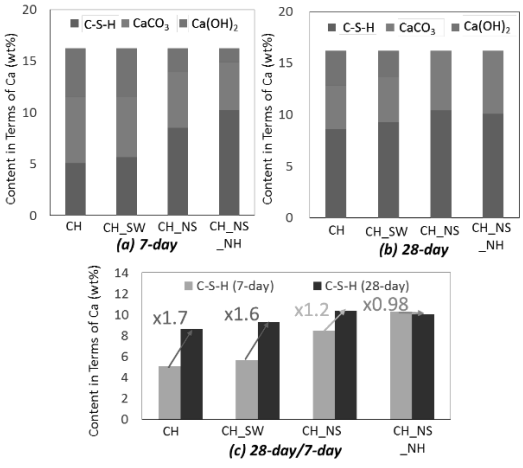


**Figure 8 Results of TG-DTA**

## 4.4 Infrared spectroscopy (FTIR)

The results of FTIR are shown in Fig. 9. The peaks which correspond to $CO_2$, $Ca(OH)_2$, $CaCO_3$, sodium silicate (NS), NaOH (NH), and O-H stretching are indicated in the graphs. The peak of 1080 $cm^{-1}$ which corresponds to Si-O symmetric vibration is the peak of raw fly ash ("FA powder" in (a)). The other peaks, 961 $cm^{-1}$, 1022 $cm^{-1}$, and 1058 $cm^{-1}$ are discussed as follows.

(1) Peak of 1022 $cm^{-1}$

The peak of 1022 $cm^{-1}$ appears in GP result (b). As shown in graph (b), the peak of 1080 $cm^{-1}$, which corresponds to the Si-O symmetric vibration peak of the raw fly ash, shifted to 1022 $cm^{-1}$ after the reaction. One of the characteristic peaks related to geopolymer is the peak of 1008 $cm^{-1}$, which corresponds to Si-O and Al-O asymmetric vibration [4]. Geopolymerization is the reaction in which Al dissolved from fly ash are inserted into Si-O-Si-O- chain and polymerize. Therefore, the peak shift from 1080 $cm^{-1}$ to 1022 $cm^{-1}$ is considered to be the increase of Al-O bond caused by geopolymerization. The peak of 1022 $cm^{-1}$ is the result of 1080 $cm^{-1}$ peak disappearance and 1008 $cm^{-1}$ peak appearance.

(2) Peaks of 961 $cm^{-1}$ and 1058 $cm^{-1}$

First, the peak of 961 $cm^{-1}$ can be observed in the all proposed mixtures, OPC, and FA70_SW after reaction. Possible chemical compounds contained in those samples are $Ca(OH)_2$ or C-S-H. $Ca(OH)_2$ does not have a peak of 961 $cm^{-1}$. Thus, the peak is considered to be the peak of C-S-H. This fact is confirmed in another research [5]. The peaks of 1058 $cm^{-1}$ were observed in CH and CH_SW clearly, and CH_NS slightly. It seems to have a relation to the alkalinity. As alkalinity becomes higher, the peak of 1080 $cm^{-1}$ and 1058 $cm^{-1}$ disappears. Therefore, it is thought that there is a tendency that the peak of the raw fly ash disappears and shifts to the peaks of smaller wavenumber as the hardening process.

# 5 Conclusions

In this study, in order to make cement-free concrete with utilizing coal fly ash, proposed mixtures are proposed and investigated from two aspects: one is from feasibility viewpoint, the other is by analysis of chemical reaction.

1) Feasibility of proposed mixtures

By increasing the water content up to 0.6 in W/B, proposed mixture concrete can be casted with sufficient workability as OPC concrete. The appearance of the CH_NS_NH concrete was as good as OPC concrete. Its compressive strength was 2.7 MPa on 28-day, which is sufficient for actual uses such as ground improvement.

2) Analysis of hardening mechanism

Both pozzolanic reaction and geopolymerization occurs in proposed mixtures. Especially, by using FTIR, those two reactions are separated to some extent. Geopolymerization is observed as peak shift from 1080 $cm^{-1}$ (Si-O symmetric vibration) to smaller wavenumber. Pozzolanic reaction is observed as a peak shift to 961 $cm^{-1}$ (C-S-H).

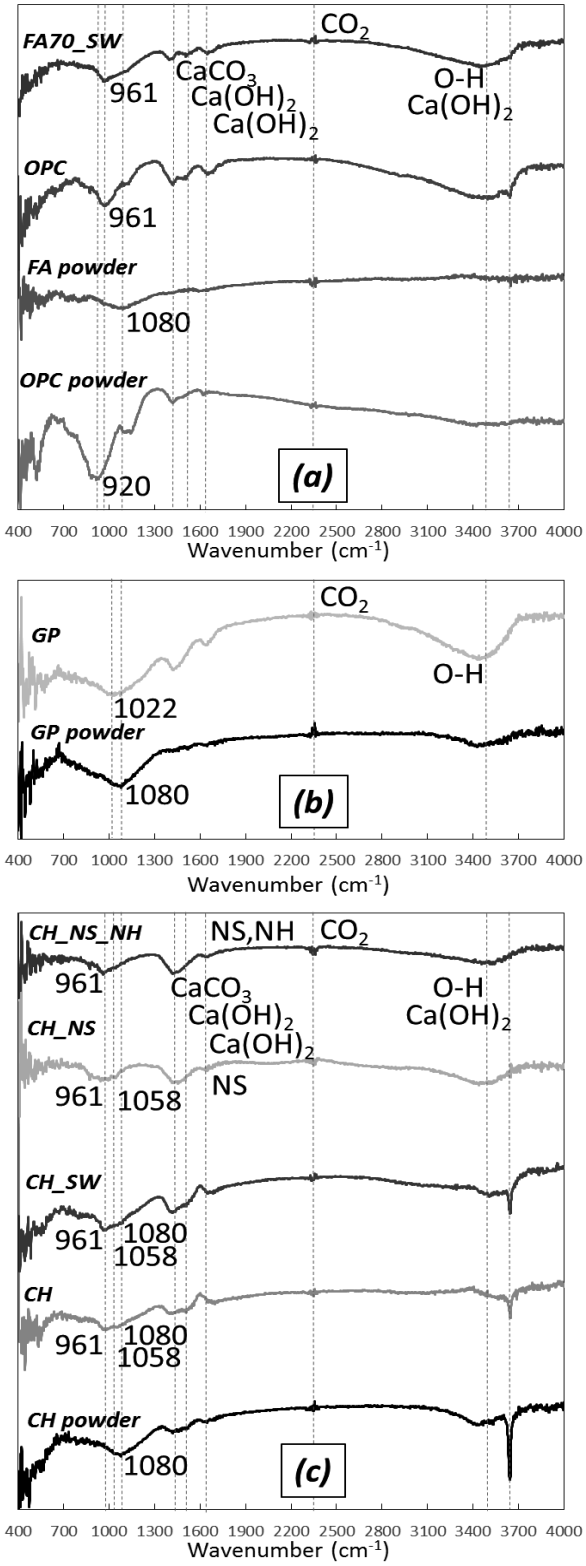


**Figure 9 Results of FTIR Analysis**

## References


[1] C. Yi (2016), "Lifetime Prediction of Reinforced Seawater Concrete Mixed with Fly Ash Which Were Produced in Japan or Philippines Against Chloride Attack", Master thesis of Tokyo Institute of Technology.

[2] K. Matsukawa, "Treatment of Solid Waste Contaminated with Heavy Metals", 2013 Proc. Seminar Workshop "Utilization of Waste Material", 2013.

[3] H. E. Schwiete and U. Ludwig (1968), "Crystal Structures and Properties of Cement Hydration Products", Fifth International Symposium on the Chemistry of Cement.

[4] J. Davidvitz, "Geopolymer: Chemistry & Applications", 4th edition, 2015.

[5] G. Igarashi and I. Maruyama (2013) , "Modeling of Water Adsorption of Calcium Silicate Hydrate", AIJ Tokai Chapter Architectual Research Meeting.

# A study on residential relocation focusing on life stage changes for compact cities

Student Number: 14M18046 Name: Kosuke Kiriyama Supervisor: Shinya Hanaoka

# 集約型都市構造実現のためのライフステージ変化を考慮した転居ターゲット層の分析

桐山　弘有助

集約型都市構造実現のためには、世帯の居住誘導が必要となる。本研究では、世帯をライフステージに分類した上で、転居傾向や交通行動、転居意向から集約型都市構造に向けたターゲット層を把握する。分析の結果、若年の単身世帯は短期的な視点において、若年の夫婦のみ世帯は長期的な視点においてターゲットになりえ、一方、退職や子の独立後の世帯を居住誘導するためには、意識の変容が求められるべきと分かった。

## 1. Background

Compact city and transit-oriented development have been introduced in many cities in the world. The Japanese government has also announced to promote compact and consolidated urban layouts with multipolar networks as a policy. Location optimization plans was established in 2014 to proceed compact city inducing the residential and urban function to the city center or the area along with railway as well. Each local government selects “areas that attract urban functions” and resident-attracting district are. Resident-attracting district is the area where residents can access public transportation easily. And people are induced to change residence to those area to stabilize the population density. Then, it is necessary to clarify the appropriate target to live in resident-attracting districts and use the service of areas that attract urban functions.

To achieve such urban form, residential relocation from suburban area to surrounding area of public transportation corridors are necessary. Decisions to change residence affect households, and are affected by life stage changes such as education, marriage, having children and retirement. It is important to induce residential relocation with considering transition of life stage. Simultaneously, trip character change such as shift from automobile to public transport is required to realize low carbon society and sustainability. Residential relocation can also act as a crucial point for a household to decide if it will own and use a family car or not.

The objectives of this study are 1) to classify household data into type of life stage and analyzing the preference to select living area of each life stage type, 2) to analyze the residential relocation pattern and the trip character after residential relocation in each life stage, and 3) to clarify the stratified groups which may be most suited to compact urban layouts and give recommendation for policy of resident-inducing.

The characteristics of households such as the number of persons per household and car ownership are considered as one of the factors of individual-unit analysis by using person trip data in many previous studies [1]. There are some thesis which analyze the relationship between residential relocation and the characteristics of households as well [2]. However, they do not treat with the relationship between residential relocation, trip character and life stage.

## 2. Data

The data of trip character of each family member and historical data of residential relocation is needed to clarify the stratified groups which may be most suited to compact urban layouts. In Japan, the National Person Trip Surveys (NPTS) has been conducted in major cities and metropolitan areas 6 times. The survey used in this research is fifth one. This Survey can be divided into “individual / household sheet” and “awareness/ experience questionnaire survey sheets”. The outline of this survey is shown in Table 1.

Table 1. Outline of the 5th Nationwide Person Trip Survey.

| Indexes | Contents |
|---|---|
| Target people | The responses from approximately 500 households per city (all member over age of 5 ) |
| Target area | Urbanization Promotion Area |
| Survey date | A weekday and a holiday in November or October, 2010 |
| Survey method | Receiving sheet by mail |
| Type of sheets | Individual survey sheets (trip character on weekday and holiday), household survey sheets and awareness/ experience questionnaire survey sheets |

## 3. Methodology

The stratified groups which may be most suited to compact urban layouts are clarified by using following two approach.

1. Clarifying **the normal targets** for compact city from trip character data and historical data of residence relocation. :

The normal targets mean households which tend to change residence from outside of resident-attracting districts to resident-attracting districts and change trip character such as shift from automobile to public transport.

2. Clarifying **the potential targets** for compact city from their determining factor to choose the location. :

The potential targets mean those who changed residence to outside of resident-attracting districts, although they had residential relocation awareness to change residence to resident-attracting districts when they change residence.

Steps of classifying the target is following;

**Step (1): Classifying household into each segmentation**

*(1-1): Classifying the household data into segmentation of life stage when thy change residence.*

*(1-2): Classifying the districts before and after residential relocation into the residential zone types.*

*(1-3):Classifying the residential zone types into segmentation of Resident-attracting district, referring the location optimization plans written by each local government.*

**Step (2): Clarifying the normal targets**

*(2-1): Analyzing the pattern of residential relocation*

Using the data of residence before and after residential relocation of each household, "the type of residence after residential relocation" and "residential relocation pattern" is analyzed in each life stage.

*(2-2): Analyzing the trip character*

"The frequency to use public transportation a year", "The variability of trip character" and "The situation of using cars" of those who change their residence to resident-attracting district are analyzed in each life stage.

*(2-3): Discussion of the normal target*

The normal target are and residential relocation inducing policy are discussed by using the result of (2-1) and (2-2).

**Step (3): Clarifying the potential targets**

*(3-1): Striking an average of the residential change awareness.*

Striking the average of the consideration degrees as the attractive area when the respondents selected the present house in two residential relocation pattern, "to resident attracting district" and "not to resident-attracting district"

*(3-2): Discriminant analysis*

Calculating the function to discriminate "the households which change residence to resident-attracting districts" and "the households which change residence to outside of resident-attracting districts", using their average score of residential change awareness.

*(3-3): Clarifying the potential target by the score of discriminant function*

Calculating the score of the discriminant function of "the households which change residence to outside of resident-attracting districts", applying the average score of the residential change awareness in each life stage.

## 4. Classifying data into each segmentation

### *4-1.Classifying the household into segmentation of life stage*

It is necessary to estimate the life stage of households when they change residence, because there is no data regarding it in NPTS. In previous studies, "relationship between household members" and "the age of household members" are used to estimate the life stage. In addition to them, "the period of living present residence" is used to estimate the life stage when household change residence in this research. Using these 3 factors, segmentations of life stage which are the combination of "present family composition" and "life event supposed to experience in each family composition when households change residence" are set.

(1) Estimating the present family composition

Each household are classified into segmentation of present family composition, using the data of "relationship between household members" and "the age of household members". Table 2 show these criteria and result.

Table 2. Family composition and its criteria

| Family composition | | Criteria |
|---|---|---|
| One-person households | | The number of household is 1. |
| Married couple only | After child's independence | 1. The number of household is 2.<br>2. The relationship between household members are husband and wife.<br>3. Present age of householder is more than 50 years old. |
| | Before giving birth | 1. The number of household is 2.<br>2. The relationship between household members are husband and wife.<br>3. Present age of householder is less than 50 years old. |
| Married couple and child(ren) | | 1. The number of household is more than 3.<br>2. The relationship between household members are husband, wife and child. |

(2) Estimating the life event which household experience in each family composition.

Firstly, the life events which household experience in each family composition are set. Secondary, the criteria to judge which life event households belong to when they change residence. This life event of each family composition is the segmentation of life stage in this research. Finally, the households are classified into segmentation of life stage when they changed residence based on criteria of life event. Table2 shows the each segmentation of life stage, its criteria and its household number of sample.

Table 3. Life stage and its criteria

| Life stage | Present family composition | | Life event when changing address | Age of householder when changing address | Number of sample |
|---|---|---|---|---|---|
| LS1 | One-person households | | Enrollment / Empolyment | less than 22 | 622 |
| LS2 | | | Others | from 22 to 60 | 7725 |
| LS3 | | | Retirement / Independence | more than 60 | 499 |
| LS4 | Married couple only | After child's dependence | Marriage / Childbirth | less than 30 | 313 |
| LS5 | | | Retirement / Independence | from 30 to 60 | 3125 |
| LS6 | | | Education | more than 60 | 391 |
| LS7 | | Before giving birth | Marriage | less than 30 | 741 |

| Life stage | Present family composition | Life event when changing address | Age of eldest child when changing address | Number of sample |
|---|---|---|---|---|
| LS8 | Married couple with child(ren) | Marriage | less than -1 | 565 |
| LS9 | | Childbirth | from -1 to 4 | 934 |
| LS10 | | Education for infants | from 4 to 12 | 1289 |
| LS11 | | Education for students | from 12 to 22 | 425 |
| LS12 | | Retirement / Independence | more than 22 | 230 |

### *4-2.Classifying districts into residential zone types.*

In order to define some districts as Resident-attracting district, it is necessary to classify the districts into residential zone types firstly, because there is no data regarding characteristics of residential area in NPTS data. Residential zone types is the classification which reflects the characteristics of residential area such as land use, distance from station, and distance from city center. This segmentation is classified in Nakamichi(2008), and the updated one in Lu(2016) is used in this research [3][4].

### *4-3.Classifying the residential zone types into segmentation of resident-attracting district*

125 residential zone types are classified into segmentation for resident-attracting districts. Based on 3 issues: "the policy issue response-based urban planning procedural guidelines drawn by Ministry of Land, Infrastructure, Transport and Tourism", "laws which is relevant to location optimization plans" and "location optimization plans drawn by each local government". This research refers 4 local governments published their official location optimization plans. And it is identified that 2 characteristics, "land use regulation" and "distance from station", have large impact to decide where resident-attracting districts are.

Using these factors, the following 3 categories are defined.

District (i): The districts which cannot be resident-attracting districts.

District (ii): The districts which may be resident-attracting districts.

Districts (iii): The districts which must be resident-attracting districts.

Table 4 shows the criteria of each segmentations for resident-attracting districts. (RZT: residential zone types)

Table 4. Criteria of segmentation of resident attracting district

| Land use regulation of RZT | Distance from station | Category | # of zones |
|---|---|---|---|
| Outside of urban planning area | - | District (i) | 7 |
| Exclusive industrial zone | | | 4 |
| Urbanization control area (50% ~) | | | 14 |
| Semi-industrial zone | 1km or more | | 3 |
| | Less than 1km | District (iii) | 1 |
| Urbanization control area (~ 50%) | 1km or more | District (i) | 6 |
| | Less than 1km | District (iii) | 3 |
| Mixed zone (mainly industrial zone) | 1km or more | District (i) | 2 |
| | Less than 1km | District (iii) | 2 |
| Other land use regulation | 1.5km or more | District (i) | 4 |
| | 1km or more / less than 1.5km | District (iii) | 30 |
| | Less than 1km | District (ii) | 47 |

## 5. Clarifying the normal target

In order to clarify the normal targets, residential relocation pattern and trip character before and after residential relocation is analyzed. Residential relocation pattern and trip character are analyzed in each life stage, "1.age of householder", "2.type of residence", "3.situation of car used", "4.ratio of households changing address to each district", "5.The number of times to use public transportation a year and the variability of trip character of people who change residence to resident-attracting districts "are calculated. (Table 5)

Discussion on the normal target is following;

The type of residence and whether to have car are important factor to induce residential relocation. One-person households tend to live in rental apartment and not to have car. After getting married, people tend to start owning their houses and car gradually. And One-person households also have characteristics to change residence to resident-attracting districts and use public transportation. The same may be said of the households after retirement or child's independence. And it can be said that the households after retirement or child's birth can adapt the characteristics of compact city because they tend to increase the frequency to use public transportation and walk after changing residence to District (ii)

Table 5. Result of residential relocation pattern and trip character

| Life stage | 1.Average Age of house holder | 2. Type of Residence | | 3. Car they can use | | 4.Resident attracting districts | | 5. Using frequency of transportaion in Disrict (ii) | | | |
|---|---|---|---|---|---|---|---|---|---|---|---|
| | | | | | | | | Times/year | | Variability | |
| LS1 | 32.4 (years old) | 2-a | 19% | 3-a | 36% | 4-a | 27% | 5-a | 298 | 5-a | 2.18 |
| | | 2-b | 4% | 3-b | 2% | 4-b | 47% | 5-b | 461 | 5-b | 0.93 |
| | | 2-c | 74% | 3-c | 61% | 4-c | 26% | 5-c | 249 | 5-c | 2.27 |
| LS2 | 54.0 (years old) | 2-a | 39% | 3-a | 54% | 4-a | 30% | 5-a | 357 | 5-a | 3.02 |
| | | 2-b | 11% | 3-b | 2% | 4-b | 40% | 5-b | 322 | 5-b | 2.07 |
| | | 2-c | 46% | 3-c | 43% | 4-c | 30% | 5-c | 187 | 5-c | 2.59 |
| LS3 | 74.6 (years old) | 2-a | 28% | 3-a | 25% | 4-a | 31% | 5-a | 297 | 5-a | 3.30 |
| | | 2-b | 15% | 3-b | 1% | 4-b | 36% | 5-b | 421 | 5-b | 0.73 |
| | | 2-c | 51% | 3-c | 70% | 4-c | 32% | 5-c | 226 | 5-c | 1.59 |
| LS4 | 59.7 (years old) | 2-a | 87% | 3-a | 78% | 4-a | 48% | 5-a | 513 | 5-a | 2.24 |
| | | 2-b | 5% | 3-b | 16% | 4-b | 26% | 5-b | 349 | 5-b | 1.03 |
| | | 2-c | 8% | 3-c | 5% | 4-c | 26% | 5-c | 166 | 5-c | 1.47 |
| LS5 | 66.3 (years old) | 2-a | 78% | 3-a | 66% | 4-a | 38% | 5-a | 451 | 5-a | 2.29 |
| | | 2-b | 12% | 3-b | 19% | 4-b | 28% | 5-b | 325 | 5-b | 2.02 |
| | | 2-c | 8% | 3-c | 14% | 4-c | 33% | 5-c | 162 | 5-c | 2.79 |
| LS6 | 72.6 (years old) | 2-a | 52% | 3-a | 52% | 4-a | 30% | 5-a | 373 | 5-a | 1.14 |
| | | 2-b | 25% | 3-b | 16% | 4-b | 36% | 5-b | 345 | 5-b | 2.63 |
| | | 2-c | 19% | 3-c | 29% | 4-c | 34% | 5-c | 130 | 5-c | 0.87 |
| LS7 | 48.2 (years old) | 2-a | 52% | 3-a | 64% | 4-a | 38% | 5-a | 444 | 5-a | 3.67 |
| | | 2-b | 7% | 3-b | 23% | 4-b | 34% | 5-b | 296 | 5-b | 4.11 |
| | | 2-c | 38% | 3-c | 13% | 4-c | 28% | 5-c | 135 | 5-c | 9.17 |
| LS8 | 47.6 (years old) | 2-a | 62% | 3-a | 69% | 4-a | 41% | 5-a | 583 | 5-a | 1.59 |
| | | 2-b | 16% | 3-b | 24% | 4-b | 33% | 5-b | 198 | 5-b | 4.51 |
| | | 2-c | 17% | 3-c | 7% | 4-c | 26% | 5-c | 210 | 5-c | 1.67 |
| LS9 | 45.0 (years old) | 2-a | 66% | 3-a | 64% | 4-a | 34% | 5-a | 470 | 5-a | 1.36 |
| | | 2-b | 15% | 3-b | 32% | 4-b | 36% | 5-b | 187 | 5-b | 2.05 |
| | | 2-c | 14% | 3-c | 4% | 4-c | 30% | 5-c | 210 | 5-c | 3.78 |
| LS10 | 46.3 (years old) | 2-a | 68% | 3-a | 66% | 4-a | 36% | 5-a | 463 | 5-a | 1.41 |
| | | 2-b | 13% | 3-b | 29% | 4-b | 30% | 5-b | 163 | 5-b | 2.76 |
| | | 2-c | 15% | 3-c | 4% | 4-c | 34% | 5-c | 203 | 5-c | 4.52 |
| LS11 | 50.4 (years old) | 2-a | 62% | 3-a | 62% | 4-a | 42% | 5-a | 407 | 5-a | 1.31 |
| | | 2-b | 18% | 3-b | 29% | 4-b | 33% | 5-b | 198 | 5-b | 1.43 |
| | | 2-c | 13% | 3-c | 8% | 4-c | 26% | 5-c | 240 | 5-c | 1.65 |
| LS12 | 68.5 (years old) | 2-a | 72% | 3-a | 56% | 4-a | 30% | 5-a | 387 | 5-a | 1.45 |
| | | 2-b | 16% | 3-b | 21% | 4-b | 41% | 5-b | 338 | 5-b | 10.4 |
| | | 2-c | 8% | 3-c | 22% | 4-c | 30% | 5-c | 184 | 5-c | 1.34 |

2-a: Owned house, 2-b: Rental house,
2-c: Rental apartment
3-a: Owned car, 3-b: Shared car, 3-c: No
4-a: District (i), 4-b: District (ii), 4-c: District (iii)
5-a: car, 5-b: on foot, 5-c: train/bus

## 6. Clarifying the potential target

### *6-1. Striking an average of the residential relocation awareness.*

Residential relocation awareness is analyzed by using the results of awareness/experience questionnaire survey sheets in the fifth NPTS. The questionnaire No. 9-(5) is the consideration degrees of eight perspectives as the attractive area when the respondents selected the present house. The perspectives are (i) City center or sub-center or the area which is close to them, (ii) The shopping district or the area which is close to it, (iii) The area where it is easy to go to shopping center in suburb, (iv) The area where there is much green, (v) The area where it is easy to get parking lots, (vi) The area where it is useful to use public transportation, (vii) The area where it is enable to use only bicycle or take a foot in daily life and (viii) The area where it is useful to drive. The average values of each consideration degrees are calculated for each life stage.

### *6-2. Discriminant analysis*

In order to clarify the potential targets, discriminant analysis is performed, using these results of 2 residential relocation pattern. Firstly, the discriminant function are calculated, which discriminate the households which change residence to District (i) and households which change residence to District (iii). Secondary, the average score of consideration degrees of those who change residence to District (i) are applied into this discriminant function in each life stage. Finally, the potential targets are clarified by the score of discriminant function in each life stage.

(1) Calculating the discriminant function

The discriminant function (eq.1) are calculated. In this function, the score of discriminant function are calculated, which is the sum of score which is the consideration degrees of eight perspectives are multiplied by the coefficients of discriminant function of each perspective. If it is positive number, the household is estimated as one which change residence to District (i), if it is negative number, the household is estimated as one which change residence to District (iii).

$$Z = w_1x_1 + w_2x_2 + w_3x_3 + \cdots + w_8x_8 \qquad \text{(eq.1)}$$

Z : The score of the discriminant function X : the average score of each perspectives
W : the coefficients of discriminant function

(2) Applying the score into discriminant function

Figure 1 shows the average score of consideration degrees of those who change residence to District (i) are applied into this discriminant function in each life stage.(Accuracy of discriminating is 61.8%.)

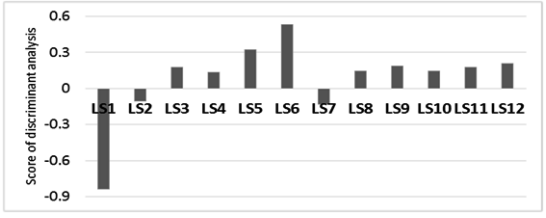


Figure 1. The score of discriminant function.

Overall, the score of discriminant function tend to be positive number. This result means that almost households could change residence as desired. On the other hand, the scores are negative number at LS1, LS2 and LS7. Especially it is really low at LS1. It can be said that they are the potential targets.

## 7. Conclusion

The discussion on targets for compact city and resident inducing policy through 3 steps is following;

One-person household, especially LS1 (life event: enrollment/employment) tend to change residence to resident-attracting districts and tend to use public transportation in Resident-attracting districts. In addition, LS1 which change residence to outside of resident-attracting districts had residential relocation awareness to change residence to resident-attracting districts. Therefore, in order to let LS1 change residence to resident-attracting districts, it is necessary to improve the environment such as money to change residence and the apartment for LS1. However, the household which people experience early, tend to staying in rental apartment and tend to change residence in short term. It can be said that they are target from the view point of short term.

On the other hand, LS7 tend to change residence to outside of resident-attracting districts. But, they also had residential relocation awareness to change residence to resident-attracting districts actually. Therefore, it can be said that they are potential targets. LS7 also tend to own cars after residential relocation, and tend to increase frequency to use car. However, they tend to adjust to the character of residential districts, such as using the public transportation often in resident-attracting districts. And the LS7 tend to change residence to districts whose character is the same as districts before residential relocation. Therefore, it is necessary to improve the environment for the households of LS7, in order to sustain compact city from the view point of long term. Especially residential relocation inducing policy such as providing a housing loan is appropriate to let them live for long time, because people tend to stay in the owned house from this life stage.

The households which change residence with opportunity of retirement or child's independence, such as LS6 and LS12, tend to change residence to resident-attracting districts. However, they do not tend to use public transportation and have residential relocation awareness to change residence to resident-attracting districts. Therefore it is necessary to change their mind of residential relocation, in order to let them change residence to resident-attracting districts.

## References


[1] Taniguchi, M., Murakawa, T., Morita, T., 1999. Designation of common segmentation for trip maker and their influence on urban transport. Infrastructure Planning Review 16, 601-607. (in Japanese)

[2] Nakamichi, K., Taniguchi, M., Matsunaka, R., 2008. The possibility for reduction of car dependence from the perspective of relocation for compact city - A study on change of trip character before and after relocation with a focus on metropolitan area -Journal of the City Planning Institute of Japan 43-3, 889-894. (in Japanese).

[3] Kumiko NAKAMICHI, Mamoru TANIGUCHI and Ryoji MATSUNAKA (2006) Development and Application of "a Pictorial Encyclopedia of Japanese Residential Zones" for sustainable urban planning, 9th Pacific Regional Science Conference Organization (PRSCO) Summer Institute, Kuala Lumpur, Malaysia.

[4]中道久美子・呂田子・花岡伸也: 大都市圏及び地方圏都市における住宅地タイプと交通行動特性の変化, 第 53 回土木計画学研究発表会, 土木計画学研究・講演集, Vol.53, CD-ROM, 2016.

# Clarification of Supply Chain in Tokyo Metropolitan Area

Student Number: 15M18196 Name: Yutaro WATANABE
Supervisor: Shinya HANAOKA, Kumiko NAKAMICHI, Tomoya KAWASAKI

# 東京都市圏におけるサプライチェーンの解明

渡邉　雄太郎

本研究では、第 5 回東京都市圏物資流動調査のデータを用いて、調査対象施設を含む物資の搬出搬入に関する OD をサプライチェーンの「上流」「中流」「下流」として捉え、品目ごとにサプライチェーンの観点から東京都市圏の物流を明らかにする。分析の結果、品目ごとにサプライチェーン上の施設の立地数や立地場所に関する物流の傾向が異なることがわかった。また、サプライチェーンの観点から物流を分析することにデータの限界があることがわかったため、次に物資流動調査を行う上での改善点を提案した。

## 1. Introduction

Tokyo Metropolitan Area (TMA) is the center of Japan's industry and economy, and it is a large consuming area with many populations [1]. In such a region, it is important to grasp the flow of goods closely related to industry/economy and people's livelihood. In addition, the main stakeholder in the logistics business is a private company, and they propound the importance of supply chain management from the viewpoint of cost reduction due to intensified competition among companies and regions with recent diversification of economic activities. There are several researches on location choice problem[2] and location of each logistics facility in TMA, while there is no research from the viewpoint of the supply chain (SC) by linking the OD (origin and destination) among facilities to capture the flow of goods as a SC. Also, since the upstream part of the SC is generally the raw material procurement and production stages, excavation areas and factories correspond. Whilst in the middle stage there are warehouses and logistics facilities in wholesale and transportation. In the downstream stage, restaurants and retailers correspond [3]. It is important to identify the "upstream", "middle" and "downstream" facilities and to clarify the SC for each item.

The objectives of this research are (1) to understand a clarified distribution in TMA by quantitatively analyzing the characteristics of the logistics of each item, from the viewpoint of "upstream", "middle" and "downstream" of the SC, (2) to visualize the facility of "upstream", "midstream", "downstream" per each item in the map within TMA, in order to understand the characteristics of the facility location for each item, (3) to show the limitation of data on Tokyo Metropolitan Area Urban Freight Survey (TMAUFS) and make proposals for future survey in the case of making SC.

## 2. Methodology

### 2.1 Data

In this research, survey result of the 5th TMAUFS conducted in 2014 is used. TMA covered in this study is Tokyo Prefecture, Saitama Prefecture, Kanagawa Prefecture, Chiba Prefecture, central and southern part of Ibaraki Prefecture, southern part of Tochigi Prefecture and southern part of Gunma Prefecture, which is the survey scope of TMAUFS. In this research, we use two questionnaires, "Establishment Sheet" and "Inflow/Outflow Sheet" obtained from the result of the "business establishment function survey" of TMAUFS. "Establishment Sheet" recognize of the facilities related to logistics in TMA on the basis of "business office", and information on each "Surveyed Facility", such as items to be handled, industry type, facility type and location. In "Inflow/Outflow Sheet", information on carry-in / carry-out of "Surveyed Facility" to which survey form of "Office Function Survey" was distributed is obtained. In other words, it is OD data of "Destination" and "Origin" of "Surveyed Facility" mainly used in this research. Figure 1 summarizes the information obtained from "Establishment sheet" and "Inflow/Outflow sheet".

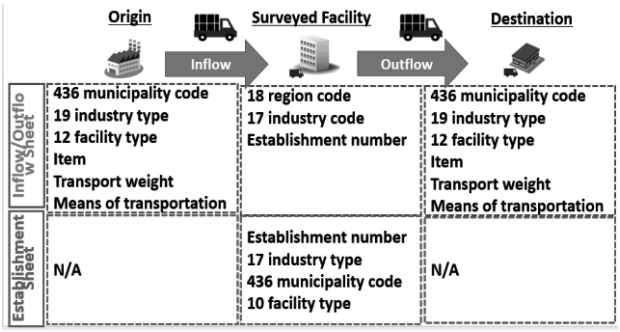


Figure 1: Contents of "Establishment Sheet" and "Inflow/Outflow Sheet"

The number of establishments surveyed in "Facility function survey" is approximately 140,000, and effective responses were obtained from approximately 44,000. (Effective answer rate is 32%) The number of OD pairs in "Inflow/Outflow Sheet" was 227,633. In this research, we excluded data that each establishment answered "unknown" or "no answer" for "municipality code", "industry type", "facility type" and "item". In addition, deleted the case where the transport company lends private cars for delivery, because there is a possibility of duplication of "Inflow/Outflow Sheet" in each between transport company and shipper, we decided not to include in this research. There are 73,471 total exclusion OD pairs, and the number of ODs used in this study is 154,162.

### 2.2 Clarification of goods flow in TMA in term of SC

#### 2.2.1 Outline of Methodology

As a method of clarifying the SC, (i) downstream facility analysis of the SC, (ii) upstream facility analysis of the SC, (iii) middle class facility analysis by aggregating the "type of industry" and "facility type" of each item and (iv) The logistics analysis with out of TMA. Figure 2 shows an image of the application point of each method on the SC. With regard to

method (iv), since the logistics are completed within only TMA by applying the method of (i) - (iii), from the method (iv), it is possible to grasp the tendency to how much items are exchanged in/out bound shipment from TMA.

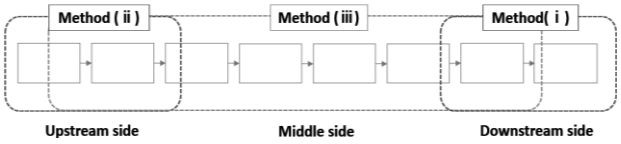


Figure 2: Range in application of each method in SC structure

### 2.2.2 Facility Analysis on Downstream side of SC

First, "Last destination" which is the most downstream part of the SC is specified. The definition of "Last destination" is "destination" which apply the facility that "19 industry type" are "various goods retailers", "retailer (except for various goods retailers), restaurants", "retailer, restaurants (unknown details)" , and "12 facility type" are "Office", "Store", "Restaurant, Hotel", "House, educational institution, etc. ". Next, connecting OD having "destination" matching "origin" of OD containing "last destination" and "origin" of OD containing "last destination". The procedure of this method is shown in Figure.3.

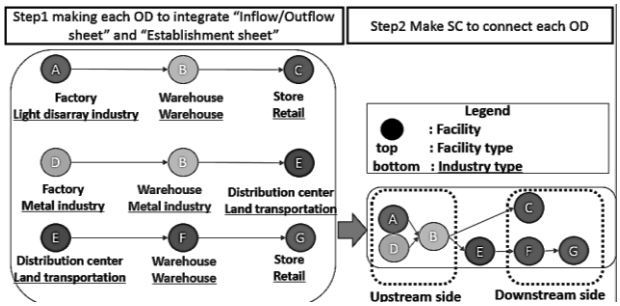


Figure 3: How to connect each OD

In Step1, when integrating "Inflow/Outflow Sheet" and "Establishment Sheet", one company has one "Establishment Number", and in order to specify one base of the company which have many bases because it is impossible to identify with just "Establishment Number". Therefore it is necessary to combine "industry type" and "436 municipality code", and to match 3 codes of "Establishment Sheet" and "Inflow/Outflow Sheet".

In Step2, it is fact that two ODs connect if "Origin" of one OD and "Destination" of other ODs have same "19 industry code", "12 facility code" and "436 municipality code". These two procedures can identify the logistics that is closest to the consumer as the most downstream part of the SC.

### 2.2.3 Facility Analysis on Upstream side of SC

In this method, we tried the two approaches of (a) and (b) on 20 items and analyzed the tendency of facilities in the upstream part of the SC.

(a) Measure the number of ODs for the combination of "19 industry type" and "12 facility type" for "Origin" of "Inflow/Outflow Sheet". From the result, we thought that we can grasp the trend of logistics in the upstream part for each item can be grasped by comparing the difference in trends by item.

(b) From (a), we considered we can say that the OD exist upstream part by investigating "industry type" and "facility type" of "Surveyed Facility" as the next facility of "Origin" which contain the OD of what "facility type" of "Origin" in "Inflow/Outflow Sheet" is "Factory". Because OD with logistics from factory to factory is more likely to be "upstream".

### 2.2.4 Facility Analysis on Middle part of SC

By analyzing the combination of "industry type" and "facility type" of all the OD data of "Inflow/Outflow Sheet", the number of combinations in each item is grasped. From the results and exclusion of the OD including the "downstream" and "upstream" facilities found from the methods (i) and (ii), it is possible to identify the facility having the combination "industry type" and "facility type" as the "middle" of the SC. We analyzed to how much "wholesaler" existed in the SC compared to other industries by examining the proportion of OD including "Surveyed Facility" of "Raw material wholesaler" and "Product wholesaler" to the number of total OD among wholesaler that are mostly in the middle of the SC. On the other hand, for items that contain the largest number of "industries" other than "wholesaler" as a percentage of "industry type" in the total OD number of each item, we select the "middle" facilities of the SC from the combination of the most "industry type" and "facility type", and it can be defined.

### 2.2.5 Goods Flow Analysis with out of TMA

By classifying the OD of "Inflow/Outflow Sheet" into OD related to logistics within TMA, OD relate to outbound shipment including overseas from TMA and OD relate to inbound shipment from outside of TMA including overseas per items, it can be measure its "the number of OD" and "weight (ton/day)".

### 2.2.6 Visualization of each facility per items on TMA

We visualized the SC of each item by mapping the latitude and longitude information of "core facility" of OD "upstream", "middle" and "downstream" of each item defined by the previous paragraph.

## 3. Result and Discussion

### 3.1 Facility Analysis on Downstream Side of SC

Figure 4 shows the number of OD including "Last destination" and the ratio of its OD to total number of ODs.

Figure 5 shows the number of ODs that have "Destination" that coincide with the "Origin" of the OD including the "Last destination" and the ratio of the number of its OD to the total number of OD. The numbers 1 to 20 shown in Figure 4 and 5 are the codes of each item. Table 2 shows the correspondence table between codes and item names.

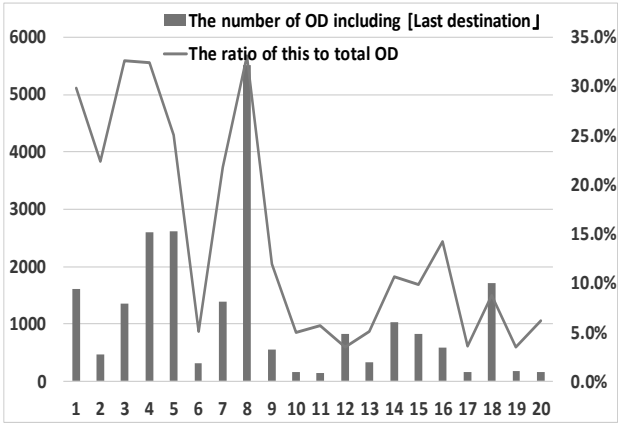


Figure 4: Number of OD including "Last destination"

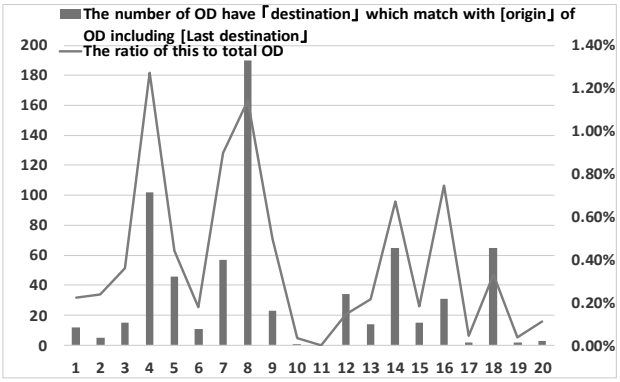


Figure 5: Number of OD have "destination" match "Origin" of OD including "Last destination"

From Figure 4, the proportion of the number of OD cases that apply to the "downstream" of the items related to daily life to the total number of ODs are that "Agricultural product (thermal)" is 30%, "Agricultural product (no thermal)" is 22.5%, "Food product (freezing)" is 32.6%, "Food product (thermal)" is 32.4%, "Food product (no thermal)" is 25%, "Daily necessity" is 33.1%, "Print product" is 21.8%. Considering that other items are between 3% and 14%, it can be said that items related to daily life have many ODs in "downstream". In addition, "Precision instrument" also has 15%, which is more than other manufacturing items. This can be inferred that the detailed items included in "Precision Equipment" are products such as watches and cameras, so that there will be many logistics close to consumers. On the other hand, from Figure 5, we also found that the number of ODs connected as a SC is considerably small. For example, even "food product (thermal)", which has the largest number of ODs connected by "the most downstream" among all items, was found to be only 1.3% of the total number of OD cases. Therefore, we concluded that it is difficult to concretely connect SC.

### 3.2 Facility Analysis on Upstream Side of SC

The contents of "Facility type" in "Origin" of "Inflow/Outflow Sheet" is shown in Figure 6 for each item. From Figure 6, there are many "factory" in the "upstream" facilities in the SC. The numbers 1 to 20 of Figure 6 are the codes of each item. Table 2 shows the correspondence table between codes and item names.

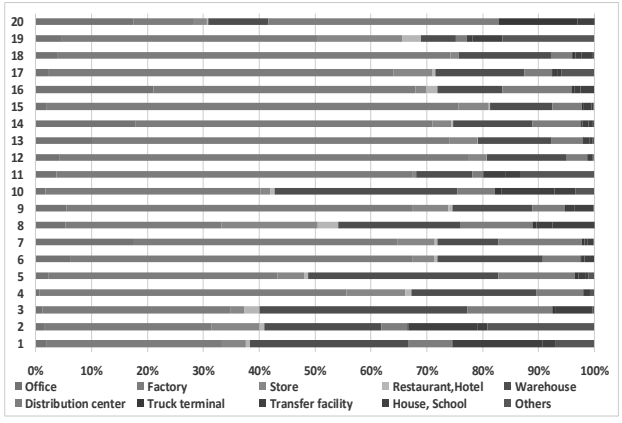


Figure 6: Share of "Facility type" in "Origin"

Meanwhile, facilities of "agricultural work place" and "mining site" in the contents of that "Facility type" is "Others" are likely to be the facility in "upstream" of SC. As shown in Figure.6, there is a large proportion of "Others" of "Facility type" in "Agricultural product (thermal)", "Agricultural product (no thermal)", "mineral product" and "Specialty". However, since "Specialty" is scrap and construction waste, it is hard to say that it is a facility located upstream of the SC among "others". In "Agricultural product (thermal)", "Agricultural product (no thermal)", "mineral product", Table 1 shows the ratio of OD including the facility have a combination of "Industry type" and "Facility type" to the number of total OD per items.

Table 1: Combination of "Industry type" and "Facility type", and its ratio

| Item | Industry type | Facility type | The ratio of a combination of "Industry tyoe" and "Facility type" |
|---|---|---|---|
| Agricultural product (thermal) | Agricultural forestry industry and fisheries | Others | 5.70% |
| Agricultural product (no thermal) | Agricultural forestry industry and fisheries | Others | 14.20% |
| Mineral product | Mining industy | Others | 10.50% |

Therefore, in these items, a combination of Table 1 contains the definition of "upstream" facility of SC.

Also, analyze the contents of the "facility type" of the "core facility" when "facility type" of "origin" is "factory" for distribution at the "upstream" of the SC. From this result, OD with logistics from factory to factory can be said to be "upstream" in all items because there are the largest proportion of factory to factory in all items.

Also, items with many OD in 'upstream' were raw material items and manufacturing items. The proportion of the number of OD that apply to "upstream" to the total OD is 77% for "mineral products" which are raw material items, 74% for "light industrial product" which are manufacturing items, 82% for "metal industry products", "chemical industry products" is 78%. It can be said that these ratios are higher than other items.

### 3.3 Facility Analysis on Middle stream side of SC

Since the facilities that apply to the "middle" of the SC are "wholesaler" or "transport company", the contents of the number of ODs including facilities of those industries to all industries is shown in Figure 7. The numbers 1 to 20 of Figure 7 are the codes of each item. Table 2 shows the correspondence table between codes and item names.

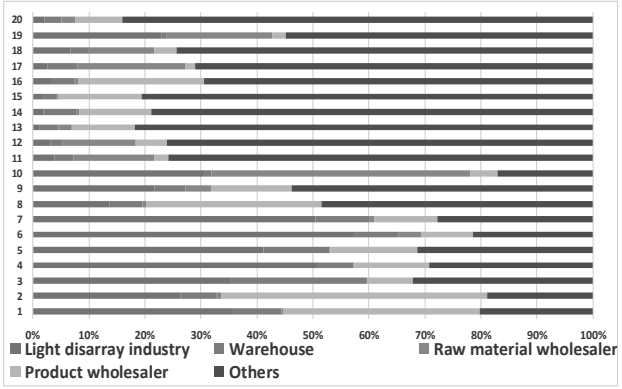


Figure 7: Share of "industry type" in "Core facility"

Items with many "product wholesaler" can be said that many OD occur in places close to consumers. Based on the above analysis, we defined the "middle" facility of SC in each items from the combination of "industry type" and "facility type". These are shown in Table 2. As a result, it turned out that there were variations in the combination of "industry type" and "facility type" depending on the item for "middle" facilities.

Table 2: Definition of “middle” facility in each items

| Code | Item | Industry type | Facility type |
|---|---|---|---|
| 1 | Agricultural product (Thermal ) | Product wholesaler | Distribution facility |
| 2 | Agricultural product (No thermal) | Product wholesaler | Distribution facility |
| 3 | Food product(Freezing) | Warehouse | Warehouse |
| 4 | Food product(Thermal) | Product wholesaler | Distribution facility |
| 5 | Food product(No thermal) | Product wholesaler | Distribution facility |
| 6 | Light industrial product | Product wholesaler | Distribution facility |
| 7 | Print product | Warehouse | Warehouse |
| 8 | Daily necessity | Product wholesaler | Distribution facility |
| 9 | Miscellaneous goods | Product wholesaler | Distribution facility |
| 10 | Forest products | Raw material wholesaler | Distribution facility |
| 11 | Mineral products | Raw material wholesaler | Distribution facility |
| 12 | Metal industry products | Raw material wholesaler | Distribution facility |
| 13 | General instrument | Product wholesaler | Office |
| 14 | Electric instrument | Product wholesaler | Office |
| 15 | Transport instrument | Product wholesaler | Distribution facility |
| 16 | Precision instrument | Product wholesaler | Office |
| 17 | Ceramic industry products | Raw material wholesaler | Office |
| 18 | Chemical industry products | Raw material wholesaler | Office |
| 19 | Specialty | Raw material wholesaler | Factory |
| 20 | Mixed | Land transportation freighter | Distribution center |

### 3.4 Goods Flow Analysis with out of TMA

Distribution within TMA was many in all items on the basis of the number of OD, but in weight-based logistics, there were more distribution with outside of TMA than those within TMA. The results of those items are shown in Figure 8.

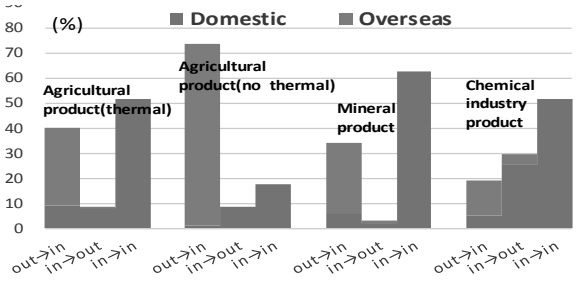


Figure 8: Distribution with in/out TMA

The means of transportation when there was a large amount of goods to be delivered was a ship. "Agriculture products (thermal)" has been carried in large quantities from overseas to factory facilities with thermal management, and has been delivered to warehouses of transport companies in Kamisu City, and food arrangement factory in Funabashi City. "Agricultural products (no thermal)" is carried in large quantities from overseas to warehouses of transport companies in Kamisu City. "Mineral products" are carried in large amounts in Kashima City. This is the Kashima coastal industrial area, which is considered to be because the steel industry is flourishing. "Chemical industry products" were imported from overseas to factory in Ichihara. This is because there is a huge Chiba port where cargo handling volume is 7% of the whole of Japan.

### 3.5 Visualization of each facility per items on TMA

We found that many of the facilities related to “Daily necessity” and “Precision instruments” were in "downstream" and many of the facilities in the manufacturing industry and instruments were in "upstream". Figure 9 and 10 show facility location of “Daily necessity” from items related to daily life and “Metal industry products” from manufacturing items.

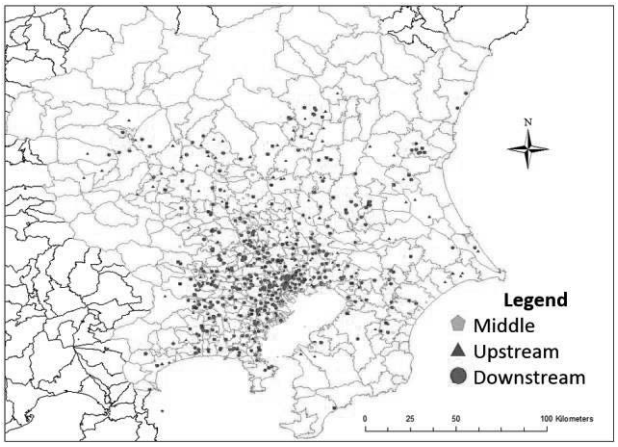


Figure 9: Map of “Daily necessity”

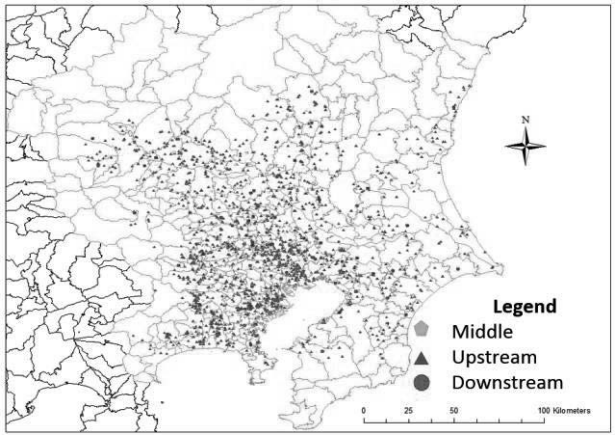


Figure 10: Map of “Metal industry products”

## 4. Conclusion

From the viewpoint of "downstream", "middle" and "upstream" of the SC, it was found that there are many "downstream" facilities in items relate to daily living and many “upstream” facilities in manufacturing items and instruments. We also found there is a tendency for logistics within TMA depending on the item.

Also, since there was a limit in using TMAUFS from the viewpoint SC, we will list the improvement points of the next survey. (1) It is necessary to unify the categories of "industry type" and "facility type" of "Inflow/Outflow Sheet" and "Establishment sheet". (2) The number of samples is increased by sending a survey form to the facility of "retailer" or "restaurant" which is highly likely to be located "downstream" of SC. (3) It is necessary to provide a field for writing the item names of both "Origin" and "Destination" of "Inflow/Outflow Sheet".

As a possibility of future research, by dividing the division according to the characteristics of the land such as the super-central area, suburbs and the coastal area where logistics warehouses are accumulated because TMA is quite huge area, so that it can be grasped a more accurate supply chain structure.

**References**

[1]東京都市圏交通計画協議会：東京都市圏の望ましい物流の実現に向けて, 2015
[2]兵藤哲朗, 首都圏における物流施設の立地とその方向性, 産業立地, vol.51, No.5, pp9-14, 2012.
[3]David Simchi-Levi: Designing and Managing the Supply Chain, 2002

# CHARACTERISTIC OF NON-SPECULAR SCATTERING ON OUTSIDE SURFACE OF BUILDINGS AT 25 GHZ

Student Number: 15M18256 Name: Hao Liu Supervisor: Jun-ichi TAKADA

# 25 GHz 帯における建物外壁面の非正規散乱の特性

劉 コウ

第 5 世代移動通信ネットワークシステムでは，準ミリ波もしくはミリ波帯を利用した高速伝送の実現が検討されている．高周波化に伴い波長が短くなり，建物外壁面の不均質性や凹凸が無視できなくなるため，平面による正規反射の仮定が成立せず，非正規散乱の影響も大きくなると予想される．本研究では，実際の建造物を対象とし，正規反射点付近の構造の違いに注目し，正規反射だけでなく非正規散乱の強度を実測した結果について分析した．

## 1 Introduction

Recently, wireless data traffic has increased rapidly [1].For the next generation of mobile network, the data rate above 10 Gbps is planned to be achieved. In order to achieve that goal, a large number of small cells, which could only cover several meters but with wide bandwidth, need to be set at the street. Normally, optical cables are used to connect between base stations(connection is called backhaul). However, there are a lot of places where it is not possible to set the optical cable, such as river and highway. Hence, the wireless backhaul is considered for the 5th generation mobile network.

In order to increase the data rate when using the wireless backhaul, one of the solution is to increase the bandwidth. This solution is based on Shannon's channel capacity theorem, which is shown in Eq. (1).

$$C = B\log_2\left(1+\frac{S}{N}\right) \tag{1}$$

Where $C$ is the channel capacity, $B$ is the bandwidth of the channel, $S$ is the average of received signal power over bandwidth, $N$ is the average power of the noise over the bandwidth.

The Ultra High Frequency(UHF) band and micro-wave frequency band, which has been used for non-Line-of-Sight wireless communication, could not provide such wide bandwidth. Hence, recently quasi-millimeter wave and millimeter wave bands are considered.

Even though it is reasonable to use high frequency to achieve high data rate, however, there are lots of challenges need to be solved from the viewpoint of wireless propagation. Firstly, when the frequency is high, the first Fresnel zone, which is the area that most part of energy will pass through, will become small. Especially for quasi-millimeter wave and millimeter wave, the first Fresnel zone could be shaded even by human body. In that case, to guarantee that the receiver could receive enough power, the non-line-of-sight path such as reflection or scattering from buildings surface will become important. Secondly, because of the high frequency, the wavelength is shorter. When the wavelength is roughly the same as the roughness of the buildings or the difference materials on building surface, the assumption that the building surface is flat becomes invalid. This implies that the scattering effect will become more significant.

Many researches have been done in outdoor environment and indoor environment [2] - [8]. For example, Takada, et al,(2002) [2] measured propagation channel in a suburban residential area at 8.45 GHz. By comparing with the measurement result and ray-tracing simulation result, the LOS component and specular reflection are correctly predicted. on the other hand, the recieved diffuse component could not be calculated correctly by ray-tracing simulation. And H.Budiarto, et al, (2004) [3] focused on one building surface and measure the scattering position. By using array antenna and estimation of signal parameters using rotational in-variance technique(ESPRIT) method, angular parameters could be estimated for each discrete position on building surface. All the result show that non-specular component will affect the propagation channel. In those literatures, frequency bands smaller than 10 GHz are analyzed, however the 5th generation is going to use the frequency above 24 GHz in order to achieve high data rate. So it is necessary to confirm the characteristic of the channel due to buildings at 24 GHz.

In this research, The final objective is to design the position and coverage of base station. Therefore, the model that can predict the received power is necessary. The propagation mechanism of the predicted model do not include the detailed scattering effect which is due to rough building surface or different building surface material. Hence, this research objective is to measure the scattering coefficient from buildings surface. In the future, by comparing with the simulation result, the final objective which is to design the position and coverage of base station could be achieved.

## 2 Analysis of non-specular scattering

### 2.1 Friis transmission equation

Friis transmission equation is used to show the relationship between transmitted power and received power at free space. Free space means there is no obstacle between transmitter and receiver. received power $P_{\mathrm{r}}$ is denoted by

$$P_{\mathrm{r}} = SA_{\mathrm{i}} = (\frac{P_{\mathrm{t}}}{4\pi d^2})(\lambda^2/4\pi) = P_{\mathrm{t}}(\lambda/4\pi d)^2 \tag{2}$$

where, $S$ is specific power, $A$ is effective area of receive antenna, $d$ is the distance between transmitter antenna and receiver antenna, $\lambda$ is wavelength, $P_{\mathrm{t}}$ is transmitted power. here $\lambda = c/f$, $c$ is speed of light, $f$ is frequency of electric

wave. Free space path loss $L_{\mathrm{p}}(d)$is defined as the reciprocal of the power gain given by Eq. (3).

$$L_{\mathrm{p}}(d) = \left(\frac{4\pi df}{c}\right)^2 \quad (3)$$

Finally, $P_{\mathrm{r}}$ could be express by Eq. (4),

$$P_{\mathrm{r}} = \frac{P_{\mathrm{t}}G_{\mathrm{t}}G_{\mathrm{r}}}{L_{\mathrm{p}}(d)} \quad (4)$$

where, $G_{\mathrm{t}}$ is the gain of transmitter antenna, $G_{\mathrm{r}}$ is the gain of receiver antenna. By using Eq. (4), receiver power could be calculated when any antenna is used.

### 2.2 Reflection and transmission

At free space, Friis transmission equation could calculate the received power. However, in reality especially in urban area, antennas are surrounded by buildings so the Friis transmission equation does not meet the conditions of free space. At this situation, the loss due to the buildings should be counted. Depending on the characteristic of material, electric wave(TE wave or TM wave), the reflection coefficient will be different. TE wave is the wave that electric field is parallel with boundary. TM wave is the wave that magnetic field is parallel with boundary(see Fig. 1).

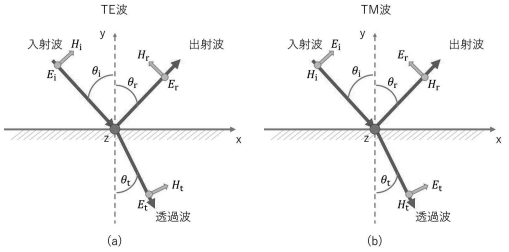


Figure 1: Reflection and transmission of TE and TM wave

Due to Snell's law, incidence angle $\theta_{\mathrm{i}}$ is equal to $\theta_{\mathrm{r}}$. The relationship between $\theta_{\mathrm{i}}$ and $\theta_{\mathrm{t}}$ is given by Eq. (5), and complex permittivity $\delta$ is given by Eq. (6).

$$\frac{\sin(\theta_{\mathrm{t}})}{\sin(\theta_{\mathrm{i}})} = \frac{\sqrt{\delta_1}}{\sqrt{\delta_2}} \quad (5)$$

$$\delta = \epsilon - j\frac{\sigma}{2\pi f_{\mathrm{c}}} \quad (6)$$

where, $j$ is imaginary unit, $\epsilon$ is permittivity, $\sigma$ is electrical conductivity, $f_{\mathrm{c}}$ is the carrier frequency.

### 2.3 Scattering and transmission coefficient

The reflection coefficient $R$ and transmission coefficient $T$ of TE wave and TM wave are different. transmission coefficient for TE wave is denoted by

$$R_{\mathrm{TE}} = \frac{\sqrt{\delta_1}\cos(\theta_{\mathrm{i}}) - \sqrt{\delta_2}\cos(\theta_{\mathrm{t}})}{\sqrt{\delta_1}\cos(\theta_{\mathrm{i}}) + \sqrt{\delta_2}\cos(\theta_{\mathrm{t}})} \quad (7)$$

$$T_{\mathrm{TE}} = \frac{2\sqrt{\delta_1}cos(\theta_{\mathrm{i}})}{\sqrt{\delta_1}cos(\theta_{\mathrm{i}}) + \sqrt{\delta_2}cos(\theta_{\mathrm{t}})} \quad (8)$$

Transmission coefficient for TM wave is denoted by

$$R_{\mathrm{TM}} = \frac{\sqrt{\delta_2}cos(\theta_{\mathrm{i}}) - \sqrt{\delta_1}cos(\theta_{\mathrm{t}})}{\sqrt{\delta_2}cos(\theta_{\mathrm{i}}) + \sqrt{\delta_1}cos(\theta_{\mathrm{t}})} \quad (9)$$

$$T_{\mathrm{TM}} = \frac{2\sqrt{\delta_1}cos(\theta_{\mathrm{i}})}{\sqrt{\delta_2}cos(\theta_{\mathrm{i}}) + \sqrt{\delta_1}cos(\theta_{\mathrm{t}})} \quad (10)$$

where, $R_{\mathrm{TE}} = E_{\mathrm{r}}/E_{\mathrm{i}}$, $T_{\mathrm{TE}} = E_{\mathrm{t}}/E_{\mathrm{i}}$ for TE wave, and $R_{\mathrm{TM}} = E_{\mathrm{r}}/E_{\mathrm{i}}$, $T_{\mathrm{TM}} = E_{\mathrm{t}}/E_{\mathrm{i}}$ for TM wave.

When the boundary is not flat, not only the specular reflection exist, but also scattering could be observed(see Fig. 2). Whether the surface is flat or rough is determined by Rayleigh standards $g$ as expressed by Eq. (11). If $g < 1$, the surface roughness could be consider as smooth surface, on the other hand, if $g > 1$, the surface roughness could be consider as rough surface.

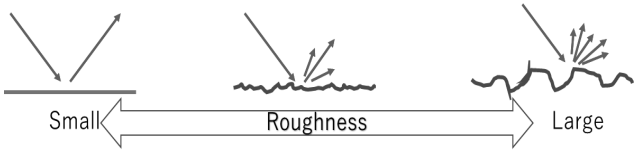


Figure 2: Relationship between roughness and scattering

$$g = \frac{4\pi\delta_h}{\lambda sin(\theta)} \quad (11)$$

In case of rough surface, the scattering coefficient$L_{\mathrm{s}}(\psi_{\mathrm{t}}, \psi_{\mathrm{r}})$ will be the function of incidence angle and departure angle as Eq. (12).

$$P_{\mathrm{r}} = P_{\mathrm{t}}\frac{G_{\mathrm{t}}(0)G_{\mathrm{r}}(0)}{L_{\mathrm{p}}(d)L_{\mathrm{c}}L_{\mathrm{s}}(\psi_{\mathrm{t}}, \psi_{\mathrm{r}})} \quad (12)$$

### 2.4 Radius of Fresnel zone

Fresnel zone is the area that phase shifting is within $\pi$, due to the difference of path length. When the incident angle is $\theta$, the radius of the $n$-th Fresnel zone is given by Eq. (13) and Eq. (14)

$$R_{1,n} = \sqrt{\frac{nd\lambda}{2}} \quad (13)$$

$$R_{2,n} = \sqrt{\frac{R_{1,n}^2(R_{1,n}^2 + d^2)}{R_{1,n}^2 + d^2\cos^2\theta}} \quad (14)$$

where, $d$ is the distance between transmitter antenna to scattering point,$R_{1,n}$ is the smaller radius of Fresnel zone, and $R_{2,n}$ is the larger radius of Fresnel zone. Depending on the percentage that first Fresnel zone is sheltered by obstacle. If the sheltered rate is lower than 60 % it can be considered as a free space environment. If half of the first Fresnel zone is sheltered, the loss will be 6 dB larger than free space. And if the hole first Fresnel zone is sheltered, the loss will be 16 dB loss larger than free space.

## 3 Measurement theory

### 3.1 Scattering modeling

To transmit the signal, antenna is an indispensable part. Comparing with the isotropic antenna, directional antenna could make signal transmit to certain direction and antenna gain could be higher than isotropic antenna in that direction. The Tx antenna used in this research is a broadband mobile access communication system(HiSWANb). The ration pattern of the antenna is

given by Fig. 3.

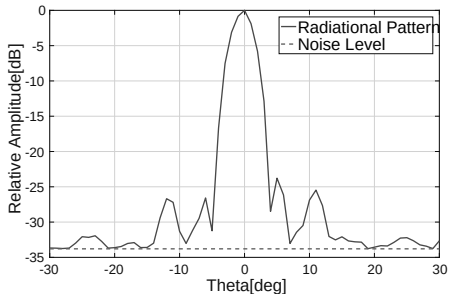


Figure 3: antenna pattern of Tx antenna

In this research, every point on the wall surface have different non-specular reflection coefficient is assumed. As Fig. 4 shows, the blue line is the path of non-specular reflection and red line is specular reflection. Scattering coefficient $L_{\mathrm{s}}(\psi_{\mathrm{t}}, \psi_{\mathrm{r}})$ is defined as the sum of specular reflection and non-specular reflection.

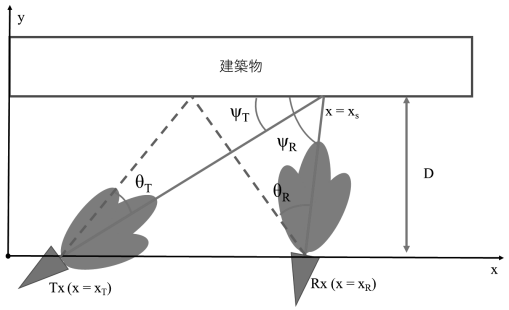


Figure 4: Parameters for calculate the scattering coefficient

### 3.2 Measurement system

In this research, by taking antenna position($x_{\mathrm{T}}, x_{\mathrm{R}}$), received power($P_{\mathrm{r}}$) and angle of Tx antenna($\psi_{\mathrm{t}}$) into Eq. (12), scattering coefficient could be calculated and analysed. The specification of antenna is shown in Table 1. Other parameters are shown at Table 2 in this measurement.

Table 1: Transmitter specification

| | |
|---|---|
| Frequency | 25GHz |
| Sample rate | 25.0MHz/40.0MHz |
| Communication | TDD |
| Modulation | 64QAM/16QAM/QPSK |
| Transmitted power | 3dBm（Max） |
| TDD ratio | AUTO/FIXED |

Table 2: Measurement parameter

| | |
|---|---|
| Frequency | 25GHz |
| Bandwidth | 25MHz |
| Transmitted power | 3dBm |
| Modulation | QPSK |
| I/Q sampling frequency | 50MHz |
| Measurement time | 20ms |

Before the measurement, loss due to cable and system must be measured. In calibration, Tx and Rx are set at certain distance and pointing to each other. The difference between measured received power and theoretical received power is the loss due to cable or other system loss.

### 3.3 Data analysis

In this research, 2 kinds of receiver signal analyzer and spectrum analyzer are used. For signal analyzer, IQ data was recorded on time axis. Since the duty cycle is 1:1, the data without signal transmitted was removed to calculate the received power by take the average of the remaining data. For spectrum analyzer, power data was recorded on frequency axis. By summing up all power within the bandwidth, received power could be calculated. For both cases, we could use the power to calculate the scattering coefficient by using Eq. (15).

$$L_{\mathrm{s}}(\psi_{\mathrm{t}}, \psi_{\mathrm{r}}) = P_{\mathrm{t}} \frac{G_{\mathrm{t}}(0) G_{\mathrm{r}}(0)}{L_{\mathrm{p}}(d) L_{\mathrm{c}} P_{\mathrm{r}}} \tag{15}$$

### 3.4 Method of calculate theoretical value

In order to know whether non-specular reflection affect the received power, it is necessary to compare the measured value to the ”theoretical value” which assumes that only specular reflection exist. If spread in x axis could be found, that means not only specular reflection, but also non-specular reflection affect the scattering reflection.

## 4 Measurement and Result

### 4.1 Measurement at NTT Yokosuka R&D Center

This measurement was held at NTT Yokosuka R&D Center. the surface of target building are mainly made from glass and metal. Environment and building surface are shown in Fig. 5 and Fig. 6.

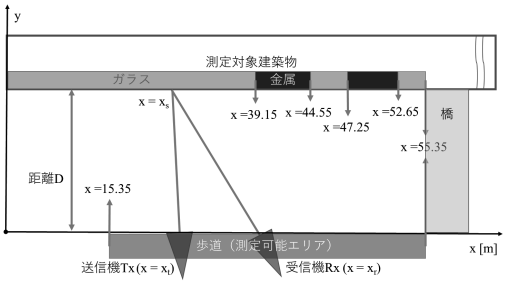


Figure 5: Measurement environment of NTT R&D Center


Figure 6: Building surface

The result is shown in Fig. 7 - Fig. 9. By analyzing the result, four results could be found. First, the spread in angle could be found at all results. That means the non-specular reflection affect the scattering coefficient. Second, material of building surface will affect the scattering coefficient. Comparing with the glass, scattering coefficient of metal has 10 dB larger than glass. Moreover, both glass and metal have 5-8 dB difference between measurement value and theoretical value around specular reflection point. Third, even for the same material, the difference is still 2-4 dB when antennas are shifted for 0.75 m. That might because the beam spot is larger than the size of window.

Thus, scattering from fence above the measurement point and window frames may lead to scattering. Four, when the incident angle is increased, the scattering coefficient is increased. This might because the increased incident angle make the beam spot became larger on building surface, thus the scattering coefficient became stronger.

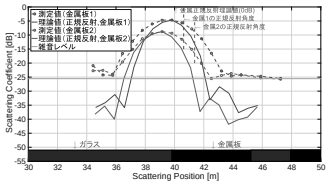


Figure 7: Result on metal

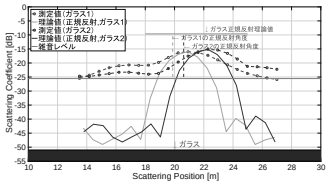


Figure 8: Result on glass

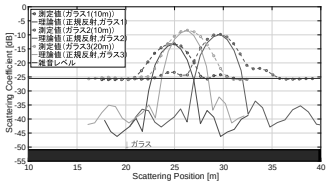


Figure 9: Result on glass(large distance)

### 4.2 Measurement at Tokyo Institute of Technology

The measurement held in Tokyo Institute of Technology is similar with NTT R&D center, but the distance between building surface and building material are different. the environment is shown by Fig. 10. The wall has 7 parts with same shape, the scattering coefficient was measured separately and compared with each other. The result that building surface material is tail, tail & glass, and tail & metal is shown by Fig.11 - Fig. 12.


Figure 10: Measurement environment of Tokyo Institute of Technology

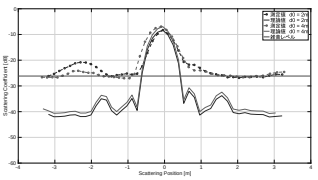

Figure 11: Result on tail

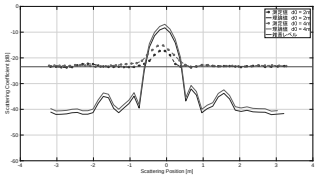

Figure 12: Result on tail and glass

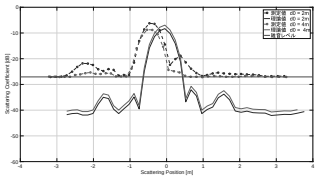

Figure 13: Result on tail and metal

As the result, first, effect from scattering could also be found due to the scattering coefficient is spread on angular axis. Second, the scattering coefficient is different due to the building material, metal have higher coefficient than tail, and coefficient of tail is higher than glass. Third, when the incident angle is increased, the scattering coefficient is increased. This might because the increased incident angle make the beam spot became larger on building surface, thus the scattering coefficient became stronger.

## 5 Conclusion

To solve the demand of data rate, The wireless backhaul utilizing more access points and high frequency was proposed. In this research, characteristic of non-specular scattering on outside surface of buildings at 25 GHz was analyzed.

The effect of scattering could be found at all measurements. when building material is different, the scattering coefficient could be different upto 10 dB. Even the material is similar there still could have 2-4 dB difference due to the different scattering object. About the effect of incident angle, when the incident angle become larger, it can find that the scattering coefficient will also become larger.

## References


[1] 総務省, ”我が国の移動通信トラヒックの現状,”, Jun. 2016.

[2] J. Takada, J. Fu, H. Zhu, and T.Kobayashi, “Spatio-Temporal Channel Characterization in a Suburban Non Line-of-Sight Microcellular Environment”, IEEE, J.Select. Areas in Coom., vol. 20, no.3, pp.532-538, Apr. 2002

[3] H. Budiarto, “Prediction Model and Measurement of the Electromagnetic Wave Scattering from Building Surface in Mobile Propagation Modeling”, Doctoral Thesis, Tokyo Institute of Technology, Mar. 2004

[4] J. S. Lu, V. Degli-Esposti, E. Vitucci and H. L. Bertoni, “Study of back-scattering from buildings using a 60 GHz scaled model,” The 8th European Conference on Antennas and Propagation (EuCAP 2014), pp. 814-816, The Hague, 2014.

[5] H. Budiarto, K. Horihata, K.Haneda, and J. Takada, “Experimental study of non-specular wave scattering from building surface roughness for themobile propagation modeling,” IEICE Trans. Comun., vol.E87-B, no.4 pp. 958-966, April. 2004.

[6] V. Degli-Esposti, “A diffuse scattering model for urban propagation prediction,” in IEEE Transactions on Antennas and Propagation, vol. 49, no. 7, pp. 1111-1113, Jul 2001.

[7] V. Degli-Esposti, D. Guiducci, A. de’Marsi, P. Azzi and F. Fuschini, “An advanced field prediction model including diffuse scattering,” in IEEE Transactions on Antennas and Propagation,” vol. 52, no. 7, pp. 1717-1728, July 2004.

[8] E. M. Vitucci, F. Mani, V. Degli-Esposti and C. Oestges, “Polarimetric Properties of Diffuse Scattering From Building Walls: Experimental Parameterization of a Ray-Tracing Model,” in IEEE Transactions on Antennas and Propagation, vol. 60, no. 6, pp. 2961-2969, June 2012.

# Web Applications for Multilingual Semi-Machine Translation based on Collective Intelligence

Student Number: 15M18240　Name: Wuning LI　Supervisor: Yukihiko YAMASHITA

# 集合知に基づく高精度多言語半機械翻訳のウェブアプリケーション化

李 呉寧

本論文では，インターネット上の一つの文書ファイルから高精度な翻訳で異なる母語の人々が情報を共有し合うことを実現するための集合知に基づく多言語半機械翻訳において，既存の研究では Java で実装されていた翻訳機を新たに JavaScript と PHP などを使って実装し，ウェブアプリケーション化する共に，現存の原文書情報付加ツールを改良する。さらに開発したシステムを評価する実験を行い，それらの有効性を確認する。

## 1. Introduction

Wiki-based online encyclopedia Wikipedia provides useful information continuously in a wide area from arts and sciences to life by collaboration. However, there is a language barrier to prepare document files for wiki in every language at the present time. Machine translation (MT) is a solution to cross the barrier and acquire the information in various languages, but it has a problem that incorrect recognition occurs in syntactic analysis or semantic selection.

In order to enable high-accuracy translation, a technique called Multilingual Semi-Machine Translation based on Collective Intelligence (Fig.1.) was proposed by Ishibashi [1]. By this technique, an XML document is described using a support tool to add the information such as syntax, grammar and meaning. Such a document is called ADAM (Auxiliary Description to Attach Meaning) document. A translator called LILITH (LInguaL Interpreter To Human) system was proposed by Negishi [2] to construct a multilingual information service system. It translates an ADAM document to one in various languages.

The existing LILITH system was written in Java so that it is difficult to work as a web application. In order to make it as a web application, I develop a new LILITH system implemented in JavaScript, PHP, etc. And I also improve the support tool to make ADAM documents. Further, I conduct two evaluation experiments to verify their effectiveness.

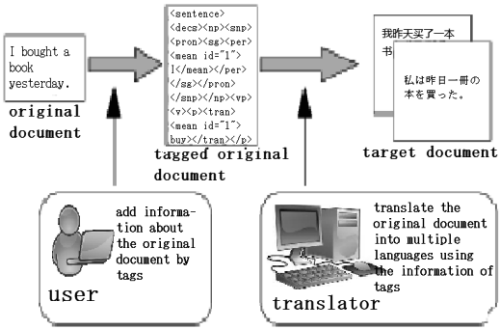


Figure 1: Multilingual Semi-machine Translation based on Collective Intelligence

## 2. Multilingual semi-machine translation based on collective intelligence

### 2.1. Overview

Multilingual Semi-Machine Translation based on Collective Intelligence enables that a user describes an ADAM document and uses the LILITH system to translate it into plural languages based on the information on tags. Because mistakes during syntactic analysis and vocabulary interpretation which are the

largest factors of the mistranslation in MT disappears, highly accurate translation is enabled by information of tags. All of these can be done on the Internet which means based on Collective Intelligence (CI).

CI is group intelligence which is treated as a synonym of “the wisdom of the crowd” [3]. In the world of the Internet, costs of collecting knowledge are extremely low and system architecture is enabled to gather a lot of participants so that CI can be realized effectively.

### 2.2. Problems of the existing system

The existing LILITH system is developed using the Java language, and it is inconvenient and incomplete since it does not have user interface (UI). To use the LILITH system, a user should install it on his/her computer and use a software such as Eclipse to work the program. Then the user can find the code to assign a path for an ADAM document.

A support tool [4] is developed to describe Adam documents. However, the following challenges remain.

- It is impossible to save data of the halfway description of an ADAM document so that once a user starts describing an ADAM document, he/she has to complete the work to the end.
- The UI of this tool is written only in English. It makes difficult for users who are not familiar with English or knowledge such as grammar and syntax of linguistics to describe an ADAM document.
- Since there is no manual on how to use this tool, a user needs to intuitively learn the way to use it.

## 3. Web Application for LILITH system and improvement on ADAM documents-making support tool

In order to solve the problems mentioned in 2.2, in this study, I newly develop LILITH system and make it as a web application with JavaScript, PHP, etc. And I also improve the support tool to describe ADAM documents.

### 3.1. Web Application for LILITH System

In order to make LILITH system easier to use on the Internet to realize CI, I developed LILITH system and made it as a web application with HTML, CSS, JavaScript and PHP. In addition, I also used jQuery and Bootstrap.

Its main functions are shown below.

- Open an ADAM document

The contents of the ADAM document can be checked.

- Translate an ADAM document

Japanese and Chinese can be chosen as the target language at the present time.

### 3.2. Improvement on ADAM documents-making support tool

In order to make the support tool to describe the ADAM documents easier to use, I improved the tool and remade it as a web application with HTML, CSS, JavaScript and PHP. In addition, I also used jQuery, jQuery UI, Bootstrap, and other techniques such as Ajax and modal window.

Its main functions are shown below.

- Input an original document

Only English is available at the present time.

- Add tags to make an ADAM document

Information of tags includes syntax, grammar and meaning.

- Save data of the halfway description

Save the data into a txt file which can be used to restart describing the ADAM document.

- Support users who are not familiar with English

In addition to English, UI language can be selected from Japanese and Chinese. And functions such as automatic input of prototype, explanation of tag and presentation of example are added.

- Improve operability

A manual on how to use this tool is added and it is possible to turn on/off to display it. And when some of buttons are hovered over, an explanation will be

displayed as "balloon".

## 4. Experiments

In order to evaluate the effectiveness of the newly developed LILITH system and the improved tool, I carried out the following two experiments.

### 4.1. Experiment 1: effectiveness of Improved ADAM document-making support tool

In this experiment, subjects used the existing tool and the improved tool to make ADAM documents of doc. 1 (I bought a book yesterday.) and doc. 2 (I think that that that that that writer used is wrong.) based on the given information. The time of making above ADAM documents is measured, and the operation burden on a user is evaluated subjectively.

6 subjects (2 Japanese and 4 Chinese) were divided into two groups of Group A and Group B. For Group A, first made the ADAM documents with the existing tool and then made the same ADAM documents with the improved tool. For Group B, first made the ADAM documents with the improved tool and then made the same ADAM documents with the existing tool.

The result of Exp. 1 is shown in Table 1. 'Time' is the time (in seconds) of describing the ADAM documents. 'Operability' and 'Experience time' were used as the five-grade evaluation index (higher is better) to evaluate the operation burden on a user.

Regarding the 'Time', it shows that using the improved tool can make description of ADAM documents faster than using the existing tool. It means that the improved tool is more practical. And as for the 'Operability' and "Experience time", the improved tool generally gained a better rating than the existing tool. In addition, all subjects had a better impression on the proposed one.

Therefore, although there is still room for improvement, it has showed the effectiveness of the improved tool.

Table 1: Results of experiment 1

| Items | | Group A | | Group B | |
|---|---|---|---|---|---|
| | | Existing | Proposed | Existing | Proposed |
| Time (s/word) | Mean. | 1136(63.1) | 723(40.2) | 933(51.8) | 735(40.8) |
| | Min. | 519(28.8) | 407(22.6) | 810(58.7) | 655(36.4) |
| | Max. | 1510(83.9) | 883(49.1) | 1056(45.2) | 814(45.2) |
| Operability | Mean. | 2.3 | 4.7 | 2.3 | 4.3 |
| | Min. | 2 | 4 | 2 | 4 |
| | Max. | 3 | 5 | 3 | 5 |
| Experience time | Mean. | 2.7 | 4.3 | 3.0 | 5.0 |
| | Min. | 2 | 4 | 3 | 5 |
| | Max. | 3 | 5 | 3 | 5 |

### 4.2. Experiment 2: effectiveness of LILITH system

In this experiment, subjects used the existing LILITH system and the proposed LILITH system to translate the ADAM documents made in Exp.1, and evaluated the operation burden on a user subjectively. Further, I compared the translation results of 4 documents by the LILITH system and other MT services.

The result of Exp. 2 is shown in Table 2. 'Operability' was used as the five-grade evaluation index to evaluate the operation burden on a user.

Table 2: Results of experiment 2

| Operability | Existing | Proposed |
|---|---|---|
| Mean. | 1.8 | 4.7 |
| Min. | 1 | 4 |
| Max. | 2 | 5 |

The following are examples of the translation results of LILITH system and other MT services.

- Doc. 1: I bought a book yesterday.
  (LILITH system) 私は昨日 1 冊の本を買った。
  (Google Translate) 私は昨日本を買った。
  (Weblio Translate) 本を昨日買った。
  (Excite Translate) 私は昨日本を買った。
- Doc. 2: I think that that that that that writer used is wrong.
  (LILITH system) 私はあの作家が使ったあの that は間違っていると思う。

(Google Translate) 私が使っている作家は間違っていると思います。
(Weblio Translate) 使われるその作家が間違っているために，私はそれをそれと考えます。
(Excite Translate) 私は考える that それ that 作家が使ったことが悪い。

- Doc. 3: Are you still playing Pokemon Go?
(LILITH system) あなたはまだポケモン Go をしていますか？
(Google Translate) あなたはまだポケモンをしていますか？
(Weblio Translate) あなたは，まだポケモン試みをしていますか？
(Excite Translate) あなたはまだ遊びポケモン行きであるか？
- Doc. 4: I want to eat rice.
(LILITH system) 私はご飯を食べたい。
(Google Translate) 私はコメを食べたい。
(Weblio Translate) 私は，米を食べたい。
(Excite Translate) 私は米を食べたい。

As for the ‘Operability’, the proposed one gained a better rating than the existing one. And all subjects had a better impression on the proposed one.

Regarding the comparison of the translation results, all of them obtained a correct translation of Doc. 1 which has a simple constitution. However, as for Doc. 2 which has a complicated constitution, in Google Translate, an error occurred in parsing that '私' which is the subject of the whole sentence was recognized as the subject of the adjective phrase modifying '作家'. In Weblio Translate and Excite Translate, an error occurred in vocabulary interpretation for 'that'. As for Doc. 3 including a proper noun, Google Translate and Weblio Translate have an error occurred in vocabulary interpretation for “Pokemon Go”, and Excite Translate has an error occurred in parsing where “playing Pokemon Go” was recognized as a noun phrase. As for Doc. 4 including a multisense word, Google Translate, Weblio Translate and Excite Translate have an error occurred in vocabulary interpretation for “rice”. On the other hand, the LILITH system translated the documents using the information of tags, so it obtained translations with higher accuracy than the others.

Therefore, the above results showed the practicality and effectiveness of the proposed LILITH system.

## 5. Conclusions

In this study, I developed a new LILITH system as a web application with JavaScript, PHP, etc. And I also improved the support tool to describe ADAM documents. Further, I conducted two evaluation experiments and the results verified their effectiveness.

As future works, it is necessary to further improve the tool and LILITH system, and it is important to increase target languages of LILITH system and vocabularies of the multilingual dictionary in order to construct a multilingual information service system. In addition, in order to be able to provide as a service based on CI, it is necessary to make an attractive web information system for users without causing a problem of security.

## References


[1] Takuya ISHIBASHI. Study of multilingual semi-machine translation based on Collective Intelligence, Master's thesis, Tokyo Institute of Technology, 2008. (in Japanese)

[2] Yuhei NEGISHI, Study of multilingual semi-machine translation based on Collective Intelligence. Bachelor’s thesis, Tokyo Institute of Technology, 2008. (in Japanese)

[3] James Surowiecki, THE WISDOM OF CROWDS, Anchor, New York, Aug. 2005.

[4] Wuning LI, Study of multilingual semi-machine translation based on Collective Intelligence. Bachelor’s thesis, Tokyo Institute of Technology, 2015. (in Japanese)

# Wavelet Based Image Coding via Linear Prediction and Improved Clustering

Student Number: 15M18049 Name: Dan WANG Supervisor: Yukihiko YAMASHITA

# 線形予測と改良されたクラスタリングに基づくウェーブレット画像符号化

王 丹

本論文では, 線形予測を用いたウェーブレット画像符号化の計算時間を削減するため, その予測器の学習に使われるクラスタリングの部分を改良することを提案する. この中で, 予測に使うブロックサイズの変更と予測誤差の大きいクラスタの削除を行う. この改良によって, 符号時にクラスタを探す計算回数を減らすことが可能であり, 予測効率と符号化効率に影響を与えずにエンコード時間を減らすことができる。また, 計算機実験によって, 提案手法の有効性を確認する.

## 1 Introduction

The rapid development of multimedia product is causing the insufficient bandwidth of network and storage of memory device. Therefore, the image coding methods have been invented to reduce or eliminate the data redundancies for saving storage costs or transmission time [1].

The discrete wavelet transform (DWT) is a tool that cuts up data, functions, or operators into different frequency components. Wavelet-based image coding is an image coding method using the DWT. By encoding the coefficients, it reduces the data size [1][2]. Predictive coding is another technique for efficient transmission or storage by sending only the difference between the original and its predicted values to reduce the data size [3]. However, it is difficult to apply predictive coding to the two-dimensional DWT that used in JPEG2000 directly because the distance of decoded pixels and pixels that have to be predicted is quite far. To solve this problem, a predictive coding method that applies prediction to one-dimensional transform part in 2D-DWT decomposition was proposed [2]. According to the experimental results, the predictive method that applies prediction to 1D-DWT transform part in 2D-DWT decomposition shows better prediction efficiency and coding efficiency than the conventional one. K-means clustering is applied in this method to partition the vectorized data of extracted blocks into $k$ clusters and to generate the coefficients of the linear predictor. However, due to the calculation of prediction, it takes more time for coding process than the method without prediction.

In this paper, in order to save encoding time without influencing coding efficiency, I propose to reduce the calculation time by changing the size of extracted block and removing the vector data belonging to the clusters which generate larger error rate than the conventional ones. I show experimental results to demonstrate the advantage of the proposed method.

## 2 Linear Prediction with Clustering

### 2.1 Linear Prediction

Linear prediction is a mathematical operation where future values of a discrete time signal are estimated as a linear function of previous samples. The most common representation of linear predictive coding is

$$\hat{s}(n) = \sum_{i=1}^{p} a_i s(n-i), \tag{1}$$

where $\hat{s}(n)$ is the predicted signal value of the actual signal value $s(n)$ from the linear combination of $p$ signal values with $a_i$ as the coefficients. The error generated by estimating the difference between the actual signal value $s(n)$ and the predicted signal value $\hat{s}(n)$. In error form in one-dimensional linear prediction can be expressed as follows:

$$e(n) = s(n) - \hat{s}(n), \tag{2}$$

In order to obtain the linear prediction coefficients $a_i$, the most common choice is to minimize the sum of squares of the errors defined in the form

$$\begin{aligned} e(n) &= s(n) - \hat{s}(n) \\ &= s(n) - \sum_{i=1}^{p} a_i s(n-i), \end{aligned} \tag{3}$$

$$E = \sum_{n} e^2(n). \tag{4}$$

where $E$ is the short-time average prediction error.

### 2.2 K-means Clustering

K-means clustering is a method of vector quantization, it aims to partition $n$ observations into $k$ clusters to which each observation belongs with the nearest mean. It is a prototype-based, partitional clustering technique.

Here, let $(x_1, x_2, ..., x_n)$ be a set of observation, and each observation is a $d$-dimensional real vector. K-means clustering aims to partition the $n$ observations into $k$ sets $\mathbf{S} = \{\mathbf{S_1}, \mathbf{S_2}, ..., \mathbf{S_k}\}$ by minimizing the within-cluster sum of squares (WCSS)

$$\arg\min_{S_1,S_2,...,S_k} \sum_{i=1}^{k} \sum_{x \in S_i} \|x - \mu_i\|^2. \tag{5}$$

where $\mu_i (i = 1, 2, ..., k)$ is a centroid that is the mean of points in $\mathbf{S_i}$.

**Algorithm 1** K-means algorithm.

Select $K$ points as initial centroids.
**repeat**
From $K$ clusters by assigning each point to its closest centroid.
Recompute the centroid of each cluster.
**until** Centroids do not change.

K-means clustering is formally described by Algorithm 1. The algorithm proceeds by repeating between two steps until only 1% of the observations change clusters.

### 2.3 Linear Prediction with Clustering

In this paper, K-means clustering is implemented for the blocks extracted from the input image according to their features to make the categories, $\mathbf{\Omega}_c$ $(c = 1, 2, ..., C)$. The prediction model in $\mathbf{\Omega}_c$ is given by

$$q = \langle \boldsymbol{a}_c, \boldsymbol{v} \rangle , \tag{6}$$

where $\boldsymbol{a}_c$ is constant for linear prediction. For training data $\boldsymbol{v}_i$ and $q_i$ $(i = 1, 2, ..., N)$ in $\mathbf{\Omega}_c$, $\boldsymbol{a}_c$ is decided to minimize the following criterion:

$$\sum_{i=1}^{N_c} |q_i - \langle \boldsymbol{a}_c, \boldsymbol{v}_i \rangle |^2. \tag{7}$$

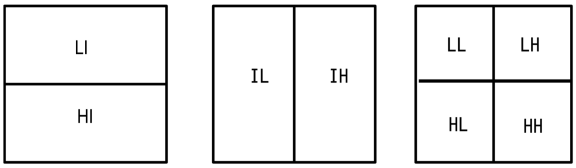


(a) vertical 1D-DWT (b) Horizontal 1D-DWT (c) 2D-DWT

Figure 1: Coefficients of 1D-DWT decomposition

## 3 Wavelet Based Image Coding with Prediction

Prediction is a key technology which can enhance the coding efficiency of image coding. If we apply predictive coding to 2D-DWT directly, it should be based on the decoded values. However, in 2D-DWT decomposition, the target pixel we want to predict is apart form the decoded pixels. Therefore, the prediction with the 2D-DWT decomposition is considered to be difficult.

To solve this problem, prediction is applied into the 1D-DWT part in the 2D-DWT decomposition [2]. Fig. 1 shows the process of 1D-DWT decomposition. Different with 2D-DWT decomposition, in 1D-DWT decomposition, we firstly decompose the input image (I) vertically into LI and HI (Fig. 1(a)) and then we respectively decompose LI and HI horizontally into LL, LH and HL, HH (Fig. 1(c)). Here L represents for low and H for high frequency coefficients. After these two steps, one stage of 2D-DWT is completed. Alternatively, horizontal 1D-DWT can also be done firstly (Fig. 1(b)), followed by vertical decomposition of IL and IH into LL, LH and HL, HH.

To predict a target pixel of the target row, a block around the target pixel is extracted and shown as Fig. 2. In 1D-DWT part, the decomposition is done row by row from top to bottom. Since the target pixels we want to predict and the reference pixels we can use are adjacent, the predictive coding can successfully be applied to 1D-DWT part .

## 4 Improved Clustering Method with Linear Prediction

The predictive method that applies prediction to 1D-DWT transform part in 2D-DWT decomposition shows better prediction efficiency and coding efficiency than the conventional one. However, due to the calculation of prediction, it takes more time for coding process than the approach with-

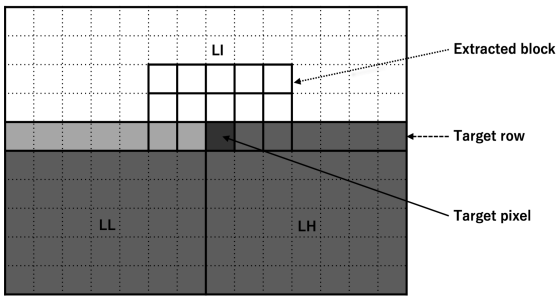


Figure 2: Extraction of blocks with size of 5 × 3

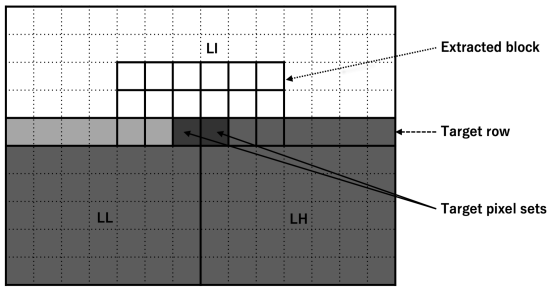


Figure 3: Extraction of blocks with size of 6 × 3

Table 1: Encoding time for different test data

| Test Data | 5×3 | Conventional |
|---|---|---|
| Intersection | 5.5412 | 0.1037 |
| Lenna | 4.2157 | 0.0777 |
| Barbara | 4.1946 | 0.0772 |

Table 2: RMSE for different test data

| Test Data | 6 × 3E | 5×3E | 6×3O | 5×3O |
|---|---|---|---|---|
| Intersection | **2.907** | 2.921 | **6.084** | 6.086 |
| Lenna | **1.947** | 1.969 | 3.843 | 3.796 |
| Barbara | 7.830 | 6.751 | 15.647 | 14.757 |

out prediction. Table 1 shows the encoding time for different test data with the same learning data. Here, the number of clusters is 128 ($nCls = 128$).

To solve this problem, I propose to reduce the times of calculation for prediction by choosing two pixels as a target set. In order to choose two pixels in the middle as a target pixel pair, the numbers of pixels from extracted block in the target row should be even. Fig. 3 shows an example of the extracted block with size of 6 × 3. With K-means clustering, we can get two parameters of liner predictor from each cluster for the target pixel pair at even and odd coordinates at the same time. In other words, instead of calculating even and odd coordinates separately, the proposed method makes it possible to calculate those at the same time. Therefore, the times of calculation for selecting the best clustering can be reduced by half.

Furthermore, the experimental results shows that there exists some clusters which generate large prediction error rate compared with the conventional one. I propose to remove the vector data belonging to the clusters which generate larger error rate than the conventional ones to improve prediction and coding efficiency. After that, I propose to reduce the number of the remaining clusters to be half of the previous one. Therefore, the times for finding the best cluster will be also reduced by half.

The estimation of the real value of target pixel $y$ can be given by:

$$\hat{y} = \langle \hat{\boldsymbol{a}}, \boldsymbol{x} - m \cdot \mathbf{1} \rangle + m. \quad (8)$$

where $\boldsymbol{x}$ represents for the vectors made from extracted blocks, $m$ is the average of $\boldsymbol{x}$. $\hat{\boldsymbol{a}}$ is the estimation of the vector of prediction parameters. $\mathbf{1}$ is the vector of which all elements are 1.

# 5 Experimental Methods and Results

In the experiment, I used 8 standard images as learning data and 3 standard images as test data. I changed the numbers of clusters ($nCls$) and the size of blocks ($b_x \times b_y$) and quantization factor $q$ to obtain the best results for prediction efficiency and coding efficiency.

## 5.1 Evaluation Methods

In this research, root mean square error (RMSE) and peak signal-to-noise ratio (PSNR) are used to evaluate the prediction efficiency and coding efficiency respectively. The smaller RMSE is, the more efficiency prediction has been done. The high PSNR value denotes the reconstructed image quality is high, and the low PSNR value denotes the reconstructed image quality is low.

## 5.2 Results and Discussion

In order to compare with the conventional one, I will show the results that image n2 was used as learning image. Furthermore, I set the numbers of clusters as 128 and changed the block size as 5 × 3 and 6 × 3.

- Prediction Efficiency

Table 2 shows the results of RMSE of test data "Intersection", "Lenna" and "Barbara" respec-

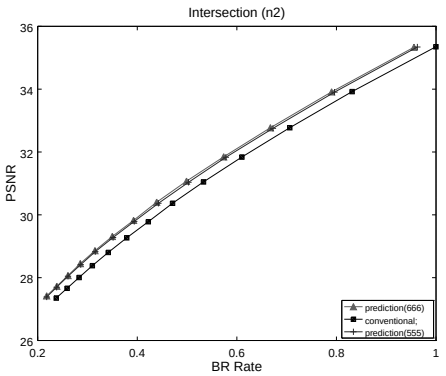


(a) Intersection

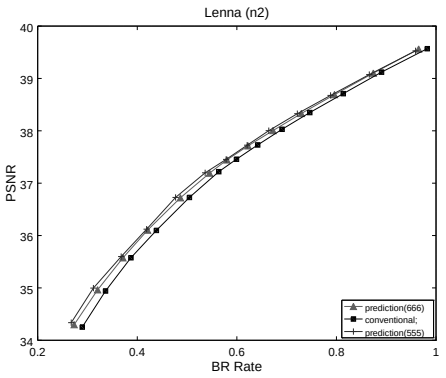


(b) Lenna

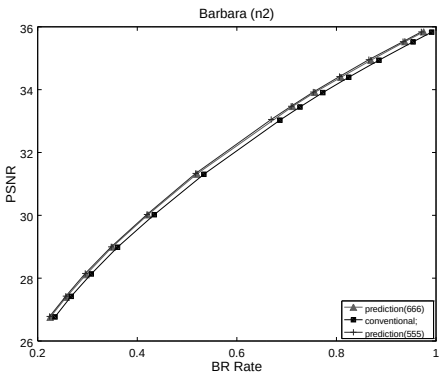


(c) Barbara

Figure 4: Rate distortion curve

tively. According to Table 2, it is obviously that there is almost no difference between the RMSEs of the proposed method ($6 \times 3$) and the previous one ($5 \times 3$).

- Coding Efficiency

Fig.4 shows the results of coding efficiency for test images Intersection, Lenna and Barbara respectively. Table 3 shows encoding times for different test data by different methods.

All of the three cases shows that the proposed method reduced the encoding time by appropriately 40% successfully without influencing coding efficiency. Especially in the case of Intersection,

Table 3: Encoding time for different test data by different methods

| Test Data | 6×3 | 5×3 | Conventional |
|---|---|---|---|
| Intersection | **3.3435** | 5.5412 | 0.1037 |
| Lenna | **2.5291** | 4.2157 | 0.0777 |
| Barbara | **2.5321** | 4.1946 | 0.0772 |

the proposed method outperformed the previous one in prediction accuracy.

# 6 Conclusions

In this paper, the background of image coding has been introduced. Followed by the basis of linear prediction, K-means clustering and the approach that applies linear prediction to 1D-DWT in 2D-DWT decomposition. Then the problem in encoding time has been figured out. To solve this problem, I introduced my proposed method to reduce the calculation time for prediction to save the coding time. Experiments are conducted to show the prediction and coding efficiencies.

According to the experimental results of the proposed method, encoding time has been reduced by appropriately 40 % without influencing coding efficiency.

For future work, it is possible to improve coding efficiency by developing a more precise prediction algorithm. For example, instead of using K-means clustering, we can apply neural network in prediction step to improve coding efficiency. Furthermore, we can apply EBCOT (Embedded Block Coding with Optimized Truncation) in coding method to improve coding efficiency.

# References

[1] Marc Antonini, Michel Barlaud, Pierre Mathieu and Ingrid Daubechies, "Image Coding Using Wavelet Transform", IEEE Transactions on Image Processing, Vol. 1, No. 2, April 1992.

[2] Shiyu Zhou, Yukihiko Yamashita, "Wavelet Based Image Coding via Linear Prediction and Clustering", Master Thesis, Jan 2014.

[3] Rajesh P.N. Rao and Dana H. Ballard, "Predictive coding in the visual cortex: a functional interpretation of some extra-classical receptive-field effects ", Nature Neuroscience 2, 79-87(1999), dol: 10.1038/4580

# Regression based Image Super Resolution through Decision Tree Learning
# 決定木学習を用いる画像回帰超解像

Number: 15M18262 Student Name : Zhengqi Zhu Supervisor: Yukihiko Yamashita

本論文では，決定木を用いる新しい画像超解像手法を提案する。これは，先に一連の回帰予測器を用意し，その中から，最適な予測器を決定木によって選択する方法である。この決定木の学習方法を具体的に与えると共に，計算機の実験によって低解像度画像から質の高い高解像度画像が復元できることを示す。

## 1 Introduction

Image super resolution (SR) is a technique for image resolution enhancement. It has various applications such as medical imaging, satellite imaging and surveillance camera. The fundamental task of image SR is to construct high resolution (HR) images by using low resolution (LR) images. It is technically easy to down-sample HR images into LR images. However, the reverse process is quite difficult, since it is necessary to create more pixels by using less pixels and the solution is not unique. Figure 1 is an example of the the general problem of SR. In this case, a desired $4\times4$ HR image patch is predicted by a $2\times2$ LR image patch. In recent years, many SR algorithms have been proposed. Interpolation-based methods utilise filters such as cubic convolution filter [1] to estimate HR pixel values. Although interpolation-based methods are widely used for their low computational cost, the estimated HR images are always with blurry edges. Reconstruction-based method use prior knowledges like Gradient Profile Prior [2] to estimate the HR images. However, the quality of estimated HR images are still lackluster. As a result, learning-based methods are being developed. Learning-based methods estimate the HR image by learning from example HR and LR image patch pairs from external datasets. Timofte et al. proposed adjusted anchored neighbourhood regression (A+) [6] which produces the state of the art result for image SR.

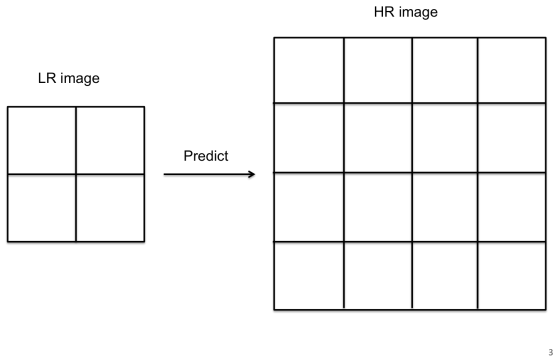


Figure 1: Super Resolution Problem

With all these methods being developed, a method to obtain more accurate HR images is still desired. Most recent learning based image SR methods, such as [5] and [7], classify image patches as groups first and then train regression models (a mapping between LR and HR image patches) for each group. However, there is not yet a study doing the opposite approach, which is training regression models first and then classifying image patches to select the best regression model for each patch. Training regression model before classification could be advantageous firstly because it can fully utilise the regressor training technology developed on other fields such as intra-prediction and secondly because the remaining problem can be simplified as a selection problem. In this study, I will demonstrate a method that utilise a binary decision tree to select optimal regressors from a set of pre-trained regressors for each LR patch. The regressors are pre-trained by using a method similar to a previous study on image intra-prediction [8]. Hyper-planes are generated based on maximum information gain to form binary tests for the decision tree. Experimental results showed that this method has the potential to reconstruct high quality HR images.

## 2 Related previous work

As it was mentioned in the previous section, the goal of this research is to select an optimal regressor from a set of pre-trained regressors to predict HR images. An advanced regressor training technology [8] from the image intra-prediction field is adopted to accomplish this goal for its ability to produce high quality regressors. Ochotorena and Yamashita proposed an effective method for regressor training [8]. Firstly, they classified image patches into small groups by using k-means clustering. They trained a regressor for each group by obtaining the least square solution of patches belong to each group. Then they started an iterative refining process to continuously regroup image patches and retrain the regressors based on errors of the predictions. This method would be explained in the next section in detail.

# 3 Proposed method

## 3.1 Regression model

As we can see in Figure 1, image SR is about predicting HR images by using LR images with less pixels. A $2 \times 2$ LR image patch can be represented as a $4 \times 1$ column vector $\vec{l}$. Similarly, a $4 \times 4$ HR image patch can be represented as a $16 \times 1$ column vector $\vec{h}$. Converting a LR patch to a HR patch is

$$\vec{h} = R\vec{l}, \tag{1}$$

where R (our regressor) is a $16 \times 4$ matrix.

As the LR image patches inherently contain less pixel information, in this method I decided to use middle image patches, of which dimension is the same as one of the HR image patches, $\vec{m}$ to predict the HR image patches. Middle image patches are created by the most commonly used bi-cubic interpolation.

$$\vec{m} = B[\vec{l}], \tag{2}$$

where B is the operator of bi-cubic interpolation.

Then the regression model can be as follows:

$$\vec{h} = R\vec{m}, \tag{3}$$

where R is the regressor in the form of a square matrix.

## 3.2 Regressor training

At first, by downsampling the images from the example HR image database $P_H$, LR image database $P_L$ can be created. Middle image database $P_M$ can be created as well by using the bi-cubic interpolation.

A set of regressors were trained by using an approach similar to the clustering and iterative refining process of the previous research [8]. Firstly, for each HR image patch $\vec{h}$, an error image patch $\vec{e}$ were created by subtract the original HR image patch $\vec{h}$ and the Middle image patch $\vec{m}$ .

$$\vec{e} = \vec{h} - \vec{m}. \tag{4}$$

k-means clustering is used to divide the set of error patches $E$ into $n$ clusters. Corresponding regressors $R_1, R_2 ..... R_n$ for each cluster are obtained afterwards. Then, the members of each cluster $H_j$, $L_j$ where $j \in \{1, 2, ..., n\}$ will be updated through a refining process by finding the minimum predicting error for each regressor.

$$H_j = \{\vec{h_i} | \arg\min_p ||\vec{h_i} - R_p\vec{m}_i||^2 = j\}, \tag{5}$$

$$M_j = \{\vec{m_i} | \arg\min_p ||\vec{h_i} - R_p\vec{m}_i||^2 = j\}. \tag{6}$$

Then the regressors will be updated too by using these updated clusters. The new regressor can be calculated by using least square method

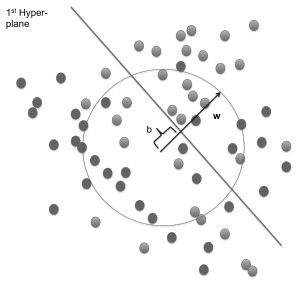


Figure 2: Hyper-plane Generation

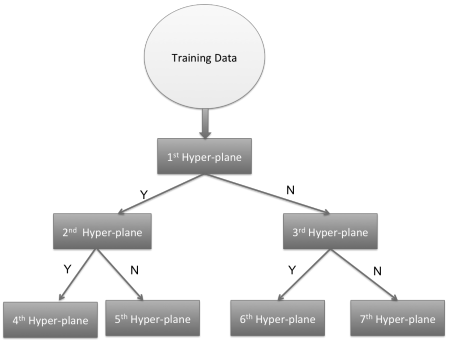


Figure 3: Decision Tree

$$R_j = \arg\min_R \sum_{\substack{\vec{H}_i \in H_j \\ \vec{m}_i \in M_j}} ||\vec{h_i} - R\vec{m}_i||^2. \tag{7}$$

By adding a Tikhonov regularization term, the new regressor is given by:

$$R_j = H_j {M_j}^T ({M_j}{M_j}^T + \lambda I)^{-1}. \tag{8}$$

This refining process will be repeated over several times to obtain the final regressors $R_1, R_2 .....$ and $R_n$.

## 3.3 Decision tree learning

The remaining problem is simplified as a selection problem, i.e. how to select the optimal regressor from $R_1, R_2 .....$ and $R_n$ for each individual middle image patch.

Hyper-planes were created to form a binary decision tree to do the selection. 500 random vectors $\vec{w_1}, \vec{w_2}, .....\vec{w_{500}}$ with the same dimension as the middle image patches with the norm of 1 are created. a set of 50 scalars $b_1, b_2, ....., b_{50}$ is created with a designated range of value. The hyper-planes can be generated by calculating the projection of the middle patch data onto the random vector subtract a certain parameter ${\vec{w_i}}^T\vec{m} - b_j$. Figure 2 is a demonstration of a hyper-plane generation. Each hyper-plane divides the original dataset into 2 subsets. Therefore, 'Which subset does the data belong to?' can be a binary test for the decision tree. The overall decision tree is illustrated in Figure 3.

The data belong to the first subset fulfils:

$${\vec{w_i}}^T\vec{m_a} - b_j \geq 0, \tag{9}$$

The data belong to the the second subset fulfils:

$$\vec{w_i}^T \vec{m_a} - b_j < 0. \tag{10}$$

Information gain is calculated for each generated hyper-plane.

$$\begin{aligned} IG = N \sum_i -P_i \log P_i - N_a \sum_i -Pa_i \log Pa_i \\ - N_b \sum_i -Pb_i \log Pb_i, \end{aligned} \tag{11}$$

where $N$ is the number of data in the parent node before divided by a hyper-plane. $N_a$ and $N_b$ represent the number of data in both child nodes respectively. $i$ is the index for the regressor. Subsequently, $P_i = N_i/N$ where $N_i$ is the number of patches which use the $i$th regressor. $Pa_i$ and $Pb_i$ is calculated similarly for both child nodes.

The optimal pair of $(\hat{\vec{w}}, \hat{b})$ that generates the hyper-plane with the maximum information gain is selected to formulate the binary test of each node for the decision tree.

$$(\hat{\vec{w}}, \hat{b}) = \arg\max_{\vec{w},b} IG, \tag{12}$$

After selecting the optimal $(\hat{\vec{w}}, \hat{b})$ for one node, the same calculation will continue at the next node. When the number of patches in a node is lower than 10 or when the total number of nodes exceeds a certain parameter, the node will be declared as an end node (node without child node). For each end node, the most used regressor will be declared as the result of that node. The binary test for each node and the result for each end node are memorised and a decision tree is constructed.

### 3.4 Test phase

Test phase is the real application of this method. In real application the only available input information is the LR image. We also have a set of regressors and a constructed decision tree for HR image prediction. We take the following steps to conduct image SR under this method.

1: Make the middle image by using LR image through bi-cubic interpolation.

2: Collect middle image patches by using a sliding window.

3: For each middle image patch $m_i$, ask binary questions on the first node and proceed to the next node until reaching the end node.

4: The result of the end node $\hat{R}_i$ is obtained.

5: Predict the HR image patch $h_i$ by $H_i = \hat{R}_i \times m_i$ and move on to the next patch until all the patch are predicted.

6: Construct the HR image by calculating the average of the overlapping sliding patches.

Finally the HR image is obtained.

## 4 Experimental results

Two test image sets were used. I down-sampled the original test images and created LR images as the input. $4 \times 4$ LR image patches were collected in order to predict $8 \times 8$ HR image patches.

### 4.1 Best Case Scenario

The best case scenario where I assumed all regressors are chosen correctly were created. This best case scenario is an ideal situation that can show both the quality of the regressors and the potential of this method. Table 1 shows the PSNR comparison between the best case scenario and the most common Bi-cubic interpolation on test image set 1. There is a significant improvement of PSNR. This suggests that this method has a good potential if the decision tree can select the optimal regressor correctly. This also suggests that the pre-trained regressors and the regression model in this method can properly conduct image SR.

### 4.2 Results of The Proposed Method

The decision tree were trained from an image database consists of 240000 LR and HR image patch pairs. On each node of the decision tree 500 random vectors $\vec{w}$ are generated and the value range of $b$ is between 0 to 0.3 with 0.006 as interval. When the total number of patches in a node is below 10, the node will be declared as an end-node. If there are still nodes that are not end-nodes, the decision tree will grow until the total hight of decision tree exceeds $\log_2 1000000 \approx 20$. Image SR was conducted by using 10, 20, 30, 40, 50, 64 as the number of regressors. Table 1 shows the PSNR results of this method with comparison to the bi-cubic interpolation where the number of regressor $n = 30$.

Table 1: PSNR (dB) Comparison 30 Regressors

| Name | Bi-cubic | Best Case Scenario | Decision Tree |
|---|---|---|---|
| Arctichare | 40.5895 | 46.8852 | 43.7192 |
| Airplane | 31.3801 | 37.5875 | 33.8867 |
| Barbara | 25.3533 | 27.9393 | 25.8367 |
| Boat | 29.9539 | 33.6441 | 31.2945 |
| Fruits | 32.2379 | 37.0949 | 34.6799 |
| Lena | 34.1440 | 38.2167 | 36.0167 |
| Baboon | 23.6435 | 26.2082 | 24.5553 |
| Goldhill | 31.2302 | 34.3052 | 32.1606 |
| Monarch | 31.6676 | 36.7382 | 34.1039 |
| Mountain | 19.4424 | 21.2262 | 20.1788 |
| Peppers | 31.8690 | 36.2276 | 33.6440 |
| Sails | 28.3114 | 32.3709 | 30.1149 |
| Average | 29.9852 | 34.0370 | 31.6826 |

There is a fair amount PSNR gain compared with the bi-cubic interpolation. We see an average of 1.7

Figure 4: Barbara: bicubic (Left), proposed method (Right)

dB gain on set 1 with 30 regressors used. We see an average of 2.1 dB gain on set 2 with 20 regressors used. Table 2 shows the PSNR gain on both test sets. As we can see in Figure 4, the visual quality has been improved particularly at the area with edge.

Table 2: Average PSNR Gain

| Number of Regressors | PSNR (dB) gain Set 1 | PSNR (dB) gain Set 2 |
|---|---|---|
| 10 | 1.5493 | 1.8941 |
| 20 | 1.6708 | 2.0664 |
| 30 | 1.6974 | 2.0643 |
| 40 | 1.5557 | 1.9983 |
| 50 | 1.6622 | 1.9837 |
| 64 | 1.5448 | 1.9846 |

I compared the result of this method to some of the state of the art methods mentioned in the introduction by using test image set 2. Table 3 shows the result comparison with 30 regressors used for this method and for the best case scenario. As we can see, the proposed method can produce similar PSNR results compared to other major methods.

# 5 Conclusion and future work

In this paper, I proposed a new regression based image SR framework. A set of regressors were trained and a binary decision tree was created to select the optimal regressor. This method produces similar PSNR results compared with the state of the art methods. I also tested a best case scenario where I assume every regressor is selected correctly. Although the current result of the proposed method is still inferior to A+ method by 0.78 dB, the best case scenario can outperform A+ by 1.62 dB. Therefore as long as the decision tree selection accuracy can be improved in the future, this method has a potential to outperform the state of the art methods. Instead of using bi-cubic interpolation, I also want to use A+ to produce middle patch. This also makes it possible to outperform A+ in the future.

# References


[1] R.G. keys,"Cubic convolution interpolation for digital image processing," IEEE Trans. Acoust.,Speech, Signal Process., vol. 29, no. 6, pp. 1153-1160, Dec. 1981.

[2] J. Sun, J. Sun, Z. Xu, H.Y. Shum, Gradient Profile Prior and Its Applications in Image Super-Resolution and Enhancement. IEEE Trans. Image Process., vol.20, no.6, pp.1529-1542, 2011.

[3] H. Chang, D.T. Yeung, and Y. Xiong, Super-resolution through neighbor embedding, Proceedings, IEEE International Conference on Computer Vision and Pattern Recognition (CVPR 2004), vol. 1., 2004.

[4] R. Zeyde, M. Elad, and M. Protter, On single image scale-up using sparse-representations, In Curves and Surfaces, Springer Berlin Heidelberg, pp. 711-730, 2012.

[5] R. Timofte, V. De Smet, and L. Van Gool, Anchored neighborhood regression for fast example-based super-resolution, Proceedings, IEEE International Conference on Computer Vision (ICCV 2013), pp. 1920-1927, 2013.

[6] R. Timofte, V. De Smet, and L. Van Gool, A+: Adjusted Anchored Neighborhood Regression for Fast Super-Resolution, IEEE Asian Conference on Computer Vision (ACCV 2014), 2014.

[7] Jun-Jie Huang and Wan-Chi Siu, "Learning Hierarchical Decision Trees for Single Image Super-Resolution," IEEE Transactions on Circuits and Systems for Video Technology, 2015

[8] Carlo Noel Ochotorena and Yukihiko Yamashita "Regression-based Intra-prediction for Image and Video Coding" (Preparing to submit)


Table 3: PSNR (dB) Results Comparison

| Test Images | Bi-cubic | Zeyde [4] | NE+LLE[3] | GR[6] | ANR[6] | A+[7] | Proposed Method | Best Case |
|---|---|---|---|---|---|---|---|---|
| Baby | 37.1 | 38.2 | 38.3 | 38.3 | 38.4 | 38.5 | 38.5 | 40.5 |
| Bird | 36.8 | 39.9 | 40.0 | 39.0 | 40.0 | 41.1 | 40.0 | 43.8 |
| Butterfly | 27.4 | 30.6 | 30.0 | 29.1 | 30.5 | 32.0 | 30.1 | 32.6 |
| Head | 34.9 | 35.6 | 35.5 | 35.6 | 35.7 | 35.8 | 35.7 | 36.9 |
| Women | 32.1 | 34.5 | 34.5 | 33.7 | 34.5 | 35.3 | 34.6 | 37.1 |
| Average | 33.66 | 35.78 | 35.77 | 35.13 | 35.83 | 36.55 | 35.77 | 38.17 |

# Energy dissipation in adhesion contact between an elastic beam and a flat rigid surface

Student number: 15M18084 Name: Takeru KUSAKARI Supervisor: Kunio TAKAHASHI

## 弾性梁と剛体平面間の凝着・脱離プロセスにおけるエネルギー散逸

草苅　太建

本論文では、弾性梁と剛体平面を凝着・脱離させたときに生じるエネルギー散逸のメカニズムをより詳細に議論するべく、梁幅が変化する台形梁と、梁の自重の影響を取り入れることで、従来の弾性梁と剛体平面間の凝着モデルを改善している。また、改善を加えた梁モデルにおけるエネルギー散逸を解析的に算出し、実験にて測定している。測定結果より、接触端部の長さがエネルギー散逸に対して影響を及ぼすことが示唆される。また、弾性梁が伸び縮みやせん断変形を起こしている可能性が示唆されるため、今後はそれらの効果を梁モデルに加える必要があることを示している。

## 1. Introduction

Force curve in adhesion phenomena is very useful for designing applications using adhesive force, such as Gecko-inspired adhesive [1-3]. In the force curve, there are differences between loading process and unloading process and it is called adhesion hysteresis. In order to predict force curve more precisely, it is significant to understand the mechanism of adhesion hysteresis.

Recent studies say that energy dissipation in adhesion contact causes adhesion hysteresis. Energy dissipation can be calculated as the difference between work of adhesion $\Delta\gamma$ and energy release rate $G$ like

$$\left.\frac{\partial U_{\text{dissipation}}}{\partial S}\right|_d = -(G - \Delta\gamma) \qquad (1)$$

$S$ is contact area, i.e. it expresses the energy dissipation per unit contact area. Because work of adhesion $\Delta\gamma$ is physical property, in order to predict energy dissipation, energy release rate $G$ is necessary to calculate. Johnson suggests a formula to calculate energy release rate $G$ in a point contact model based on JKR theory [4]. It is expressed as

$$G = \Delta\gamma/(1 \pm \alpha) \qquad (2)$$

$\alpha$ is dissipation factor and it is a fixed value defined by property [5]. Meanwhile, Baek suggests a different formula expressed as

$$G = \Delta\gamma + f/(2\pi a) \qquad (3)$$

$a$ is contact radius in a point contact model and $f$ is dissipation force [6]. But these two theories have contradiction expressed as Fig.1. So, in point contact model, the mechanism of adhesion hysteresis hasn't been clarified yet.

As the different model, there is adhesion contact model between an elastic beam and a flat rigid surface [7]. Kusakari measured the energy release rate in adhesion contact between a rectangular elastic beam and a flat rigid surface. He suggests that energy release rate in beam model can be adapted to both Johnson's and Baek's. But this beam model has two problems. Firstly, because of rectangular beam, contact width is fixed and the effect of contact width can't be discussed. Secondly, the weight of the beam is ignored. Therefore, in order to understand the mechanism more precisely, this beam model needs to be modified.

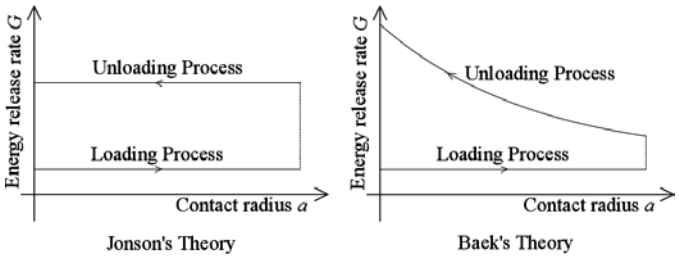


Fig.1 Comparison between Johnson's theory and Baek's theory related to energy release rate

In this study, in order to clarify the mechanism of adhesion hysteresis, existing beam model is modified in two points. Firstly, trapezoidal beam model is introduced to discuss the effect of contact width on adhesion hysteresis. Secondly, the weight of the beam is considered. And then, energy dissipation is measured and discussed based on the modified model.

## 2. Modified Beam Contact Model to Calculate Energy Dissipation

Fig.2 shows schematic illustration of modified beam contact model. In trapezoidal beam, the width changes linearly. Change rate of the width $m$ is expressed as

$$m = \frac{W_1 - W_0}{W_0} \qquad (4)$$

By using change rate of the width $m$, trapezoidal beam can be considered theoretically. And also when $m = 0$, it expresses a rectangular beam.

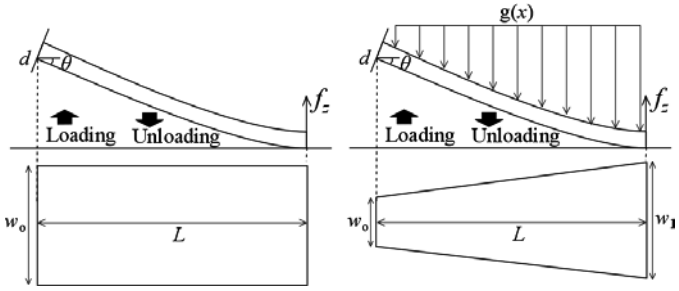


Fig.2 Schematic illustration of modification of beam contact model

Based on the assumption that the density of the beam is uniform, the weight of the beam is considered as

$$g(x) = \frac{f_g}{L}(1 + m\frac{x}{L}) \tag{6}$$

$f_g$ is the total weight of the beam and $L$ is the length of the beam. In modified beam model, this is considered in calculation of the force $f_z$ and energy dissipation $U_{\text{dissipation}}$.

The force $f_z$ between an elastic beam and a flat rigid surface can be calculated based on linear beam theory. In this model, it is assumed that the friction force can be neglected. The force $f_z$ in the line contact is expressed as

$$f_z = \frac{1}{\alpha_1}\frac{EI_0}{L^2\cos^2\theta}\left(\frac{d}{L} + \sin\theta\right) + \frac{\alpha_2}{\alpha_1}f_g \tag{7}$$

$EI_0$ is the bending stiffness at the root of the beam. $d$ is the displacement of the root of the beam. $\theta$ is the contact angle. And $\alpha_i$ is the parameter related to change rate of the width $m$. In area contact, the force $f_z$ can be calculated as

$$f_z = \frac{1}{\beta_1}\frac{EI_0}{l^2\cos^2\theta}\left\{\frac{d}{l} + (1-\beta_2)\sin\theta\right\} + \frac{\beta_3}{\beta_1}f_g \tag{8}$$

$l$ is the length of non-adhesion area. $\beta_i$ is the parameter related to change rate of the width $m$ and the length of non-adhesion area $l$. When change rate of the width $m \to 0$, the force $f_z$ equals to the force $f_z$ in a rectangular beam. Whether this theoretical model is valid is discussed based on experimental result later.

As for the calculation energy dissipation, the energy release rate should be calculated. Energy release rate is defined as

$$G = \left.\frac{\partial U_{\text{elastic}}}{\partial S}\right|_d \tag{9}$$

Therefore, in order to calculate energy release rate, elastic energy must be calculated. In this model, because the tangential force is assumed as ignorable value, it can be considered that bending deformation only occurs. Accordingly, elastic energy in this model can be calculated as

$$U_{\text{elastic}} = \frac{\beta_1}{2}\frac{{f_z}^2 l^3\cos^2\theta}{EI_0} + \beta_4\frac{EI_0}{l}\tan^2\theta + \beta_5\frac{{f_g}^2 l^3\cos^2\theta}{EI_0} - \beta_3\frac{f_z f_g l^3\cos^2\theta}{EI_0} \tag{10}$$

After all, by using formulas (1), (9), (10), energy dissipation in adhesion contact between an elastic beam and a flat rigid surface can be calculated.

## 3. Experiment to Measure Energy Dissipation

In order to calculate energy dissipation, the parameters shown at Tab.1 need to be known.

The parameters from 1 to 5 are fixed by initial condition. The parameters from 6 to 8 are measured experimentally. 9 and 10 are estimated based on experimental result later.

Tab.1 Parameters to calculate energy dissipation

| | | |
|---|---|---|
| 1. | $L$ | Length of a beam |
| 2. | $I_0$ | Moment of inertia at the root of a beam |
| 3. | $m$ | Change rate of width |
| 4. | $\theta$ | Contact angle |
| 5. | $f_g$ | Weight of whole beam |
| 6. | $d$ | Displacement of the root of a beam |
| 7. | $f_z$ | Force between a beam and a surface |
| 8. | $l$ | Length of non-adhesion area |
| 9. | $E$ | Yong's Modulus |
| 10. | $\Delta\gamma$ | Work of adhesion |

Therefore, in order to measure displacement of the root of a beam $d$, force between a beam and a surface $f_z$, and length of non-adhesion area $l$, the experiment system are prepared as shown at Fig.3. Displacement of the root of a beam $d$ is controlled by stepping motor(KZL06075-C1-GA, SURUGA SEIKI). Force between a beam and a surface $f_z$ is measured by electronic scale(Practum®612-1S, Sartorius). Length of non-adhesion area $l$ is observed by microscope(SKM-3000B-PC, SAITOH KOUGAKU). And the elastic beam used in this experiment is PDMS(SYLGARD®184 SILICORN ELASTORMER KIT, Dow Corning). As a flat rigid surface, slide glass(MICRO SLIDE GLASS S9213, MATSUNAMI) is used. And also, in order to reduce the effect of friction force, still balls are set between the surface and the electronic scale.

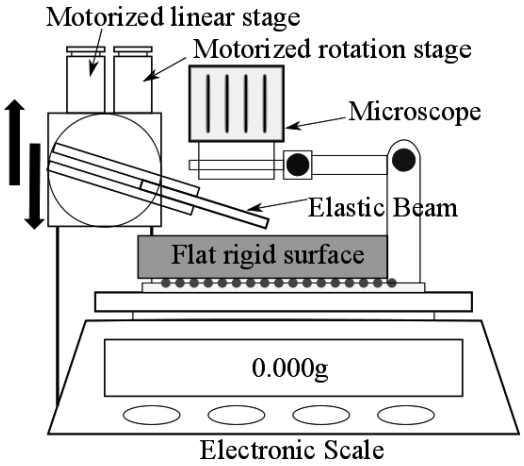

Fig.3 Schematic illustration of experimental system

In this study, viscoelasticity is not considered. Therefore the experiment need to be performed as static state as possible. Accordingly, the displacement is controlled by a step of 50μm and waiting duration between steps is 30 seconds. And the maximum displacement is chosen 3500μm.

After all, force curves are measured as shown at Fig.4-5.

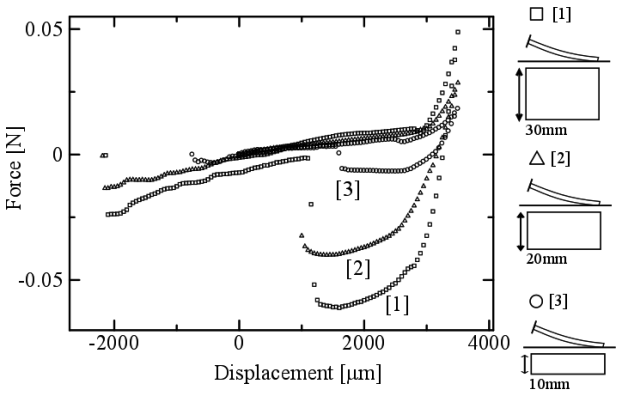


Fig.4 Force curve between a rectangular elastic beam and a flat rigid surface

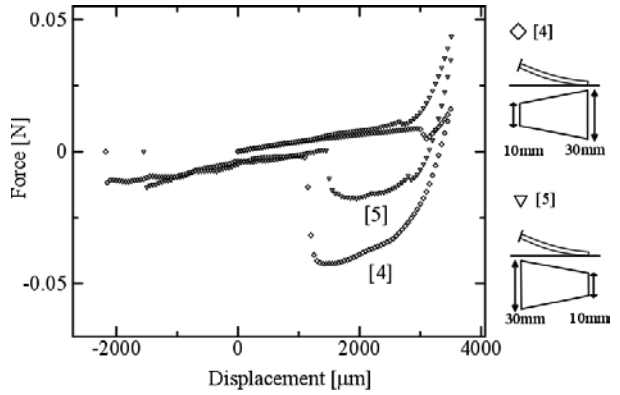


Fig.5 Force curve between a trapezoidal elastic beam and a flat rigid surface

Comparing theoretical force given by formula (7) and (8) with the measured force curves, Yong's Modulus is estimated. One example of the comparison is shown at Fig.6.

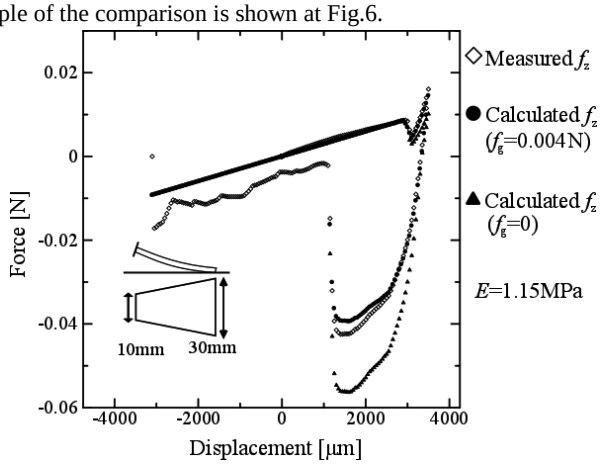


Fig.6 Comparison between measured force and calculated force

From Fig.6, in the trapezoidal beam whose edge is wide, the weight of the whole beam $f_g$ is very influential on the force curve. And by using modified model which considers the weight of the whole beam $f_g$, fitting of force curve can be performed better. From this result, Yong's modulus $E$ is estimated as 1.15MPa.

Because Yong's modulus $E$ has been estimated, energy release rate $G$ can be calculated using formula (9) and (10) as shown at Fig7-8.

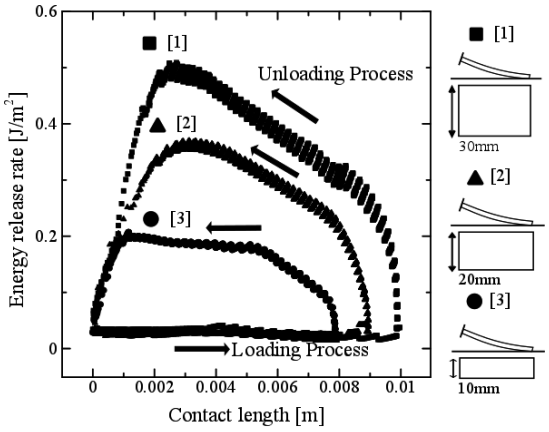


Fig.7 Energy release rate between a rectangular elastic beam and a flat rigid surface

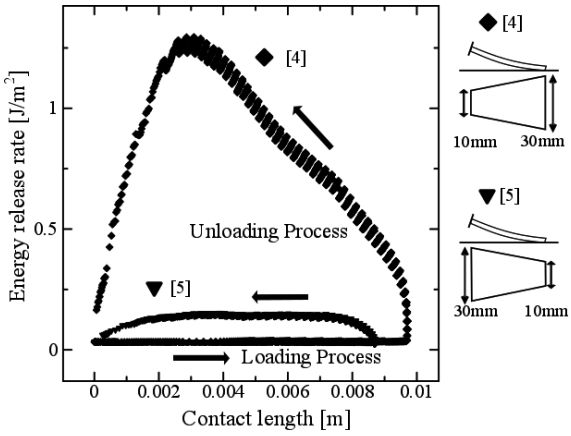


Fig.8 Energy release rate between a trapezoidal elastic beam and a flat rigid surface

In the loading process, all the results show the same tendency and the same fixed value. Therefore the energy release rate in loading process can be considered as physical property and it is assumed as work of adhesion $\Delta\gamma$. Accordingly, $\Delta\gamma$ is estimated as 0.031J/m$^2$ and this value almost equals to the $\Delta\gamma$ of a point contact model [6].

After all, all the parameters to calculate energy dissipation have been decided. The results of the energy dissipation are shown at Fig.9-10.

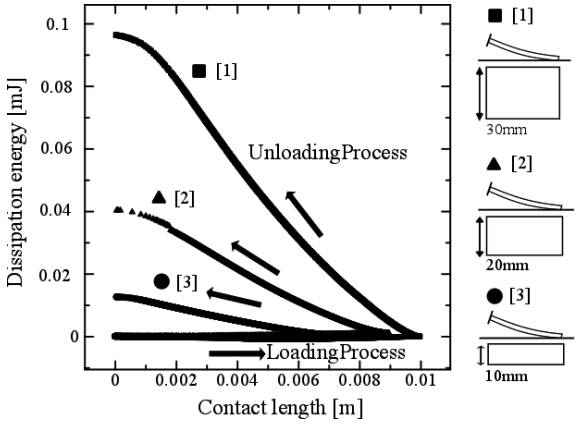


Fig.9 Dissipation energy between a rectangular elastic beam and a flat rigid surface

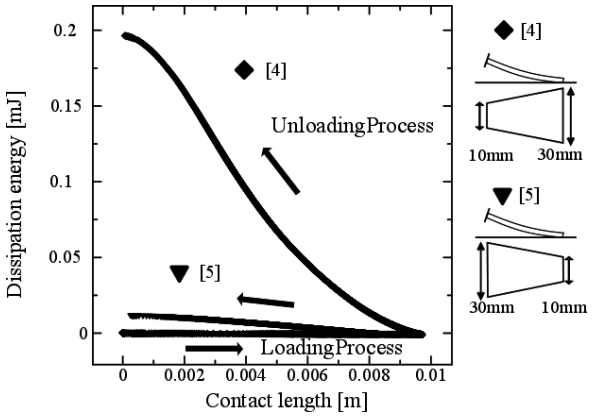


Fig.10 Dissipation energy between a trapezoidal elastic beam and a flat rigid surface

## 4. Discussion

In using rectangular beam, the energy release rate in unloading process tends to increase if the width of the beam gets wide as shown at Fig.7. On the other hand, in using trapezoidal beam, the beam [4] whose contact width increase in unloading process has much more energy release rate than another one, i.e. the beam [4] needs more energy to separate from the surface as shown as Fig.8.

And also, in energy dissipation, wider the width of the rectangular beam is, more energy is dissipated as shown at Fig.9. In the trapezoidal beams, the beam [4] has much more energy dissipation as shown at Fig.10.

From the results of energy release rate and energy dissipation, it can be suggested that the width of contact edge effects on the energy dissipation, i.e. adhesion hysteresis. However, in using the rectangular beam, the energy release rate increases as the beam is separated from the surface. Based on existing theories such as Johnson's one and Baek's one, when width of contact edge is fixed, the energy release rate is also fixed. Therefore these results contradicts to the exiting studies. The reason why is that there are some factors which are not considered in this model.

In fact the shear deformation induced by the friction force can be thought as one of the factors causing the contradiction, although steel balls are set to reduce the effect of the friction force. In order to estimate the effect of the friction force, the displacement of the edge of the beam $\delta$ is measured by micro scope. And based on geometric conditions, the displacement of the edge $\delta$ is calculated theoretically as,

$$\delta = -\tan\theta\,(d + l\sin\theta) \qquad (11)$$

In Fig.11 the relation between the $\delta$ calculated theoretically and the measured $\delta$ is shown. Around the start point of the loading process and the end of the unloading process, both the measured $\delta$ and the calculated $\delta$ are almost same value. On the other hand, as the loading is getting advanced, the difference is increasing. Accordingly, there is a possibility of the friction force working on the beam. Therefore the deformation induced by the friction force could effect on the energy release rate and energy dissipation. And it could causes the contradiction between the result in this study and the existing theories. So ,based on the result, it can be suggested that the shear deformation induced by the friction force should be considered in order to calculate energy dissipation more correctly in the future works.

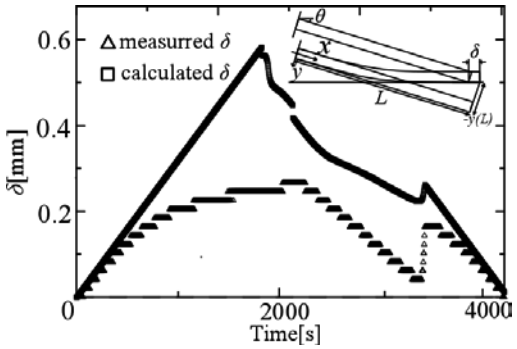


Fig.11 Comparison between $\delta$ calculated theoretically and $\delta$ measured experimentally

## 5. Conclusion

Introducing trapezoidal beam model and the effect of the weight of a beam, the existing beam model is modified theoretically. Also, it is shown experimentally that this model can fit to the measured force curves and the weight of the beam effects on the force curve. It can be the indication to design applications using adhesive force. Regarding the energy release rate, in loading process, it is fixed value regardless of the shape of the beam. And considering this value as work of adhesion, energy dissipation can be calculated. However the result contradicts to the existing theories in some points. One of the reasons is considered as the deformation induced by the friction force based on the result of the displacement of the edge $\delta$. Therefore, it is suggested that the shear deformation induced by the friction force should be considered in order to calculate energy dissipation more correctly in the future works.

## References

[1] Geim A. K., Dubonos S. V., Grigorieva I. V., Novoselov K. S., Zhukov A. A. and Shapoval S. Y., "Microfabricated adhesive mimicking gecko foot-hair", *Nature Materials* **2**, 461-463, 2003

[2] Santos, D., Spenko, M., Parness., A., Kim, S. & Cutkosky, M., "Directional adhesion for climbing: theoretical and practical considerations", *Journal of Adhesion Science and Technology*, **21**, pp. 1317-1341, 2007.

[3] Jeonga, H. E., Leeb, J. K., Kima, H. N., Moonb, S. H., Suha, K. Y., "A nontransferring dry adhesive with hierarchical polymer nanohairs", PNAS vol.**106** no.14, 5639-5644, 2009

[4] K. L. Johnson, K. Kendall and A. D. Roberts: *Proc. R. Soc. London A* **324** (1971), pp. 301-313.

[5] K. L. Johnson, et al.: *Tribol. Int.*, 31., 8, p.413-418 (1998)

[6] D. Beak, et al., a master thesis of Tokyo Institute of Technology (2013)

[7] T. Kusakari, et al., a bachelor thesis of Tokyo Institute of Technology (2015)

# A condition-based maintenance policy for Electric Vehicles (EVs)

Student Number: 15M18010 Name: Toshiro Abe Supervisor: Naoya Abe

# 電気自動車のための状態に基づく最適なメンテナンス制度

阿部 敏朗

本論文は、今後の更なる普及が見込まれる電気自動車に対し、車両を構成するコンポーネントの劣化過程を過去のデータを用いて予測し、適切なタイミングで故障を未然に防ぐメンテナンスを行う戦略を提案した。分析結果から、 従来の車検制度のタイミングでメンテナンスを行う場合と本手法を比較した場合、車両の信頼性を同等に保った上で、最大で 40%程度の整備費削減が見込まれることが示唆された。

## 1. Introduction

### 1.1 Inspection and Electric Vehicles (EVs)

Mandatory inspection and the maintenance being carried out for vehicles are assumed to play an important role to ensure road safety by reducing breakdowns as well as to mitigate environmental problem such as air pollution created by the emission from poorly maintained automobile traffic. In Japan, despite the fact that vehicles have experienced dramatic technological development, the periodical mandatory inspection system was revised only twice since it was firstly introduced in 1953.[1]

According to the Ministry of Land, Infrastructure, Transport and Tourism, a vehicle owner typically pays JPY 91,000 to JPY166,000 on every inspection.[2] In fact, it was suggested that the vast majority of current vehicle owners feel maintenance/inspection expenditure as a critical financial burden.[3] This expenditure also refrains potential owners (i.e. people who possess a driving license but choosing not to own a vehicle) from purchasing a vehicle.[4] Even though the target of these surveys was associated with conventional vehicle owners, this tendency may apply to EV owners.

EVs and Internal Combustion Vehicles (ICVs) are different in some respects. Firstly, EVs emit no tailpipe pollutants while they are driven. Secondly, an EV has relatively non-complex mechanical structure compared to an internal combustion vehicle especially in the number of moving parts. For example, a combustion engine consists of 20,000 to 30,000 parts, on the other hand, an electric motor has only 30 to 100 parts.[5] In accordance with the complexity of the structure, it is logical to speculate that EVs may have higher reliability.

When it comes to the future perspective of the diffusion and adoption of EVs in Japan, the Japanese government released its strategy in 2010, which suggests that EVs will account for 20-30% of passenger vehicle sale in 2030.[6] In order to meet the target, the price of an EV, and charging infrastructure have been considered as major obstacles. However, as of 2016, there are more than 40,000 places nationwide where electric car owners could recharge their vehicles.[7] This is more than the number of existing petrol stations in Japan. In addition, battery cost which has been a reason for EV's high price is decreasing. Björn Nykvist et al. (2015) reported EV manufacturers lowered battery price from US$1,000 per kWh to around US$300 per kWh, during 2007 to 2014.[8] They also suggested that the cost of Li-ion batteries continue to decline which makes EVs economically more viable to consumers. The wide diffusion of EVs makes it important to consider new inspection policy mainly designed for EVs.

### 1.2 Design of a maintenance strategy

As the inspection was initially intended to reduce the mechanical breakdown on a vehicle to ensure the road safety, an ideal maintenance strategy for EVs should also maintain vehicles mechanical reliability and preferably financially efficiency. The trade-off here is that the more frequent maintenance actions to keep a vehicle in a good condition, the higher the resulting cost can be. In this respect, condition-based maintenance (CBM) which has been used in many industries such as Information Technologies or Energy, is a promising approach.[9] This approach gives a strategy to perform the minimal number of preventive maintenance actions that can restore the reliability of aged components to avoid costly breakdowns based on the components failure rates in the system.

The CBM approach mainly contains of two steps: a system modeling based on failure rates and an optimization of maintenance decisions according the system modeling, which often involves Monte Carlo simulation, which is the calculation that generates random objects or processes with using a computer.[10] This method enables one to perform a simulation to see how a quasireal-life system which consists of many components with non-linear deterioration mode behaves. However, the difficulty of using the Monte Carlo approach is the computing time, because one has to run several hundred or thousands of simulations for every single step of optimization of maintenance decision.

In order to run the Monte Carlo practically, good solutions which meet demand upon evaluation function must be chosen from the solution space with using an optimization algorithm. Since the function being optimized is a decision of preventive maintenance actions which is expressed as a discrete problem where information of the function is expressed as an independent bit, typically {0,1}, Genetic Algorithms (GAs) which employs binary strings is suitable as an optimization approach.

## 2. Objectives and Contribution

### 2.1 Objectives

A CBM approach with flexible interval maintenance policy based on the vehicle condition is proposed. This aims to identify: (i) the times in which preventive maintenance actions should be performed to minimize the necessary total

maintenance cost, including the recovery cost for breakdowns, and (ii) how CBM is effective in reducing the lifetime maintenance cost compared to existing inspection policy.

## 2.2 Significance of the study

EVs have been adopted to the Japanese market at unprecedented speed. Despite the penetration, there have not been proactive discussions for the reform of their inspection policy. This study is proposing a financially favorable maintenance strategy for EVs through a quantitative analysis, and the outcome of the study is expected to provide policy-makers insights for the introduction of new inspection policy specifically for EVs.

# 3. Methodology

## 3.1 System modeling

The system resembling an EV consists of eight critical components connected in series, and the system shows a breakdown when single component causes a malfunction. (See Figure 3-1). Due to the similarity of mechanical structure between an EV and a conventional vehicle, the selection of critical components follows current inspection practice which is speculated to be designed upon the consideration of road safety. On top of that, components unique to an EV (electric motor and battery) are added in the system.

The deterioration process of each component is assumed to follow a Weibull distribution, which is commonly used within reliability engineering due to its versatility and relative simplicity. The most general expression of the Weibull distribution is given by the two parameters: $\beta$ as a shape parameter and $\eta$ as a scale parameter. The values of these parameters used in the study can be found in Figure 3-1.

Figure 3-2 describes the transition of failure rate on each component. It can be seen that a component with larger $\eta$ generally shows higher reliability. The failure data for the components were retrieved from a report from the Japanese government and a non-profit organization called Plug in America.[10 11] In addition, in this study, it is assumed that a preventive maintenance action returns the components to an "as good as new" condition.

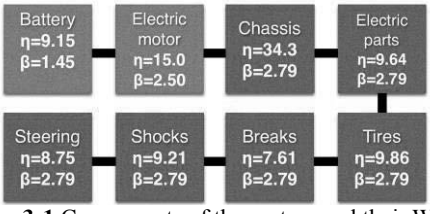


**Figure 3-1** Components of the system and their Weibull parameter settings

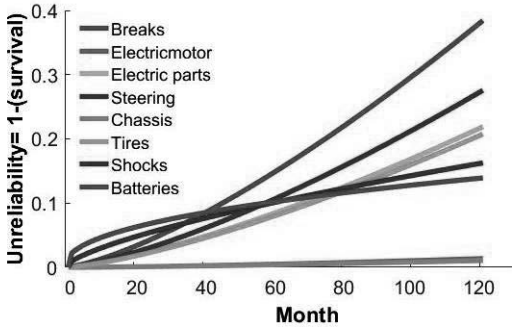


**Figure 3-2** Transition of unreliability on components over time

## 3.2 Optimization

### *3.2.1 Genetic Algorithms*

In this problem, an individual must encode all possible scheduling combinations for all system components. Since we want to know when and how many actions must be carried out, in this sense, a binary string so-called individual is employed. Each individual has a length of *Nc* bits ($T_M \times 12 \times$number of component), and its decoding is such that a '1' means that component is selected to have preventive maintenance, while '0' means no action is carried out on that time-unit. Multiple numbers of individuals are the population. After initialization of the first population, the fitness of each individual in population is evaluated by objective function. Then, two individuals are chosen and mated to produce new individuals for the next generation. These new individuals can be modified again by mutation. This continues until a termination condition is met. (See Figure 3-2 right)

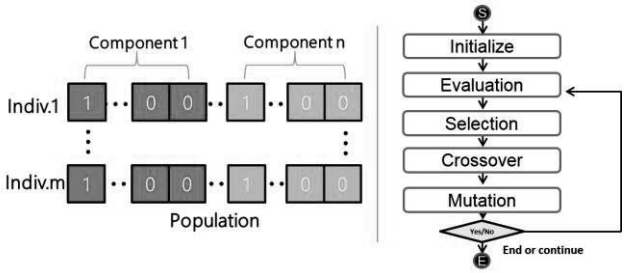


**Figure 3-2** A string representation of maintenance strategy and an outline of GAs

### *3.2.2 Objective function*

The objective function for evaluating a given set of individuals is to reduce the sum of preventive maintenance cost $C_M$ and corrective maintenance cost $C_R$ and repair cost within the mission time $T_M$.

$$\mathrm{G} = \min\ (C_M + C_R) \qquad \text{(eq.4.1)}$$

Preventive maintenance cost $C_M$ can be written as eq.4.2 $Nc$ is the number of components, $n_M$ is the number of maintenance activities in total through the mission time. $n_{Mi}$ is the number of preventive maintenance on component *i*. $C_{MB}$ is the base cost per single maintenance intervention and $C_i$ is the component specific cost.

$$C_M = n_M C_{MB} + \sum_{i=1}^{Nc} n_{Mi}\, C_i \qquad \text{(eq.4.2)}$$

$C_M$ consists of the component dependent cost $C_i$ and the base cost $C_{MB}$, which represents the minimum cost to carry out preventive maintenance actions including agency fee, and basic labor cost. This setting encourages one to perform preventive maintenance on several components at the same timing to save $C_{MB}$.

$$C_R = \sum_{i=1}^{Nc} \sum_{t=1}^{T_M} C_{Ri} \cdot I_{Ri}(t) \qquad \text{(eq.4.3)}$$
$$C_{Ri} = \mu_{Ri} + L_c \qquad \text{(eq.4.4)}$$

$C_R$ is the total corrective maintenance cost which occurs after a breakdown of a component. $C_{Ri}$ is the repairing cost per time on component *i* which consists of labor cost $L_c$ and base cost $\mu_{Ri} I_{Ri}(t)$ is a characteristic function equal to 1 if the component *i* is under repair at time-unit *t* and 0 otherwise.

*3.2.3 Cost parameters and simulation settings*

Cost parameters are the crucial factors that determine the lifetime maintenance cost of an EV. Since these parameters heavily depend on a variety of factors such as the type of a vehicle, the situation of breakdown, the type of maintenance garage and so forth. However, this study is focusing on the comparative analysis of flexible maintenance strategies; therefore, considerably appropriate cost parameters are estimated based on the available data. The mission time here is set as 13 years with the consideration of the average ownership period for passenger cars in Japan as well as the battery lifetime. In order to save computational time, one month is the minimal time unit.

**Table 3-1** Cost parameters for preventive maintenance and corrective maintenance

| Comp. | $C_{MB}$ (JPY) | $C_{MBi}$ (JPY) | $l$ (JPY) | $C_R$ (JPY) | Source |
|---|---|---|---|---|---|
| **Steering** | 70,000 | 10,000 | 8,000 | 165,000 | Yourmechanic.com |
| **Breaks** | 70,000 | 10,000 | 8,000 | 58,000 | Costhelper.com |
| **Tires** | 70,000 | 10,000 | 8,000 | 19,000 | Costhelper.com |
| **Shocks** | 70,000 | 10,000 | 8,000 | 85,000 | Costhelper.com |
| **Electric parts** | 70,000 | 10,000 | 8,000 | 56,000 | Nationwide Inspections |
| **Chassis** | 70,000 | 10,000 | 8,000 | 400,000 | Rakuten insurance |
| **Electric Motor** | 70,000 | 10,000 | 8,000 | 200,000 | Alibaba |
| **Batteries** | 70,000 | 10,000 | 8,000 | 620,000 | Inside EVs |

## 4. Results

This study mainly focuses on whether a CBM strategy could reduce the lifetime maintenance cost compared to the 3-2-2-year fixed maintenance interval where inspection is performed after three years from the purchase of an EV and then every two years. This corresponds to the current vehicle inspection policy.

Three types of maintenance strategies are employed; a zero-maintenance with no preventive maintenance actions, fixed interval strategy, and flexible interval CBM strategy.

Table 4-1 shows the result of the CBM strategy. CBM suggests the four times of preventive maintenance activities on a vehicle within $T_M$ (=13 years) and the resulting lifetime maintenance cost was JPY 490,000, which is approximately 48% less than the zero maintenance strategy.

**Table 4-1** Simulation result of CBM and zero maintenance

| Component | 1st (Month) | 2nd (Month) | 3rd (Month) | 4th (Month) |
|---|---|---|---|---|
| 1.Breaks | 5 | | 63 | 96 |
| 2.Electric | 5 | | | |
| 3.Electric parts | | 21 | | 96 |
| 4.Steering | | 21 | | 96 |
| 5.Chassis | - | - | - | - |
| 6. Tires | | 21 | | 96 |
| 7.Shocks | 5 | | 63 | |
| 8.Batteries | - | - | - | - |
| Cost for flexible interval strategy (JPY) | | | | 490,000 |
| Cost for zero maintenance strategy (JPY) | | | | 1,011,100 |

Figure 4-2 indicates that the optimization of the CBM strategy has decreased both maintenance cost and numbers of breakdown on all components. In the end of the optimization (generation=10,000), for the average of 8 components, it showed only 11% of breakdowns compared to the no maintenance strategy before the optimization.

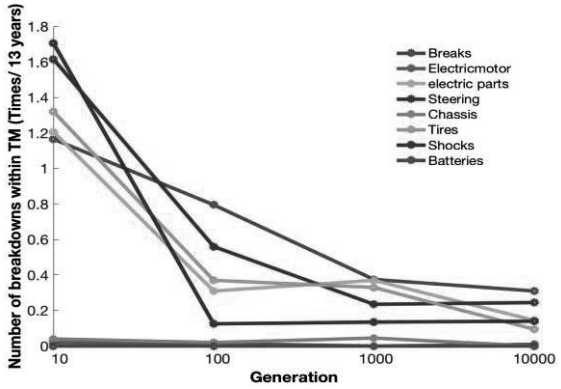


**Figure 4-2** Number of expected breakdowns on components by GAs generation

Figure 4-3 suggests the lifetime maintenance cost of an EV with different maintenance intervals. The lifetime maintenance cost of the 3-2-2-year strategy was JPY 815,240. This was approximately 40 % more expensive than the CBM strategy. Among all fixed interval strategies, the 5-year interval showed the highest cost efficiency of maintenance, which was JPY 567,700. In the figure, when the intervals are relatively shorter or longer, the maintenance costs were high. In the former case, this is because excessive numbers of preventive maintenance actions were performed, and in the latter case, the lack of preventive maintenance actions resulting in higher chances of getting breakdowns.

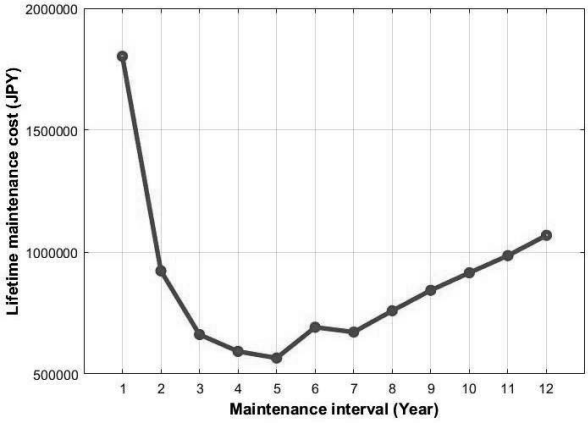


**Figure 4-3** Lifetime maintenance cost as a function on maintenance interval

Figure 4-4 illustrates the comparison of reliabilities among three different strategies: CBM strategy, 3-2-2-year fixed interval strategy and zero maintenance strategy respectively. CBM and fixed interval maintenance strategies showed dramatically higher reliabilities compared to the zero-maintenance strategy. It could be inferred that the right number of maintenance actions have reduced failures. However, it is also reasonable to point out that every preventive maintenance action leaps the system reliability to as good as the initial condition in the simulation.

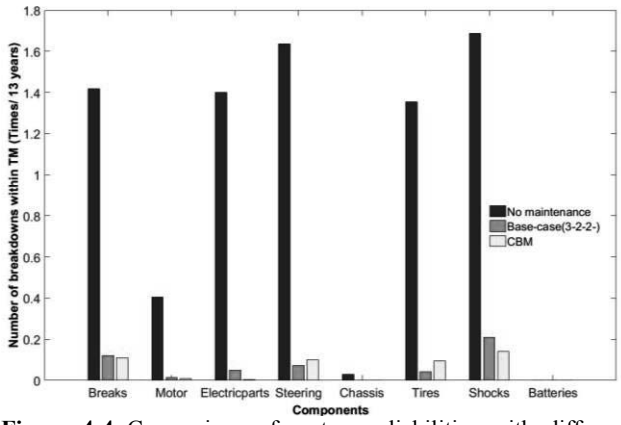


**Figure 4-4** Comparison of system reliabilities with different strategies

Figure 4-5 and Figure 4-6 report the reliability of the system and lifetime maintenance cost obtained by flexible-interval CBM when the cost parameters $C_R$ (corrective maintenance) and $C_M$ (preventive maintenance) are multiplied by the factors $C_T$ as well as $P_T$ that vary from 0.2 to 5.0.

In Figure 4-5, when $C_T$ is small, fewer preventive maintenance actions were preferred. This is because when the corrective maintenance cost was small, the incentive to decrease the number of breakdowns also became small. However, the increase of the factor $C_T$ encouraged frequent preventive maintenance actions which result in smaller number of breakdowns at $C_T$ =2.0 and $C_T$ =5.0 in the figure.

In Figure 4-6, when the cost for preventive maintenance activities was as small as $P_T$=0.2, a strategy with frequent preventive maintenance actions was performed since one can hold a high system reliability and a low lifetime maintenance cost at the same time. On the other hand, when $P_T$ is larger than 2.0, it was inevitable to experience higher maintenance expenditure since the replacement cost generally is high, and preventive maintenance, that can decrease the number of breakdowns, became expensive.

It is worthwhile noticing that the cost parameter regarding the cost of preventive maintenance actions greatly affected the lifetime maintenance cost. By changing $C_T$, the cost varies from JPY 430,600 to JPY 670,000 so that the maximum cost with this setting has increased by approximately 150%. However, the change in cost parameter $P_T$ from 0.2 to 5.0 resulting in the increase of lifetime cost of JPY 430,510 to JPY 1,201,900 that is equivalent of 258 % of increase.

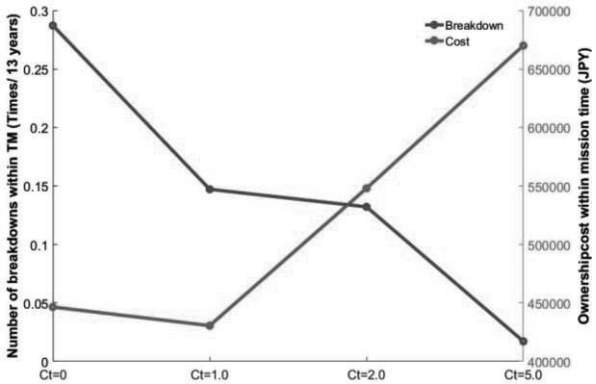


**Figure 4-5** Sensitivity of reliability and maintenance cost to different corrective maintenance cost parameters

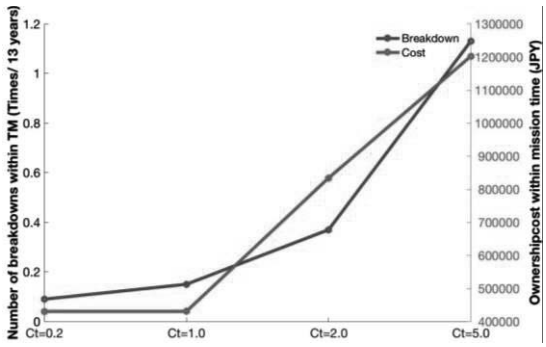


**Figure 4-6** Sensitivity of reliability and maintenance cost to different preventive maintenance cost parameters

## 5.Conclusion

The result is confirming that not only CBM can possibly cut down the maintenance cost within vehicle lifetime, but also it enables to operate a vehicle with high reliability comparable to the maintenance actions under the current inspection policy. Several remarks are summarized as follows: (i) the lifetime maintenance cost for the CBM strategy was JPY 490,000 and the preventive maintenance actions were performed for four times within $T_M$, and (ii) CBM strategy can potentially decrease approx. 40% of the maintenance cost compared to the current 3-2-2-year fixed interval strategy which was JPY 815,240.

In addition, in the fixed-interval case, the 5-year interval was optimal and it showed the highest cost efficiency with maintenance cost being 38% smaller compared to the one with the 3-2-2-year strategy, however, it was still 15% more costly than the CBM strategy. Furthermore, the sensitivity analysis revealed that the amount of lifetime maintenance expenditure is more sensitive to preventive maintenance cost parameters than corrective maintenance cost parameters, and therefore it is logical to assume that decreasing the cost per single preventive maintenance action possibly has a strong impact on the reduction of an EV's lifetime maintenance cost.

Our result is encouraging the introduction of the CBM maintenance strategy for EVs. However, several works remain to be done for future studies as listed following:(i) identifying the effect of imperfectness of the preventive maintenance by conducting several different scenarios and evaluate the effect both on reliability and lifetime maintenance cost,(ii) increasing the number of components with more precise component structure (e.g., try a different kind of model such as parallel logic),and (iii) designing a simulation program for the run on TSUBAME (a large-scale supercomputer) which enables us to obtain a more precise result with a more complex system.

## References

[1] Japan Automobile Manufacturers Association. (2014). *History of automobile inspection system and significance and role of automobile inspection*.vol.48. pp. 2-8.
[2] Ministry of Land, Infrastructure and Transport Vehicle Transportation Bureau. (2005). *Basic Survey Results Report on Automobile Inspection*, Inspection and Maintenance Report
[3] Life media. (2014). *Survey on vehicle owners*. Retrieved January 12, 2017.
[4] Sony Assurance. (2014). *National Car Life Survey*, Retrieved January 12, 2017.
[5] NIKKEI, Inc. (2010). *Disappearance of parts on a vehicle -The identity of an electric car (4)*. Nikkei Shimbun. Retrieved January 12, 2017.
[6] METI (2010) *Next Generation Vehicle Strategy*. http://www.meti.go.jp/english/press Retrieved January 12, 2017
[7] Coutler,T.(2015). *Japan Now Has More EV Chargers Than Gas Stations*. Bloomberg Retrieved January 12, 2017
[8] Nykvist,B & Nilsson,M.(2015). Rapidly falling costs of battery packs for electric vehicles, Nature Climate Change 5, 329–332
[9] Gray,C- Watson,S.(2009).*Physics of Failure approach to wind turbine condition based maintenance.* Wind Energy.vol. 13(5) ,pp. 395–405.
[10] Marseguerra,M. E,Zio.(2000).*Genetic algorithms and Monte Carlo simulation for optimal plant design*, Reliability Engineering & System Safety Volume 68, Issue 1, pp 29–38.

# A study of leasing scheme and its perception for the diffusion of residential electricity storage system

Student Number: 15M18026 Name: Junya ISHIDA Supervisor: Naoya ABE

# 一般家庭用蓄電池システム普及におけるリース制度と利用者意識に関する研究

石田純也

本論文では、家庭レベルの蓄電池システムの普及を促す方策を検討するため、日本における蓄電池リース事業の契約者を対象にアンケート調査を行った。調査では、導入に至る経緯や使用実態を把握するとともに、システム導入に伴う満足度や要望と経済的便益の関係を明らかにした。その結果、蓄電池システムの満足度に対して、経済的便益や蓄電システムに対する理解度、技術的に新しい製品を使用することに対する満足感が統計的に有意に影響を及ぼし、また当該リース制度により経済的便益を享受していない利用者の存在を推定した。

## 1. Introduction

### 1.1 Background

Electricity storage system (ESS) is becoming one of the key options for grid stabilization and distributed power system, under the given state of the rapid growth of renewable energy sources (RES) in Japan, partially due to the Great East Japan earthquake in 2011. Because of feed-in tariff started in 2012, photovoltaic (PV) system is rapidly being diffused in household sector. One of the expected uses and roles of ESS is to be installed in households and help to cope with those issues in addition to bringing to the benefits to the ESS users.

There are two ESS's representative benefits for households. ESS can provide them with opportunities to save electricity bill and can be used as an emergency power source. Since ESS literally stores electricity, users can shift the timing of purchasing electricity, allowing ESS users to buy cheaper night-time power for the electricity consumption in daytime when the tariff is higher. Also, ESS users with PV systems can charge surplus electricity produced by a peak difference between the generated electricity from a PV systems and household electricity demand. Currently, due to feed-in tariff scheme, selling such surplus electricity to utilities is more profitable than self-consumption. However, the profitability in the future is uncertain as FITs is becoming less financially attractive, implying that self-consumption will become financially more important. The role of ESS can become more significant in the future and thus its further diffusion is expected.

ESS has, however, several issues to be overcome such as expensive introduction cost and recovering the cost. [1] [2] Hence, this study focused on residential ESS leasing as it is an affordable introduction form of ESS to its users. Lease scheme is a financial contract to introduce new equipment with paying fixed monthly costs. Its main advantage for consumers is to mitigate the burden of initial payment. For companies, one of the advantages is to capture more customers, which in turn contributes to modestly stable revenue streams, even though the sale per contact is relatively lower.

**Table 1** Pros and Cons of lease scheme [3][4]

| | Consumer | Companies |
|---|---|---|
| Pros | •Mitigating initial cost<br>•Avoiding obsolescence<br>•Tax saving | •Sales promotion<br>•Certain and fast money collection |
| Cons | •Losing salvage value<br>•Unsatisfaction due to no ownership<br>•Fixed financial burden | •Disposal of property after termination |

**Table 2** Example of ESS lease by ONE energy [5]

| | |
|---|---|
| Contract period | 10 years |
| Monthly cost | 9,396 JPY (Tax included) |
| Total of monthly costs | 1,127,520 JPY (Tax included) |
| Charging capacity | 5.53kWh |
| Other services | Monitoring, Performance guarantee |

In Japan, ONE Energy Corporation (ONE Energy) is a leading company for ESS leasing business since 2013, and this study was conducted in partnership with this firm.

### 1.2 Previous studies

#### 1.2.1 Profitability of ESS

For profitability of ESS, there are several studies, which focus on a combination of PV system and ESS. Researchers generally mentioned the significance of electricity consumption pattern in addition to technical characteristics and the introduction cost of them. [6][7] Conformity of that pattern to PV's electricity generation profile is important in terms of economics. Thus, life style is one of the significant factors for profitability of ESS.

Also, some researchers pointed out the economic importance of self-consumption in the future where electricity selling price is very low after feed-in tariff is expired. [8][9] To achieve more economically effective PV system use in the future, ESS is expected to play a significant role since it can stock surplus electricity and increase self-consumption.

#### 1.2.2 Consumer preference for ESS

In 2013, Sekisui Chemical Company, Limited and Environmental Research Institute, Inc. conducted a questionnaire survey targeting actual ESS users in Japan. [10] So far, there are no similar surveys. It revealed that many users are satisfied with ESS because of saving electricity bill and the potential use as an emergency power source. In addition, this study found that some household run out charged electricity within a day while the others does not, which resulted in difference of their satisfaction. Since if or not a user runs out charged electricity depends on amount of discharged electricity and capacity of ESS, the importance of life style and introduction of ESS with an adequate capacity was confirmed. In addition, this survey implies that users with deeper understanding of ESS and Home Energy Management System (HEMS) are more satisfied with ESS.

### 1.2.3 Consumer preference for leasing scheme

Some studies investigated consumer preference for leasing scheme of home appliances and cars. [11][12][13] They revealed that the users were satisfied with cheapness of monthly payment and found that leasing scheme caused concerns about damages to borrowed equipment and unsatisfaction due to the lack of ownership.

## 2. Objectives and Contribution

Since there are no surveys targeting actual ESS leasing users, their situation and attitudes toward ESS and its leasing are not revealed. For the further diffusion of ESS, it is significant to know consumers' actual situation, especially their subjective satisfaction and economic benefits, and to empirically propose further ESS diffusion strategies. Therefore, the objectives of this study are to investigate:

(1) the ESS users' motivation and satisfaction with ESS

(2) the relationship between the satisfaction level and economics benefits for the users under leasing scheme

By suggesting further ESS diffusion strategies based on empirical results, companies can improve consumers' satisfaction with ESS. Higher satisfaction and solving user's complaints contribute to further ESS diffusion and its sustainable use.

## 3. Data collection and methodology

### 3.1 Data collection

With the cooperation of ONE Energy, questionnaires were sent to 500 customers. They used ESS for at least 1 year or longer and live in Japan, except in both Hokkaido and Okinawa as there are no users in those two regions. The collection period for the survey was between 11th November 2016 and 16th December 2016. For those who responded this survey, honorarium was provided, which was equivalent to JPY1,000. All private information about the users were kept confidentially so that the questionnaires were sent and collected by ONE Energy while the design of the questionnaire was made by the author and the author's affiliated research group.

The questionnaire consisted of three sections: section A) Questions about your behavior and opinion to electricity and its system, section B) Questions about your behavior and opinion to ESS and its leasing, and section C) Questions about your basic information. For example, there were questions for electricity bill, electricity bill saving by ESS, introduction of PV system, and so on in section A, questions for satisfaction of ESS leasing, financial satisfaction of ESS leasing, a sense of security from ESS, and so on in section B, and questions for gender, age, household income, and so on in section C.

### 3.2 Methodology

### 3.2.1 Ordered logistic regression analysis

In order to find the factors affecting satisfaction of ESS leasing (eq.1) and financial satisfaction (eq.2), analyses with ordered logistic regression were conducted. The variables are shown in Table 3. The model equations are:

$$\ln\left\{\frac{P(Y_1 > j|x)}{P(Y_1 \le j|x)}\right\} = \sum_{i=1}^{10} \beta_{1.i} x_{1.i} - \mu_j \qquad \text{eq.1}$$

$$\ln\left\{\frac{P(Y_2 > j|x)}{P(Y_2 \le j|x)}\right\} = \sum_{i=1}^{11} \beta_{2.i} x_{2.i} - \mu_j \qquad \text{eq.2}$$

**Table 3** Variables for regression and clustering

| eq.1 | eq.2 | CA | Meaning (Unit) | Range |
|---|---|---|---|---|
| $Y_1$ | - | $V1$ | Satisfaction of ESS leasing (C5) | 1~5 |
| $x_{1.1}$ | $Y_2$ | $V2$ | Financial satisfaction (C5) | 1~5 |
| $x_{1.2}$ | - | $V3$ | Sense of security from ESS (C5) | 1~5 |
| $x_{1.3}$ | - | $V4$ | Satisfaction with having a technically new equipment (C5) | 1~5 |
| $x_{1.4}$ | $x_{2.1}$ | $V5$ | Demand for new plan which is suitable with future price menu for ESS (C5) | 1~5 |
| $x_{1.5}$ | $x_{2.2}$ | $V6$ | how much your consciousness about electricity bill and electricity menu is changed after installing ESS (C5) | 2~5 |
| $x_{1.6}$ | $x_{2.3}$ | - | Understanding for ESS (C4) | 1~4 |
| $x_{1.7}$ | $x_{2.4}$ | - | Gender (Dummy) | - |
| $x_{1.8}$ | $x_{2.5}$ | - | Age (C5) | 0~4 |
| $x_{1.9}$ | $x_{2.6}$ | - | PV system (Dummy) | - |
| $x_{1.10}$ | $x_{2.7}$ | - | Contraction (C4) | 1~4 |
| - | $x_{2.8}$ | - | Household income (C7) | 1~7 |
| - | $x_{2.9}$ | - | Average monthly electricity bill saving (JPY) | -2,000 ~ 13,500 |
| - | $x_{2.10}$ | - | Amount of monthly electricity consumption (kWh) | 5 ~ 1,592 |
| - | $x_{2.11}$ | - | Monthly lease fee (JPY) | 1,000 ~ 4,900 |

CA = Cluster analysis
C(n) = Categorical variable which is n grade evaluation

Here, $\beta$ is a coefficient. $\mu$ is a threshold. Since both $Y_1$ and $Y_2$ are categorical variable with 5 grade evaluation, $j = 1,2,3,4$. $Y_1$ is the overall satisfaction of ESS leasing. $x_{1.1}$ ( $Y_2$ ), $x_{1.2}$, $x_{1.3}$, $x_{1.4}$ ( $x_{2.1}$ ), and $x_{1.5}$ ( $x_{2.2}$ ) are specific satisfactions and opinions. $x_{1.6}$ ($x_{2.3}$) is understanding which is how precisely you know capacity of your ESS and how deeply you understand function of ESS. $x_{1.9}$ ($x_{2.6}$) is if or not you own a PV system. $x_{1.10}$($x_{2.7}$) is how deeply you were involved in your leasing contraction, for example, if or not you are a contractor. $x_{2.9}$ is an estimation of monthly electricity bill saving by ESS. In the questionnaire survey, respondents were firstly asked which month's electricity bill was the highest/lowest in the latest one year after installing ESS. Secondly, they were asked how much the months' electricity bill were changed. Hence, electricity bill savings of "highest-electricity-bill month" and "lowest-electricity-bill month" were obtained, respectively. $x_{2.9}$ is an average of those two electricity bill savings. $x_{2.10}$ is monthly electricity consumption in May 2016. $x_{2.11}$ is monthly lease fee. This fee varies depending on subsidies from the central government and local governments, and also some users are compensated for lease fee by house manufactures.

Sample numbers are 223 for eq.1 and 104 for eq.2. Considering multicollinearity, all VIFs were confirmed to be less than 10.

### 3.2.2 Cluster analysis

To identify group of users and their common characteristics, cluster analysis was conducted. Table 3 shows variables for this analysis. All of them are 5-ranked categorical variables. With regarding them as quantitative variable, they were not standardized. The detailed calculation method is hierarchical cluster analysis with ward's linkage method by Euclidean distance.

# 4. Result

## 4.1 Results of Questionnaire survey

As the result of the survey, 316 responses were received, and 315 of them were valid. Response rate was 63.0%. 149 of 315 respondents perfectly answered, and the other answers included blanks or mistakes.

In section C, respondents were asked their basic information. Majority of respondents are male (74.3%). Their ages are relatively older such as 30s (22.5%), 40s (31.7%), 50s (25.7%), 60s (18.1%). Household income is also high. Those whose income is more than 4 million JPY accounts for 80.0%. The median of Japanese household's income is 4.27 million JPY. [14] In addition, they are assumed to be households consuming large amount of electricity. 67.6% of them live in all-electric houses.

In section A, respondents were asked their behavior and opinion to electricity and its system. Regarding PV system, only 37.2% of them own the systems. The respondents who do not have PV systems were asked how much they would like to introduce PV systems. 23.2 % of them expressed positive response. For electricity bill, respondents answered two electricity bill saving as already explained in 3.2.1. Figure 1 is a comparison of average monthly electricity bill saving and monthly lease fee. For the horizontal axis, right-side households have higher lease fee and higher average electricity bill saving. Although this calculation is not mature, there are 25.8% of the respondents who might not obtain financial benefit from ESS leasing.

In section B, respondents were asked their behavior and opinion to ESS and its leasing, for example, satisfaction of ESS leasing, its reasons, financial satisfaction, sense of secure from ESS, and understanding for ESS. For satisfaction of ESS leasing, 69.5% (223 people) of the respondents are satisfied, 21.3 % (67 people) are "satisfied and unsatisfied", and 6.6 % (21 people) are unsatisfied. For the reason of "satisfied", 73.5% of 223 people chose "saving electricity bill". Only 17.0 % of them chose "sense of secure". For the reason of "unsatisfied", 38.1 % of 21 people chose "Not saving electricity bill". 19.0 % of them said "The capacity of ESS is not enough". Another 19.0 % of them chose "The merit of ESS is not clear". Also, 152 people answered free comments about their unsatisfaction and anxiety for ESS leasing. 29 people of them complained or wondered about financial benefit of ESS leasing. 25 people worried about what would happen when ESS leasing is expired, for example, if or not they can continue ESS leasing after it, and some of them complained about additional costs when removing ESS. 23 people of them complained about the capacity of ESS in this question as well.

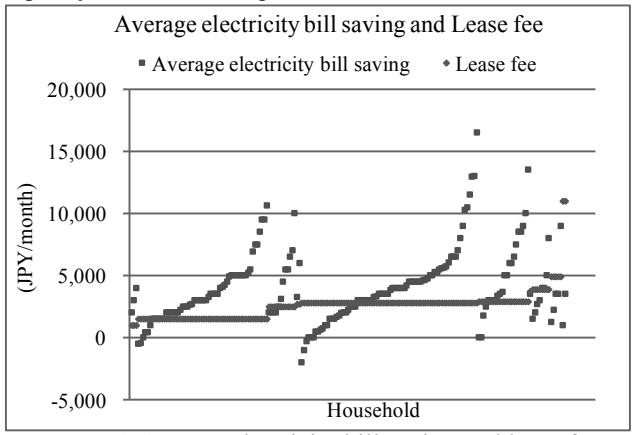


**Figure 1** Average electricity bill saving and lease fee

**Table 4** Result of ordered logistic regression

| eq.1 | Odds ratio | | eq.2 | Odds ratio | |
|---|---|---|---|---|---|
| $x_{1.1}$ | 6.21 | *** | $x_{2.1}$ | 1.0296 | |
| $x_{1.2}$ | 0.89 | | $x_{2.2}$ | 1.6450 | * |
| $x_{1.3}$ | 2.15 | *** | $x_{2.3}$ | 1.2772 | |
| $x_{1.4}$ | 1.01 | | $x_{2.4}$ | 3.8831 | * |
| $x_{1.5}$ | 0.83 | | $x_{2.5}$ | 1.1353 | |
| $x_{1.6}$ | 2.08 | *** | $x_{2.6}$ | 0.9125 | |
| $x_{1.7}$ | 1.47 | | $x_{2.7}$ | 0.4921 | |
| $x_{1.8}$ | 0.83 | | $x_{2.8}$ | 1.0924 | |
| $x_{1.9}$ | 1.79 | * | $x_{2.9}$ | 1.0004 | *** |
| $x_{1.10}$ | 0.66 | | $x_{2.10}$ | 1.0004 | |
| - | - | | $x_{2.11}$ | 0.9991 | *** |
| AIC | 371 | | AIC | 250 | |
| Puseudo-$R^2$ | 0.329 | | Puseudo-$R^2$ | 0.174 | |
| Sample Number | 223 | | Sample Number | 104 | |

(Note) *** : p<0.01、** : p<0.05、* : p<0.1

## 4.2 Results of ordered logistic regression

Table 4 shows the results of ordered logistic regression. Puseudo-$R^2$ of eq.1 is 0.329, and that of eq.2 is 0.174. In eq.1, $x_{1.1}$ (Financial satisfaction), $x_{1.3}$ (Satisfaction with having a technically new equipment), and $x_{1.6}$ (Understanding for ESS) are statistically significant at 1 % level. Those odds ratio is more than 1, which means that those have positive effect on satisfaction of ESS leasing. On the other hand, in eq.2, $x_{2.9}$ (Average monthly electricity bill saving) and $x_{2.11}$(Monthly lease fee) are statistically significant at 1 % level. Odds ratio of $x_{2.9}$ is more than 1 and has a positive effect on Financial satisfaction. That of $x_{2.11}$ is less than 1 and has a negative effect.

## 4.3 Cluster analysis

Figure 2 shows dendrogram for cluster analysis. Because of data availability for V1, V2, V3, V4, V5 and V6, sample number is 278. To understand detailed characteristics of user groups, dividing respondents into 7 clusters are chosen here. Figure 3 shows average scores of each variable for each cluster. V1 and V2 have a strong positive correlation. Relationships between $V_1$ and the others are conditional on each cluster. Reviewing it, each cluster's characteristics are described in Table 5.

# 5. Discussion

From questionnaire survey, it was firstly confirmed that respondents were elder and rich. Even though the introduction cost is mitigated due to leasing scheme, users, who are early adopters, are such wealthy people. Also, they seem to be households consuming a large amount of

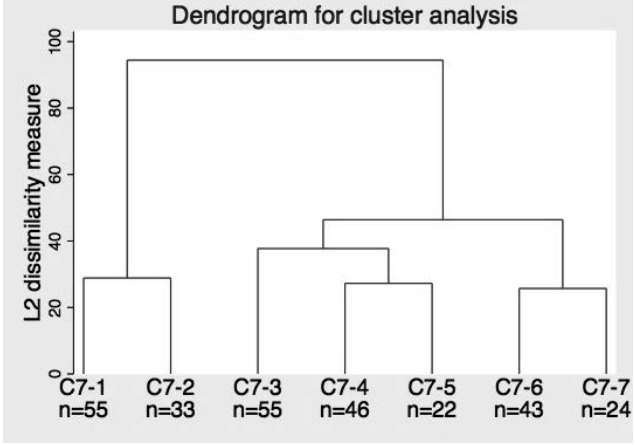


**Figure 2** Dendrogram for cluster analysis

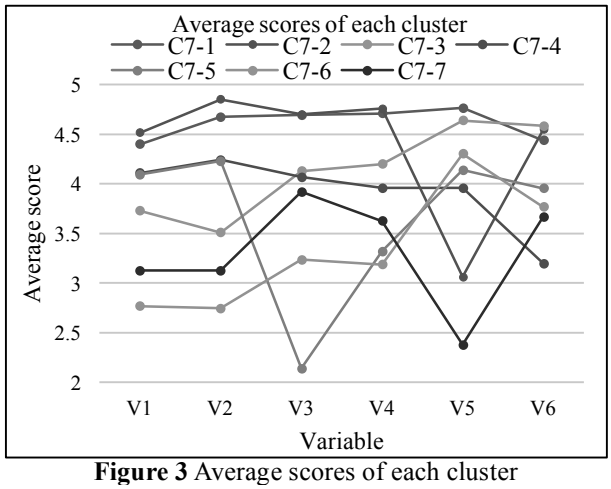


**Figure 3** Average scores of each cluster

**Table 5** Characteristics of clusters

| Cluster | Expected characteristics |
|---|---|
| C7-1 (n=55) | They are very satisfied with current situation and strongly desire optimized ESS usage plan. |
| C7-2 (n=33) | They are very satisfied with current situation and do not strongly desire optimized ESS usage plan. |
| C7-3 (n=55) | They feel relatively little financial benefit and strongly desire to improve it. |
| C7-4 (n=46) | They are satisfied with current situation, but their attitude toward electricity bill was not so changed. |
| C7-5 (n=22) | They focus on financial benefit more than other clusters. |
| C7-6 (n=43) | Their satisfaction is very low but strongly desire optimized ESS usage plan. |
| C7-7 (n=24) | Their satisfaction is very low and do not strongly desire optimized ESS usage plan. |

electricity. In fact, 215 of 315 respondents agreed that electricity bill saving was one of the reasons to start ESS leasing. Secondly, introduction of PV systems was checked. Majority of respondents do not own PV systems and did not express high motivation to introduce PV systems in the future. It may imply that a use of ESS itself does not directly cause PV system introduction. Since a tangible reason for this result was not revealed in this study, future works are hoped to identify it. Third, it was confirmed that many users were satisfied with ESS leasing, and it is mainly because of electricity bill saving. However, as shown in reasons of unsatisfaction and Figure 1, some of users does not feel financial benefit or does not obtain financial benefit, and they are not satisfied. Financial issue is, of course, significant. In fact, because of termination of governmental direct subsidy to ESS, lease fee is recently increasing. If all lease fees in Figure 1 were 4,900 JPY/month, 68.8 % of the respondents would not obtain profit. Although this is not accurate calculation, it is obvious that relationship between electricity bill saving and lease fee is very sensitive, considering current assumed electricity bill saving. Finally, it is also considered that lack of capacity can be a reason of unsatisfaction. In the questionnaire survey, this point was not directly asked, but some respondents complained about it.

From ordered logistic regression analysis, it was confirmed that satisfaction of ESS is increased by financial satisfaction, satisfaction with having a technically new equipment, and understanding for ESS. Since high satisfaction with having a technically new equipment and deep understanding for ESS are considered to be unique characteristics of early adopters, satisfaction of ESS leasing will be decreased in the future where users are more ordinal. Therefore, financial satisfaction will be more significant in the future to keep or increase current satisfaction level, and understanding of ESS will be also important because it can be controlled by others while satisfaction with having a technically new equipment cannot. On the other hand, it was not statistically confirmed that sense of secure affected satisfaction of ESS leasing, though it is one of the main merits of ESS.

From cluster analysis, respondents are divided into 7 groups, and each cluster has specific characteristics. It is confirmed that a cluster (C7-7) had very low average of V1, V2, and V5. This might mean that they do not have strong motivation to improve current situation. If there is no help for them, their motivation of continuous ESS use might be lost.

## 6. Conclusion

This study conducted questionnaire survey and analyses with ordered logistic regression and cluster analysis, aiming for investigating (1) the ESS users' motivation and satisfaction with ESS and (2) the relationship between the satisfaction level and economics benefits for the users under leasing scheme. In cooperation with ONE Energy, questionnaires were distributed to 500 customers, and 315 responses were obtained. For (1), most of ESS leasing users are satisfied with it, and it is mainly because of financial benefit. For (2), the satisfaction level is increased by economics benefit. Additionally, it was confirmed that satisfaction with having a new equipment and understanding for ESS also increased the satisfaction level. However, it is assumed that future ESS users will have less satisfaction with a technically new equipment, and financial benefit and understanding for ESS will be more significant. Thus, it is necessity to be considered that the border line of loss and gain might be susceptible to changes of lease fee, and there is an unsatisfied group which does not have a strong motivation for more financial benefit.

Therefore, in order to achieve further ESS diffusion and its sustainable use, it is significant for users to know an effective use of ESS, which leads users' financial states above the border line and which can provide opportunities to deepen understanding for ESS. However, it should be considered that the effective use needs to be friendly enough for those who do not have a strong motivation for more financial benefit.

## Reference

[1] DBJ, (2013), 蓄電池産業の現状と発展に向けた考察
[2] 田頭直人, 池谷知彦, 土屋依子, 馬場健司, (2012), 電気自動車の蓄電機能と家庭用蓄電池に対する一般消費者の意向, 電力中央研究所報告, Y11021
[3] 宮内義彦, (2008), リースの知識<第 9 版>, 日本経済新聞出版社
[4] 加藤建治, (2015), 図解入門ビジネス 最新リース取引の基本と仕組みがよ～くわかる本[第 6 版], 株式会社秀和システム
[5] ONE エネルギー株式会社, ホームページ
[6] 遠藤弘, 小川洋, (1991), 個人住宅用太陽光発電システムの経済性, 電気学会論文誌 D, 112(3), 235-243
[7] 山城迪, 小山貴之, 仲村宏一, 手塚博文, 柿添重光, (1995), 蓄電池機能付き住宅用太陽光発電システムの運用と経済評価, 電 気学会論文誌 B, 115(10), 1234-1241
[8] 大嶺英太郎, 小林広武, 浅利真宏, 上野剛, (2013), PV 設置需要家における蓄電池の経済性評価 -蓄電池設置により経済メリットが生じる条件の検討-, 電力中央研究所報告, R12018
[9] Cucchiella, F., D'Adamo, I., Gastaldi, M., (2016), Photovoltaic energy systems with battery storage for residential areas an economic analysis, Journal of Cleaner Production, 1-15
[10] 積水化学工業株式会社, (2013), 「家庭用蓄電池利用実態アンケート調査」について
[11] 和田安彦, 中野加都子, (2006), サービサイジング普及に向けた家電リース・システムの消費者意識に関する研究 –液晶テレビ を事例として-, 土木学会論文集 G, 62(2), 211-219
[12] 今堀洋子, (2006), 家電のグリーン・サービサイジングに対する利用者の需要性と事業化の方策, 環境科学会誌, 19(4), 347-353
[13]石井康夫, 寺見佑弥, (2013), 個人向け自動車リースに関する生活意識の調査分析, 国際研究論叢, 27(1), 37-58
[14] 厚生労働省, (2015), 平成 27 年 国民生活基礎調査の概況

# Estimation of environmental and economic impacts induced by the promotion of accommodation sharing services based on input-output table

Student Number: 15M18109 Name: Yosuke SOEJIMA Supervisor: Naoya ABE

# 産業連関表に基づく民泊事業推進による環境影響と経済波及効果の推定

副島 洋介

本研究は 2020 年の東京都を事例に、民泊事業の推進を増大する宿泊需要に対する新規宿泊施設建設の代替案として捉え、その環境影響と経済効果を産業連関表に基づき定量化した。その結果、2020 年までに民泊の客室を現行の計画より 10%増やす毎に年間あたりの経済効果を 2.3%～3.2%失うが、$CO_2$ 排出量を 1%～2%削減でき、これは東京都が 2020 年までに掲げる目標 $CO_2$ 削減量の 0.067%～0.13%に相当することが示された。

## 1 Introduction

### 1.1 Accommodation capacity problem and rise of accommodation sharing services

Today, the capacity of accommodation facilities in Japan has drawn serious attentions as the country will host the Olympic and Paralympic Games in Tokyo in 2020 and the accommodation capacity in that year may be insufficient for inbound foreign visitors for the significant event. Along with this concern, ICT based accommodation services are now growing rapidly. For instance, Airbnb [1], ICT based accommodation matching service, has 60 million users all around the world since its foundation in 2008. The Japanese government is also testing the impact of accommodation sharing by deregulating the laws in Ota ward, Osaka and Kitakyushu city in 2016. These insufficient accommodation and accommodation sharing could be inter-related with each other as the growth of latter may mitigate the concern of the shortage of the accommodation in 2020 and beyond.

An important property of the promotion of accommodation sharing is that it doesn't require large scale construction so that there is little cost and time for infrastructure development, which can consequently mitigate environmental burden too. In contrast, traditional hotels need large scale construction which can induce larger economic impact as well as environmental impact since construction involves various industries' production activity such as materials and machineries. In short, there can be trade-off relationship between economic and environmental effect of these two accommodation modes. Therefore, it is important to quantify the effects of the two aspects for the two different approaches to accommodate the increasing foreign visitors to Tokyo.

### 1.2 Energy consumption and GHG emission in accommodation sectors

The increase of accommodation facilities can be divided into construction stage and operation stage with different main operators: construction industry and accommodation service industry or hosts of accommodation sharing respectively. According to Tokyo metropolitan government [2], the amount of $CO_2$ emission in Tokyo was 54M t-$CO_2$ in 2010, and construction industry accounted for 2.8% (1.5M t-$CO_2$), and accommodation service industry accounted for 1.8% (1.0M t-$CO_2$) among them. Accommodation sectors including construction and operation emitted relatively huge amount of $CO_2$. Similarly, average $CO_2$ emission by the operation of hotel rooms was 125.2 kg-$CO_2$/$m^2$ while general household sector was 59.3 kg-$CO_2$/$m^2$ in 2012 [3], which is about half of the emission from the hotel operation.

There is a case that the increasing visitors' demand might decrease after 2020. In that cases, hotels which will be constructed in the future would be a problem in terms of profitability and environmental burden. Once hotels are constructed, it should be used for decades so that decision making whether constructing traditional hotels or promoting accommodation sharing services should be carefully concerned.

### 1.3 Existing studies relating construction and accommodation service industries

There are several studies, which estimate economic impact of tourism activities. Musha [4] examined economic impact throughout several prefectures induced by a tourism event held in Nara. Sakurai et al. [5] evaluated the contribution of tourism industry in Hokkaido economy by setting some future scenarios.

In addition, estimation of environmental impact induced by construction and operation of buildings have been investigated for a long time. National institute for environmental studies [6] developed database which reflect environmental impact per unit of production among 400 industrial sectors. Urushizaki et al. [7] analyzed time series $CO_2$ emission generated by construction sector. Yoshioka et al. [8] estimated the change of $CO_2$ emission including construction stage and operation stage after the introduction of energy saving facilities in general houses.

Some studies pointed out characteristic of users of accommodation sharing services and analyzed its effect to accommodation service industry in economical point of view. Hamari et al. [9] and Tussyadiah et al. [10] investigated people's motivation of using Airbnb. Zervas [11] analyzed correlation between traditional hotels and the diffusion of Airbnb.

However, those existing research mainly focused on one aspect, either of economic or environmental aspect, and there is little study demonstrating the effect of certain economic activity from multiple sides.

While accommodation sharing services are expected to contribute to solve the concern, it is still unclear that what kind of specific impacts will be generated by the promotion of these services. In this study, Tokyo is chosen

as targeted areas where lack of accommodation facilities is especially a significant problem.

## 2 Objectives and contribution

The objectives of this study are (1) to demonstrate induced effects by the promotion of accommodation sharing services in terms of environmental and economic aspects quantitatively, (2) to estimate exactly how much $CO_2$ emission will be reduced by the avoidance of new construction and to prove its effectiveness, and (3) to provide the range of environmental and economic impact based on some scenarios in Tokyo in 2020.

Through this study, the trade-off relationship between environmental and economic impacts triggered by the promotion of accommodation sharing services and its significance are clarified. The main contribution of this research will be to help decision making of Japanese government and municipalities regarding the promotion of accommodation sharing services which is currently under discussion.

## 3 Data collection and methodology

### 3.1 Input-output analysis

In this analysis, input-output table which indicates how much products and services are sold and bought in each industry in a given year in a single country or region is used. $CO_2$ emission (t-$CO_2$) and production amount (yen) induced by the change of final demand are estimated for environmental and economic impacts respectively.

The calculation flow and its boundary are shown in Fig. 1. More specifically, in the case of economic impact analysis, at first, there is increased demand to various industrial sectors (e.g., construction, retail & transportation), and then producers react to meet these increased demand (direct effect). This increased production results in additional supply to the above mentioned industrial sectors (indirect effect). These direct and indirect effects raise the level of household income, which will be re-spent on final goods and services (induced effect). The sum of these three effects is economic impact. Similarly, environmental impact is also estimated by calculating how much $CO_2$ emission will be generated by the increased final demand.

Basic input-output analysis model is given as follows:

$$\boldsymbol{\Delta X_1} = \left[\boldsymbol{I} - \left(\boldsymbol{I} - \widehat{\boldsymbol{M}}\right)\boldsymbol{A}\right]^{-1}\left(\boldsymbol{I} - \widehat{\boldsymbol{M}}\right)\boldsymbol{\Delta F}d,$$

$$\boldsymbol{\Delta X_2} = \left[\boldsymbol{I} - \left(\boldsymbol{I} - \widehat{\boldsymbol{M}}\right)\boldsymbol{A}\right]^{-1}\left(\boldsymbol{I} - \widehat{\boldsymbol{M}}\right)\boldsymbol{c}k\boldsymbol{w}\boldsymbol{\Delta X_1}$$

where
$\boldsymbol{\Delta X_1}$: Direct effect + Indirect effect
$\boldsymbol{\Delta X_2}$: Induced effect
$\boldsymbol{I}$: Identity matrix
$\boldsymbol{I} - \widehat{\boldsymbol{M}}$: Self-sufficiency rate matrix
$\boldsymbol{A}$: Input coefficient matrix
$\boldsymbol{F}d$: Domestic demand vector
$\boldsymbol{c}$: Private final consumption expenditure rate vector
$k$: Propensity to consume (scalar)
$\boldsymbol{w}$: Employees' compensation rate vector.

Here $\left[\boldsymbol{I} - \left(\boldsymbol{I} - \widehat{\boldsymbol{M}}\right)\boldsymbol{A}\right]^{-1}$ is called Leontief inverse matrix, which represents how output rises in each sector due to the unit increase in final demand. The change of final demand is represented by $\boldsymbol{\Delta F}d$. Moreover, for the environmental impact analysis, modified Leontief inverse matrix $\boldsymbol{d}\left[\boldsymbol{I} - \left(\boldsymbol{I} - \widehat{\boldsymbol{M}}\right)\boldsymbol{A}\right]^{-1}$ is used. Here $\boldsymbol{d}$ is diagonal matrix whose components are $d_i = \frac{D_i}{X_i}$ (t-$CO_2$/M yen), where $d_i$ represents environmental impact per unit of production in industry $i$, $D_i$ is annual $CO_2$ emission in industry $i$ and $X_i$ is annual production amount. Regarding construction effect, annual impacts are calculated by dividing average operation duration of hotels and general houses (35 years for hotels and 30 years for general houses). Finally, annual economic and environmental impacts are estimated for construction effect and operation effect respectively.

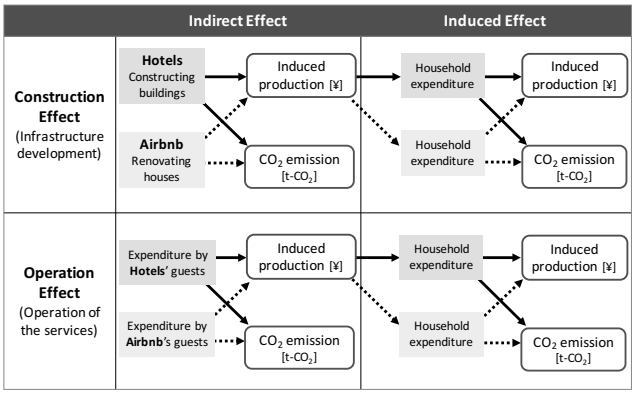


**Fig. 1** Analytical flow and its boundary

### 3.2 Dataset

Dataset indicating the situation of accommodation demand and supply in Tokyo in 2020 was collected from statics of Japanese government and research institutes (Table 1).

**Table 1** Estimation of accommodation demand and supply situation in Tokyo in 2020 [12] [13] [14]

| | |
|---|---|
| Expected no. of increasing foreign visitors' stay (comparison with 2014, million people's stay) | 9.31 |
| Required no. of rooms (comparison with 2014, thousand rooms) | 13.84 |
| Ave. construction fee per hotel room (million yen) | 9.91 |
| Ave. renovation fee per accommodation sharing room (million yen) | 0.98 |
| Ave. expenditure of foreign visitors (thousand yen) | 100.48 |

### 3.3 Scenario setting

Environmental and economic impacts are estimated based on scenarios, which represent accommodation demand and supply situation in Tokyo in 2020. Table 2 represents scenarios depending on accommodation modes to cover insufficient accommodations. Scenario (a) assumes that hotels will be constructed as planed in 2020 and the rest of rooms will be covered by accommodation sharing. Scenario (b) and (c) suppose the situation that accommodation sharing will be actively promoted and scenario (d) and (e) assume the situation that hotels will be strongly promoted. In addition to these five scenarios, other scenarios which assume expenditure of guests will be decreased by -10% and -20% except for accommodation fee are established (Table 3). Since guests of accommodation sharing tend to have consciousness of cost reduction, scenario (2) and (3) are considered as more realistic scenarios. By combining scenarios in Table 2 and

Table 3 as Scenario 1-a, 1-b, etc., environmental and economic impacts are estimated.

**Table 2** Scenarios depending on accommodation modes (AS: accommodation sharing)

| Scenarios | No. of hotel rooms | No. of AS rooms |
|---|---|---|
| a. BAU | 9,690 | 4,153 |
| b. AS +10% | 8,306 | 5,537 |
| c. AS +20% | 6,922 | 6,922 |
| d. Hotels +10% | 11,074 | 2,769 |
| e. Hotels +20% | 12,459 | 1,384 |

**Table 3** Scenarios depending on guests' expenditure (yen)

| Scenarios | Hotel guests | AS guests |
|---|---|---|
| 1. Same as hotels' guests | 100,476 | 100,476 |
| 2. Expenditure of AS guests -10% | 100,476 | 91,633 |
| 3. Expenditure of AS guests -20% | 100,476 | 82,790 |

## 4 Results

### 4.1 Economic impact and environmental impact of planned case in 2020

The amount of economic and environmental impacts of scenario 1 are considered as upper bound since scenario 2 and 3 are more feasible scenarios. In scenarios 1-a. BAU case, economic impact induced by hotels is 259 billion yen in Tokyo and 98 billion yen in the other area of Japan, while environmental impact is 214K t-$CO_2$ in Tokyo and 164K t-$CO_2$ in the other area of Japan. Economic impact by accommodation sharing services is 96 billion yen in Tokyo and 4 billion yen in the other area of Japan, while environmental impact is 92K t-$CO_2$ in Tokyo and 69K t-$CO_2$ in the other area of Japan. 70% of economic impact induced by both hotels and accommodation sharing services are spread inside Tokyo, while over 40% of environmental impact are induced outside of Tokyo. This is because industrial structure of Tokyo is service intensive and most economic activity done by service industries whose $CO_2$ emission per unit of production is quite low stays in Tokyo while economic activity by raw materials and infrastructure whose $CO_2$ emission per unit of production is high flows out of Tokyo.

Moreover, operation effect accounted for over 90% of each impact. This is because in terms of annual impact, construction effect was divided by operation duration and thus its annual impact was decreased. Consequently, operation effect induced by the guests of hotels and accommodation sharing services had significant impact.

### 4.2 Trade-off relationship between environmental and economic impacts

Table 4 shows total economic and environmental impacts including hotels and accommodation sharing services depending on scenarios. The change rate from BAU case is shown in bracket. In scenario 1, if accommodation sharing is promoted by 10%, 37 billion yen economic impact and 30.6K t-$CO_2$ environmental impact of hotels will be lost, instead 32 billion yen economic impact and 30.7K t-$CO_2$ environmental impact of accommodation sharing will be produced. In total, there is 5 billion yen loss and 61 t-$CO_2$ increase, and its elasticity is -0.014 (Table 5). In this scenario, the promotion of accommodation sharing services decreases economic impact and increases environmental impact in Tokyo. This result attributes to higher $CO_2$ emission per unit of production in operation effect of accommodation sharing services, which was determined in the process of guests' expenditure setting.

As seen in Table 4, if hotel rooms are replaced by accommodation sharing rooms, environmental impact will gradually decrease. In scenario 2, if accommodation sharing is promoted by 10%, environmental impact will be decreased by 0.94%, and there is 8 billion yen loss and 2,795 t-$CO_2$ reduction, and its elasticity is 0.41 (Table 5). In scenario 3, if accommodation sharing is promoted by 10%, environmental impact will be decreased by 2%, and there is 11 billion yen loss and 5,650 t-$CO_2$ reduction, and its elasticity is 0.60 (Table 5). Among the three scenarios, scenario 3 will lead the most effective outcome in terms of $CO_2$ reduction, which implies that reduction of final demand involving operation effect has significant effect for the $CO_2$ reduction.

**Table 4** Total economic and environmental impacts per year depending on scenarios

| | Scenario a. BAU | | Scenario b. AS+10% | | Scenario c. AS+20% | |
|---|---|---|---|---|---|---|
| | EC (bil. yen) | ENV (K t-$CO_2$) | EC (bil. yen) | ENV (K t-$CO_2$) | EC (bil. yen) | ENV (K t-$CO_2$) |
| Scenario 1 | 355 | 307 | 350 (-1.40) | 307 (0.02) | 345 (-2.81) | 307 (0.04) |
| Scenario 2 | 346 | 298 | 338 (-2.30) | 295 (-0.94) | 330 (-4.59) | 293 (-1.88) |
| Scenario 3 | 337 | 290 | 326 (-3.24) | 284 (-1.95) | 315 (-6.47) | 278 (-3.90) |

**Table 5** Trade-off relationship between promotion of accommodation sharing and decrease of hotels

| | Economic impact (bil. yen) | Environmental impact (t-$CO_2$) | Elasticity ($\Delta CO_2\%/\Delta yen\%$) |
|---|---|---|---|
| Scenario 1 | -5 | 61 | -0.014 |
| Scenario 2 | -8 | -2,795 | 0.408 |
| Scenario 3 | -11 | -5,650 | 0.603 |

Fig. 2 shows the transition of $CO_2$ emission per 100 rooms and year depending on the setting of operation duration. As seen in this figure, the longer the operation duration is, the lower the $CO_2$ emission of hotels per year. The main reason of this reduction is that construction effect which is induced in the initial stage is divided by operation duration so that the impact per year is gradually decreased. On the other hand, there is few change for the $CO_2$ emission of accommodation sharing services due to a few construction effect. As shown in the figure, even if hotels are operated for 15 to 30 years, its annual $CO_2$ emission will be still higher than upper bound $CO_2$ emission of accommodation sharing services. If it will be operated for over 30 years, its $CO_2$ emission will be lower than the upper bound $CO_2$ emission of accommodation sharing at last. In scenario 2 and 3, $CO_2$ emission will constantly be lower than $CO_2$ emission of hotels regardless of operation duration. This result implies that hotels have to be operated in long duration when considering environmental impact, however accommodation sharing services have no such limitation.

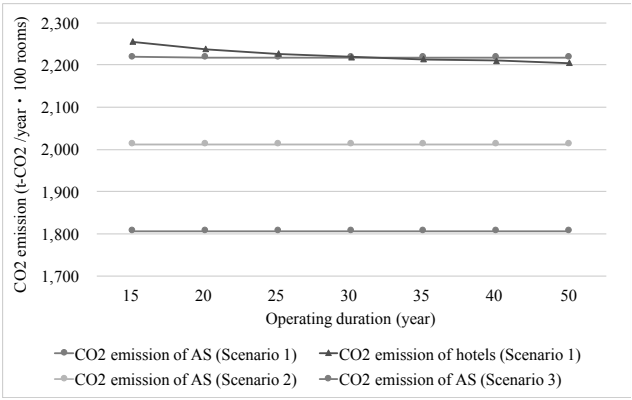


**Fig. 2** Transition of $CO_2$ emission per 100 rooms & year

### 4.3 Evaluation of environmental impact of promotion of accommodation sharing services

Amount of reducible $CO_2$ emission also need to be evaluated. As mentioned above, $CO_2$ emission of construction industry was 1.5M t-$CO_2$, and accommodation service industry was 1.0M t-$CO_2$ in Tokyo in 2010. Table 6 shows reducible $CO_2$ emission in each scenario and its ratio in each industrial sector in Tokyo. Ratio of $CO_2$ emission in construction effect corresponds to construction industry and operation effect corresponds to accommodation service industry. In scenario 2, 0.03% $CO_2$ reduction in construction industry and 0.24% $CO_2$ reduction in accommodation service industry will be possible with 10% increased accommodation sharing rooms. In scenario 3, its contribution will be 0.03% and 0.53% respectively.

Tokyo metropolitan government set a goal that aims to reduce GHG emission by 25% by 2020 (comparison with 2000). In other words, $CO_2$ emission need to be reduced to 44M t-$CO_2$ per year, where required reduction amount is 4.2M t-$CO_2$ (comparison with 2014). If scenario 2-b and 2-c are achieved, totally 2,795 t-$CO_2$ and 5,590 t-$CO_2$ reduction will be possible, and these amount is equivalent to 0.067% and 0.13% of required $CO_2$ reduction, respectively. If scenario 3-b and 3-c are achieved, totally 5,650 t-$CO_2$ and 11,300 t-$CO_2$ reduction will be possible, and these amount is equivalent to 0.13% and 0.27% of required $CO_2$ reduction, respectively. As a result, if the accommodation sharing is increased by 10%, it can lead to 0.067% to 0.13% of required $CO_2$ reduction, and if the accommodation sharing is increased by 20%, it can contribute to 0.13% to 0.27% of required $CO_2$ reduction.

**Table 6** Reducible $CO_2$ emission and its ratio in each industrial sector in Tokyo

| | | Scenario b. AS+10% | | Scenario c. AS+20% | |
|---|---|---|---|---|---|
| | | Difference from BAU (t-$CO_2$) | $CO_2$ ratio (%) | Difference from BAU (t-$CO_2$) | $CO_2$ ratio (%) |
| Scenario 1 | Construction effect | -425 | 0.03 | -850 | 0.06 |
| | Operation effect | 486 | 0.05 | 971 | 0.10 |
| Scenario 2 | Construction effect | -425 | 0.03 | -850 | 0.06 |
| | Operation effect | -2,370 | 0.24 | -4,739 | 0.48 |
| Scenario 3 | Construction effect | -425 | 0.03 | -850 | 0.06 |
| | Operation effect | -5,225 | 0.53 | -10,450 | 1.06 |

## 5 Conclusion

The environmental and economic impacts induced by the promotion of accommodation sharing services to compensate insufficient accommodation in Tokyo in 2020 was demonstrated depending on several scenarios through this study. By regarding the impacts in scenario 1 as upper bound, the following findings were obtained:

- If 10% of planned hotel rooms are replaced by accommodation sharing rooms, there will be 8 billion yen loss and 2,795 t-$CO_2$ reduction in scenario 2, and 11 billion yen loss and 5,650 t-$CO_2$ reduction in scenario 3. It indicates 2.3% to 3.2% economic impact loss, and 1% to 2% of $CO_2$ reduction comparing with planned case.
- 70% of economic impact induced by both hotels and accommodation sharing services are spread inside Tokyo, while over 40% of environmental impact are induced outside of Tokyo.
- Hotels need to be operated for over 30 years to be lower the upper bound $CO_2$ emission by accommodation sharing services.
- If 10% of planned hotel rooms are replaced by accommodation sharing rooms, it will result in 0.067% to 0.13 % of required $CO_2$ reduction to achieve the goal setting in Tokyo by 2020, and if it becomes 20%, it will be 0.13% to 0.27% of required $CO_2$ reduction.

The achievement of scenarios that the number of accommodation sharing rooms will increase by 10% to 20% could be feasible if there are more deregulation and diffusion of ICT based services. Accordingly, the accommodation sharing services are considered as effective solution to cover insufficient accommodations in terms of easy infrastructure development, mitigation of environmental burden, and sustainable ways when considering after 2020 as well.

There are several points to be improved regarding methodology and scenario setting for more accurate estimation. Furthermore, the estimation is required not only in Tokyo but also in Osaka and Kyoto, where the lack of accommodation facilities will also be significant problem because the impacts would vary depending on industrial structure and energy supply configuration.

## Reference

[1] Airbnb, Inc. (2016). Airbnb. https://www.airbnb.jp/ (accessed 2016.12.12).
[2] 東京都環境局. (2013). 都における温室効果ガス排出量総合調査(2010 年度実績).
[3] 東京都環境局. (2016). 低炭素ベンチマーク.
[4] 武者加苗. (2010). 地域経済における観光事業の産業連関分析. 産研論集(関西学院大学), 37 号, pp.113-124.
[5] 櫻井賢一郎, 細江宣裕. (2005). 北海道観光振興計画はアド・バルーンか? 外国人観光客数予測と産業連関分析. 運輸政策研究, Vol 8, No.1.
[6] 南齋規介, 森口祐一, 東野達. (2002). 産業連関表を用いた環境負荷原単位データブック(3EID). 国立環境研究所.
[7] 漆崎昇串, 水野稔, 下田吉之, 酒井寛二. (2001). 産業連関表を利用した建築業の環境負荷推定. 日本建築学会環境系論文集, Vol. 549, pp.75-82.
[8] 吉岡完治, 早見均, 池田明由, 菅幹雄. (1993). 環境分析用産業連関分析表の応用(3)：省エネ住宅のすすめ. イノベーション&I-O テクニーク, Vol.4, No.2, 環太平洋産業連関分析学会.
[9] Hamari, J., Sjöklint, M., and Ukkonen, A. (2015). The sharing economy: Why people participate in collaborative consumption. *Journal of the Association for Information Science and Technology*, 67(9), pp.2047-2059.
[10] Tussyadiah, I. P., and Pesonen, J. (2015). Impacts of Peer-to-Peer Accommodation Use on Travel Patterns. *Journal of Travel Research*, 55(8), pp.1022-1040.
[11] Zervas, G., Proserpio, D., and Byers, J. (2014). The Rise of the Sharing Economy: Estimating the Impact of Airbnb on the Hotel Industry. *Boston University School of Management Research Paper No. 2013-16*.
[12] 大和香織. (2015). インバウンド観光と宿泊施設不足. みずほ総合研究所. http://www.mizuho-ri.co.jp/publication/research/ (accessed 2016.12.24).
[13] 国土交通省. (2016). 建築物リフォーム・リニューアル調査報告. http://www.mlit.go.jp/toukeijouhou/chojou/rrs.htm (accessed 2016.12.24).
[14] 東京都産業労働局. (2016). 平成 27 年東京都観光客数等実態調査. http://www.metro.tokyo.jp/INET/CHOUSA/2016/05/60q5q300.htm (accessed 2016.12.24).

# Effects of ICT based urban mobility as a case of collaborative economy in Indonesia

Student Number: 15M18227 Name: Benny LEONO Supervisor: Naoya ABE

# ICT を活用した都市内モビリティーの効果
# ーインドネシアにおける共有型経済の事例研究ー

Benny LEONO

本論文は、インドネシアにおける情報通信技術（ICT）を活用した都市内の二輪モビリティーサービスの基礎効果を検討し、同サービスが利用者と提供者（運転手）にもたらす影響という観点から、その実態把握を行ったものである。その結果、スマートフォンに代表される ICT の普及により、都市内モビリティーの利用及び提供方策が効率化され、特にサービス提供者の労働時間における柔軟性、満足度、所得水準が向上したことを明らかにした。同時に課題として、提供者の「専門性」の向上余地が限られているため，同サービスが将来，彼らの自立に対する影響がまだ不明瞭である。

## 1. Introduction

### 1.1 Motorcycle rise and its use

In Indonesia, mass transport modes are still lacking, private vehicles are the primary modes of transport that provide everyday trips among the urban commuters. Motorcycle is a common transportation mode which is preferable than any other modes because it is cheaper than a car and more importantly because it can travel faster. In 2015, motorcycle ownership in Indonesia has reached the number of 92.9 million, while Indonesia population itself is 257.5 million people (Badan Pusat Statistik, 2016). It means 36% of the citizen commute with motorcycles and no wonder that the streets today are filled with motorcycles. In the 1980s, realizing that there was an arbitrage, those who started to work, illegally, as a motorcycle-taxi driver, which is known as Ojek, responding promptly to provide mobility needs when other public transport modes are not so available. The perceived performance of public transportation system is considered as very low in Indonesia, therefore, the role and contribution from ride-hailing service, Ojek to support mobility needs becomes significant (S.B. Nugroho, 2010). Local government has no choice but to allow Ojek service going on as far as no alternative which may give a better solution. Ojek at very beginning also supported the society by providing job for those who possess low skill (A.K.M. Tarigan, 2010). However, for most of its history, Ojek is known as a low-income job and becomes an option when people have no choice but to make use full of their motorcycles for earnings. As these issues remain a problem in Indonesia, Sustainable Development Goal 8 encourage everyone especially the low-income groups to work efficiently to achieve productive employment, and decent work in order to get an equal pay for work of equal value.

### 1.2 ICT based ride-hailing with collaborative economy

Today people are living in digital and informatics era, when everything is connected and information transfers fast. Technology is transforming transportation, the ability to work efficiently and conveniently request, track, and pay for trips via mobile devices is changing the way people get around and interact with city. GoJek is a technology based ride-hailing service, one of the phenomenon that connect Ojek drivers and ride hailers in real time, by using app platform in smartphone. Gojek enhances available advanced technology to enable people fulfill mobility demands in a more efficient way, hints to the term of collaborative economy. Over the last few years, there has been much speculation as to whether the so-called collaborative economy will impact positively or negatively (Santi et al., 2014; Carvero, R. G. 2007), but little hard evidence exists to support either position. In this paper, we consider workers who choose to provide motorcycle rides service using the Gojek app platform. Drivers who partner with Gojek provide transportation and life-style services to users requesting rides via Gojek's app on smartphones devices.

Gojek realize how collaborative economy idea may able to clarify the previously unregulated Ojek system to enable the circulation of activities and generate potential benefits by fostering access over ownership of motorcycle and enhance the advance of Information and Communication Technologies (ICT). It is still unclear whether Gojek as a new disruptive innovation of urban transport is truly could enhance people with productive working environment and generate a more efficient option for mobility. (A. Schlze, 2015) mentioned that the turbulence from global demand towards advanced innovation technology has always affect the market and impact to people afterwards. Another study (Horpedahl, 2015) highlighted that innovation in technology nowadays allow people to bypass traditional ways. Moreover, (B. Cohen, 2014) also reminded that the developments of ICT have started to challenge traditional thinking, and mentioned that collaborative economy in mobility provide solutions which can be attributed to multiple stakeholders.

## 2. Objectives and Contribution

### 2.1 Objectives

This study aims to shed some light to see what collaborative economy is all about and what the impacts to the society are by providing the first analysis of a representative, sample of Gojek driver-partners and Gojek users. Gojek, which enhance the use of information technologies to provide services can now benefits not only

Gojek users but also Gojek driver-partners. Regardless of the technological aspect, the underdeveloped performance of public transportation system and working environment may be related to Gojek driver-partners and Gojek user's views of this new ICT-based ride-hailing service.

The objective of this study is to examine the basic effects of collaborative economy through a case of Gojek under following two perspectives:

- To explore the benefit of ICT use in increasing social welfare for Gojek driver-partners.
- To study how this new ICT based ride-hailing service affect Gojek user preference for commuting while capture the reduction of potential time saving.

## 2.2 Significance of the study

From the result of this study, the basic effects of ICT based ride-hailing service Gojek has been identified. Therefore, this research hopes will contribute to propose a better transportation policy-making by ICT in the future, to enhance solution for efficient working life-style, and to understand how transport mode combined with ICT can save time.

# 3. Data collection and methods of analysis

## 3.1 Data collection

This study attempts to examine people's view or perspective toward Gojek. Some approaches like questionnaire, face-to-face interview were employed. Target respondents were people with Indonesian nationality. Should be noted, respondents in this study were divided into 2 groups, Gojek partner-drivers and Gojek users. Paper version of questionnaires was prepared and distributed from November to December 2016 in Surabaya, Indonesia.

## 3.2 Methods of Analysis

### 3.2.1 Cross Tabulation

A total of 220 responses was gathered, including 68 and 152 responses from Gojek driver-partners and Gojek user respondents respectively. Cross tabulation analysis is employed to analyze the results of the survey data. The data collected provides a bunch of information regarding to relationship between variables. Then, visualization by using chart bar, diagram, or graph is used to comprehend the relationship.

### 3.2.2 Clustering Analysis

To elicit different types of group among Gojek driver-partners, clustering analysis is employed. This study selects Agglomerative Hierarchical Clustering to produce a hierarchical series of nested clusters, which finally displayed as a tree diagram called a dendrogram. Equation (1) shows the formula of the calculation of dissimilarity measures by using Euclidean distance.

$$D(i,j) = \sqrt{\sum_{k=1}^{N} \left(X_{ki} - X_{kj}\right)^2} \quad \dots (1)$$

$i,j$ : $Number\ of\ observation$
$k$ : $Variables$
$N$ : $Total\ variables$

# 4. Findings to Gojek driver-partners

## 4.1 Change of income level

Many of previously Ojek driver are attracted to partner with Gojek by the level of income Gojek offers at the first time. While other respondents who worked at labor market attracted by the flexibility, as data result computed in Table 1. Combining the advanced technology, Gojek attracted more users by using smartphone app, which results in increasing orders for Gojek driver-partners to earn at any time.

Table 1. Cross tabulation of motivation to partner with Gojek and driver-partners' age range [unit: %]

| Motivation to join as Gojek driver-partner | Range Age | | | Total |
|---|---|---|---|---|
| | 21-30 | 31-40 | 41-50 | |
| Increase in Income | 17 | 19 | 11 | 47 |
| Flexibility | 11 | 26 | 15 | 52 |
| Loan (smartphone etc.) | 1 | 0 | 0 | 1 |
| Others | 0 | 0 | 0 | 0 |
| Total | 28 | 46 | 26 | 100 |

Table 2 shows the competitive analysis between Ojek and Gojek according to interview result which elaborate significant differences between the two modes.

Table 2. Competitive analysis between Ojek and Gojek

| Analysis Item | Ojek (Traditional) | Gojek (ICT-Based) |
|---|---|---|
| **Advance Booking** | YES | NO |
| **Hiring Method** | On the spot/Reservation Call/Flag | Smartphone App |
| **Payment** | Cash | Account Charge/Cash/Credit card |
| **Pricing Structure** | Negotiation | Transparent |
| **Rating System** | NA | Available |
| **Reliability** | Low | High |
| **Working Style** | Unsecure | Flexible and Independent |
| **Age Limit** | No limitation | 17-55 |
| **Value Capture to company** | NA | Reward and Bonus |
| **ETA to pick up point** | NA | Available |
| **Route to destination** | Self-skill | Smartphone GPS /Self-skill |
| **System** | NA | Organized and modernized |
| **Law and regulation** | Grey Area | Structured and formalized |

From the survey results, most of Gojek driver-partners (61 respondents) experienced in increased-income level after partnered with Gojek, depicted by dots above 45 degrees' line in Figure 1.

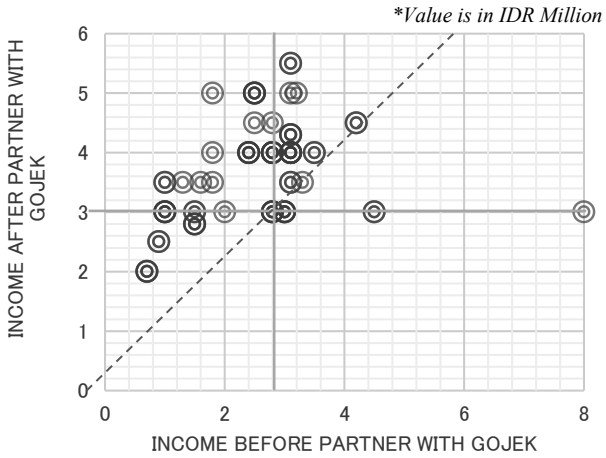


Figure 1. Most of Gojek driver-partners experienced in increased-income level and earned the minimum wage compared to before they partnered with Gojek

The 45 degrees' line indicates no change in income level even after partnered with Gojek. Thus, from the figure we also captured some driver-partners who experienced in no change of income level (4 respondents) and decreased-income level (3 respondents), which indicated by dots running on the 45 degrees' line and dots below the 45 degrees' line, respectively. In addition, green vertical and horizontal line indicates the minimum wage of IDR 3.05 million. From Figure 1, we figured out that most driver-partners earn minimum wage of IDR 3.05 million after partnered with Gojek, indicated by dots above green horizontal line. Previously, most of driver-partners did not earn as much as the minimum wage before partnered with Gojek.

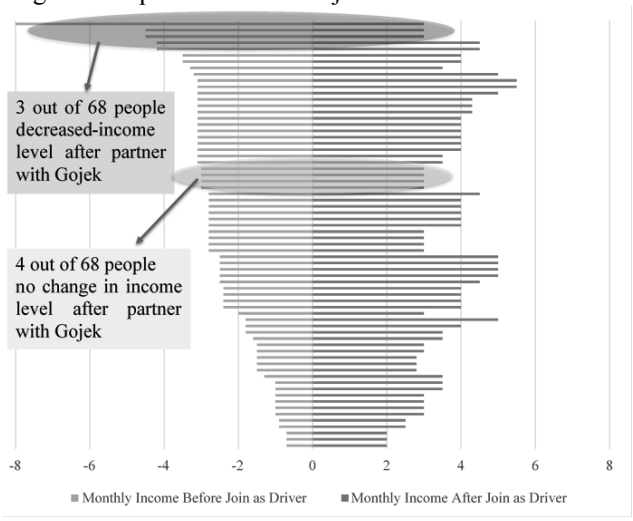


Figure 2. Comparison of drivers' income in monthly basis, before and after partnered with Gojek

Figure 2 shows a more detail illustration in change of income level from 68 driver-partners before and after partnered with Gojek. The x-axis is in IDR million unit. Only 7 drivers experienced in decreased- or no change in income level after partnered with Gojek. While 61 drivers generated more income after joined as Gojek drivers.

## 4.2 Cluster analysis of 68 driver-partners

In order to take a different perspective on the survey result data of Gojek driver-partners, we conducted Cluster Analysis. The result of clustering 68 driver-partners simply aims to segment drivers' survey data into meaningful clusters, and to further investigate the difference in motivation towards working as Gojek drivers. As shown in Table 3, we divide Gojek driver-partners into 3 clusters.

Table 3. Cluster centroid of 68 Gojek driver-partners

| Cluster | Age | Income Before | Income After | Daily Income | Working Hour |
|---|---|---|---|---|---|
| 1 | 39.607 | 2.704 | 3.996 | 0.173 | 9.107 |
| 2 | 32.727 | 2.464 | 2.864 | 0.109 | 9.091 |
| 3 | 32.643 | 2.389 | 3.675 | 0.142 | 10.571 |

| Cluster | Total Trips | Running Distance | Income Satisfaction | Flexibility Satisfaction | Working Satisfaction |
|---|---|---|---|---|---|
| 1 | 13.179 | 2.714 | 4.679 | 4.714 | 4.821 |
| 2 | 9.364 | 1.909 | 3.455 | 4.818 | 3.909 |
| 3 | 14.286 | 3.286 | 4.036 | 3.643 | 3.714 |

From the cluster results, we made investigation by examining variable by variable to reveal which variable that leads to the clusters. We assumed that Cluster 1 belongs to driver-partners focusing on both earnings and working-flexibility. Cluster 2 is driver-partners who prefers working-flexibility, while Cluster 3 is driver-partners focuses more on earnings.

Cluster 1 has the highest value in increased-income level after partnered with Gojek. This group of drivers put earnings as important value to maintain a decent life. All drivers in this group are married, we consider family to be an influencing factor on how drivers work and earn for their family. Moreover, drivers in Cluster 1 earn as much as above the minimum wage of IDR 3.05 million in average. The average of working hour per day in Cluster 1 shows 9.107, which is almost similar to Cluster 2 by 9.091. But in fact, Cluster 1 could generate more earnings than Cluster 2. This means Cluster 1 group knows how to work more efficiently. Satisfaction level shows high scale for all variables income, flexibility and overall working.

Result from Table 3 also shows that the level of income in average for Cluster 2 as 2.864, although the income level indeed has increased, the value is less than the minimum wage. When we investigate further, the average result in other variables such as total working hours, total trips, and total running distances, indicate the lowest value among other clusters. We assumed that driver-partners in Cluster 2 are more attracted to work due to flexible working schedule Gojek offers. Satisfaction level towards flexibility shows highest value of 4.818 compared to other satisfaction variables and other clusters. In addition, driver-partners who experienced in decreased-income level, are belong to cluster 2. From interview result, one driver stated that the earning from Gojek still enough to maintain life for the whole family even he experienced in decreased-income level. The driver previously worked as a truck driver and often leave the hometown, which result in almost no time for family. Now he can manage to increase more time for family as he can settle his schedule for work.

Cluster 3 shows the highest in value of total working hours, total trips, and total running distance variables among all clusters. From interview result, drivers in Cluster 3 tend to take any orders regardless of distance. We assumed that driver-partners from Cluster 3 are not picky in taking orders and work for earnings. They earned as much as the minimum wage in average. All not-married drivers belong to Cluster 3. From the interview result, indeed the drivers mentioned that they have more time for themselves without any responsibilities for the family yet, but planning to save up for one. The time results in willingness to run further distance and to focus on earnings. Satisfaction level towards income level shows high value of 4.036 compared to other satisfaction variables.

## 5. Findings to Gojek users

Gojek users was divided into 2 groups, the students from universities in Surabaya with ninety-seven (97) respondents and the local workers with fifty-five (55) respondents. Gojek users' behavior towards Ojek seem to have changed, which leads to preference of using Gojek. As Gojek combined technology in delivering service, fewer people use Ojek recently. Some of Gojek users are

*partly*- and *fully-shifting* their transport mode from Ojek to Gojek, as shown in Figure 3. From the survey result, we found out that fifty-nine (59) over one hundred and fifty-two (152) user respondents are *new-users* of ride-hailing service. These respondents never used Ojek previously, yet they ever used the ICT based Gojek for the very first time. Gojek had attracted many young people in Indonesia, who are more likely to be updated with ICT innovation.

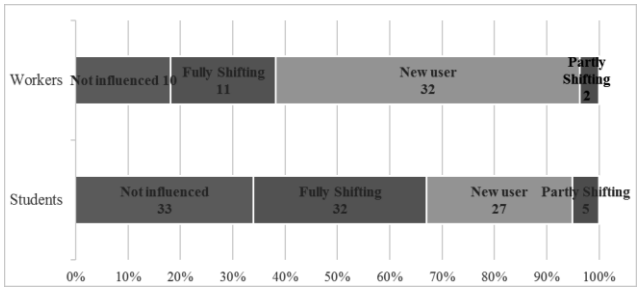


Figure 3. Two groups of respondents' view towards Gojek service with comparison to the use of Ojek.

We compared Gojek with other transportation modes used previously by Gojek new-users, and found out that Gojek contributed in terms of time-saving. From survey result as shown in Table 4, Gojek users can cut travel time of other modes used previously by 57% of angkot and taxi, 52% of car, bus, and Bemo, 43% of Becak.

Table 4. Comparison of travel time (TT) and time cut between Gojek and previous mode trips

| Mode | Ave. TT by mode (minutes) | Ave. Gojek TT (minutes) | Time Cut |
|---|---|---|---|
| Car | 41.51 | 21.60 | 52% |
| Taxi | 41.52 | 23.79 | 57% |
| Angkot | 33.61 | 19.17 | 57% |
| Bus | 31.11 | 16.11 | 52% |
| Bemo | 31.43 | 16.43 | 52% |
| Becak | 17.50 | 7.50 | 43% |

Gojek seemed to contribute in convenience and time-saving for the users. Survey result shows one hundred and twenty-four (124) respondents among one hundred and fifty-two (152) respondents answered they experienced in time-saving after using Gojek.

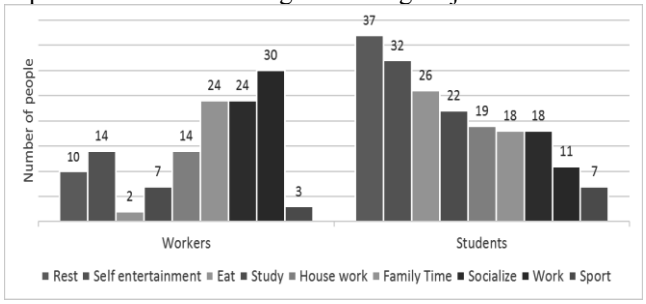


Figure 4. Result of the two groups towards possible activities engaged from the time saved after using Gojek.

Respondents mentioned activities they prefer to engage from the time-saving after using Gojek, as depicted in Figure 4. Workers group are more likely to work, socialize and spend time for family. While students group are more likely to rest, and spend time for self-entertainment such as, reading books, café, or internet browsing, and eat.

## 6. Conclusion

This paper has provided the first comprehensive analysis of Gojek's driver-partners and users, based on survey data. Gojek permits flexible work and increases income of level to some group of driver-partners, who seemed satisfy to have partnered with Gojek. Moreover, the availability of modern technology, like the Gojek app, provides advantages for Gojek users compared with the traditional Ojek, and this has boosted new demand for ride services, and proved to cut travel time of previously used mode.

With more demands in ride services, Gojek increased demand for driver-partner, who appears to be attracted in large part because of the flexibility Gojek offers, the level of compensation, and the income. Many driver-partners valued the flexibility to choose their hours of work. Gojek also becomes an attractive option to those who want to work part-time, as other part-time jobs in the labor market typically disadvantages in terms of pay. With the help of ICT development, Gojek serves as a bridge for many seeking employment opportunities. Most Gojek driver-partners experienced in increased income and earnt the minimum wage. Cluster analysis reveals 3 main types of drivers who prioritize: income, flexibility, both income and flexibility. Easy access by smartphone also has made a way to commute much more convenient because driver can now come to pick-up location with estimated time arrival displayed on Gojek app. Gojek driver now able to come to pick-up location which reduces Gojek users' walking time compared to when they commuted by Ojek previously.

Finally, increasing Internet use by citizens in Indonesia have resulted in opportunities to support urban mobility while public transportation system still not able to compete with mobility demands. The high ownerships of private motorcycle and smartphone users which linkages the advances in technology, can now make it possible to respond to specific needs in increasing social welfare to some group of people and providing option for mobility inside the city.

## Reference


- A. Schlze, J. M. (2015). Introduction: Knowledge Generation and Innovation Diffusion in the Global Automotive Industry. Change and Stability during Turbulent, Industrial and Corporate Change, Oxford University Press.
- A.K.M. Tarigan, Y. S. (2010). Negative experiences and willingness to use paratransit in Bandung, Indonesia: An exploration with ordered probit model. Proceeding of the 89th Annual meeting of Transportation Research Board.
- B. Cohen, J. K. (2014). Ride on! Mobility business model for the sharing economy. Organ. Environ. 27 (3).
- Badan Pusat Statistik Indonesia (2016). Link source: http://www.bps.go.id/linkTabelStatis/view/id/1413
- Carvero, R. G. (2007). Informal transport: A global perspective. Transport Policy 14, 445-457.
- Horpedahl, J. (2015). Ideology Uber alles? Economics bloggers on Uber, Lyft, and other transportation network companies pp. 360-374. Econ. J. Watch 12 (3).
- S.B. Nugroho, T. L. (2010). Measuring Social Capacity for Urban Air Quality Management in Megacities in South East Asia based on Attitudinal Survey in Jakarta and Hanoi. Proceeding of the 16th Conference of Sustainable Development Research Conference. The Kadoorie Institute, University of Hongkong.
- Santi, P. (2014). Quantifying the benefits of vehicle pooling with share ability networks. Proc.Natl.Acad.Sci.111, 13290–13294.

# Current status of subsidized taxi operations by NPOs in Tokyo for the elderly and disabled mobility

Student Number: 15M18167 Name: Kazuhiko MATSUMURA Supervisor: Naoya ABE

# 東京都における高齢者・障がい者モビリティのための福祉有償運送事業の現状

松村和彦

本論文は東京都内の 33 の福祉有償運送事業所のサービス充実度を分析し、移動困難者モビリティの地域差を明らかにした。「補助金受給額」「重度移動困難者へのサービス充実度」、「サービス供給量」、「サービス確実性」の観点からまとめ、その結果から地理的特性の顕著な差は見られなかった。また、補助金受給額と他のサービス充実度との関連が見られないことから、補助金交付基準の見直しが必要であることが明らかになった。

## 1. Introduction

### 1.1 Current situation of mobility for movement limited person

Nowadays, Japan is facing a serious problem from aging society. The ratio of population over 65 years people in Japan will continue to increase to over 30% by 2030 [1]. Since the number of people certified for long term care in Japan has also increased to 6,077,435 in 2015 from 5,250,404 in 2012 [2]. Almost all of them have difficulty to go out due to their physical disability. Some of them can go out by using a KAIGO taxi[1] or transfer from their family. However, others face financial limitation and no chance of access of transfer from their family or the people they can rely on. These people who have physical and financial limitation of going out and no people to rely on when they want to go out are defined as “movement limited persons”. Movement limited persons are not only the elderly people but there are three kinds of disabled people who fulfilled the above conditions: physical disability, mental disability and intellectual disability people.

Limitations in movement lead to be bedridden [3]. Besides, mobility of elderly and disabled people is defined as likely to be human right in Western countries and it is ensured by law [4]. Therefore, mobility of movement limited person must be secured.

Since movement limited people are suffering from going out, FUKUSHI-YUSHOUNSO[2] is the vest way for them. It is because that the service provided by FUKUSHI-YUSHOUNSO has fulfilled the preferences of movement limited person; it is not necessary for family help, it has a welfare car that makes movement limited person easier to get on and off the car and service fee is about half of the price of normal taxi in operation area. However, actual service operation might be different from each NPO.

[1] KAIGO taxi is a taxi service for those people who have difficulty of going out which is conducted by ordinal company [5].

[2] FUKUSHI-YUSHOUNSO is a taxi service for those people who have difficulty of going out which is conducted by NPO [6].

### 1.2 FUKUSHI-YUSHOUNSO

Figure 1 shows that relations between total cars of FUKUSHI-YUSHOUNSO and population density of people certified for long term care in each area of Tokyo. Twenty areas are selected that ten areas are the largest number of total cars and ten areas are the smallest number of it in Tokyo area. Ten areas in Tokyo don’t provide a FUKUSHI-YUSHOUNSO service even though some movement limited persons live in these areas. Thus, these gaps might have an effect on their mobility depending on where they live. Therefore, this study focuses on the actual operation of FUKUSHI-YUSHOUNSO.

Considering the actual operation, subsidy is an important factor because NPO has only limited budget for operation. It means subsidy is directly related to service context.

### 1.3 Selection of targeted area

There are two reasons why this study has targeted Tokyo area to investigate the actual operation of FUKUSHI-YUSHOUNSO.

First, Tokyo has a characteristic of like that of small Japan on the perspective of population density. It means that investigating Tokyo area is important to get the picture of whole Japan.

Second, it will continue to increase the number of movement limited person in Tokyo. Tokyo is the largest number of migrants from other prefectures that are over 65 years old.

### 1.4 Objectives

This research categorizes the NPOs which conduct a FUKUSHI-YUSHOUNSO service based on their characteristics. There are two purposes of this research:

1. To clarify the relation between adequacy of FUKUSHIYUSHOUNSO service and subsidy for FUKUSHI-YUSHOUNSO.

2. To clarify regional differences of mobility of movement limited person.

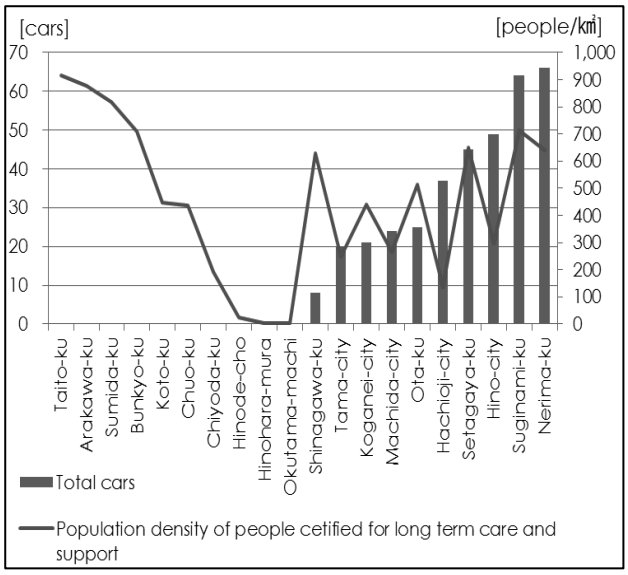


Figure 1 Relations between total cars of FUKUSHI-YUSHOUNSO and population density of people certified for long term care in each area of Tokyo

## 2. Significance of the study

From previous researches, there are three issues about FUKUSHI-YUSHOUNSO.

① The recent actual operation of FUKUSHI-YUSHOUNSO is unclear.
② The information of subsidy for FUKUSHI-YUSHOUNSO is not organized.
③ The relation between adequacy of FUKUSHI-YUSHOUNSO service and subsidy for FUKUSHI-YUSHOUNSO is unclear.

## 3. Data collection and methodology

### 3.1 Data collection

This research used the data of NPOs which conduct a FUKUSHI-YUSHOUNSO service in Tokyo. Table 1 shows the data of NPOs. These data which are subsidy, trip, the number of registered user and the number of driver are collected by hearing survey since 2016 August 26 to November 24. These data of total car and wheelchair car are collected from Director-General of Tokyo District Transportation at 2016 July 8.

Table 1: The data of NPO (n=33)

| Variable | Duration | Average |
|---|---|---|
| Subsidy [JPY/year] | In 2015 | 2,880,050 |
| Trip [time/year] | In 2015 | 3,100 |
| Total car [car] | In 2016 at June | 6.1 |
| Wheelchair car [car] | In 2016 at June | 3.7 |
| The number of registered user [people] | In 2015 | 118 |
| The number of driver [people] | In 2015 | 12.9 |

### 3.2 Methodology

#### 3.2.1 The flow of methodology

There are three steps to categorize the NPOs. First step is data standardization to be able to compare with each indicator. Second step is to extract synthetic variable from the data table 1 as show by principal component analysis (PCA). It is a method to shorten the multivariate data to prevent from data deviation. Third step is to categorize the NPOs by cluster analysis based on new indicators which are extracted by PCA.

#### 3.2.2 Principal component analysis

PCA extracts few numbers of independent data that can simply indicate service adequacy. Equation (2) shows principal component. Later $P$ means the number of variables. In this study, $P$ would be six. Later $m$ means the number of principal component.

$$Z_m \equiv \sum_{p=1}^{P} a_{pm} x_p \tag{2}$$

$Z_m : principal\ component$
$a_{pm} : coupling\ coefficient$
$x_p : variable$

But there is a condition, if $m$ is 1.

$$\sum_{p=1}^{P} a_{pm} x_p = 1 \tag{3}$$

This study uses principal components as indicators by over around 80% of cumulative contribution ratio because the number can present the original data.

#### 3.2.3 Cluster analysis

Cluster analysis is a multivariate analysis method to make a group according to some analogy data. The cluster is made of samples that are the highest similarity of dissimilarity matrix in samples. There are some calculation methods of dissimilarity matrix. This study uses Mcquitty method because this method is suitable to deal with outlier minority sample when cluster number is over four [7]. Equation (4) shows how to calculate the dissimilarity matrix by Mcquitty method. The formula simply means taking an average between two clusters.

$$\mathrm{D}(C_{kl}, C_i) = \frac{\mathrm{D}(C_k, C_i) + \mathrm{D}(C_l, C_i)}{2} \tag{4}$$

$\mathrm{D}(C_{kl}, C_i) : distance\ between\ clusters$
$C : cluster$

## 4. Hearing survey and results

### 4.1 Hearing survey

This study conducted hearing survey to collect the data of NPOs and understand what factor is important to evaluate actual operation for movement limited person. Five factors are clarified.

Ⅰ. Whether the NPO conducts bed-to-bed service or not?
Ⅱ. How many wheelchair cars does the NPO have?
Ⅲ. What is the operation style of NPO?
Ⅳ. Who are the targeted people?
Ⅴ. Does the NPO motivate to help going out for many people?

Recently, the demand of bed-to-bed service and wheelchair car is growing for severe movement limited person according to aging society. and Ⅰ factors Ⅱ can help going out for them.

Additionally, operation style is strongly related to financial resources of NPO. Basically, NPO of single operation style gains operation fee from municipality as a subsidy. NPO of multi operation style is operated by money from the other businesses which are almost nursing care.

On the other side, targeted people are different by NPO based on the types of disability and physical condition. Besides, some NPOs don't motivate to help going out for many people. The service is just part of the other care service for them.

## 4.2 Results

Six variables in table 1 are extracted by PCA. The result of this analysis can express about 83% of cumulative contribution ratio by third principal component (table 2).

These principal components are named based on these numbers on Table 2 as; first principal component is comprehensive service adequacy axis. Second principal component is independent large scale service engagement axis. Third principal component is dependent on municipality service engagement for light movement limited person axis.

First to third principal components are used by cluster analysis as the indicators of NPOs. The result of cluster analysis shows that thirty three NPOs are categorized into eighteen clusters (Figure 2). The number of clusters is minimum requirement that any cluster doesn't have NPOs which are not different motivation by hearing survey (Ⅴ).

Table 2 Result of PCA

| Items | First PC | Second PC | Third PC |
|---|---|---|---|
| Subsidy [JPY/year] | 0.35 | -0.58 | 0.40 |
| Trip [time/year] | 0.36 | 0.41 | 0.55 |
| Total car [car] | 0.35 | 0.64 | -0.076 |
| Wheelchair car [car] | 0.41 | -0.17 | -0.65 |
| The number of registered user [people] | 0.46 | -0.24 | 0.20 |
| The number of driver [people] | 0.51 | 0.029 | -0.27 |
| Eigenvalue | 2.87 | 1.17 | 0.85 |
| Contribution ratio | 0.48 | 0.20 | 0.14 |
| Cumulative contribution ratio | 0.48 | 0.68 | 0.82 |

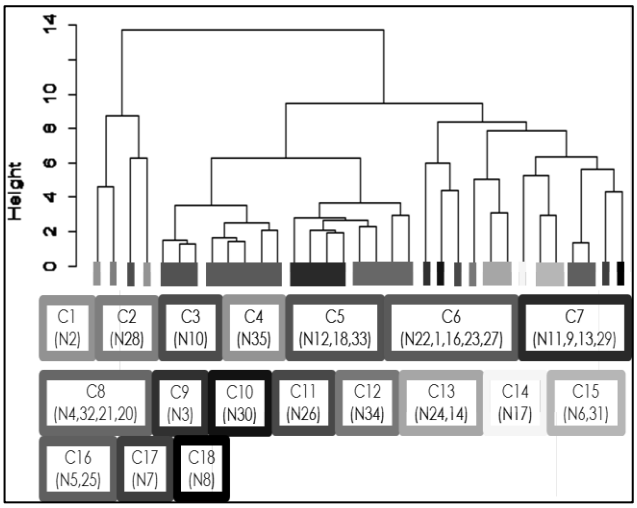


Figure 2 Result of cluster analysis

Six indicators which are about NPO data used by PCA before, kinds of operation style and targeted people are comprehensively considered to evaluate a FUKUSHI-YUSHOUNSO service adequacy by each cluster.

The two research objectives are clarified as explained below;

In the first, the information about NPOs are organized into four aspects; the amount of subsidy, service adequacy for severe movement limited person, the amount of trips and service certainty.

The service adequacy for severe movement limited person is composed by the number of wheelchair car and provision of bed-to-bed service. Service certainty is composed by the number of total cars, user and driver. It is because higher these numbers indicates lower rate of rejection of a service provided from NPO due to their high capacity.

Second step is to clarify the relationship between the amount of subsidy and service adequacy. As a result, the amount of subsidy is not related to service adequacy perspective of three aspects; service adequacy for severe movement limited person, the amount of trips and service certainty.

Third step is to clarify the regional characteristics of FUKUSHI-YUSHOUNSO service adequacy. Based on above conditions except the amount of subsidy, the FUKUSHI-YUSHOUNSO service adequacy is considered.

First cluster is composed by only NPO2. Total car (8 cars), user (270 people) and driver (19 people) are far higher than the average number. It means first cluster is high service certainty. Additionally, wheelchair car (8 cars) is higher than the average and bed to bed service is conducted. First cluster is high service adequacy for severe movement limited person. But trip (886 times/year) is much lower than average. Thus, first cluster is high service certainty and service adequacy for severe movement limited person. The other clusters by eighteenth have been evaluated like the above steps.

Summarizing the result, seven clusters which are composed by ten NPOs are high service adequacy for severe movement limited person. Targeted operation areas are shibuya-ku, tama-shi, kita-ku, kiyose-shi, itabashi-ku,

inagi-shi, shinagawa-ku, koganei-shi, hino-shi and tachikawa-shi.

Six clusters which are composed by eight NPOs are high amount of service provided. Targeted operation areas are mitaka-shi, inagi-shi, higashiyamato-shi, edogawa-ku, koganei-shi, hino-shi, tachikawa-shi and setagaya-ku.

Six clusters which are composed by eight NPOs are high service certainty. Targeted operation areas are shibuya-ku, tama-shi, mitaka-shi, kokubunzi-shi, higashiyamato-shi, edogawa-ku, koganei-shi and setagaya-ku.

Furthermore, some NPO have fulfilled multi conditions. NPO2 and NPO28 are high service adequacy for severe movement limited person and service certainty. Targeted operation areas are shibuya-ku and tama-shi. NPO5 and NPO25 are of high amount of service provided and high service adequacy for severe movement limited person. Targeted operation areas are hino-shi and tachikawa-shi. NPO35 and NPO7 have high amount of service provided and high service certainty. Targeted operation areas are mitaka-shi and setagaya-ku. NPO30 and NPO17 are satisfied three conditions. Targeted operation areas are kokubunzi-shi and koganei-shi.

On the other hand, four clusters which are composed by fourteen NPOs have not fulfilled any conditions. Targeted operation areas are fussa-shi, ota-ku, nishitokyo-shi, mizuho-cho, kodaira-shi, adachi-ku, Machida-shi, katushika-ku, ome-shi, hamura-shi, komae-shi, akiruno-shi, fuchu-shi and nerima-ku. Figure 3 shows of the result of regional characteristics of mobility for movement limited person on map of Tokyo area.

Overall, some NPOs which are evaluated above three conditions are mixed. Moreover, middle area of Tokyo has some NPO which fulfilled with multi conditions of service adequacy. But that area also has other NPOs which are not fulfilled with any conditions. Therefore, peculiar trend of regional characteristic of FUKUSHI-YUSHOUNSO service adequacy have not bene found.

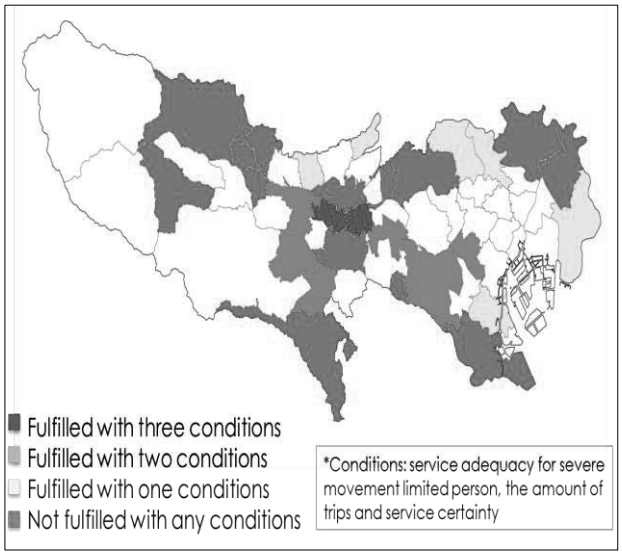


Figure 3 regional characteristics of mobility for movement limited person in Tokyo

## 5. Conclusion

According to research objectives, this research has clarified two points:

1. The amount of subsidy is not related to service adequacy perspective of three aspects; service adequacy for severe movement limited person, the amount of trips and service certainty.

2. Peculiar trend of regional characteristic of FUKUSHI-YUSHOUNSO service adequacy have not been found.

It is necessary for the municipality to reconsiders the standard of subsidy delivering. The municipality should consider severe movement limited persons when they decide to how much they deliver subsidy for NPO. It is because that the most of NPOs which conducts bed to bed service don't gain subsidy even though the service demand is large and it is expensive to deliver bed to bed service.

However, the subjects of this study are only 33 NPOs out of 120 in Tokyo. It means that this research cannot understand operation of whole FUKUSHI-YUSHOUNSO NPOs in Tokyo. Additionally, the way of choosing NPOs in this study may have involved a selection bias. Moreover, service adequacy doesn't include operation fee even though Operation fee is important to choose a FUKUSHI-YUSHOUNSO service for movement limited person. In the case of including operation fee in service adequacy, it must consider use characteristics as well.

## Reference


1. 高齢社会白書(2015) 「第 1 章 高齢化の状況 第 1 節 高齢化の状況」 http://www8.cao.go.jp/kourei/whitepaper/w-2015/html/gaiyou/s1_1.html （アクセス日 2016 年 1 月 19 日）

2. 介護保険事業報告(2015) 「介護保険事業状況報告（暫定）平成 27 年 4 月分」 http://www.mhlw.go.jp/topics/kaigo/osirase/jigyo/m15/1504.html （アクセス日 2016 年 1 月 19 日）

3. 藺牟田洋美・安村誠司・阿彦忠之（2004 年）「準寝たきり高齢者の自立度と心理的 QOL の向上を目指した Life Review による介入プログラムの思考とその効果」『日本公衛誌』第 51 巻第 7 号,471-482

4. 清水浩志郎（1995）「高齢者・障害者交通研究の意義と今後の展望」『土木学会論文集』第 518 巻第 28 号,17-29

5. 阿部名保子（2010）「福祉有償運送事業の運営実態から見た持続可能な移動サービスの現状と今後のあり方」『運輸政策研究』第 13 巻第 3 号,24-34

6. 国土交通省(2008)「福祉有償運送ガイドブック」 http://www.mlit.go.jp/jidosha/sesaku/jigyo/jikayouyushoryokaku/GB-honbun.pdf （アクセス日 2016 年 1 月 19 日）

7. 金森弘昇・松田眞一（2010）「周期性のあるデータを中心とした独立成分分析の考察」http://www.seto.nanzan-u.ac.jp/st/nas/academia/vol_010pdf/10-011-025.pdf （アクセス日 2016 年 1 月 19 日）

8. 総務局（2015） 「東京都の人口（推計） 平成 27 年 4 月」 http://www.metro.tokyo.jp/PROFILE/map_to.htm （アクセス日 2016 年 1 月 19 日）

9. 都道府県別人口密度（2015）「都道府県，年齢（3 区分），男女別人口ー総人口 平成 27 年 1 月」 http://www.stat.go.jp/data/jinsui/2014np/ （アクセス日 2016 年 1 月 19 日）

10. 高齢社会白書(2015) 「第 1 章 高齢化の状況 第 2 節 高齢者の姿と取り巻く環境の現状と動向」 http://www8.cao.go.jp/kourei/whitepaper/w-2015/html/zenbun/s1_2_1.html （アクセス日 2016 年 1 月 19 日）

# FACTORS AFFECTING MONGOLIAN PRIMARY SCHOOL LEADERS' ATTITUDES TOWARD ICT IN EDUCATION

Student Number: 15M18055 Name: Yusuke Ohya
Supervisors: Shinobu Yamaguchi and Jun-Ichi Takada

During the multiple education reforms with policy development and project implementation since late 1990s in Mongolia, responsibilities of school leaders have increased. One of the focuses of its policy is to integrate ICT in education, and thus, school leaders' positive perceptions on use of ICT have become essential. This study aims to explore the factors that affect the attitudes of primary school leaders in Mongolia toward ICT use in educational activities. The study of 222 school leaders found that two factors, namely, teacher cooperation and availability of ICT resources are affecting school leaders' attitudes toward ICT in education. These identified factors are expected to help policy makers in Mongolia to develop effective education policies. Further, this study also revealed that other factors such as school leaders' age, school location, and availability of ICT specialist are not found to be significant factors. This finding also contributes to the current literatures on attitudes of school leaders.

# 1 Introduction

After the collapse of the Union of Soviet Socialist Republics (USSR), Mongolia faced financial difficulties in every sector. Especially in education sector, as education expenditure decreased by 56% between 1990 and 1992, both an access to schooling and its quality were deteriorated [1]. In this context, education reform has been taken place in Mongolia with policy development and project implementation. In 2006, "Master Plan to Develop Education of Mongolia in 2006-2015" was established, and one of the focuses of its policy is to explore the use of ICT to improve education, contributing to increased access to education and teacher development. Mongolian governments have developed plans to intensify their investments regarding ICT integration in education .

Given new national policies, responsibilities of school leaders have increased to effectively utilize ICT in school activities. As the role of school leaders is vital in making decisions on educational activities, the positive perceptions of school leaders on the use of ICT at school have become essential.

Given this background, this study aims to explore the factors affecting the attitudes of Mongolian primary school leaders toward ICT use in education.

# 2 Literature Review

## 2.1 Educational change theory

There are two important theories supporting this study. One is the Fullan's educational change theory. The educational change is recognized as a synonym to education reform [2]. The theory states that transformation of beliefs of educators is the fundamental component for the sustainable implementation of educational change. School leaders, especially, are expected to lead changes as facilitators among those who are involved in educational reform. A considerable amount of evidence exists that school leaders are crucial for determining the success of changes within the schools [3] [4].

As discussed earlier, Mongolia is experiencing educational reform supported by policies and project implementation. Hence, it is important to look at the attitudes of school leaders toward ICT use in educational activities, which is one of the significant factors in the success of the educational change.

## 2.2 Attitude study

There are multiple definitions of people's attitudes. Kreijns, Acker, & Vermeulen defined attitudes as person's overall feeling of sympathy or antipathy toward an object. Further, number of studies supported that attitudes are the most distinctive and indispensable concept determining people's behavior [5].

In developing scales to measure people's attitudes, Smith established the tripartite model. It categorized the concept of attitudes into three aspects: 1) affective domain; 2) behavioral domain; and 3) cognitive domain. Affective domain reflects feelings toward an object/event. Behavioral domain reflects behavioral intentions and action with respect to an object/event. Cognitive domain refers to perceptions and beliefs about an object/event [6].

This model has been adopted and utilized in different types of attitude studies in both developed and developing countries [7] [8].

## 2.3 Potential factors affecting school leaders' attitudes toward ICT in education

An extensive literature review identified the following eight potential factors which affect school leaders' attitudes toward ICT in educational activities: 1) teacher cooperation; 2) school ICT strategy; 3) pedagogy using ICT; 4) school ICT specialist; 5) ICT resources; 6) gender; 7) age; and 8) location of school. Accordingly, eight hypotheses

were developed as follows (Fig 1):

**Hypothesis 1**: School culture that teachers cooperate and share their experiences is positively affecting school leaders' attitudes toward ICT in education

**Hypothesis 2**: Development of school strategies for ICT is positively affecting school leaders' attitudes toward ICT in education

**Hypothesis 3**: School culture that teachers share and discuss the pedagogy using ICT is positively affecting school leaders' attitudes toward ICT in education

**Hypothesis 4**: Availability of school ICT specialist is positively affecting school leaders' attitudes toward ICT in education

**Hypothesis 5**: Availability of ICT resources is positively affecting school leaders' attitudes toward ICT in education

**Hypothesis 6**: Gender is affecting school leaders' attitudes toward ICT in education

**Hypothesis 7**: Age is negatively affecting school leaders' attitudes towards ICT in education

**Hypothesis 8**: School location is affecting school leaders' attitudes toward ICT in education

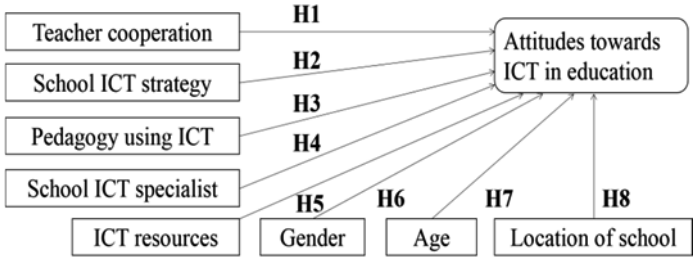


Fig 1. Hypotheses on potential factors affecting school leader's attitudes

# 3 Methodology

## 3.1 Significance of focusing on cognitive attitudes toward ICT in education

Applying the tripartite model to measure school leaders' attitudes, this study particularly focuses on cognitive aspect for the following reasons.

First, in discussing technology introduction into school setting, the previous studies found the importance of cognitive domain to analyze the attitudes of school leaders. For instance, Pelgrum found that there is a clear association between cognitive attitudes of school leaders and the emphasis on computer integrated learning at schools [9]. Further, regarding the Mongolian context, local experts emphasized the importance of people's positive cognitive attitudes to promote ICT usage in school settings. The expert pointed out that some Mongolian people are not enthusiastic to utilize ICT tools due to the lack of belief of positive impact of ICT [10].

## 3.2 Data source

For quantitative analysis, data were retrieved from the baseline survey of "Quality Improvement of Primary Education Teachers Through Development of Training Materials Using ICT", conducted in 2012. A total of 222 responses were collected for data analysis from school principals and training managers from five regions, reflecting geographical differences. (Fig 2). This sample represents 9.9% of primary school leaders in Mongolia. As for the qualitative analysis, face-to-face interviews and questionnaire survey took place in Khentii, Khovd, Bayankhongor provinces, and Ulaanbaatar city. A total of 13 school leaders and local government representatives participated in the survey.


Fig 2. Data collection sites in Mongolia

## 3.3 Data analysis process

The quantitative data analysis had four steps. First, data cleaning including data re-coding and creating dummy variables were performed. Second, question items were categorized into different variables based on the literature review. Third, exploratory factor analysis was conducted to avoid redundancies in question items and examine the structure or relationship between variables. Forth, multiple regression analysis was employed to identify the significant factors affecting school leaders' attitudes toward ICT use in education. Descriptive analysis of the data sample supplements the analysis to understand its characteristic. A set of demographic information, including position in school, gender, age, years of service at the position, and school location is described.

# 4 Findings

## 4.1 Demographic information

The respondents are composed of school principals (48.4%, N=104) and training managers (51.6%, N=111). Nearly three quarters are female (73.2%, N=161). As for its age distribution of the respondents, 44.7% (N=93) are age of 40-49, followed by 30-39 years olds (26.0%, N=54). In terms of years of experience as school leaders, 45.7% (N=85) worked for 20-29 years and another 18.3% (N=34) worked for 30-39 years. As for the location of the schools, 74.4% (N=157) are located in villages while 13.7% (N=29) are situated in provincial center, and 11.8% (N=25) are in Ulaanbaatar.

### 4.2 Exploratory factor analysis

A set of 15 question items measuring school leaders' attitudes and affecting factors were extracted from the baseline survey. Factor analysis was conducted on these items to avoid redundancies in question items. Kaiser-Mayer-Olkin (KMO) test and Bartlett's test were conducted to detect sampling adequacy and correlation between variables. As a result, the KMO measure is 0.843 which confirmed the adequacy of data. Also, Bartlett's test of sphericity was found statistically significant, which indicates that null hypothesis (there are no correlations between any of the variables) is rejected. Hence, these result proved that the data are suitable for factor analysis.

Subsequently, factor rotation was conducted to recategorize the factor structure of question items for adequate interpretations. It was found that 15 question items were recategorized into four latent variables with 13 question items. As for the reliability of each category, Cronbach's alpha ($\geq 0.7$) confirmed an internal consistency (Table 1).

Table 1. Cronbach's Alpha for latent variables

| Latent variables | Number of items | Cronbach's Alpha |
|---|---|---|
| Pedagogy using ICT | 3 | .777 |
| Teacher cooperation | 4 | .833 |
| Leaders' attitudes in ICT integrated education | 3 | .847 |
| School ICT strategies | 3 | .804 |

In addition to four categories, variables which were not tested in factor analysis such as ICT resources, school ICT specialist, gender, age, and school location are also utilized for multiple regression analysis.

### 4.3 Multiple regression analysis

Multiple regression analysis was conducted to identify the factors affecting school leaders' attitudes toward ICT use in education activities. Nine independent variables, namely, teacher cooperation (TC), school ICT strategy (SS), pedagogy using ICT (PI), school ICT specialist (IS), ICT resources (IR), gender (G), age (A), and location of school (LS1 and LS2). Dependent variable in this model is school leaders' attitudes toward ICT use in educational activities (ATTD). The regression model is developed as follows.

$$ATTD = \gamma + \delta_1 TC + \delta_2 SS + \delta_3 PI + \delta_4 IS + \delta_5 IR + \delta_6 G + \delta_7 A + \delta_8 LS1 + \delta_9 LS2 \quad (1)$$

Table 2 summarizes the result of regression analysis. Based on the analysis, model of Mongolian primary school leaders' attitude was shown as the following.

$$ATTD = 0.937 + 0.384\,(TC) + 0.153\,(IR) \quad (2)$$

Equation (2) shows that there are two statistically significant variables affecting school leaders' attitudes toward ICT use in educational activities, namely, teacher cooperation and ICT resources. Regarding the model fits, this model explains 27.7% of the variance of Mongolian primary school leaders' attitudes toward ICT in educational activities.

Table 2. Regression and Multicollinearity Statistic

| Variables | B | Std. Error | t | Sig. | VIF |
|---|---|---|---|---|---|
| (Constant) | .937 | .457 | 2.053 | .041 | |
| **Teacher cooperation** | **.384** | **.113** | **3.412** | **.001** | **1.523** |
| Pedagogy using ICT | .127 | .081 | 1.571 | .119 | 1.580 |
| School ICT strategies | .070 | .089 | .783 | .435 | 1.396 |
| **ICT resources** | **.153** | **.045** | **3.406** | **.001** | **1.124** |
| School ICT specialist | -.030 | .121 | -.251 | .802 | 1.091 |
| Gender | -.020 | .099 | -.198 | .844 | 1.084 |
| Age | -.001 | .006 | -.125 | .900 | 1.189 |
| Location of school 1 | -.021 | .140 | -.151 | .880 | 1.890 |
| Location of school 2 | -.093 | .177 | -.525 | .600 | 1.831 |

($R^2_{adj} = .277$)

As for the Variance Inflation Factor (VIF), the result revealed no infringement on multicollinearity issue, suggesting that the independent variables do not exhibit strong correlation to each other. On the other hand, other factors including school ICT strategy, pedagogy using ICT, school ICT specialist, gender, age, and location of school were not found statistically significant factors affecting school leaders' attitudes. These results are discussed further in the latter sections. The data analysis supports two hypotheses introduced in this study.

**Hypothesis 1**: School culture that teachers cooperate and share their experiences is positively affecting school leaders' attitudes toward ICT in education

**Hypothesis 5**: Availability of ICT resources is positively affecting school leaders' attitudes toward ICT in education

## 5 Discussion

This section discusses five major findings in relation to current literature.

First, teacher cooperation was found significant for school leaders' attitudes toward ICT use in educational activities. This finding is consistent with previous studies [11] [12]. The qualitative survey result also supports this finding. School leaders recognized that teacher cooperation is essential for teachers to promote the use of ICT for educational activities. Especially, rural schools are located in dispersed environment with limited educational resources, and thus, sharing knowledge, skills and new information were essential to cope with new ICT tools to be introduced into their educational activities. Further, improvement of ICT infrastructure also created the culture of sharing among teachers.

Second, availability of ICT resources are also found to be a significant factor affecting Mongolian

school leaders' attitudes toward ICT use in education. In Mongolian primary school context, with national policies and strategies of expanding ICT into educational settings, school principals have become more responsible to establish school ICT infrastructures. Therefore, the level of ICT environment is a vital question for school leaders to be dealt with on daily basis.

Third, the analysis found that an availability of school ICT specialist does not affect school leaders' attitudes toward ICT in education. This finding was contradictory with the current literature indicating the importance of the ICT specialist. Further, in the interviews and survey conducted in urban and rural schools, the majority of the respondents agreed with the current literature emphasizing the role of ICT specialists in schools. This contradiction cannot be explained at this moment. A comment of a training manager, however, indicates that hiring an ICT specialist may prevent closer collaboration among teachers as they could rely on the specialist. The view point might imply less importance of a specialist in schools in Mongolian context.

Fourth, the analysis found that age is not important for the school leaders to promote ICT integration in schools. As mentioned earlier, Mongolian government implements ICT policies and strategies through multiple project activities throughout Mongolia. School leaders are in the position to put these strategies into action at school level. Thus, they are obliged to train themselves to upgrade their ICT skills and knowledge regardless of their age.

Fifth, location of school was not found to be a factor affecting school leaders' attitudes toward ICT use in educational activities. This finding was not supported by the previous study in Mongolia [13]. This contradiction of finding can be explained by rapid ICT infrastructure improvement in rural area. Due to those efforts nationwide, school location is not an important issue to affect leaders' attitudes toward ICT use in educational activities.

# 6 Conclusion

Since early 2000s, the Mongolian government has been promoting the use of ICT into teaching and learning through different policies and project implementations. The responsibilities of school leaders have increased to effectively utilize ICT in school activities, and thus, their positive perceptions on the ICT integration at schools have become indispensable. The study found that teacher cooperation and ICT resources are the two important factors affecting Mongolian primary school leaders' attitudes toward ICT use in education. If schools can build an environment for teacher cooperation and improved ICT infrastructure, it would affect positively to the attitudes of school leaders to integrate ICT in teaching and other school activities. It is hoped that this finding can contribute to further policy development in primary education.

This study also found the importance of national policies and strategies. The national efforts nationwide focusing on ICT use in educational activities are so powerful that demographic information such as gender, age, school location are not as much as influential for the school leaders.

Further research is recommended to explore other potential factors influencing school leaders' attitudes toward ICT in education. Additional qualitative data help to understand the local context in Mongolia. Further sampling is also recommended to illustrate school leaders' attitudes more precisely.

# References


[1] Wu, K. (1994). Mongolia: Financing Education during Economic Transition. World Bank Discussion Papers 226. East Asia & Pacific Region Series.

[2] Education Resources Information Center. (1966). ERIC - Thesaurus - Educational Change.

[3] Fullan, M. (2002). The change. *Educational Leadership*.

[4] Hallinger, P. (2003). Leading educational change: Reflections on the practice of instructional and transformational leadership. *Cambridge Journal of Education*.

[5] Ajzen, I., & Fishbein, M. (1977). Attitude-behavior relations: A theoretical analysis and review of empirical research. *Psychological Bulletin*, *84*(5), 888–918.

[6] Ajzen, I. (1988). Attitudes, personality, and behavior.

[7] Albirini, A. (2006). Teachers' attitudes toward information and communication technologies: the case of Syrian EFL teachers. *Computers & Education*, *47*(4), 373–398.

[8] Kay, R. (1994). An exploration of theoretical and practical foundations for assessing attitudes toward computers: The computer attitude measure (CAM). *Computers in Human Behavior*.

[9] Pelgrum, W. (1993). Attitudes of school principals and teachers towards computers: does it matter what they think? *Studies in Educational Evaluation*.

[10] USA International Business Publications. (2015). *Mongolia Investment and Business Guide: Strategic and Practical Information*.

[11] Peansupap, V., & Walker, D. (2005). Factors affecting ICT diffusion: a case study of three large Australian construction contractors. Engineering, Construction and Architectural Management, 12(1), 21–37.

[12] LLouis, KS, HM Marks, and S Kruse. 1996. "Teachers' Professional Community in Restructuring Schools." American Educational Research.

[13] Tsogtsaikhan, O. (2014). Factors Affecting Information Communication Technology (ICT) Integration of Primary School Teachers in Mongolia.

# APPLICATION OF DRONE FOR RIVERBANK LANDSCAPE MONITORING IN THE WORLD HERITAGE SITE OF LUANG PRABANG, LAO P.D.R.

Student Number: 15M18180 Name: Hironari Yu
Supervisors: Shinobu Yamaguchi and Jun-Ichi Takada

With the rapid increase in tourists in the world heritage town of Luang Prabang, there is an urgent need to manage riverbank landscape of the main heritage zone using an appropriate ICT tool. In collaboration with the Department of World Heritage, Luang Prabang (DPL), drone was selected as a tool to effectively visualize the current conditions along Mekong river. Landscape analysis was conducted to identify the gaps between current conditions and the preservation criteria. Analysis found the followings: 1) riverbank areas accessible from the street intersections are particularly not meeting preservation criteria; 2) five areas with large scale temporary tents and storages are located near boat parkings on Mekong river; and 3) restaurant owners are prioritizing tourist needs rather than preservation criteria. These findings may imply that local residents have limited understanding about the preservation criteria, and therefore, raising preservation awareness targeting these populations is found to be essential. A set of video data of riverbank landscape produced in this study serve as baseline data for future preservation policy development.

## 1. Introduction

### 1.1. Site background

Luang Prabang of Lao P.D.R was inscribed as a World Heritage site of UNESCO in 1995 for its outstanding values [1]. Since its inscription, the town has faced drastic increase of tourists. Furthermore, there is a concern that its landscape may change due to unplanned urban expansion [2]. UNESCO monitoring report of 2008 noted the possibility for Luang Prabang to be listed as World Heritage in Danger [3]. Thus, there is a keen need to keep a balance between development and preservation in Luang Prabang. Tokyo Institute of Technology (Tokyo Tech) has been collaborating with DPL aiming at the sustainable development management of heritage site using Information and Communication Technology (ICT) since 2004. In 2015, riverbank landscape management is identified as one of the core activities to keep the value of Luang Prabang as a World Heritage site.

### 1.2. Problem statement

The Heritage Master Plan of Luang Prabang states that Mekong riverbank and Namkhan riverbank were originally covered by greenery such as vegetable gardens. However, after its inscription, decreasing tendency of greenery was found in both riverbanks [3]. These potentially contribute to the degradation of Luang Prabang as a World Heritage site. The Riverbank Management Plan was developed in 2015 to preserve its landscape as riverbank landscape is one of important heritage in Luang Prabang. However, little information on current condition of riverbank landscape is available, and thus, an urgent need was identified to understand and analyze current riverbank landscape to effectively implement Riverbank Management Plan.

### 1.3. Research objectives

Four research objectives were formulated: 1) to identify the appropriate tool for visualization and to analyze its use; 2) to collect riverbank landscape visual data; 3) to develop an evaluation tool to analyze riverbank landscape; and 4) to evaluate and analyze the current landscape in Mekong riverbank.

## 2. Literature Review

### 2.1. Importance of riverbank management

There are two importance points in riverbank management in Luang Prabang. First, riverbank landscape is recognized as a part of outstanding values by UNESCO. Heritage Preservation and Development Master Plan (PSMV) established in 1999 specifies the importance of riverbank landscape, and thus, it is a responsibility of DPL to preserve. Second, green environment on riverbank has the important function for preventing landslides by strengthening the root networks of trees and plants. Therefore, the protection of greenery is the key in maintaining the safe environment along the riverbank. This research collects detailed information about riverbank landscape and analyzes the current landscape with DPL.

### 2.2. Riverbank Management Plan

Riverbank Management Plan covers the protection area of 4.5 km of both Mekong riverbank and Namkhan riverbank. The plan shows the comparison between the current landscape and the ideal landscape synthesized from the photos of current landscape on 11 important

preservation points. This management plan contains characteristics of the protected zone together with protection criteria. The management plan only restricts the landscape from the street side. However, landscape conditions in the riverside are also important for future management, and therefore this study focuses on the visualization of the riverbank.

### 2.3. Landscape monitoring tools

Five potential monitoring tools were identified to examine appropriate tools in the field from existing or ongoing projects around the world: 1) drone; 2) balloon; 3) kite 4) crane; 5) manned helicopter [4][5][6][7]. These tools are utilized to monitor coastal situation to prevent natural disaster, to analyze damages caused by earthquake, as well as to monitor biodiversity of the world heritage site. Each tool contains both advantages and shortcomings. This study analyzes the use of these tools reflecting local conditions of Luang Prabang.

## 3. Methodology

Four major steps were involved prior to the landscape analysis: 1) identification of monitoring tools; 2) visualization of riverbank landscape; 3) development of a landscape analysis method; and 4) selection of landscape evaluators. As a first step, the comparative analysis of the five possible monitoring tools was conducted through field survey. Considering seven selection criteria, i.e. recording from riverside, recording from high view, distance to the objects, cost, training needs for operation, difficulty in maintenance, and possible recording time, drone was selected as an appropriate monitoring tool. Four aspects were found important: 1) capabilities of recording from riverside; 2) capabilities of recording from high view; 3) capabilities of close monitoring to the objects; and 4) relatively low cost.

For a second step, riverbank landscape visualization took place using the drone in 2016. This step includes 1) selection of pilot site, 2) identification of landscape monitoring indicators, 3) collection of landscape visual data focusing on the indicators, and 4) improvement of landscape data. First, 1.5 km of protected zone along Mekong riverbank was selected (Fig. 1).

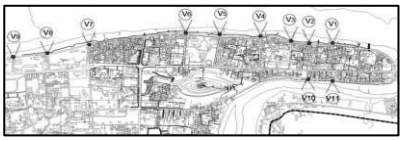

**Fig. 1 Important intersections**
Source: Riverbank Management Plan, 2015, p. 9

Second, landscape analysis was carried out on green environment and built architectures in the pilot site. Third, video shooting instead of photo taking was conducted to record the continuous views of Mekong riverbank landscape using Parrot Bebop drone with recording documentation written in English. Forth, the video data were improved by editing, stitching and tagging with a map using GPS. These processes produced a video of green environment (9.15 minutes) and a video of built architectures (11.15 minutes) (Fig. 2).

**Fig. 2 A sample green environment video**
Source: Created by the author, 2016

As for the third step, an evaluation tool was developed. In this process, important landscape preservation criteria for greenery and built architectures were clarified reflecting the Riverbank Management Plan and discussion with DPL staff members. Four specific criteria were identified: 1) no temporary tents; 2) no temporary storages; 3) no other temporary objects; and 4) no piling of fire woods, sands and gravels. These criteria are important because such temporary objects on the riverbank degrade the landscape of Luang Prabang. On the other hand, the criteria of built architectures focus on the location and interior of the architectures. Three specific criteria were: 1) (restaurants) not located in front of intersections; 2) no roof (white umbrella can be used); and 3) no wall. Riverbank landscape is considered important from both riverside and street side, and thus, the view of the built architectures needs to be evaluated accordingly. Finally, these criteria are reflected to produce a set of evaluation sheets for landscape analysis.

As a fourth step, landscape evaluators were selected within DPL. Specifically, ten and nine evaluators were selected for analysis of green environment and built architectures respectively from different units in DPL. Landscape analysis was performed using the landscape video data and evaluation sheets in October and November, 2016.

## 4. Results / Analysis

### 4.1. Analysis results of green environment

The greenery landscape analysis found the gaps between current landscape and the preservation criteria. Specifically, 14 areas were identified as not meeting the criteria by evaluators. Among them, five areas were identified by all ten evaluators (Fig. 3).

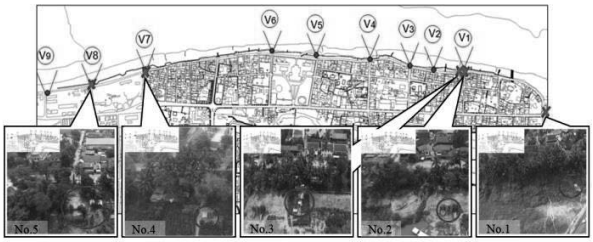


**Fig. 3 Analysis results for greenery**
Source: Created by the author utilizing Riverbank Management Plan (2015, p.9), 2016

In these five areas, large temporary tents and storages were found against the preservation criteria. This result suggests that these five areas are subject to careful monitoring for landscape preservation. In the analysis, seven areas out of 14 were situated in riverbank accessible from the intersections. Interviews with local residents clarified that tents or storages found in nine areas were owned and utilized by the boat owners. Their preservation awareness is vital for the sustainable riverbank management.

## 4.2. Analysis results of built architectures

The landscape analysis for built architectures also found the gaps between current condition and the management plan. Twenty-two restaurants out of 32 in the pilot site were not meeting the preservation criteria. For example, 20 restaurants had roofs that are not permitted.

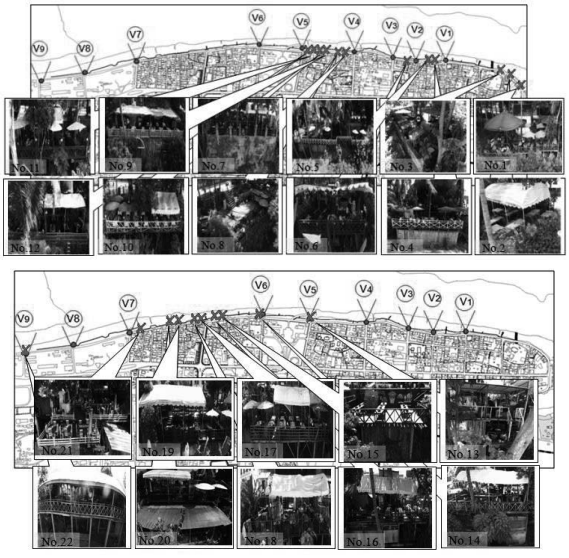


**Fig. 4 Analysis results for architectures**
Source: Created by author utilizing Riverbank Management Plan (2015, p.9), 2016

Further, figure 4 illustrates 14 restaurants against the criteria were situated in the areas between V4 and V5 and between V6 and V7. These areas have multiple tourist attractions such as Luang Prabang Main Street, Mt. Phousi and the National Museum. This result shows that restaurant owners prioritize the tourist needs rather than the preservation criteria. At the local workshop in DPL, difficulties of satisfying both tourist needs and preservation criteria were discussed. Specific measures to raise awareness of the residents to understand the importance of preservation criteria are needed for the future activities. Furthermore, 11 restaurants out of 22 were using white tents. White tents are not permitted for the restaurants although white umbrella are allowed. It was interpreted in the local workshop that such regulation may not be understood precisely by the restaurant owners. Therefore, the importance of effective dissemination of regulation was recognized.

## 4.3. Advantages of landscape analysis method

The landscape analysis method makes the long-term monitoring of Mekong riverbank landscape. There are two reasons. First, all evaluators from different units of DPL could identify areas and architectures not meeting the preservation criteria. It suggests that this analysis method can be utilized by any staff members regardless of their technical background. Second, it enables to analyze the current landscape in detail through the comparison between landscape video data and preservation criteria. This method can be applied to understand the changing situations of the landscape contributing to the chronological landscape comparison over time.

## 4.4. Issues of landscape analysis method to be discussed

Three issues were identified to be considered for the improvement. Two technical issues specific to the drone used for video shooting were identified. First, the current digital zoom function of the video processing software of Parrot Bebop drone cannot capture detailed information on the landscape. Therefore, it is suggested to use the drone with optical zoom which can which can shoot specific objects with magnified images. Second, the video data taken by drone contained some blurred images. Evaluators experienced difficulties to evaluate the landscape due to the low resolution. To tackle this problem, it is necessary to develop recording manual including important check points for clear images. Third, the study found that some of the preservation criteria of Riverbank Management Plan are not clear

enough for the evaluators to make decision in the analysis. For the effective landscape analysis, it is necessary to carefully define the preservation criteria.

## 5. Discussion

Through the landscape analysis using drone, two findings were identified. First, the training of drone operation on the site is vital for its effective use. Because the operators should have the ability not only to operate it smoothly but also to respond unexpected incidents when capturing the images. This is consistent with the previous study that the specific training on the site can contribute to efficient workload and wide range of applications [8]. Second, countermeasures for risk of crash were identified. They are: 1) to keep a short distance between operators and drone for prevention of unstable Wi-Fi connection during the flight; and 2) to refrain from operating drone near the trees and other objects, 3) to avoid rainy and windy weather conditions. These countermeasures were partly confirmed by a previous study [4].

Further, based on the analysis results of both green environment and built architectures of the pilot site of Mekong riverbank area, three effective measures were clarified for future landscape preservation. As for green environment, there are two specific activities to be promoted from the landscape analysis. One is to promote boat owners' preservation awareness. The other is to cooperate with local residents in order to monitor the riverbank areas accessible from the intersections more frequently. Large scale tents and storages are owned by the boat owners, and awareness campaign targeting them would be a vital strategy for DPL. For another measure, it is important to plan and implement activities to motivate residents to participate in preservation of their village. One suggestion is to introduce mobile application developed by Tokyo Tech that include quizzes and important information on riverbank management [9]. Cooperative monitoring with local residents can contribute to the preservation in these areas. Regarding built architectures, discussion sessions between local residents and DPL are highly recommended. The landscape analysis clarified: 1) difficulties to keep a balance between satisfying tourist needs and following preservation criteria, and 2) possibilities of misunderstanding about the criteria among local residents. To cope with these issues, opinion from the restaurant owners is considered vital for an effective preservation.

## 6. Conclusion

Riverbank landscape management is an important part of heritage preservation in the world heritage town of Luang Prabang. The landscape analysis identified the gaps between current conditions and the Riverbank Management Plan. To deal with the gaps, it is necessary to raise preservation awareness understanding the criteria among local residents. Although this study covered 1.5 km of protected zone along Mekong riverbank as a pilot site, it is suggested that future study applies the monitoring method to the extended 3 km along Namkhan riverbank to achieve complete data collection.

### Reference


[1] UNESCO. (1995): Town of Luang Prabang, UNESCO World Heritage Center, [Online], Available: http://whc.unesco.org/en/list/479/, (Accessed on January 9, 2017)

[2] Leong, C, Yamaguchi, S, Takada, J, Sitthirath, R, Vannathy, P, Phonesawat, X, Sengraly, P. (2010): Introducing GIS (Geographical Information System) to monitor development in world heritage site of developing country: Case of Luang Prabang, Lao P.D.R, 3rd joint international conference on information & communication technology electronic engineering (JICTEE), pp. 503-507, Luang Prabang Lao P.D.R.

[3] ICOMOS. (2008): Reactive monitoring mission to the town of Luang Prabang world heritage property Lao People's Democratic Republic, WHC-07/31.COM/7B , pp. 22-28 November 2007, [Online], Available: http://whc.unesco.org/document/10057 (Accessed on January 12, 2017)

[4] Mariella, D., Giuseppe, D, C., Massimo, R., & Antonio S. (2012). Use of unmanned aerial vehicles (UAVs) for photogrammetric surveys in rockfall instability studies, Società Geologica Italiana, Roma 2012.

[5] Boike, J & Yoshikawa, K. (2003). Mapping of Periglacial Geomorphology using Kite/Balloon Aerial Photography. Permafrost Periglac. Process. 14: 81-85

[6] Terunuma, H., Yokouchi, N., & Okada, T, (2007): 日本映画にみる海の風景の意味と演出方法に関する研究. 景観・デザイン 研究講演集. No.3

[7] Uchiyama, S. (2015). 有人ヘリコプターによる空撮画像を用いた平成 27 年 9 月豪雨における災害対応地図の作成. Research Abstracts on Spatial Information Science: CSIS DAYS 2015.

[8] Hing, J, T, Oh, P, Y. (2008): Development of an unmanned aerial vehicle piloting system with integrated motion cueing for training and pilot evaluation, J Intell Robot Syst, 54:3–19.

[9] Poong, Y, S, Yamaguchi, S, Takada, J. (2016): Study of perceptions on behavioral expectation to preserve world heritage site through mobile learning application in Luang Prabang, Lao P.D.R. doctoral thesis, International Development Engineering, Tokyo Institute of Technology, Japan

**Estimating Near-surface Wind Field by Aerial Thermal Image Velocimetry**

Student Number: 15M18138 Name: Motoyuki HIJIKATA Supervisor: Manabu KANDA

熱画像地表面風速場推定法の航空機観測への応用

土方 基由

本論文では，熱画像地表面風速場推定法（TIV）をヘリコプターからの観測に適用し，数百メートルスケールにおける移流の可視化及びベクトルの推定を行った．Scale Invariant Feature Transform (SIFT)を用いた座標系統一補正と時系列及び空間フィルタリングを施すことにより，本観測に対してTIV を適用することができ，その結果時間及び空間的に局所性を有する風速場の測定に成功した．さらに，追跡している乱流構造のスケールや地表面パラメータの空間分布の推定手法の提案，TIV 速度と地表観測値とのバリデーションを行った．

# 1 Introduction

Turbulent structure inside an atmospheric boundary layer is dependent on atmospheric conditions and the geometric nature of the surface. However, measurement method for horizontal wind velocity distribution is limited. Recently, a method to estimate two-dimensional wind velocity called thermal image velocimetry (TIV) was established. The concept behind it lies in the relationship between the changes in surface temperature measured by a thermographic camera and the near-surface wind speeds. TIV has successfully detected wind fields near building walls and vortices similar to dust devils, which are tens of meters in scale [1]. To date, the application to larger spatial scales is still limited [2]. In this study, I applied TIV to a larger scale by conducting an aerial observation on-board a helicopter. The outcome of this study suggests the possibility of applying TIV to wider scales, hundreds of meters despite the thermographic camera being not stationary.

# 2 Principle of TIV

Consider a case where the surface is heated and the temperature difference between air and surface becomes extreme. Active turbulence will develop near the surface. As air circulates horizontally aloft, heat transfer between surface and air occurs, resulting to a non-uniform surface temperature distribution. This phenomenon is captured using a thermographic camera and afterwards brightness will be extracted. Applying an image correlation analysis to retrieve brightness temporal variation similar to the particle image velocimetry, horizontal wind distribution is derived.

# 3 Observation Location and Set-up

## 3.1. Meiji Shrine

The observation above the Meiji Shrine was conducted from 11:45 to 11:50 at March 21, 2013 on a clear sunny condition. Surface temperature data at 100Hz were captured using an FLIR SC5000 Thermal IR camera, which was mounted on the helicopter flying 900 m above ground level. The spatial field of view and grid size are 624 m×764 m and 256×320 respectively. The left side of figure. 1 shows the observation site.

## 3.2. Tamagawa Riverbed

Another observation above the Tamagawa riverbed was conducted from 14:35 to 14:50 at December 21, 2016 on a sunny condition. The installed camera and the helicopter altitude were same with that of the Meiji Shrine observation. However, frequency of filming was set to 50Hz. The spatial field of view and grid size are 666 m×800 m and 256×308, respectively, as shown in the right side of figure. 1. In addition, field observation of wind velocity using a supersonic anemometer (Model 81000 Ultrasonic Anemometer) set-up on the ground was simultaneously conducted. The location is indicated in figure. 1.

# 4 Analysis Procedure

Figure. 2 shows the analysis procedure of aerial TIV (henceforth called ATIV). There are three steps in the process, namely: coordinate correction, filtering analysis, and image correlation analysis.

In the first step, coordinate correction was conducted to adjust the images to have a common perspective, a necessary requirement for TIV. Differences in image coverage and perspective was due to the helicopter's

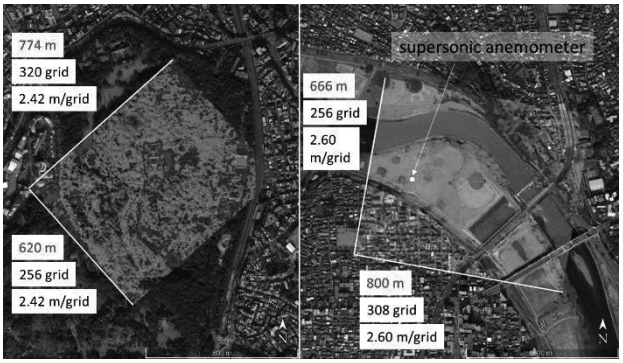


Fig. 1: observation site and scale of Meiji Shrine (left), and Tamagawa riverbed (right)

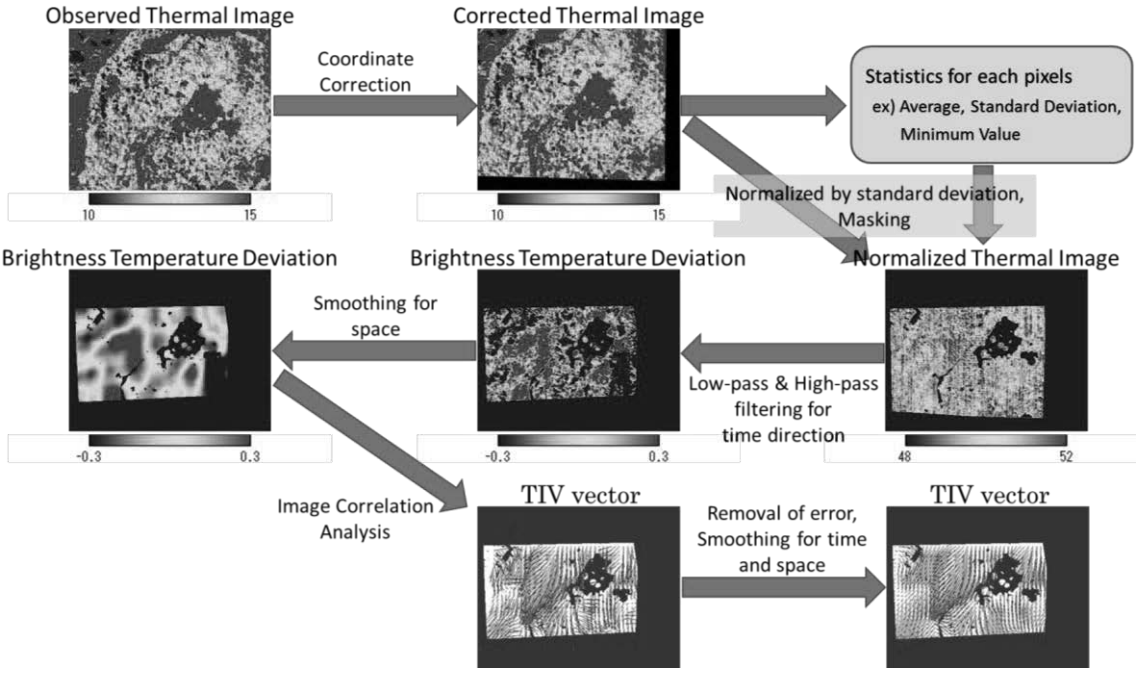


Fig. 2: analysis procedure of ATIV

movement. In this study, SIFT (Scale-Invariant Feature Transform), which can detect a feature point and match them between images was conducted [3]. Subsequently, the Homography matrix based on the detected feature points were multiplied to original images, and then corrected coordinates of each images were acquired. This study achieved the first-ever application of SIFT to TIV.

In the second step, filtering analysis, which is composed of the temporal and spatial direction, was conducted. In the temporal direction, firstly, the pixel value was normalized by the standard deviation value of that pixel. Thereafter, low-pass and high-pass filtering were performed. This process can remove high frequency and low frequency fluctuation, respectively. This enables the detection of turbulence structure at certain desired scaling for each observations. In this study, low-pass × high-pass filter was set to 80(s) × 40(s) for Meiji Shrine, and 30(s) × 15(s) for Tamagawa riverbed. In the spatial direction, spatial smoothing using surrounding pixels was performed. Generally, pixels that correspond to top of trees have larger fluctuation of temperature than internal gaps of trees of low turbulence intensities. In this study, the area considered was the top of trees. In the smoothing process, averaging was conducted in which each pixels were weighted by the standard deviation. Images obtained through this process are called brightness temperature deviation.

In the final step, image correlation analysis, which is the same methodology with PIV was applied. In TIV, the pattern of brightness temperature deviation is used, while particles in images is used in PIV. In this procedure, two images of brightness temperature deviation that have a specified time difference were initially acquired. Next, the inspection domain, which is a square surrounding the focused pixels were set. Thereafter, the area in the second image having the most similar pattern to the first image's focus pixel was detected. This was evaluated by correlation function. Divided by the time difference, TIV vectors between those time differences were estimated. Selected inspection domain and time differencing were 31 grid (75m) and 1(s) for Meiji Shrine, and 31 grid (81m) and 3(s) for Tamagawa riverbed respectively.

In this study, coordinate correction part and normalization by standard deviation in the filtering analysis for temporal direction were added to the standard TIV methodology to make it applicable to aerial-acquired thermal images. The former effectively considers the helicopter's movement, and the latter is for the spatial difference of heat properties in a wide area, of few hundreds meters in scale.

# 5 Result and Discussion

## 5.1. Meiji Shrine

After the filtering analysis, the movement of turbulence fluctuation was visualized using the

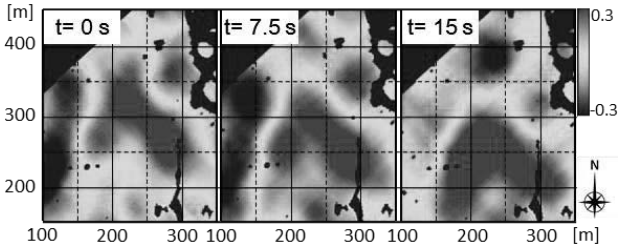


Fig. 3: brightness temperature deviation at a part of Meiii Shrine observation

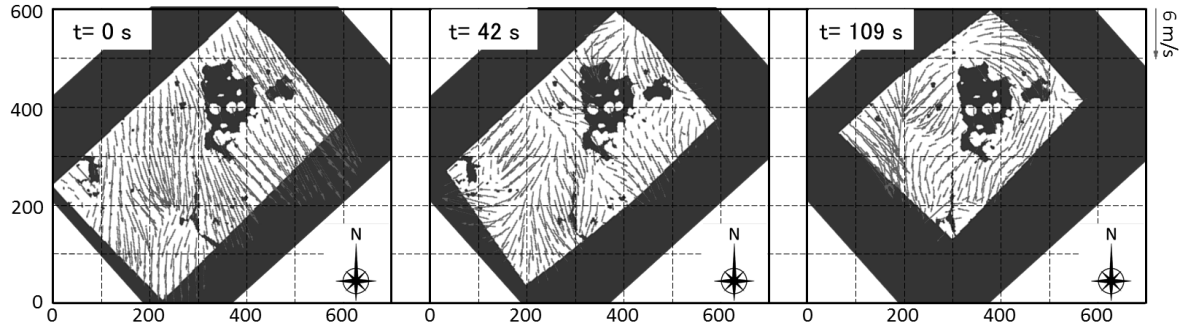

Fig. 4: spatial distribution of TIV vectors in Meiji Shrine

brightness temperature deviation (for example, see Figure. 3). From 0(s) to 15(s), advection from north is visible. In summary, apparent motion-like behavior in brightness temperature deviation from north to south in Meiji Shrine and from southeast to northwest in Tamagawa riverbed were detected.

Figure. 4 shows TIV vectors in Meiji Shrine resulting from image correlation analysis. Initially, the vectors are from northwest direction in almost uniformly, however after 42(s), divergence occurred at around (200, 200) and (400, 500) resulting in the upset of uniformity. After 109(s), another divergence at (300, 500) occurred and flow seems to be going around the building. In figure. 4, spatial and temporal change of TIV vectors were confirmed in Meiji Shrine and Tamagawa riverbed throughout the whole area.

Figure. 5 shows the temporal averaging of spatial distribution of TIV vectors in Meiji Shrine observation (left) and Tamagawa riverbed observation (right). In Meiji Shrine, 83.2% was north-northwesterly wind, while in Tamagawa riverbed, 66.5% was south southeasterly. At the same time, the observed wind direction was north-northwest and south-southeast respectively at Otemachi weather station (AMeDAS), which is 5 km east-northeast from Meiji Shrine and 14 km northeast from Tamagawa riverbed observation site. However, there are slight differences between the TIV result and AMeDAS data in both wind condition, good accuracy between them were confirmed. The average wind velocity was 2.44ms$^{-1}$ and 1.42ms$^{-1}$ in Meiji Shrine and Tamagawa riverbed respectively.

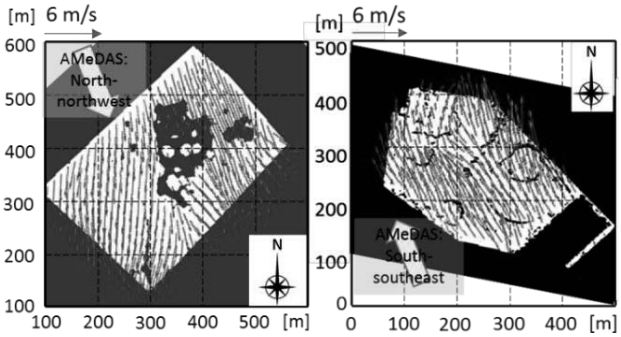

Fig. 5: temporal averaging of spatial distribution of TIV vectors in Meiji Shrine observation (left) and Tamagawa riverbed observation (right)

## 5.2. Estimation of the height of turbulent structure

As shown in Fig. 3, the brightness temperature deviation means a visualization of the footprint of turbulent structure, and TIV velocity corresponds to the velocity of the center of that structure. From this assumption, the height of turbulent structure that TIV has been focusing on can be estimated using the Monin-Obukhov similarity in unstable condition as shown in equation 1. From the result of Meiji Shrine observation, that height of turbulent structure was calculated.

$$\frac{u_{adv}}{u^*} = \frac{1}{k}\frac{1}{z_{coh}}\int_0^{z_{coh}}\left[\ln\left(\frac{z}{z_0}\right)+\ln\left\{\frac{\left(x_0^2+1\right)\left(x_0+1\right)^2}{\left(x^2+1\right)\left(x+1\right)^2}\right\}+2\left(\tan^{-1}x-\tan^{-1}x_0\right)\right]dz$$
$$x=\left(1-16\frac{z}{L}\right)^{1/4},\ x_0=\left(1-16\frac{z_0}{L}\right)^{1/4} \quad (1)$$

$z_{coh}$ corresponds to the height of turbulent structure. $L$: Obukhov length and $z/L$: atmospheric stability were referenced to the observed data at the top of M05 building of Tokyo Tech. $z_0$ was 1.09 derived by $z_0/h$=0.07 [4], and $u^*$: friction velocity was assumed by Rossby number similarity using MSM data provided by JMA [5]. As a result, the height of turbulent structure was evaluated as 122m from top of the forests. From the low-pass for 40(s) and high-pass for 80(s) multiplied by 2.44 ms$^{-1}$, horizontal scale of turbulent structure could be assumed as 97.6–195.2m. We can confirm that the estimated height of turbulence structure is consistent with this result.

## 5.3. Estimation of spatial distribution of friction velocity

Friction velocity is the vital velocity scale to describe turbulence and is used in many similarity theories in meteorology field. Therefore, the attempt to obtain the spatial distribution of friction velocity was conducted using TIV velocity and equation 1 in neutral condition in Meiji Shrine. $z_{coh}$ was assumed equal to the product of 2.44 ms$^{-1}$ and 60(s), the average of low-pass and high-pass filtering. The result is shown in Figure. 6. In accordance with the TIV velocity distribution, the friction velocity has spatial locality too. Especially,

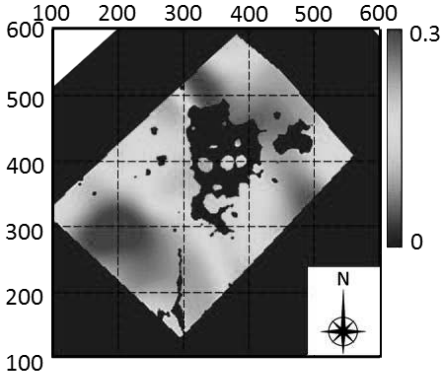


Fig. 6: the spatial distribution of friction velocity

windward side of the building and the area where we can confirm strong divergence in the 42(s) of Figure. 4 have higher value than in other areas.

### 5.4. Validation with the ground observation

In Tamagawa riverbed observation, the validation of TIV velocity with the ground observation using supersonic anemometer was conducted. TIV velocity has proportional relationship between surface wind velocity; however, the ratio between them is unpredictable [6]. Therefore, for validation, the observed wind direction and TIV vector direction at the observation point were compared. The result is shown in Figure. 7. The blue line shows the ground observation and red line shows the TIV vectors. In this figure, 0° shows the southerly wind, and positive is westerly, while negative is easterly. From the comparison, ground data was about south-southeast wind, which matches with the AMeDAS data shown in Sect. 5.1. Changing the value of parameters: inspection domain (*dom*) =10, 20, 30, 40 grid, time step in calculating TIV vectors (*step*) =1, 3, 5 (s), the highest correlation $r$ = 0.44 were obtained in the case (*dom*) = 30 grid, (*step*) = 3(s). However, there are some large fluctuation in TIV vectors that were not observed by the ground measurements at 14:43:20, 14:45:20 and 14:48:00. From the original thermal image, it was found that during these times radial noise were found that led to significant errors arising from the sudden movement of the helicopter. The noise is expected to be removed by calibrating the thermal camera using a black body furnace before observation. Another possibility for the error is the presence of stratus clouds, that might have passed below the helicopter slightly affecting the measured ground temperature.

## 6 Conclusion

The visualization of turbulent structure and TIV vectors in a few hundreds of meters in scale were attempted by applying TIV to aerial observation.

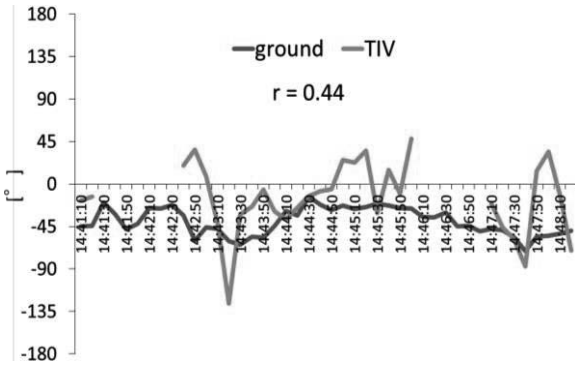


Fig. 7: validation of TIV vector direction and ground observation

Proper filtering analysis and coordinate correction using SIFT algorithm made it possible to realize ATIV and rough agreement with AMeDAS data was confirmed.

For Meiji Shrine observation, using obtained TIV velocity and Monin-Obukhov similarity, the height of turbulent structure that TIV is focusing on was estimated. Compared with the low-pass and high-pass filtering scale, the result was appropriate. In addition, a methodology to estimate the spatial distribution of friction velocity was also suggested.

For Tamagawa riverbed observation, validation of TIV vector direction using ground observation was conducted. Some errors in TIV vectors were found due to the stratus clouds that might have passed below the helicopter or enhanced noise due to the sudden movement of the helicopter. Despite this, moderate agreement was confirmed ($r$ = 0.44).

## Reference

[1] Inagaki, Atsushi, et al.: 'Thermal image velocimetry.' Boundary-layer meteorology 149.1, 1-18, 2013

[2] Inagaki A.: '熱画像風速測定法(TIV)による風の空間分布計測', 水文・水資源学会誌, Vol.29, No.3, pp.186-195, 2016

[3] David G Lowe.: 'Object recognition from local scale-invariant features', International Conference on Computer Vision, Corfu, Greece, pp.1150-1157, 1999.

[4] Javis P G., James G B., Landsperg J J.: 'Coniferous forest in Vegetation and atmosphere', Vol.2, Monteith J L. Ed, Academic, London, pp171-240, 1976

[5] Kondo J.: '水環境の気象学', 朝倉書店, 2014 年第 16 刷

[6] Iwatsuka E.: 'サーモカメラで観測した屋外地表面温度の移流速度と近傍風速の関係', 土木学会論文集 B1 (水工学), Vol.71, No.4, I_427-I_432, 2015

**Projection of High Tide Inundation under Rapid Land Subsidence and Sea Level Rise**

**—Effectiveness and Limitation of Coastal Dykes in Jakarta**

Student Number: 15M18144 Name: Daisuke Fujii Supervisor: Hiroshi TAKAGI

ジャカルタ沿岸域における地盤沈下と海面上昇に伴う将来浸水域予測 —海岸堤防の効果と限界

藤井 大祐


## Abstract

ジャカルタは近年の急激な人口増加・経済発展に伴い，飲料用水・産業用水として地下水を大量に揚水しており，その結果著しい地盤沈下が起きている。低平な沿岸域ではすでに頻繁に洪水被害が発生しているが，最も沈下の激しい Pluit 地区で行った現地調査では海岸堤防は高潮を防ぐには不十分な高さであり，貧弱な構造のため決壊の可能性があることがわかった。本研究では，地盤沈下と海面上昇を予測した複数のシナリオを作成し，2050 年までの浸水シミュレーションを行うことで海岸堤防整備の効果と限界を検証した。沈下が止まらない状況で異常潮位が発生すると，越流により 2050 年の浸水範囲は 40 $km^2$ に広がりジャカルタ全域の問題に発展する。陸地が海面より低いため自然に水が引くことはなく，浸水は 2 週間程度続く可能性がある。堤防は洪水抑止の対策となり得るが，地盤沈下が止まらない場合その効果は一時的であり，逆に引き潮時に堰として働き，浸水を長期化させる要因となることが示された。


## 1 Introduction

Jakarta, the capital of Indonesia, is one of the largest coastal megacities with a recent high population increase and economic growth. A resident population exceeding 9.6 million in 2010 is estimated to reach 30 million by 2030. The population growth rate reached 1.39%/year over the period of 2000-2010. Although Jakarta has also been experiencing rapid economic growth over the last decades, Jakarta has resorted to extract groundwater for domestic and industrial use because of insufficient water supply system. This led to drastic extraction of groundwater and consequently to sinking groundwater level and severe damage to buildings and infrastructures due to land subsidence. Land subsidence rate in Jakarta is the highest among Asian megacities at over 21.5 cm/year (Fig.1.1). This trend is showed notably in coastal areas. Rapid land subsidence causes approximately half of land areas in Jakarta to be lower than sea surface. This problem makes it difficult to drain water to the sea and frequently causes an extended flood due to high tide.

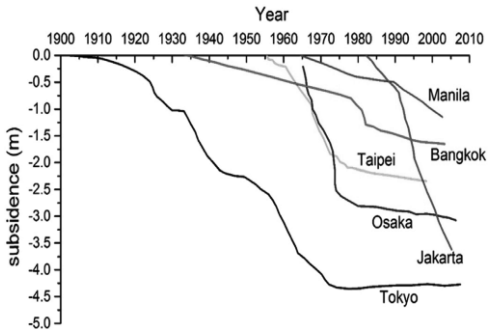


Fig. 1.1 Land subsidence in Asian megacities

The range of tide level in Jakarta Bay is as small as 1 m. However, there is a long-period tide constituent referred to as the “18.6-year lunar nodal cycle” aside from the general diurnal or the semi-diurnal tide constituents. This tidal oscillation can be generated by the positional relationship between the moon’s orbit and the earth's equatorial surface and these inclinations have a period of 18.613 years. In this term, there are regional and extreme sea levels added to the water levels for dozens of centimeters to typical tide in Jakarta. Pluit district, which is sinking at over 10 cm/year in the northwest of Jakarta, has suffered damage due to flooding as often as when extreme high tides occur. It is especially considered that an amplification of tide in November 2007 flooding is caused by these abnormal high tides.

Fig. 1.2 Flood due to high tide in Pluit district, 2007

Jakarta’s government is planning to construct greater dykes with a distance of 34 km along the coastline of Jakarta, the outer sea wall over 50 km and 17 of the artificial islands. The total investment costs are between $8.6 and $20.1 billion (present value). However, the feasibility of the project is not ascertained yet because of many uncertainties such as financial issue and environmental impact.

It is important to understand effectiveness and limitation of coastal dykes against future flood events under rapid land subsidence in Jakarta in order to consider mitigation strategies for those critical issues such as sea-level rise, abnormal high tide and land subsidence. Thus, the author applied the model, which was adjusted to the abnormal tide that happened in 2007, to project future coastal flood under land subsidence and sea level rise.

## 2 Methods

The present study is mainly consisted of two components: (1) understanding the situation of Jakarta’s coast by conducting field surveys and (2) performing numerical simulations, all aiming at discussing future flood and the effectiveness of dykes under land subsidence.

### 2.1 Field Survey

The author conducted a series of field surveys in order to identify coastal issues and measure ground elevations and sea levels around the district of Pluit, where the most

severe land subsidence in Jakarta is taking place. The Pluit district also has the reservoir and the largest pump station (drainage capacity of 50m$^3$/s) to drain water from upstream to the sea.
Actual effect of sinking was observed visually for a few days in September 2015, February 2016, and May 2016. The distance between sea surface and ground elevation was measured by a measuring staff and calibrated the mean sea level at 0 m. The ground elevation in the village behind the dyke was examined using a laser distance meter. The ground elevation was measured at a large number of locations along small residential paths. The sea levels in Jakarta Bay were observed by using a water pressure gauge at the interval of 10 minutes from September 2015 to January 2016.

## 2.2 Numerical Simulation

### 2.2.1 Model outline

The hydrodynamic model Delft-3D was applied to the detailed simulation of future flood in Jakarta. Calculation settings are listed in Table2.1. Flood simulation was performed by using the topography and tidal condition showed Section 2.2.3.
Moreover, hypothetical dykes with different heights were placed all along the coastline in order to investigate whether coastal floods can be effectively mitigated by such flood protections (Fig.2.1, blue).

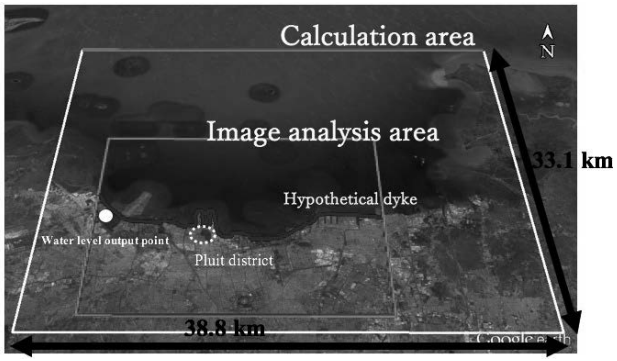


Fig.2.1 Calculation area

Table 2.1 Setting

| | |
|---|---|
| Calculation area | 38.8km × 33.1 km |
| Tide condition | High tide in 2007 flood event ※2.2.3<br>Mean sea level at Tanjung Priok(+0.0 m) |
| Grid size | Number of grid: 434×290<br>Minimum size: 150m × 20 m (near dyke) |
| Time step | Δt = 0.5 min |
| Calculation time | 2 weeks |
| Topography<br>Bathymetry | SRTM satellite data in 2000 ※2.2.3 |
| Roughness (Manning) | Water areas: 0.02, downtown: 0.04, mangrove: 0.3 (s/m$^{1/3}$) |

### 2.2.2 Scenarios

Simulation scenarios were assumed between 2030 and 2050 which were split every 5 years with the year 2015 used as a reference. These scenarios were further separated into two: 1) one scenario is that land subsidence stops by 2030 and only sea level rise continues afterwards and 2) the other assumed that both land subsidence and sea level rise continue by 2050.
It is assumed that coastal dykes were built along the coastline at 2030, and a total of 6 cases of dyke height were considered between 0.5 m and 5 m above mean sea level to see how the characteristics of coastal flood could be influenced by initial heights of the dyke.

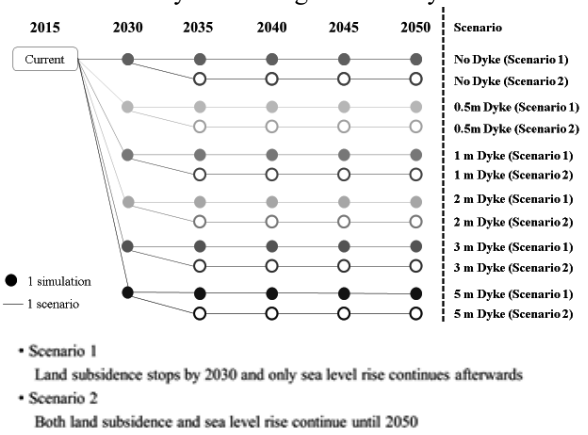


Fig.2.2 Simulation scenarios

### 2.2.3 Input Data

The tidal condition in this study was calibrated by tide data observed during the 2007 coastal flood event, which demonstrated an abnormal high tide component up to 20-30 cm. Topography data between 2030 and 2050 were created by subtracting annual land subsidence continuously observed at 10 points in Jakarta between 1997 and 2001 from the satellite data of SRTM Digital Elevation as of 2000.

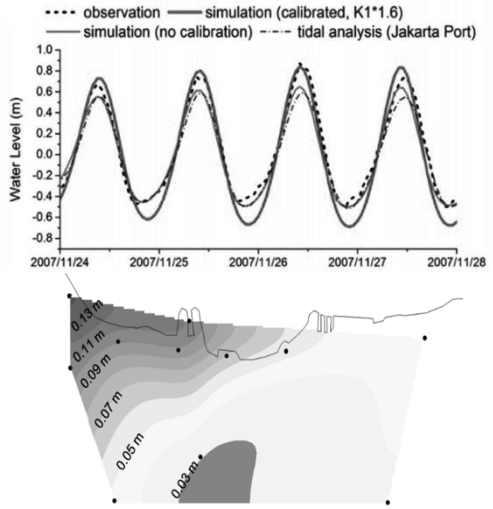


Fig.2.3 Tide calibration and annual land subsidence

Flood area maps were made by masking the output of flood areas from calculation result with water areas at mean sea level in 2015. Future flood areas and flood volume were analyzed from these results and subsequently images were created. Additionally, simulation outputs of the change of water level behind the dyke (Fig.2.1, water level output point) were generated.

# 3 Results

## 3.1 Field Survey

The crest width of dyke in Pluit district was measured to be 50 cm. Because of the thinness, the dyke could be breached in the not too distant future. The height of the dyke was 70 cm above mean sea level, which was as low as the high tide level. These results showed that the dyke

height is not sufficient enough to prevent the sea water from overflowing.

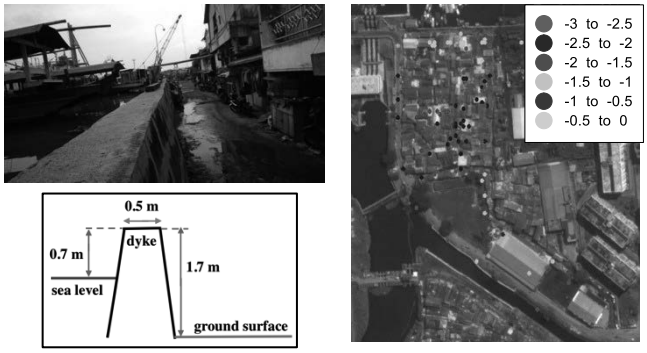


Fig. 2.4 The height of coastal dykes and community behind

The elevation of the coastal community behind a thin coastal dyke is lower than 1.5 m on average and 3 m at maximum below sea level (Fig.2.4).
Although these dykes were raised by about 1 m after the 2007 abnormal tidal flood event, the present height of the dyke appears to be not enough and the concrete has been badly corroded with many cracks.

### 3.2 Numerical Simulation

Fig.2.5 shows the expansion of flood areas in Jakarta, simulated for several scenarios (no dyke, 2 m and 3 m dyke in 2030, 2040 and 2050).
Overflow starts from the northwest coast. Flood event is currently happening within the coastal area, but it is anticipated to expand into the entire Jakarta area by 2050.

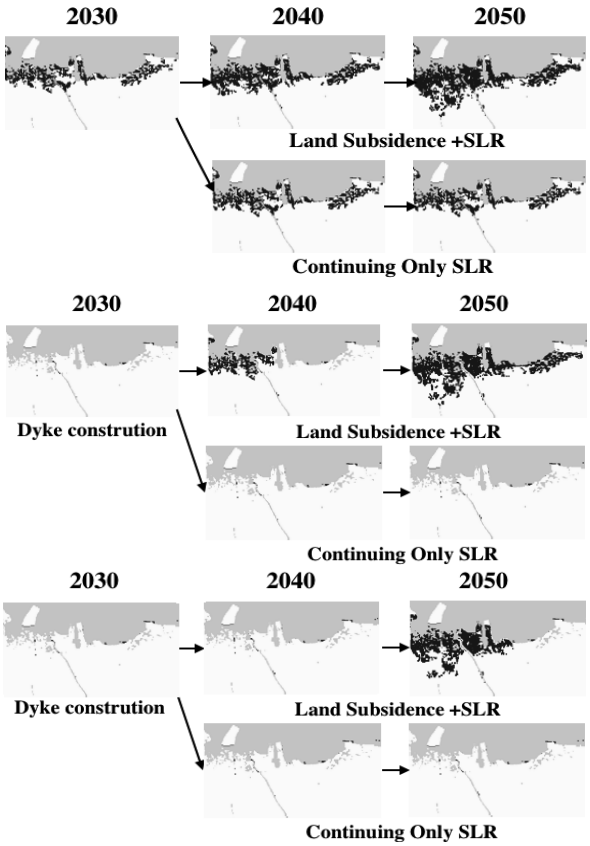


Fig.2.5 Projections of future flood areas

In the case where land subsidence would continue, a 2 m dyke will undergo an extensive overflow from 2040, and even if the 3 m dyke were built, it will be overflowed in 2050. Projected flood areas are similar with those in the case of no dyke.
Fig.2.6 shows the behavior of water level behind the dyke under abnormal tide in 2050.
Compared to the case of without dyke, the case of with 1 and 2 m dyke both make the velocity slower when the sea water returns to the sea, causing stagnant water behind the dykes. In the case of 3 m dyke, the seawater that once overflowed the dyke is trapped by the dyke and not returned to the sea and consequently the water level rises up to the high sea level.

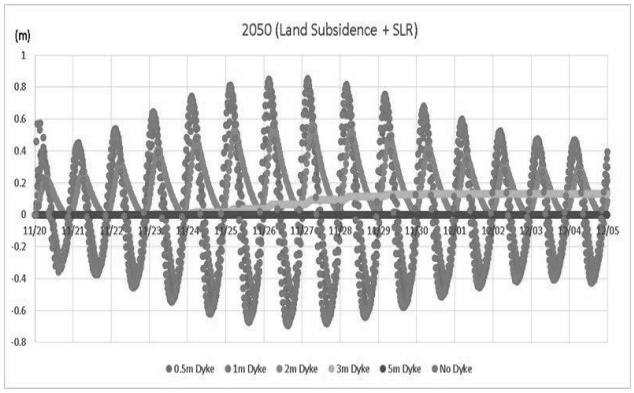


Fig.2.6 Water level behind the dykes

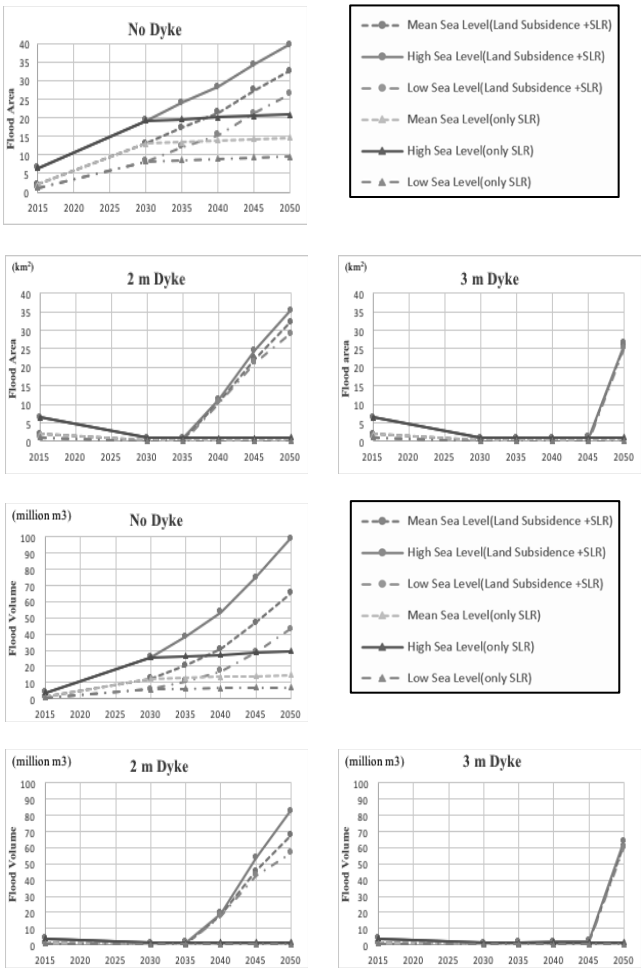


Fig.2.7 Future flood areas and volumes

Fig.2.7 shows the future flood areas and volumes in the different heights of dyke. In continuing land subsidence scenarios, 40 $km^2$ sea water will flow at high sea level in 2050, and it will be 20 $km^2$ in the discontinued sinking scenarios.

If dykes were built and land subsidence was terminated, flood areas would be less than 10% of those of the continuing land subsidence case. Furthermore, in the continuing land subsidence case, the extent of flooding will expand severely even if the initial dyke elevation is as high as 3 m. Lastly, compared to the no dyke case, the higher the built dyke is, the smaller the difference in the resulting flooded areas between high and low sea level.

## 4 Discussion

Field survey revealed that ground elevations in the community of Pluit district are 1 m or even lower than sea level, and that the sea water that once flowed over the dyke is considered to spread to the lowest center of the village rapidly. Seawater cannot return to the sea only by gravity. Therefore, mechanical treatments such as pumps are necessary to drain seawater out to the reservoir and ultimately to the sea.

Even though the local government raised the thin dykes by about 1 meter after the flood event, the difference between the top of the dyke and sea level is only 70 cm in the present condition. This indicates that ground is sinking together with the dyke. If land subsidence is continuing at its current rate, the dyke elevation will be the same as the sea surface within the next 10 years. The cracks and inclination on the dyke due to increasing sea pressure can accelerate the risk and the expanded effect can induce collapse by itself.

The current condition on the dyke renders long periods of flooding induced by the sea water in the adjacent coastal communities. Subsequently, human damages would be more tragic mainly due to the boats and trees being drifted towards the shore.

The simulation results such as the future flood maps, the water levels behind coastal dyke and the future flood volumes due to high tide all illustrate the difference of future flood damage between the continuing and discontinued land subsidence cases.

The present (2015) no-dyke condition induces a maximum of 7 $km^2$ of flood area. In the year 2030, the maximum flood area would be expanded to 20$km^2$, which is twice as large as the minimum flood area (10$km^2$). The flooded area would then be drastically expanded to 40$km^2$ by 2050.

This indicates that the effect of land subsidence is higher than that of the abnormal tide events such as that in 2007 and that the flood damage in the future high tide days is much worse due to the influence of land subsidence.

Although the dyke construction is effective as a flood reduction strategy under the discontinued land subsidence case, the 3-m high dyke will still allow overflow by 2050 if the sinking continues. As water overflows across the dyke, the dyke acts like a wall that prevents the floodwater to return to the sea. The overflowed water could remain inland for a long period. These prolonged inundations may occur regardless of the height of the dyke. Even if a 3-m dyke was constructed in 2030, seawater would start to overflow after 2045 and cause extensive inundation up to 59.7 million $m^3$ by 2050. The pump station with a maximum drainage capacity of 50 $m^3$ in the Pluit district would not be able to drain out this amount of inundation in a short period of time. The residential areas and main roads in Pluit would suffer from both economic loss and sanitation issues.

## 5 Conclusions

The dyke construction has a great reduction effect against abnormal tide. However, if the land subsidence is not mitigated appropriately, the effect of this coastal dyke would only work for short term as it would allow the sea water to overflow in the near future and further cause longer periods of inundation. On the other hand, if land subsidence is terminated by 2030, flooding could be prevented by a short dyke with 1-m or slightly higher.

Even if the government of Jakarta can complete the construction of the extensive coastal dyke along the shoreline by 2030 as planned, the simulation results reveal the occurrence of both the overflow of sea water and the collapse of dyke unless the issues of land subsidence is completely solved. The flood projections by 2050 show that damaged flood areas could expand over five times as large as the present flood area.

It is expected that it would take more than 10 years or a few decades to be able to completely terminate land subsidence. Given the magnitude of the catastrophe as resulted from the simulation scenarios, therefore, coastal flood mitigation plans should not only be focused on building dykes and floodgates against abnormal tide but more importantly, eliminating the ground subsidence issue should be more prioritized.

## References


1) Takagi H., Esteban M., Mikami T., Fujii D. Projection of coastal floods in 2050 Jakarta, Urban Climate, No.17 p.135-145,2016a.
2) Takagi H., Mikami T., Fujii D., Esteban M. Mangrove Forest against Dyke-break induced Tsunami in Rapidly Subsiding Coasts, National Hazards and Earth System Sciences, doi:10.5194/nhess-2016-128, 2016b.
3) Djaja, R., Rais, J., Abidin, Z.H., Wedyanto, K. Land subsidence of Jakarta Metropolitan Area. 3rd FIG Regional Conference, Jakarta, Indonesia, October 3–7, 2004 (14 pp.).
4) Farr, T.G., et al. The shuttle radar topography mission. Rev. Geophys. 45, RG 2004. http://dx.doi.org/10.1029/2005RG000183, 2007.
5) Hasanuddin Z. Abidin, H Andresa, Rochman Djaja, Dudy Darmawan, M. Gamal. Land subsidence characteristics of Jakarta between 1997 and 2005, as estimated using GPS surveys, GPS Solut, 12:23-32 doi 10.1007/s10291-007-0061-0, 2008.
6) IPCC. Working group I contribution to the IPCC Fifth Assessment Report Climate Change 2013, 2013.
7) JICA, YACHIYO Engineering Co., LTD.
8) The Institutional Revitalization Project for Flood Management in JABODETABEK http://open_jicareport.jica.go.jp/pdf/11995024_02.pdf. p.2-56-p.2-62, 2010.
9) NCICD. NCICD Implementation Model 2025, 2013.

# Photocatalytic Degradation of Methylene Blue Using $TiO_2$ supported on Natural Zeolite and Activated Carbon

Student number: 14_18106　Name: Takahiro Takamatsu　Supervisor: Hirofumi HINODE,

## 担持光触媒を用いたメチレンブルーの分解

高松　貴大

染料廃水は 1 ppm 以下のわずかな濃度でさえも染料は色を放ち、環境に悪影響を与える。新規の処理方法として酸化チタンによる光触媒分解があるが、処理後の分離が困難であるという問題を抱えている。そこで光触媒をゼオライトと活性炭の表面に担持することで触媒の粒径を大きくし、反応系からの分離をより簡単にすることを目的として研究を行なった。本研究ではゼオライトと活性炭の表面にチタニアを担持し、粒径が大きく、かつ光触媒能力の高い触媒を合成しその担持条件等を検討した。

## 1. Introduction

Dye pollutants are one of the primary sources of environmental contamination[1][2]. It has been estimated that 15% of produced dyes worldwide is disposed in wastewater during the synthesis and processing [2,3].

Even in small amounts (< 1 ppm), dyes are clearly visible and can affect the water environment [3]. So it is necessary to treat water contaminated with dyes.

The usual methods that are employed to remove dye from wastewater streams are activated sludge method and coagulation method. However, these methods have some concerns. Activated sludge method produce excess sludge and is difficult to control[4]. Coagulation method produces waste aggregates[5]. Treatment and disposal of the excess sludge and waste aggregates entails costs and landfill space. While in the landfill, these wastes can also leach in the groundwater[6].

One of the alternative methods to remove dyes in the water is by photocatalytic degradation using $TiO_2$. Photocatalytic degradation of dyes using $TiO_2$ have a distinctive advantage. During photocatalysis, $TiO_2$ completely mineralizes the dye pollutant and does not produce excess sludge, so there is no need for secondary treatment. However, separation of $TiO_2$ from the wastewater stream after treatment is another problem, because $TiO_2$ particle size is very small[7].

To address this setback, this study aims to support $TiO_2$ photocatalyst on different materials to increase its particle size and make the separation of the photocatalyst from the wastewater stream after the treatment process easier. Different amounts, (by wt. percent) of commercial $TiO_2$ (DeGussa P25), were supported onto natural zeolite and activated carbon (AC). These materials are known as adsorbent, and using them as support of $TiO_2$ may also be beneficial. The photocatalytic activity of the supported $TiO_2$ photocatalysts were tested for degradation of methylene blue.

## 2. Experimental

### 2.1 Synthesis of $TiO_2$ / zeolite (TZ) or $TiO_2$ / AC(TC)[8]

#### 2.1.1 Pretreatment of adsorbent supports (Zeolite and AC)

Zeolite used in this study was natural zeolite taken from Sukabumi, Indonesia. Zeolite or AC powder was placed in a beaker and then 0.1 mM HCl was added. The mixture was placed in a magnetic stirrer for 6h, and then rinsed with deionized water afterwards. The powder was filtered and dried at 80℃.

#### 2.1.2 Supporting $TiO_2$ onto adsorbent

Deionized water, the adsorbent, and commercial $TiO_2$ (Degussa P25) were mixed in the beaker and ultrasonicated for 1 h. $TiO_2$ loading rate was 25, 40, 60, and 90 wt%. Afterwards, the mixture was washed thoroughly by deionized water and dried at 80℃. The zeolite samples were named, TZ25, TZ40, TZ60,

TZ90 and activated carbon samples were named TC25, TC40, TC60, TC90, accordingly.

### 2.2 Catalyst characterization

The synthesized catalysts were subjected to X-ray diffraction to identify any crystal structures present in TZ and TC samples. Their morphologies were observed using SEM and their particle sizes were determined using laser diffraction particle sizing technique.

### 2.3 Photocatalytic activity test

Methylene blue (MB) was used as a representative cationic dye to test the photocatalytic activity of the synthesized catalysts. The initial concentration of MB was adjusted from 40-80 ppm to become around 35 ppm after dark adsorption. Catalyst (0.01g) was added into the beaker and MB was allowed to adsorb on the surface of the catalyst in the dark for 30 min. After dark adsorption, UV lamp was switched on, and the solution was sampled every 15 or 30 min. The MB concentration in each sample was measured by UV-vis spectrophotometer.

### 2.4 Test of anchoring strength of $TiO_2$ onto adsorbents

To test how stable the $TiO_2$ was supported on the absorbents, test of anchoring strength was conducted, In this test, the amount of $TiO_2$ detached from adsorbent during prolonged time of stirring was measured.

TZ or TC samples (0.5 g) were put into beaker with 300 ml deionized water and stirred for 1 h and settled for 2 h. Afterwards, The cloudy liquid part was removed and the $TiO_2$ samples were washed with deionized water. This procedure was repeated twice, and then the catalysts were dried at 80℃. The washed samples were named TZa and TCa.

### 2.5 Measurement of $TiO_2$ loading amount in TZ and TZa

After TZ or TZa was dissolved by hydrofluoric acid (HF), Ti cation concentration was measured by ICP-AES and loading rate of $TiO_2$ of TZ and TZa was calculated.

HF(27M, 20 ml) and TZ or TZa (50 mg) was put into tefron beaker and the mixture was stirred for 24 h. The concentration of Ti cation was adjusted by deionized water. Afterwards, Ti cation concentration was measured by ICP-AES and loading rate of $TiO_2$ of TZ and TZa was calculated.

### 2.6 Measurement of loading rate of $TiO_2$ in TC and TCa

AC can not be dissolved by HF, so $TiO_2$ loading rate of TC and TCa was calculated from weight reduction rate by heating. $TiO_2$ weight reduction rate by heating is negligible, thus all weight loss after heating can be attributable to the weight loss of AC, as shown in the following formula:

**Loading rate of TiO2(%) = 100 – Weight reduction of TC(%)÷ Weight reduction of AC(%)･･･Eq (1)**

In this study, TC or TCa is heated at 800℃ and weight reduction was measured by TG.

## 3.Results and discussion

### 3.1 XRD analysis

The anatase, rutile, clinoptilolite-Ca and mordenite peaks can be observed in TZ's XRD pattern. Clinoptilolite-Ca and mordenite are kinds of zeolite structure. As $TiO_2$ loading rate became higher, $TiO_2$ peak became higher and zeolites peak became lower.

The anatase and rutile peaks could also be observed in TC's XRD pattern. $TiO_2$ loading rate of TC did not effect these peak intensity.

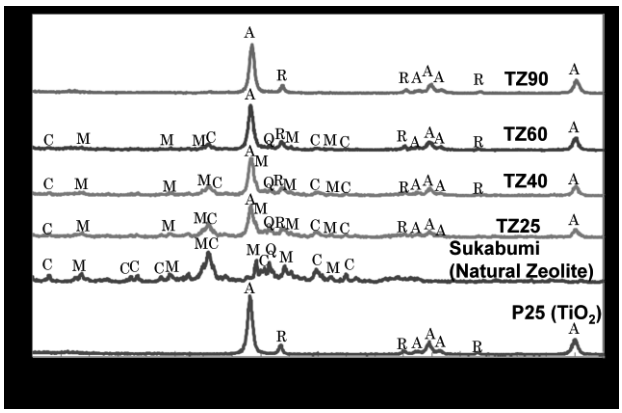


(a)

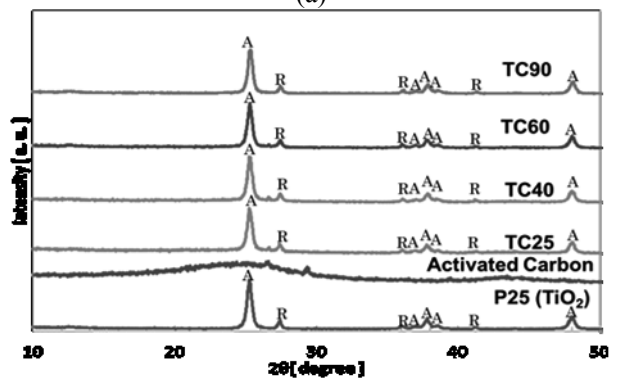


(b)

C: Clinoptilolite-Ca ($KNa_2Ca_2(Si_29A_{l7})O_{72}$ · $24H_2O$)
M: Mordenite ($(Ca, Na_2, K_2)Al_2Si_{10}O_{24}\cdot 7H_2O$)
Q: Quartz ($SiO_2$) A: Anatase ($TiO_2$)
R: Rutile ($TiO_2$)

Fig.1. XRD patterns of TZ(a) and TC(b) at different $TiO_2$ loading rate.

### 3.2 Morphology

The morphology of the synthesized samples was studied via SEM, and the SEM images of TiO2 - coated zeolite and AC are shown in Fig.2. Small white particles observed on surface of samples are $TiO_2$ particles.

These SEM images show support of $TiO_2$ on zeolite or AC was successful.

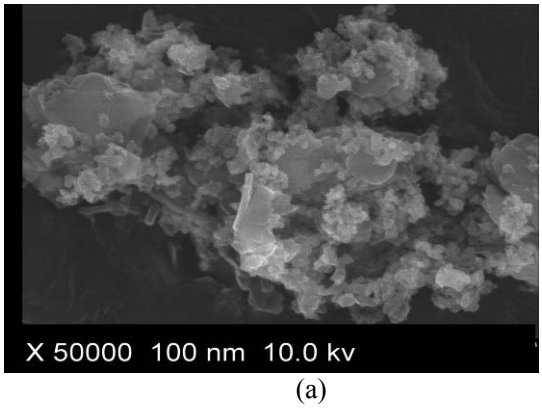


(a)

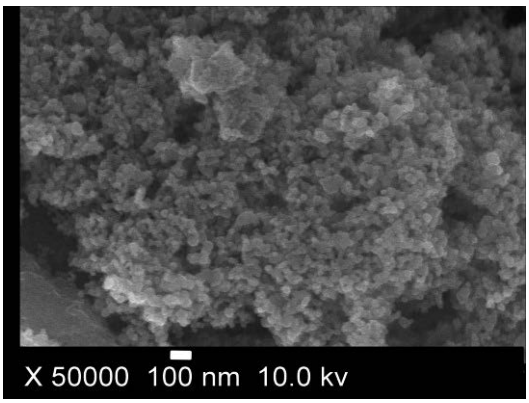


(b)

Fig.2. SEM image of (a) TZ25 and (b) TC25

### 3.3 Loading rate of $TiO_2$

Table1. Result of loading rate of $TiO_2$

| | TZ25 | TC25 | TZ40 | TC40 | TZ60 | TC60 | TZ90 | TC90 |
|---|---|---|---|---|---|---|---|---|
| TiO2 wt% (Theoretical) | | 25.0 | | | | | | |
| TiO2 wt% (Analyzed) | | 32.2 | | | | | | |
| TiO2 wt% (After anchoring) | | 30.8 | | | | | | |

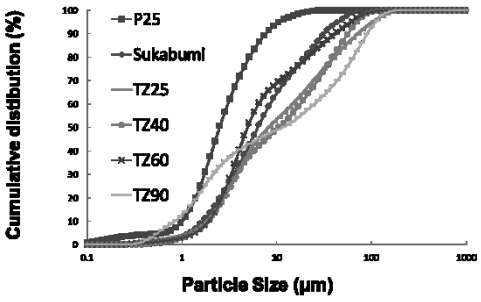


(a)

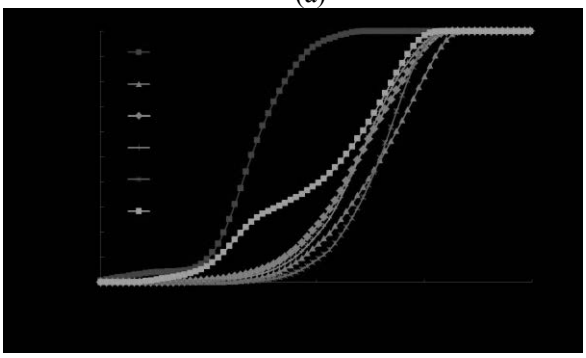

(b)

Fig.3.Particle sizes distribution of (a) TZ and (b) TC by laser diffraction particle size analyzer

Result of loading rate of $TiO_2$ is shown in table 1. The result indicates that $TiO_2$ was strongly anchored on TZ and TC. Analyzed loading rate of $TiO_2$ is almost same theoretical.

### 3.4 Particle size distribution

Table 2 shows the mean volume diameter (MV) of TZ and TC was about 2~15 times bigger than that of P25. The particle size of TC is bigger than TZ because of the bigger particle size of AC. TC60 have the biggest MV (39.2 μm). TZ90 and TC90 have high amount of small particle (< 1.0 μm). This is attributable to the presence of small $TiO_2$ particles. From this result, it can be concluded that some of TiO2 was not supported on the adsorbent.

Table 2. Mean Volume Diameter（MV）

| Sample name | P25 | Sukabumi | AC | TZ25 | TC25 | TZ40 | TC40 | TZ60 | TC60 | TZ90 | TC90 |
|---|---|---|---|---|---|---|---|---|---|---|---|
| Mean Volume Diameter (μm) | 2.5 | 6.3 | 40.8 | 8.1 | 25.0 | 10.5 | 14.0 | 4.9 | 39.2 | 11.5 | 18.2 |

### 3.5 Degradation removal rate

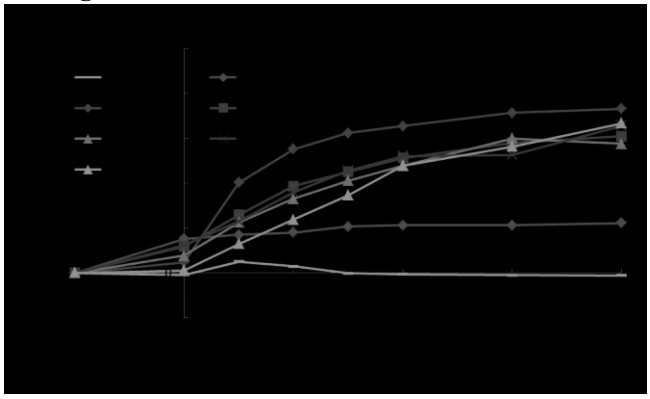

(a)

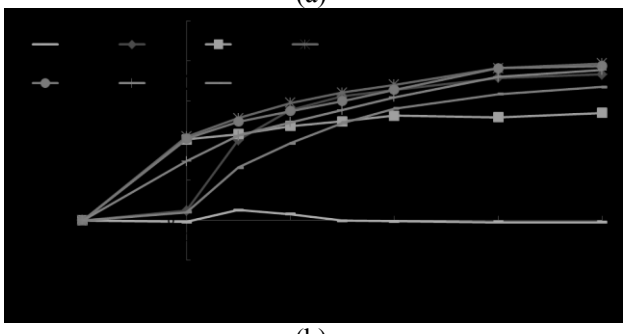

(b)

Fig.4. Degradation removal rate of MB by (a) TZ and (b) TC

Fig.4 shows the removal rates of TZ and TC. Degradation removal rate were compared with adsorption amount in table 3.

TC25 had the highest degradation removal rate of 78.7 %. TC25 have higher degradation removal rate and MV (78.7 %, 25.0 μm, respectively) than P25 (73.3 %, 2.5 μm, respectively). Excess loading rate of $TiO_2$ caused decrease of adsorption amount. Too little loading rate of $TiO_2$ caused decrease of active site, which lead to the decrease in degradation removal rate. Adsorption amount of TC is higher than TZ because of high adsorption amount of AC.

Table 3. Adsorption amount and degradation removal rate

| Sample name | P25 | TZ25 | TC25 | TZ40 | TC40 | TZ60 | TC60 | TZ90 | TC90 |
|---|---|---|---|---|---|---|---|---|---|
| Adsorption amount (mg/g) | 8.6 | 21.2 | 135.5 | 13.9 | 119.4 | 22.3 | 75.4 | 1.9 | 7.1 |
| Degradetion removal rate (%) | 73.3 | 61.1 | 78.7 | 65.7 | 77.5 | 52.1 | 75.4 | 66.8 | 66.9 |
| Mean Volume Diameter (μm) | 2.5 | 8.1 | 25.0 | 10.5 | 14.0 | 4.9 | 39.2 | 11.5 | 18.2 |

## 4. Conclusion

Support of $TiO_2$ was successfully support a zeolite and AC. TC25 had the highest degradation removal rate of 78.7 %. TC25 have higher degradation removal rate and MV (78.7 %, 25.0 μm) than P25. Excess loading rate of $TiO_2$ resulted in the decrease of adsorption amount and caused the presence of $TiO_2$ particles that can not be supported on the adsorbents. Too little loading rate of $TiO_2$ caused decrease of active site, which lead to the decrease in degradation removal rate.

Test of anchor strength showed $TiO_2$ was strongly anchored on TZ and TC.

Particle sizes of TZ and TC are bigger than that of P25.

Reference


[1] K. Nakata, A. Fujishima, TiO2 photocatalysis: Design and applications, J.
Photochem. Photobiol. C Photochem. Rev. 13 (2012) 169–189.
[2] A. Fujishima, T.N. Rao, D.A. Tryk, Titanium dioxide photocatalysis, J.
Photochem. Photobiol. C Photochem. Rev. 1 (2000) 1–21.
[3] A. Fujishima, X. Zhang, D. Tryk, TiO2 photocatalysis and related surface
phenomena, Surf. Sci. Rep. 63 (2008) 515–582.
[4] 羽賀清典、農業技術研究機構畜産草地研究所
http://lin.alic.go.jp/alic/month/dome/2003/oct/CHOUSA-2.HTM
[5] 前馬恵美子、富山大学、中和凝集沈殿法とは？
http://www3.u-toyama.ac.jp/environ/shige/lecture/2004/b04_02_2.htm
[6] 三菱総合研究所、平成 22 年度地球温暖化問題等対策調査事業
http://www.meti.go.jp/meti_lib/report/2011fy/E001477.pdf
[7] R.L Pozzo et al,Catalysis Today 39 (1997) ,219-231
[8] 水中に分散した TiO2 光触媒による水浄化 – Panasonic
https://www.panasonic.com/jp/corporate/technology-design/ptj/pdf/.../p0105.pdf

# Estimation of $CO_2$ Emission from Chinese Manufacturing Industry using Hybrid Method

Student Number: 15M18061 Name: GUAN Jianxin Supervisor: Shinya HANAOKA

ハイブリッド手法を用いた中国製造業 $CO_2$ 排出量の推計

関 建新

本研究ではプロセス分析と産業連関分析を組み合わせたハイブリッド手法を用いて中国の乗用車一台当たりの素材，生産，輸送，使用段階の $CO_2$ 排出量を推計する．また，シナリオ分析のため産業構造の変化，技術進歩，工場移転及び需要の予測も行う．推定結果から，使用段階の排出量が最も多く，今まで算定されていない素材段階の排出量も無視できないほど多いことが分かった．シナリオ分析により，技術進歩が排出量削減に最も効果的である一方，需要増加による全体の排出量は現状の 2.6 倍となることを示した．

## 1. Introduction

The IPCC concluded that the rapid rise of GHG emissions concentration is the result of human activities in its 5th assessment report (AR5)[1]. Carbon dioxide ($CO_2$) accounts for 65% of GHG emissions in 2014, $CO_2$ emission reduction is a very important issue all over the world.

China started the reform and opening-up policy since 1978. In these 30 years, Chinese government changed its planned economy to market economy, which resulted in rapid increase of economy. On the other hand, with the economy increasing, $CO_2$ emissions of China increased as well. On the basis of Emissions Database for Global Atmospheric (EDGAR) [2], Chinese $CO_2$ emissions surpassed U.S., became the world`s largest $CO_2$ emission country in 2005. Moreover, in 2013 the $CO_2$ emission of China is 10.64 Gt-$CO_2$, which accounted for 29% of global emission. One of the reason is that depending on fossil energy.

Amongst $CO_2$ emission in China, manufacturing industry is the biggest emission sector, the direct emission of the manufacturing sector is 6.6 Gt-$CO_2$. Manufacturing of automobile and other transportation equipment is the 6$^{th}$ among contained emission of manufacturing sector[3]. Moreover, manufacturing is the sector which is most sensitive to economy increasing in China. On the other hand, not only automobile manufacturing industry has a very high $CO_2$ emission, the sector of transportation emitted 0.95Gton $CO_2$ as well, which is 5$^{th}$ of all sectors. Therefore, increasing $CO_2$ emissions, especially of automobile industry is a serious problem in China.

Looking at automobile industry in China, total sales of vehicle already became world largest in 2009, and exceed 25 million in 2015. However, car ownership per 1000 people, is only 71.42 in China, only a half of world average (140), and much less than developed countries (727). Because of increase of economy, population and purchasing power, it can be assumed that demand of automobile in China will rapidly increase in the future.

In U.S.-China Joint Announcement on Climate Change in November 2014, the Chinese government announced that China would strive to bring its spiraling $CO_2$ emissions to a peak by 2030. In the 21st annual Conference of Parties (COP21) [4] of UN Framework on Climate Change (UNFCCC) in Paris, Chinese government submitted the Intended Nationally Determined Contributions (INDCs): to lower carbon dioxide emissions per unit of GDP by 60% to 65% from the 2005 level by 2030. Considering the automobile ownership in the future, the sector of transportation and automobile equipment`s emission will increase as well, which will become a big influence factor of INDC in COP21.

$CO_2$ emission of automobile method still remains startup step. There are only some studies using process based analysis or I-O table analysis. However, estimate $CO_2$ emission only by one of them is difficult to get a high accuracy result. There are some studies propose a hybrid method in other country, but not appropriate to Chinese automobile industry.

Because of the high demand of Chinese automobile market, $CO_2$ emission of automobile industry is a big problem as well. And it can be estimated increase rapidly in the future. Therefore, a high accuracy estimation method to quantify $CO_2$ emission of Chinese automobile industry is necessary.

However, the existing method to estimate automobile industry`s $CO_2$ emission in China, process based analysis and I-O table analysis, have their own limitation, it is difficult to estimate $CO_2$ emission accurately.

The objective of this study is to estimate $CO_2$ emissions by a hybrid methodology of I-O table analysis and process based analysis of automobile industry in China. Furthermore, because of the structure of Chinese industry changes, technology improvement, and factory shift in the future, this study make several scenarios to quantify the effect of these changes, and to clarify which is the policy contribute to $CO_2$ emission reduction in the future.

## 2. Methodology

This study using life cycle viewpoint, estimate one automobile`s $CO_2$ emission from material phase, production phase, transportation phase and using phase (Table 1). And estimate whole automobile industry`s emission by using sales data of different body type and car level.

Table 1 Emission phase of car life cycle

| Phase | | Emission sector |
|---|---|---|
| Material Phase | | Manufacturing |
| Production Phase | Parts Production | Manufacturing |
| | Assembly | Manufacturing |
| Transportation Phase | Parts Transportation | Transportation |
| | Assembled car Transportation | Transportation |
| Using Phase | | Transportation |

### 2.1 Data

To estimate $CO_2$ emission by a hybrid method, the data of process based analysis and I-O table analysis is necessary as follows,

I-O table: the I-O table used in this study is from national bureau of statistics of the People`s Republic of China. The year of 2002, 122 sectors, 2007, 135 sectors and 2012, 139 sectors is be used.

China Energy Statistical Yearbook: to calculate basic unit of direct and indirect emission, the energy using of every sector is obtained. In this study, 2008 China Energy Statistical Yearbook is used.

Price of material: there is no official statistic data of price of material in China, therefore this study collect material`s price from the biggest E-commercial website, Alibaba

Data about parts production and assembly: because these are no this kind of database in China. The energy using of production and assembly, type and weight of parts are obtained from a Japanese database, JLCA database.

Data about transportation: this study uses number and location of supplier and dealer to estimate transportation phase`s $CO_2$ emission.

Using data: this study use`s Shanghai Volkswagen`s car Lavida as a case study to calculate $CO_2$ emission of using phase. Hence using phase data obtain from Shanghai Volkswagen`s official website.

## 2.2 Hybrid Method

In this study, firstly to apply process based analysis to estimate production phase, transportation, and using `s $CO_2$ emission. I-O table analysis is used for material phase. To combine this two analysis`s boundary (Figure. 1) is the estimation methodology of hybrid method.

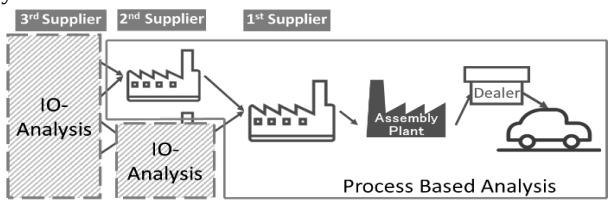


Figure 1 Boundary of 2 analysis

Process Based Analysis

(i) Parts production

In this study, $CO_2$ emission of parts production is estimated as Eq. (1) use JLCA database.

$$E_p = \sum_j \sum_n g_{n,j} \cdot EMF_j \quad \text{.....(1)}$$

$E_p$: $CO_2$ emission of parts production per car (t-$CO_2$);
$g_{n,i}$: electricity use of producing parts $n$ in region $j$ (mWh);
$EMF_j$: emission factor of region $j$ (t-$CO_2$/mWh);
n : number of parts, $n$=1~31;

(ii) Assembly

Similar as parts production, $CO_2$ emission of assembly also estimated by using JLCA database. Electricity of assembly is used in Eq. (2).

$$E_a = g \cdot EMF \quad \text{.....(2)}$$

$g$: electricity use of assembly phase (mWh)
$EMF$: emission factor (t-$CO_2$/mWh) ;

(iii) Transportation

Calculation of transportation phase is divided into parts transportation and assembled car transportation. And also divided into road, maritime and rail transportation. Road transportation is calculated by improved tonnage method while railway and maritime transportation are calculated by tonnage method. These calculations are made by estimation tool of the Policy Research Institute for Land, Infrastructure, Transport and Tourism (PRILIT). This tool was established under Ministry of Land, Infrastructure, Transport and Tourism (MLIT) of Japan[5].

According to improved tonnage method, $CO_2$ emission of parts transportation is calculated by Eq. (3).

$$E_i = \frac{W_i \cdot d_{ij} \cdot C \cdot H \cdot F \cdot 44/12}{u} \quad \text{.....(3)}$$

Assembled car transportation from assembly factory to dealer can use improved tonnage method (road, Eq. (4)) or tonnage method (rail or maritime, Eq. (5)).

$$E_c = \frac{W_c \cdot d_{ij} \cdot C \cdot H \cdot F \cdot 44/12}{u} \quad \text{.....(4)}$$

$$E_R = \frac{W_c \cdot d_{rn} \cdot F_R}{q} \quad \text{.....(5)}$$

Assembled car transportation from port of assembly factory to port of dealer can use Eq. (6)

$$E_M = \frac{W \cdot d_{lm} \cdot F_M}{q} \quad \text{.....(6)}$$

Since there are all 876 dealers considered in this research, emissions of assembled vehicles transportation phase from assembly plant to dealers can be calculated as follows:

$$E_D = \sum_s \frac{n_s (E_M + E_C)}{876} or \sum_s \frac{n_s (E_r + E_C)}{876} or \sum_s \frac{n_s E_C}{876} \quad \text{……(7)}$$

From Eq. (1) to Eq. (7) $CO_2$ emission from transportation phase is:

$$E_T = \sum_i E_i + \sum_c E_c + E_D \quad \text{.....(8)}$$

$E_T$: $CO_2$ emission of transportation phase per car (t-$CO_2$);
$Ei$: $CO_2$ emission of parts transportation per car (t-$CO_2$);
$Ec$: $CO_2$ emission of assembled car transportation by road per car (t-$CO_2$);
$E_R$: $CO_2$ emission of assembled car transportation by rail per car (t-$CO_2$);
$E_M$: $CO_2$ emission of assembled car transportation by maritime per car (t-$CO_2$);
$E_D$: $CO_2$ emission of assembled car transportation per car (t-$CO_2$);
$n_s$: Dealer number in province $s$;
$W_i$: Weight of parts (t);
$d_{ij}$: Transportation distance (km);
$c$: Basic unit of improved tonnage method (l/tkm);
$H$: Heat generation per unit (GJ/kl);
$F$: emission factor (t-C/GJ);
$i, j$: number of supplier $i$=1~97;
$u$: number of unit;
$q$: number of assembled car;
$W$: weight of assembled car (t);
$d_{kl}$ $d_{rn}$ $d_{lm}$: Distance from assembly factory to dealer (km);

(iv) Using

To estimate $CO_2$ emission of using phase, it is necessary to consider how consumer use car. Which means to setup car using pattern. Based on Chinese car using habit, 3 different car using patterns are set in this study.

Heavy user: commuting every day by car and use car at weekend for leisure as well. This kind of patter, annual travel distance is set as 20,000KM.

Normal user: sometimes commuting by car on weekdays, and use car at weekend for leisure. Annual travel distance is set as 10,000KM.

Light user: only user car on weekend for leisure. This kind of patter, annual travel distance is set as 3,000KM. $CO_2$ emission of using phase is calculated in Eq. (9).

$$E_U = \frac{d \cdot y}{e} \cdot den \cdot f \quad \text{.....(9)}$$

$E_U$: $CO_2$ emission of using phase (t-$CO_2$);
$d$: annual travel distance (km);
$y$: service life of car (set as 10 years);
$e$: fuel consumption (km/L);
$f$ : emission factor of gasoline (kg- $CO_2$/kg);
$den$: density of gasoline (kg/L);

I-O Table Analysis

To apply I-O table analysis, firstly to calculate emission basic unit by using I-O table. After calculating basic unit, it is able to estimate $CO_2$ emission of different material by using Eq. (10).

$$E_m = \sum_i e_{k,i} \cdot Price_i \quad \text{.....(10)}$$

$E_m$: $CO_2$ emission of using phase;
$e_{k,i}$: emission basic unit of sector $i$;
$Price_i$: material price of material $i$;

Hybrid method

The flow of a hybrid method shows as Figure 2. Firstly, use process based analysis to estimate using, transportation and production phase`s $CO_2$ emission, then the phase of material which can`t estimate by process based analysis, I-O table analysis is applied. Finally, add the result of process based analysis and I-O table analysis is the result of hybrid method.

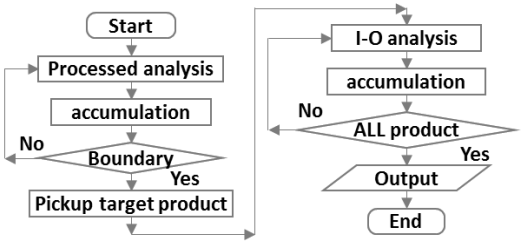


Figure 2 Hybrid method

## 2.3 Scenario Building

(i) Scenario 0: BAU

It assumed that there is no change of Chinese industry structure, develop as the same pattern at present. Therefore, it is necessary to forecast I-O table in the future.

To forecast I-O table in the future, RAS method is applied in this study. RAS is a method to forecast the input coefficient matrix of target year. To forecast the input coefficient matrix, total output, intermediate demand, value added and intermediate input have to be forecasted beforehand.

(ii) Scenario 1: 3rd industry development

China is the biggest manufacturing country in the world, which call "the world's factory". However, consider the future condition of China, to develop an environment-friendly and sustainable society, it can be assumed that the 3rd industry will increase. Refer to the developed countries such as U.S. and Japan, it can also assume that the main industry will shift from 2nd industry to 3rd industry.

However, China has its own industry structure, because of protection of domestic industry, even in the future, 1st and 2nd structure will not decrease as low as U.S. or Japan.

Therefore in this study, the percentage of Chinese industry structure in 2050 set as 1st industry – 1%, 2nd industry – 35%, 3rd industry – 64%.

Table 2 Industry share setting

| | 1st Industry | 2nd Industry | 3rd Industry |
|---|---|---|---|
| BAU | 2.4% | 66.5% | 31.1% |
| 2030 | 5.6% | 46.4% | 47.9% |
| 2050 | 1% | 35% | 64% |

(iii) Scenario 2: technology improvement

Scenario 2.1: electricity generation improvement

Firstly, according to Nakamichi et al[3]: the efficient of coal power generation increase. The emission factor of coal was decreasing from 2004 (1.112 kg-$CO_2$/kWh), became 0.934 kg-$CO_2$/kWh in 2009. This study assumes that it will decrease to 0.57 kg-$CO_2$/kWh in 2050.

About the share of power generation method, Chinese government does a lot of work on nuclear power, wind power and solar power, try to make the share of non-fossil fuel up to 30%.In this study, the share of nuclear set as 10% in 2050. About wind power, assume that government will stop subsidy from 2020, the share of wind power will set as 6% in 2050. About solar power, because of subsidy, the share will be 2% in 2050. Finally, water power is 17% at present, and it will keep this percentage in the future.

Scenario 2.2: fuel consumption improvement

There are several technology improvements these years of Volkswagen. Firstly, a decrease of displacement, for example, the displacement of car golf is almost 2.0, but it decreases to 1.4 in 2013. Secondly, in order to keep performance at lower displacement, turbo technology is widely utilized. Similarly, same car of golf, in 1992 all of them are naturally aspirated engine, but in 2013 all changed to turbo engine. Finally, for decrease fuel consumption at same speed, transmission technology also improvement form MT to 4AT, 6AT, and DSG in these years.

It can be assumed technology improvement will also continue in the future to decrease fuel consumption, therefore in this study, fuel consumption set as 2.79 L/100KM in 2050.

(iv) Scenario 3: factory shift

Because of increasing of Chinese income, the labor cost of automobile company increased these years, and will increase in the future as well. Therefore automobile company will shift their manufacturing factory to somewhere with lower labor cost.

Scenario 3.1: domestic factory shift: the tariff to import assembled car is 25% in China. If automobile company shift their assembly factor aboard, although labor cost decrease, tariff will be the new cost, and it will reflect in the price of car. Therefore in this study, automobile company will shift their assembly factory to another different province with a lower labor cost. The shift target set as Gansu province, which is the lowest income in 2050[3]. Parts will transport from parts factory as present to Gansu, assembled car transport from Gansu to dealers.

Scenario 3.2: aboard factory shift: in this scenario, automobile company will shift their parts factory to the country of lower labor cost. Because of the import policy of China, the main parts of car (engine, frame, transmission parts) have a 25% tariff, so only unimportant parts factory will shift to abroad in the future. The target will set as Myanmar which is near to China and have lower labor cost among ASEAN countries. Prats will transport from Myanmar to assembly factory in China.

# 3. Result

## 3.1 Present Emission Estimation

(i) Result of one car

The emission estimation result of one car by hybrid method shows in Table 3.

Table 3 Emission result of one car (t-$CO_2$)

| | | | |
|---|---|---|---|
| Material Phase | | | 0.429 |
| Production Phase | 0.777 | Parts Production | 0.271 |
| | | Assembly | 0.506 |
| Transportation Phase | 0.218 | Parts Transportation | 0.008 |
| | | Assembled car Transportation | 0.210 |
| Using Phase | | | 6.6~44.2 |

Estimation result shows the largest emission comes from using phase. However, the result of using phase is very sensitive to service life and annual travel distance (car using pattern). The second is production phase, in this study, part production and assembly factory are located in China mainland, which has a very high emission factor. The third is material phase. In other studies this phase always be omitted, but according to result in this study, emission of this phase is also very high and should be noticed. Finally, transportation phase`s emission is the lowest. The reason is that both supplier and dealer of Shanghai Volkswagen are located in south-east coastal areas in China, transportation distance is not that long.

(ii) Result of automobile industry

The $CO_2$ emission result of Chinese automobile industry different by body type and level shows in Figure 3. The total emission in 2015 is 36.10 Mt-$CO_2$. Sedan is the highest emission body type. Among the level, A level is the highest emission level because the demand is highest. Non sedan is the second, although the demand of non sedan is not that high, but because non sedan always heavier than the same level sedan, emission of non sedan also very high. Crossover is a niche market, so the

emission only very less.

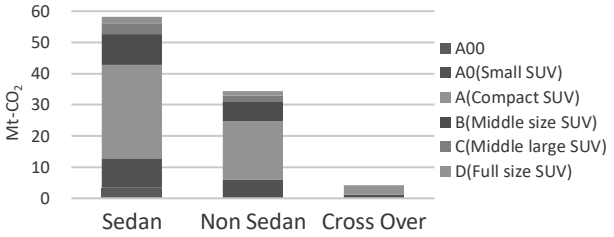


Figure 3 Emission result of automobile industry in 2015

### 3.2 Future Forecast

As the result shows in Figure 4, different scenarios have different emission reduction result in the future. Firstly, the most effective way to reduce $CO_2$ emission is technology improvement (scenario 2). It can contribute 34% of $CO_2$ reduction. And the industry structure changes (scenario 1) can reduce 21% of $CO_2$ emission. Secondly, manufacturing factory shift scenario (scenario 3.1, 3.2) also contribute to $CO_2$ emission reduction, because the emission factor is much lower. However, because of the location change of manufacturing factory, $CO_2$ emission of transportation increased dramatically. Especially, if transportation keeps using truck or trailer, it will even higher than current situation.

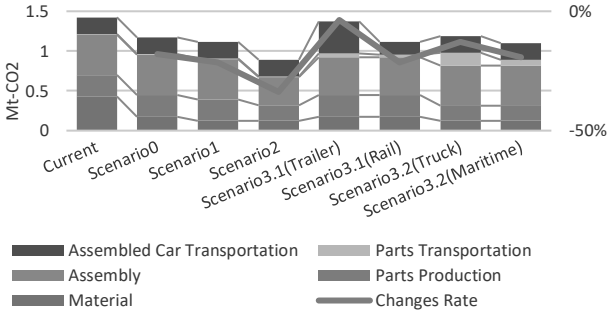


Figure 4 Forecast result of scenarios in 2050

Figure 5 shows automobile industry`s $CO_2$ emission of each province in China. $CO_2$ emission of all province increased in 2050. The reason is that although emission of on car decrease to 0.841 t-$CO_2$ in 2050, demand is increased of car leads to $CO_2$ emission increase of automobile industry from 36.10 Mt-$CO_2$ to 117.48 Mt-$CO_2$ in 2050. U.S. Energy Information Administration (EIA)[6]`s data shows that in 2015 the emission of transportation equipment is 28.57 Mt-$CO_2$ in U.S. Compare to U.S., $CO_2$ emission of automobile industry is a very big problem.

Therefore, to reduce $CO_2$ emission of one car`s lifecycle is important. On the other side, to reduce $CO_2$ emission of all automobile industry, some policy to reduce automobile demand such as improve public transportation, automobile tax, limitation of parking also plays a very important role.

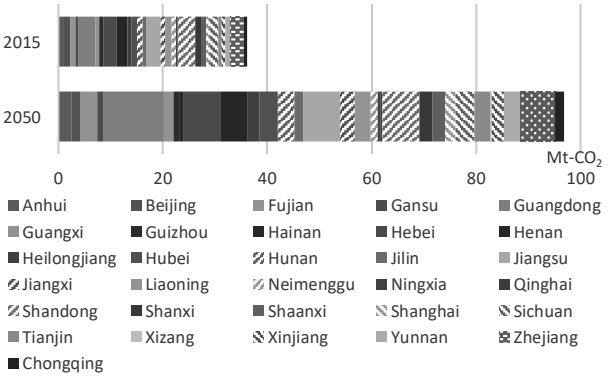


Figure 5 forecast result by province

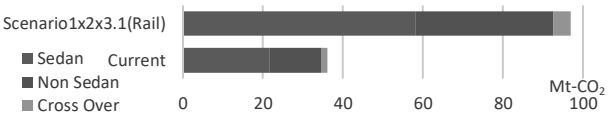


Figure 6 Forecast result by body type in 2050

Table 4 Emission per GDP

| | 2015 | 2030 | 2050 |
|---|---|---|---|
| Emission/GDP(t-CO2/GRMB) | 5.24 | 6.59 | 2.59 |
| Percentage | 100% | 126% | 49% |

Finally, compare $CO_2$ emission per GDP of 2015, 2030 and 2050, the GPD data of HSBC is used. The result shows in Table 4, $CO_2$ emission per GDP is 5.24 in 2015, 6.59 in 2030 and 25.89 in 2050. Consider about automobile industry, the ability to achieve INDC of COP21 difficult, but because of GDP increasing and population reduction, it substantially decrease in 2050.

## 4. Conclusion

The estimation result of one car shows, the highest emission phase is using phases. On the other hand, $CO_2$ emission of material phase shows a very high result as well, which cannot be ignored. According to scenario analysis, technology improvement is the most effective way to reduce $CO_2$ emission of one car. The scenario of manufacturing factory changes can reduce $CO_2$ emission of one car, however, transportation phase`s $CO_2$ emission will increase dramatically. Moreover, although $CO_2$ emission of one car can be decreased to 0.841 t-$CO_2$ in the future, because of demand of car increase, total emission of automobile industry will increase finally.

To achieve INDC of COP21, improvement of power generation is a fundamental solution. Moreover, to reduce $CO_2$ emission of total automobile industry, a solution of one car`s emission is not enough. Some policy to reduce automobile demand such as improve public transportation, automobile tax, limitation of parking also plays a very important role.

In this study, data of parts obtain from a Japanese database – JCLA database. These data are collected in Japan, may have some difference from China. In the future, if parts data can be collected in China domestic, uncertainty of result can decrease still more.

I-O table used in this study is only 139 sectors, much less than Japan and U.S., it also makes some uncertainty because of aggregation of I-O table. In addition, the price of I-O table is an assumed average price, not the real price of products, it also makes some uncertainty to result.

To calculate $CO_2$ emission of material phase, a price of material is necessary, these data are collected from Chinese E-commercial site, so the price changes in the future also affect $CO_2$ emissions of this study.

Finally, this study only considers about GV, however in the future EV, HEV or other new energy car also become popular in the market. Therefore in the future effect of new energy car should be included in this study.

## References


[1] Intergovernmental Panel on Climate Change: Fifth Assessment Report (AR5), 2014, http://www.ipcc.ch/.

[2] EDGAR: $CO_2$ time series 1990-2013 per region/country. http://edgar.jrc.ec.europa.eu/overview.php?v=CO2ts1990-2013.

[3] 中道久美子, 花岡伸也, 関建新: 中国における家計消費に基づく省市区別 $CO_2$ 排出量の推計と削減策の検討, 土木学会論文集 G(環境), Vol.72, No.6 (環境システム研究論文集, 第 44 巻),pp.II_95-II_106,2016.10

[4] Conference of the Parties. http://www.cop21paris.org/.

[5] 経済産業省　国土交通省：ロジスティクス分野における $CO_2$ 排出量算定共同ガイドライン Ver.3.0, 2007.

[6] EIA: Fuel Consumption, 2010,https://www.eia.gov/consumption/manufacturing/data/2010/pdf/Table3_1.pdf

# Production of high concentration bioethanol from cassava stem

Student Number: 15M18115 Name: Kazumasa TANAKA

Supervisor: Ryuichi EGASHIRA Cosupervisor: Kiyohiko NAKASAKI

## キャッサバの茎を原料とした高濃度バイオエタノール発酵

田中一正

本研究はキャッサバの茎からの高濃度エタノール発酵を目的としてキャッサバの茎の酸加水分解法を検討した。キャッサバの茎の酸加水分解液を再利用することで液中のグルコース濃度を従来の約 2 倍に濃縮することに成功した。濃縮した酸加水分解液に *Saccharomyces cerevisiae* IAM4178 を接種してエタノール発酵することで最大 40 g/L 程度のエタノールを得ることができ、ほとんどが有効利用されていないキャッサバの茎から高濃度のエタノールを生産する方法を示した。

# 1 Introduction

Recently, there is a growing concern about the depletion of petroleum based-fuels reserves. Carbon dioxide which is produced in combustion of petroleum based-fuels tends to increase the temperature of the planet. It leads to many negative effects to environment. Furthermore, the intensive demand of petroleum based-fuels increases the crude oil price. These factors have heightened the need to search for alternative energy resources.

Bioethanol is an attractive solution to address above problems as it is a carbon neutral energy source. Bioethanol is produced by the fermentation of sugar by microorganism. Today, almost all bioethanol is produced from corn and sugarcane. However, the production of bioethanol from food crops causes interference between food demands.

Agricultural residues are collecting attentions as alternative substrate of bioethanol fermentation, owing to its low cost and abundant amount in the world. It is estimated that 491 billion liters of bioethanol can be produced from sum of agricultural residues and food wastes in the world which is 16 times higher than the current total production. During bioethanol fermentation, the ethanol concentration should reach at least approximately 40-50 g/L, because several studies have concluded that this target concentration can make the process economically feasible, especially by saving energy for the distillation [1]. So, it is important to produce high concentration ethanol in fermentation of agricultural residue.

Agricultural residue is composed of lignocellulose. Starch in the crops can be fermented directly, but lignocellulose has to be pretreated before fermentation. The acid hydrolysis by hydrochloric acid or sulfuric acid is the most common method to break the lignocellulosic structure. However, acid hydrolysis pretreatment produces fermentation inhibitors such as furfural and phenolic compounds which can lead low ethanol productivity. So, it is required to remove these inhibitors by detoxification.

The research purpose is to produce around 40 g/L of bioethanol from cassava stem. In this study, cassava stem was used as bioethanol substrate. The amount of cassava stem produced in a year is 35 million tons, but about 80% of cassava stem is abandoned or burned in the wild [2]. For the purpose, fermentation of synthetic broth, fermentation of cassava stem broth and fermentation of condensed cassava stem broth were conducted.

# 2 Materials and methods

### 2-1 Fermentation of synthetic broth

The fermentation ability of IAM4178 on glucose and xylose was examined using synthetic broth. IAM4178 was precultivated in 50 mL of YM broth at 30ºC for 2 days. Then, 50 mL of the preculture was centrifuged at 6,000 rpm for 5 min. The supernatant was discarded and the wash solution which was composed of 5 g/L of peptone and 3 g/L of yeast extract was added to wash the pellet. The mixture of wash solution and the pellet was centrifuged again in the same condition. After centrifuging, the supernatant was discarded and the pellet was inoculated to 50 mL of synthetic broth which was composed of 40 g/L of glucose, 20 g/L of xylose, 5 g/L of peptone and 3 g/L of yeast extract. Fermentation was conducted at 30ºC, 120 rpm.

The chemical formulas of ethanol production from glucose is shown below.

$$C_6H_{12}O_6 \rightarrow 2\ C_2H_5OH + 2\ CO_2$$

According to the formula, 0.51 g of ethanol is produced from 1 g of glucose. The ethanol fermentation efficiency was calculated for all experiments based on an assuumption that the ethanol concentration calculated from above formula is 100%.

### 2-2 Fermentation of cassava stem broth

#### 2-2-1 Fermentation of CS 200

Cassava stem hydrolysate was fermented by IAM4178 to investigate the fermentation ability of IAM4178 in the cassava stem hydrolysate and compare the fermentation characteristic of the CS broth and synthetic broth. Cassava stem (CS) was obtained from Trang Bom region, Dong Nai prefecture, Vietnam. Firstly, CS was ground to make the particle size smaller than 0.5 mm. The ground CS was stored in the desiccator. Ground CS and 72wt% sulfuric acid were mixed at the weight ratio 1:1.25. The mixture was put in the incubator at 30ºC for 1 hour. During incubation, the inside content was stirred evey 15 min to make it uniformity. After 1 hour, distilled water was added to decrease the acid concentrarion to 16.4% and the mixture of CS and acid was heated in autoclave at 111ºC for 1 hour. The hydrolysate was kept stand at room temperature for 1 hour, and calcium carbonate wad added to adjust pH around 5.5. The hydrolysate after neutralization was centrifuged at 6000 rpm for 5 min and supernatant was filtered with a paper which has pore size of 0.45 μm. Then, 5 g/L of peptone and 3 g/L of yeast extract were added to the filtered hydrolysate. The hydrolysate after these procedures was used as CS 200. The theoretical sugar concentration is shown in Table 1. The value was calculated using CS composition measured by NREL method [3]. IAM4178 was inoculated to CS 200 in the same manner with chapter 2-1.

#### 2-2-2 Fermentation of CS 400

In order to produce high concentration of ethanol, condendsation of sugar in CS broth by two times hydrolysis and fermentation characteristic of the cndensed CS broth were investigated. Ground CS and 72wt% sulfuric acid were mixed at the weight ratio 1:1.25. The mixture was put in the incubator at 30ºC for 1 hour. During incubation, the inside content was stirred evey 15 min to make it uniformity. After 1 hour, distilled water was added to decrease the acid concentrarion to 16.4% and the mixture of CS and acid was heated in autoclave at 111ºC for 1 hour. The hydrolysate was kept stand at room temperature for 1 hour, and filtered with a paper which has pore size of 0.45 μm.

Ground CS and 72wt% sulfuric acid were mixed and incubated for 1 hour in the same manner, and the filtered hydrolysate mentioned above was added to the mixture. The volume of the added hydrolysate was same with the volume of distilled water which was added before the first heating. Acid concentrarion after adding the hydrolysate became 28%. The mixture of CS and hydrolysate was heated in autoclave at 111ºC for 1 hour. The hydrolysate was kept stand at room temperature for 1 hour, and calcium carbonate wad added to adjust pH around 5.5. The hydrolysate after neutralization was centrifuged at 6000 rpm for 5 min and supernatant was filtered with a paper which has pore size of 0.45 μm. Then, peptone and yeast extract, 5 g/L and 3 g/L each were added to the filtered hydrolysate. The hydrolysate after these procedures was used as CS 400. The theoretical sugar concentration is shown in Table 1. The value was calculated using CS composition measured by NREL method. IAM4178 was inoculated to CS 400 in the same manner with chapter 2-1. After the fermentation started, IAM4178 was inoculated again in 6d as the cell density decreased.

### 2-3 Analytical methods

Sugar, ethanol, and furfural were measured with a HPLC system with a Shodex Sugar SH1011 column and a refractive index detector. Mobile phase was 5 mM $H_2SO_4$, flow rate was 0.6 mL/min and the temperature in the column oven was 60°C. Cell density was measured by dilution plating method with YM agar plate. Incubation of the plates was conducted at 30°C, for 2 days. Phenolic compound was measured by Folin-Ciocalteu method referred from [4].

## 3 Results and discussion

### 3-1 Fermentation of synthetic broth

The courses of sugars, ethanol and cell density are shown in Fig. 1 and 2. IAM4178 consumed 40 g/L of glucose within 1 day and 20 g/L of xylose was decreased to 10 g/L in 96h. As a result, ethanol and xylitol were produced. The ethanol fermentation efficiency was 84.4%. The cell density was stable around $10^8$ CFU/mL. These results indicated that IAM4178 can produce ethanol from glucose at high efficiency and can produce xylitol from xylose as a byproduct. The present study also demonstrated that the xylitol production from 5 g/L of xylose by IAM4178 in the exisitence of 10 g/L of glucose was higher than 5 g/L of xylose alone (data not shown). So, the xylitol production was enhanced possibly by the existence of glucose.

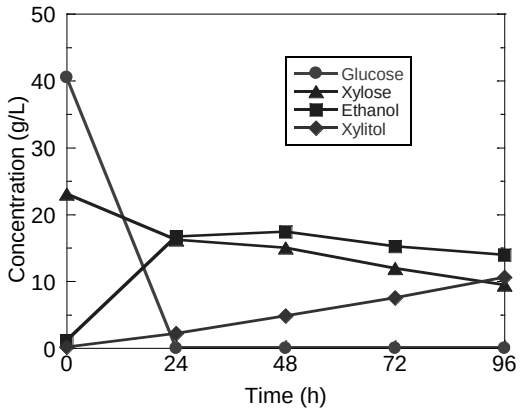

Fig. 1 The courses of sugars and ethanol

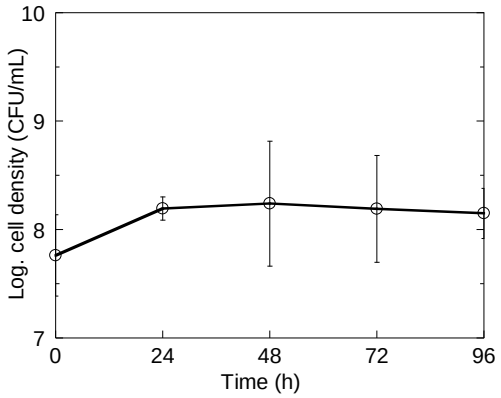

Fig. 2 The course of cell density

### 3-2 Fermentation of CS 200

The courses of sugars, ethnaol, furfural and cell density are shown in Fig. 3 and 4. The initial sugar concentration of CS200 was 63 g/L, which was about 90% of the theoretical value (see Table 1). All glucose was consumed within 12h while about a half (i.e. 10 g/L) of xylose was consumed in 36h. Ethanol was produced with the decrease of glucose but xylitol was not produced altough xylose decreased. Schirmer-Michel, Ângela Cristina, et al. [5] reported that the *Candida guilliermondii* produces xylitol from xylose in the synthetic broth, but does not produce xylitol in the rice hull hydrolysate. The author speculated the existence of inhibitor of xylose reductase activity in the rice hull hydrolysate. In this study, CS 200 might also contained xylose reductase inhibitor. The ethanol fermentation efficiency from CS200 was 73.4%, and the cell density was almost stable at $10^8$ CFU/mL (see Fig. 4). These results indicate that IAM4178 can produce ethanol in the CS hydrolysate without any detoxification. However, the ethanol fermentation efficiency was 10% lower than that of the synthetic broth. It is possibly because of the delay in glucose consumption by furfural [6], and/or the consumption of ethanol by the yeasts.

Table 1 The theoretical sugar concentration

| Run | Glucose (g/L) | Xylose (g/L) |
|---|---|---|
| CS 200 | 73.94 | 31.08 |
| CS 400 | 136.79 | 57.50 |

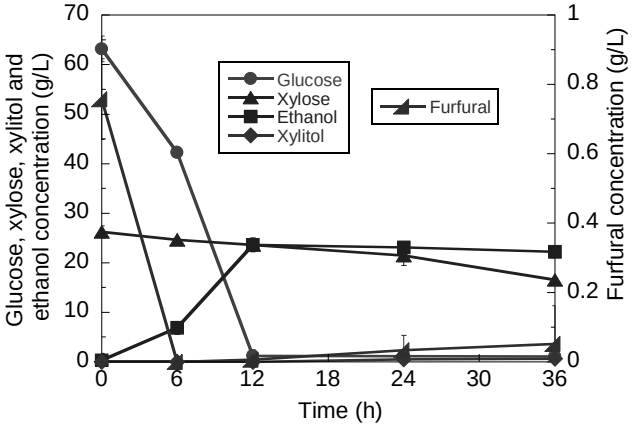

Fig. 3 The courses of sugars, ethanol, and furfural

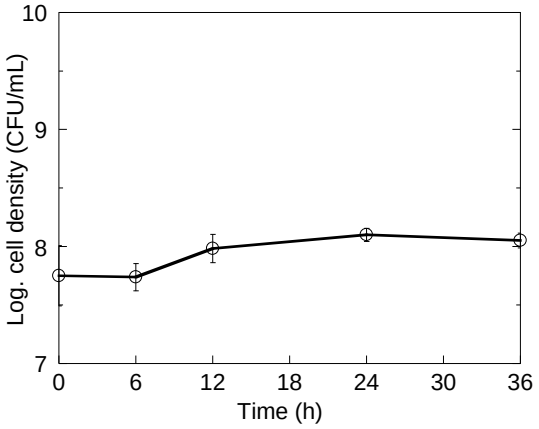

Fig. 4 The course of cell density

### 3-3 Fermentation of CS 400

The courses of sugars, ethanol, furfural, cell density, and phenolic compound are shown in Fig. 5, 6 and 7. The sugar concentration in CS 400 was about 70% of theoretical value in Table 1. This is possibly because some sugar was degraded excessively by two times hydrolysis. From 0d to 2d, about 40 g/L of glucose was consumed. However, the glucose consumption was ceased from 2d to 6d. The glucose consumption begun after IAM4178 was inoculated in 6d, and all of the remaining glucose was consumed in 9d. The glucose consumption was slower than that of CS200, which showed the degradation of 60 g/L glucose within 12h. It suggests that the inhibitor concentration increased by condensation, and caused the delay in glucose consumption.

The final ethanol concentration and ethanol fermentation efficiency of CS 400 were 40 g/L and 73.3%, respectively. It showed that 40 g/L of ethanol concentration is achieved by condensation in the new hydrolysis method. The ethanol fermentation efficiency was similar value with CS 200. These results indicated that the inhibition delayed the sugar consumption but did not affect the fermentation efficiency.

The cell density decreased from $10^8$ CFU/mL in 0d to zero in 4d. Then, the cell density recovered to $10^8$ CFU/mL because of second inoculation in 6d, but it decreased again to zero in 9d. The total phenol was around 2.5 g/L and it was almost stable. In the previous research, 2 g/L of phenoic compound could inhibit the ethanol fermentation [7]. Thus it can be said that 2.5 g/L of phenolic compound in the CS 400 was enough high to affect the cell increase of IAM4178. High concentration of ethanol could be produced from CS 400, but IAM4178 decreased during the fermentation. In summary, the present study indicated that the condensation of CS broth increases both fermentable sugars and inhibitors, but high concentration ethanol is produced by the addition of yeast during the fermentation. The removal of the inhibitory substances will be the next challenge.

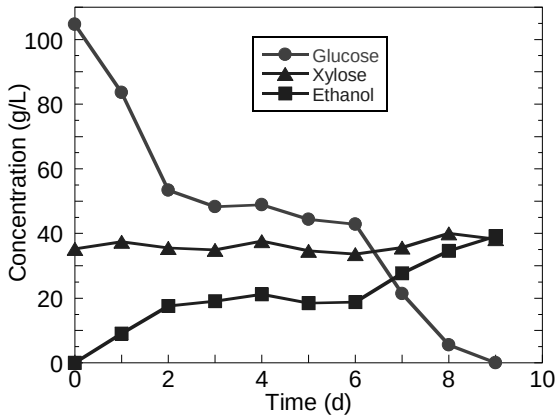

Fig. 5 The courses of sugars and ethanol

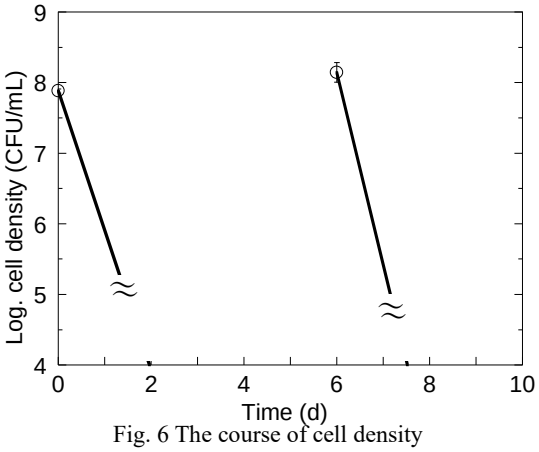

Fig. 6 The course of cell density

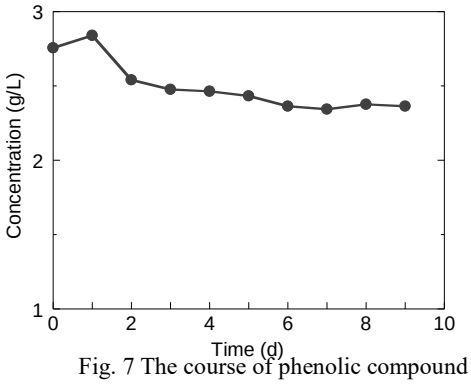

Fig. 7 The course of phenolic compound

# 4 Conclusions

The cassava stem broth (CS 400) was successfully condensed by two times hydrolysis. Fermentation of the condensed broth with IAM4178 achieved ethanol concentration of 40 g/L, which is the target concentration of bioethanol from agricultural residue.

# References


[1] Mitsunori Yanagisawa, Kanami Nakamura, Osamu Ariga, Kiyohiko Nakasaki, Production of high concentrations of bioethanol from seaweeds that contain easily hydrolyzable polysaccharides Process Biochemistry 46 (2011) 2111–2116.

[2] Minhee Han, Yule Kim, Youngran Kim, Bongwoo Chung, and Gi-Wook Choi, Bioethanol production from optimized pretreatment of cassava stem, Korean J. Chem. Eng. 28(1) (2011) 119-125.

[3] A. Sluiter, B. Hames, R. Ruiz, C. Scarlata, J. Sluiter, D. Templeton, and D. Crocker, Determination of Structural Carbohydrates and Lignin in Biomass, Technical Report NREL/TP-510-42618 Revised July (2011).

[4] Matteo Bonoli, Vito Verardo, Emanuele Marconi, and Maria Fiorenza Caboni, Antioxidant Phenols in Barley (Hordeum vulgare L.) Flour: Comparative Spectrophotometric Study among Extraction Methods of Free and Bound Phenolic Compounds, J. Agric. Food Chem. 52 (2004) 5195−5200.

[5] Angela Cristina Schirmer-Michel, Simone Hickmann Flores, Plinho Francisco Hertz, Gilvane Souza Matos, Marco Antonio Zachia Ayub, Production of ethanol from soybean hull hydrolysate by osmotolerant *Candida guilliermondii* NRRL Y-2075, Bioresource Technology 99 (2008) 2898–2904.

[6] L. J. Boyer, J. L. Vega, K. T. Klasson, E. C. Clausen and J. L. Gaddy, The Effects of Furfural on Ethanol Production by *Saccharomyces Cerevisiae* in Batch Culture, Biomass and Bioenergy Vol. 3 No. I (1992) 41-48.

[7] J. P. Delgenes, R. Moletta, and J. M. Navarro, Effects of lignocellulose degradation products on ethanol fermentations of glucose and xylose by *Saccharomyces cerevisiae*, *Zymomonas mobilis*, *Pichia stipitis*, and *Candida shehatae*, Enzyme and Microbial Technology 19 (1996) 220-225.

# Liquid-liquid equilibrium in concentration and purification of bioethanol by solvent extraction

Student Number: 15M18150 Name: Tomonori MASUDA Supervisor: Ryuichi EGASHIRA

# 溶媒抽出法によるバイオエタノールの濃縮および精製における液液平衡

増田 知徳

エタノール水溶液を原料，直鎖アルカン又は軽質軽油を溶媒として液液平衡を実測及び活量係数モデルにより推算した。エタノールは水よりも選択的に溶媒相中に移動した。分子中の炭素原子数（炭素数）の大きい溶媒及び平衡時の温度の低い範囲の条件においてはエタノール−水系の共沸混合物よりもエタノール濃度の高い範囲への濃縮が可能であった。平衡時の温度の上昇又は溶媒の炭素数の減少と共に，エタノールの分配係数は増加し水に対する分離の選択性は低下した。

## 1. Introduction

Bioethanol is well known for the substitute of motor gasoline and considered to the promising fuel since it is obtained from renewable source. Although it is necessary to concentrate ethanol more than 99.5vol% to blend with motor gasoline [1], it is impossible to attain the high concentration by the conventional distillation, because of azeotrope mixture at the ethanol mass fraction of 0.96. The techniques to concentrate ethanol other than distillation have been studied for a long time. One of the typical methods of ethanol concentration is azeotropic distillation, whereas this method should require much energy. Other concentration methods for less energy requirement have been proposed to replace the method with high energy requirement, such as adsorption and membrane separation and so on. The solvent extraction is also one of them. For most cases, the ethanol extraction was studied with the solvents giving relatively high ethanol solubility. Generally these kinds of solvents showed lower separation selectivity of ethanol relative to water, and it was difficult to concentrate ethanol up to the specified concentration. Therefore it is necessary to study the application of the extraction with the solvents of high separation selectivity of ethanol for the bioethanol production.

This study aims the application of solvent extraction to concentration and purification of ethanol for the bioethanol production. The extraction solvents which have potential to concentrate ethanol more than azeotrope composition were selected and the liquid-liquid equilibrium (LLE) of the ethanol-water-solvent was measured under various conditions. The measured LLE was compared with the estimation results by the activity coefficient model. Then the development of bioethanol concentration process with the employed solvent was discussed.

## 2. Liquid-liquid equilibrium measurement

### 2.1. Experimental

According to previous studies, alkane compounds of higher carbon numbers in molecule were expected to show higher separation selectivity of ethanol relative to water [2]. Tridecane (C13), tetradecane (C14), and light gas oil (LGO), consisting mainly of alkane compounds, were selected as solvent. The Physical properties of materials are shown in Table 1. The selected solvents are expected to separate from ethanol easily by distillation, because each boiling point of solvents is much higher than that of ethanol.

The experimental conditions of the mutual solubility and LLE measurement are summarized in Tables 2 and 3. The specified amounts of feed and solvent were put in conical flask and shaken in isothermal bath. After the specified time, raffinate and extract phases were separated into each other by separating funnel. The obtained solutions were analyzed by gas chromatograph (GC) with flame ionization detector, and Karl Fischer titration (KFT) to determine their compositions.

**Table 1 Physical properties of materials**

| Component | Boiling point[K] | Density[kg/L] |
|---|---|---|
| Ethanol | 351.5 | 0.789 |
| Tetradecane | 526.6 | 0.764 |
| Tridecane | 507.1 | 0.756 |
| Light gas oil | 443~643 | 0.840 |

**Table 2 Conditions of experiment of mutual solubility of solvent-ethanol and solvent-water**

| | | |
|---|---|---|
| Feed, F | | Ethanol(e), Water(w) |
| Solvent, S | | Tridecane (C13), Tetradecane(C14), Light gas oill(LGO) |
| Mass of feed | [g] | 10~30 |
| Mass ratio of S to F | [-] | 1~1.5 |
| Temperature, T | [K] | 289~308 |
| Time | [h] | 48 |

**Table 3 Conditions of experiment of liquid-liquid equilibrium in ethanol-water-C14 system**

| | | |
|---|---|---|
| Feed, F | | Ethanol aqueous solution |
| Solvent, S | | Tetradecane(C14) |
| Mass of feed | [g] | 10~30 |
| Mass fraction of ethanol in feed | [-] | 0.20~1.00 |
| Mass ratio of S to F | [-] | 1 |
| Temperature, T | [K] | 298~333 |
| Time | [h] | 48 |

## 2.2 Results and discussion

Figure 1 shows the mutual solubilities between ethanol and solvent under several temperatures. Although the solvent used formed a heterogeneous phase with ethanol, the systems formed a homogeneous phase at higher temperature. The temperature required to form a homogeneous phase rose in order of C13 (298K), LGO (303K), and C14 (313K), and this might follow the order of increasing number of carbon atom in molecules (CN). The mutual solubility of ethanol with solvent increased, as temperature was elevated and CN decreased.

The solvent compound in the raffinate phase and water in the extract phase were not detected by GC or KFT analysis, in other words, the mutual solubility between water and C14 or LGO was negligibly small. Then it could be expected that this kind of solvent should give high separation selectivity of ethanol relative to water. Moreover it must be unnecessary to consider the separation between solvent and water.

Figures 2 and 3 show the phase diagrams of ethanol, water, and C14 systems. The solubility of ethanol and water in the extract phase and that of C14 in the raffinate phase increased with temperature, that is to say, two phase region became smaller as the temperature rose. In this measuring conditions, C14 formed homogeneous phase with some kinds of the feed solutions of higher ethanol concentrations, and the temperature and feed compositions are shown in Table 4. Then, by adjusting temperatures and other conditions appropriately, it is possible to concentrate ethanol up to higher than that specified for the bioethanol production by extraction.

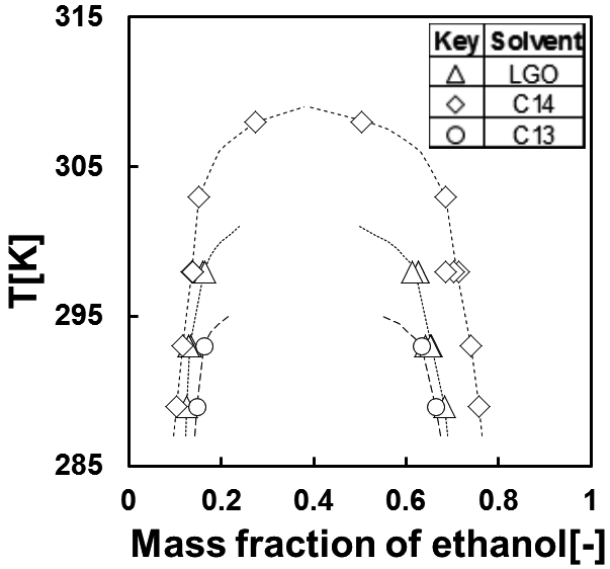


**Fig.1 Mutual solubility of ethanol and solvent**

**Table 4 Conditions which C14 and feed became homogeneous phase**

| T[K] | Mass fraction of ethanol in feed |
|---|---|
| 313 | 1.00 |
| 323 | 0.99, 1.00 |
| 333 | 0.98, 0.99, 1.00 |

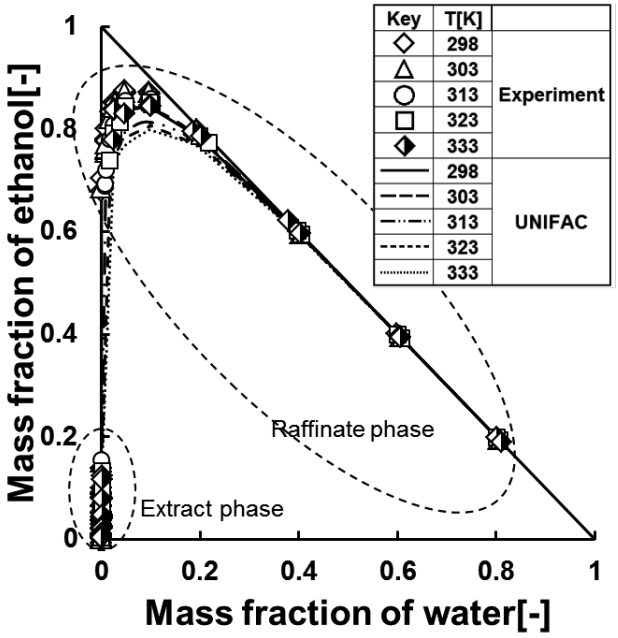


**Fig.2 Phase diagram of C14-water-ethanol (experimental results show by points, estimated results show by curves)**

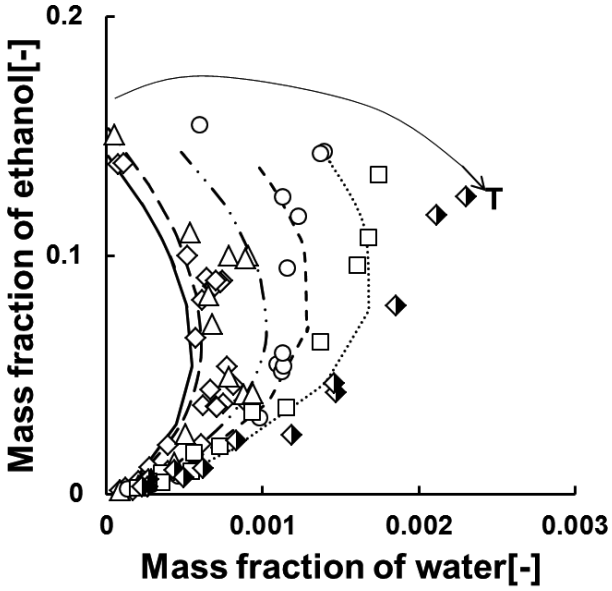


**Fig.3 Enlarged view of extract phase on Fig.2 (experimental results show by points, estimated results show by curves)**

The LLE of the systems measured in this study were estimated by the UNIFAC method, one of the thermodynamic techniques to estimate activity coefficients with interaction parameters between functional groups composing molecular of component and so on[3]. The interaction parameters were determined by fitting the experimental results at the respective temperatures. The estimation results in the case of ethanol-water-C14 system are also shown in Figures 2 and 3 by the curves. The UNIFAC method could favorably estimate the LLE of C14-water-ethanol, especially the compositions of the extract phases.

The distribution ratio of component $i$, $m_i$, the separation selectivity of component $i$ against component $j$, $\beta_{i,j}$, solvent-free mass fraction of ethanol in extract, $Z_E$, and solvent-free mass fraction of ethanol in raffinate, $Z_R$ were defined as follows:

$$m_i = y_i / x_i \quad (1)$$
$$\beta_{i,j} = m_i / m_j \quad (2)$$
$$Z_E = y_e / (y_e + y_w) \quad (3)$$
$$Z_R = x_e / (x_e + x_w) \quad (4)$$

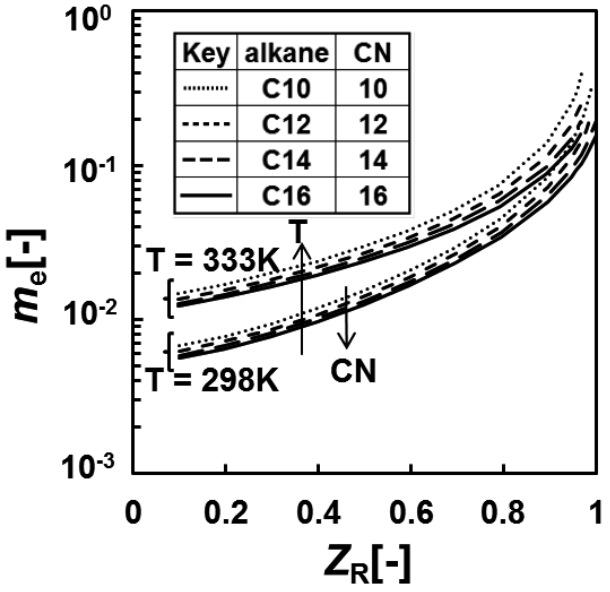


**Fig.5 Relation between distribution ratio of ethanol and solvent-free ethanol concentration in the raffinate phase**

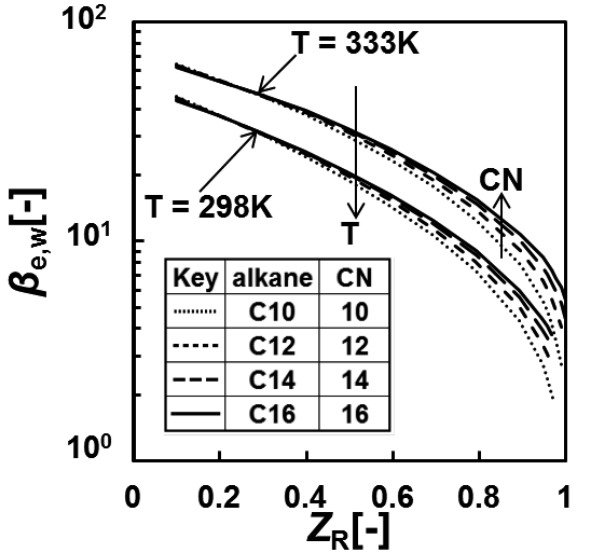


**Fig.6 Relation between separation selectivity of ethanol relative to water and solvent-free ethanol concentration in the raffinate phase**

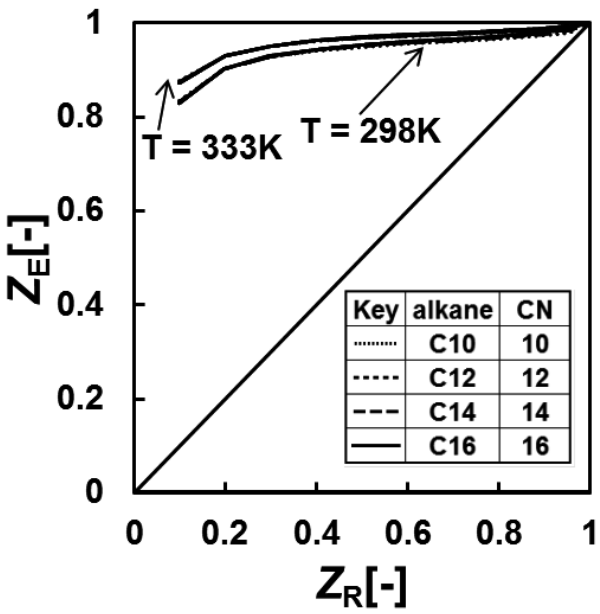


**Fig.4 Relation of solvent-free ethanol concentration in each phase**

The LLE of alkane-water-ethanol system was estimated by the UNIFAC method under various temperature. Figure 4 shows the relation between $Z_E$ and $Z_R$. The $Z_E$ was always larger than $Z_R$. In other words, ethanol could be concentrated in the extract relative to water. The $Z_E$ increased as the temperature increased, and that was larger than that with CN. Figure 5 shows the relation between $m_e$ and $Z_R$. The $m_e$ increased with $Z_R$, temperature, and decreasing CN. Figure 6 shows the relation between $\beta_{e,w}$ and $Z_R$. The $\beta_{e,w}$ decreased with increase of $Z_R$, elevation of temperature and decrease of CN. The actual feed solution from the fermentation step generally contained ethanol of 0.1 by mass fraction. In this concentration range, $m_e$. was so small whereas $\beta_{e,w}$ was large. Then the recovery of ethanol from the feed solution must be difficult even though $m_e$ could be improved by temperature elevation.

## 3. Bioethanol concentration process by solvent extraction

Figure 7 shows the outline of extraction process for bioethanol concentration and purification. The solvent should form heterogeneous two liquid phases with highly pure ethanol in the enriching section between the feed entry point and the top of the extractor, where the ethanol is enriched up to nearly pure with concentration higher than in azeotrope by reflux operation.(shows on Figure 8) On the other hand, high solubility of ethanol into the solvent is required in the stripping section lower than the feed entry to reduce ethanol flowing out as a raffinate product. Although these two criteria of the solvent conflict with each other as results of the equilibrium shown in Figures 5 and 6, they can be satisfied at the same time by selecting different operating temperatures for the enriching and stripping sections, for example.

Other method for reduction of ethanol flowing out as a raffinate product is use of distillation before extraction.

Mass fraction of ethanol in vapor phase and that of ethanol in liquid phase were defined as $Z_V$ and $Z_L$. Figure 8 shows $Z_E$ and $Z_R$ on LLE of C14-water-ethanol system and $Z_V$ and $Z_L$ on vapor-liquid equilibrium(VLE) of ethanol-water system. The VLE data was quoted from the literature.[4] Within the range of high concentration of ethanol(around 96wt%), the difference between $Z_V$ and $Z_L$ is much small, so distillation is difficult. On the other hand, in the range of relatively low concentration of ethanol (60-80wt%), the difference between $Z_V$ and $Z_L$ is large enough to distill raw bioethanol feed into 60-80wt% ethanol easily. Figure 9 shows outline of extraction and distillation. The raffinate containing ethanol is introduced into distillation column, then the ethanol in raffinate is distilled into a distillate product. Accordingly it is possible to recover ethanol from raffinate product by using distillation.

The technique which needs lower energy is required of bioethanol purification process. When operating conditions of extraction process are optimized for reduction of energy consumption, these plans such as above are important.

## 4. Conclusions

The mutual solubility of alkane compounds and ethanol, or alkane compounds and water was measured, and alkane compounds were employed as the solvent for the bioethanol production. Liquid-liquid equilibriums of ethanol-water-solvent were clarified, and it was possible to concentrate ethanol up to more than ethanol azeotrope composition in the range of lower temperature and larger number of carbon in molecules. The distribution ratio of ethanol increased, with elevate of temperature and decrease of number of carbon in molecules, and the separation selectivity of ethanol relative to water decreased with increase of distribution ratio of ethanol.

Based on LLE of experimental results and estimation results by activity coefficient model, bioethanol production process employing extraction using product reflux, and distillation was discussed.

### Nomenclature

x = mass fraction of component in raffinate phase, y = mass fraction of component in extract phase, Z = mass fraction of ethanol without solvent, CN = number of carbon in molecule, T = temperature, m = distribution ratio, $\beta$ = separation selectivity, $\gamma$ = activity coefficient, a = interaction parameter, C10 = decane, C12 = dodecane, C13 = tridecane, C14 = tetradecane, C16 = hexadecane, LGO = light gas oil, CN = number of carbon atom in molecule, LLE = liquid-liquid equilibrium, VLE = vapor-liquid equilibrium

### Subscript

E = extract phase, R = raffinate phase, V = vapor phase, L = liquid phase, w = water, e = ethanol, s = solvent, i = component i, j = component j, p = phase

### References


[1] JIS K 2190:2011 燃料用エタノール
[2] Roddy.J.W Ind. Eng. Chem. Proc. Des. Dev. p104 (1981)
[3] Fredenslund A AIChE Journal vol.21 p1086-1099(1975)
[4] 社団法人日本化学工学会 “化学工学基礎編改訂第 5 版”(2004)


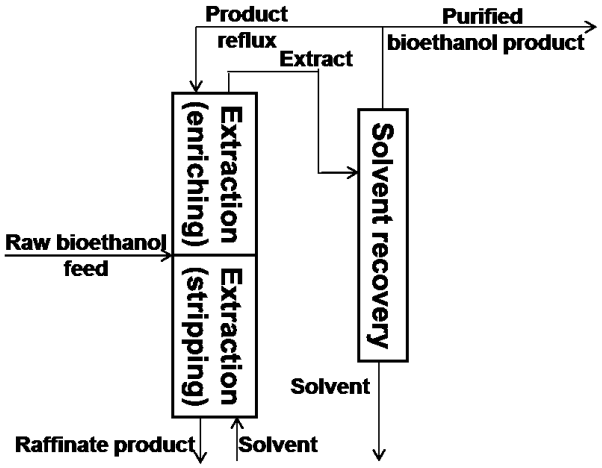


**Fig.7 Outline of extraction with product reflux**

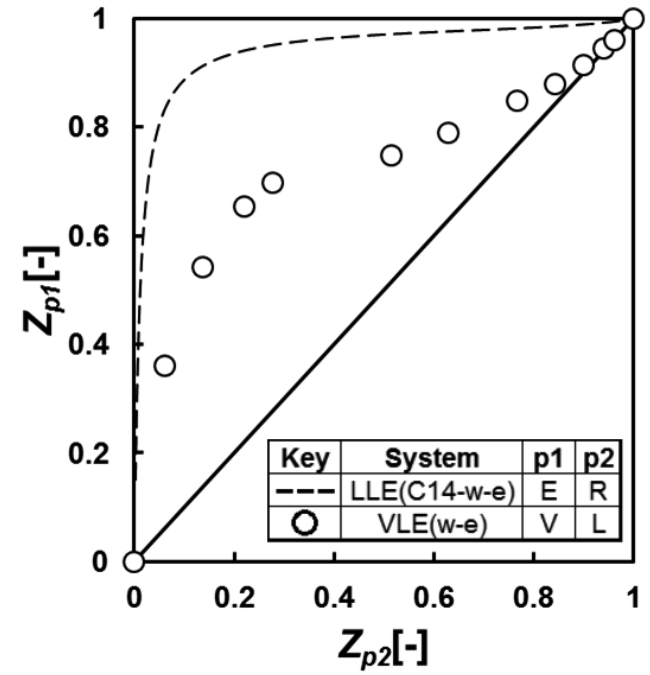


**Fig.8 LLE of C14-water- ethanol system and vapor-liquid equilibrium of ethanol-water system**

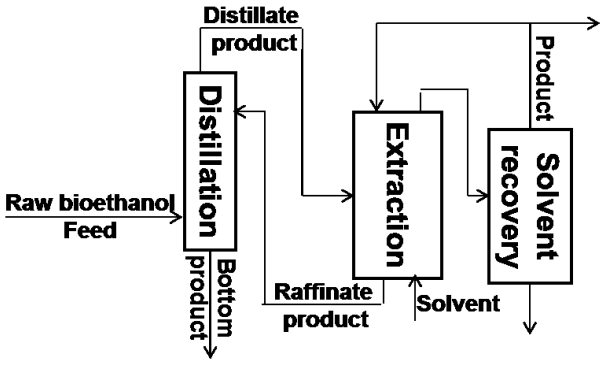


**Fig.9 Outline of extraction and distillation**

Forecasting extreme storm surges in Manila Bay-
an adverse combination of unusual tropical cyclone tracks and southwest monsoon

Student Number: 15M18279 Name: Jerome SILLA Supervisor: Hiroshi Takagi

During the last 56 years, 4% or 66 cases of the total tropical cyclones (TC) that matured over the Northwestern Pacific Basin developed originally in the South China Sea (SCS) and traversed northeast towards the northern Philippines including Metro Manila. Despite the rarity of these tropical systems, their wind speeds may be exacerbated by an interaction with southwest monsoon (SWM) which could further induce disastrous storm surges. Analysis of the NCEP FNL wind data revealed an average wind speed of 5.4 m/s and a maximum wind speed of 14.1 m/s southwest monsoon in Manila Bay. Two east-tracking hypothetical tropical cyclones, TD W28 (1993) and TY Halong (2008), were utilized in the simulation based on 2013 Typhoon Haiyan's characteristics. The largest surge induced by TD W28 was simulated at Navotas station with a peak water level of 5.5m. The largest surge induced by TY Halong was also observed at Navotas station with a maximum surge of 6.6m. The results demonstrated that the additional 5.4 m/s average monsoon produced up to 40cm increased surge (7% relative change) and the additional 14.1 m/s maximum monsoon increased by 70cm in water level (13% relative change).

# 1 Introduction

Tropical cyclones (TC) that enter the Philippine Area of Responsibility typically come from the east in the Pacific Ocean. In addition to this predominant source of TC, low pressure systems that eventually develop into tropical cyclones in the South China Sea (SCS) (hereby referred to as SCS TC) also endanger the western side of the Philippines (Figure 1). Although these SCS TCs have relatively weaker wind speed and are less frequent, this paper stresses that the existence of such is clearly indisputable and potentially disastrous.

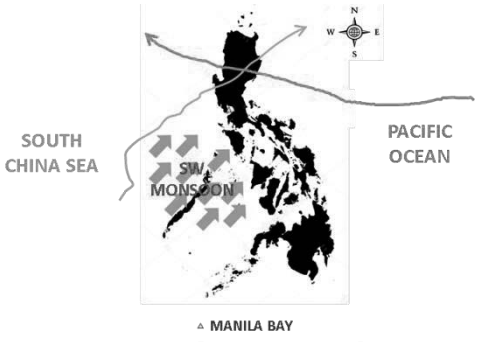


Figure 1. Tropical systems that enter the Philippines develop from either the west (South China Sea) or the east (Pacific Ocean)

Although Manila Bay at first glance may seem to be sitting safely on the western side of the Philippines which faces the opposite landfall point of most TCs from the Pacific Ocean, the bay is particularly vulnerable to coastal disaster due to the presence of extremely densely-populated communities over a low-lying coast. In September 2011, despite being 200 kilometers north of Manila Bay and only having 80 knots maximum sustained wind speed, Typhoon Nesat (TY Nesat) generated one of the most destructive storm surges to ever hit the bay. The maximum storm surge coincided with the high tide of the tidal cycle and tropical cyclone winds interacted with southwest monsoon (SWM) that contributed to an augmented wind field (Morin, 2016), battering the low-lying informal housing scattered around the Manila Bay shoreline.

The objective of this research is to place an increasing emphasis on the vulnerability of Manila Bay to, not just storm surge *per se*, but also to the disasters brought about by the peculiar characteristics of tropical cyclones affecting the Philippines. This research assumes a worst-possible scenario in Manila Bay by incorporating a straightforward approach of integrating tropical cyclone, southwest monsoon and high tide components.

# 2 Data Analysis

## 2.1 SCS TC Component

Tropical cyclones that originated in the South China Sea may track either eastward towards the northern Philippines and Taiwan or westward away from the Philippines and towards Vietnam and southern China. Using the typhoon track data from the Joint Typhoon Warning Center (JTWC) from 1959-2014 (56 years), it was found that among the total tropical systems (1477 cases) that matured in the entire Northwestern Pacific Basin, 153 cases or 10% originated from the South China Sea and tracked either eastward (4%) or westward (6%). It should be stressed out that the scope of tropical cyclones in this study focused only on those that initially tracked eastwardly in which 66 cases were observed. Any indication of fluctuation in the number of occurrence of these SCS TCs was investigated in an annual basis although no pattern was observed. Further, these tropical systems were classified into two — 1) cyclogenesis above 14°N and 2) cyclogenesis below 14°N — on the basis that the southernmost latitude of Manila bay is 14°16′N (Figure 2.1).

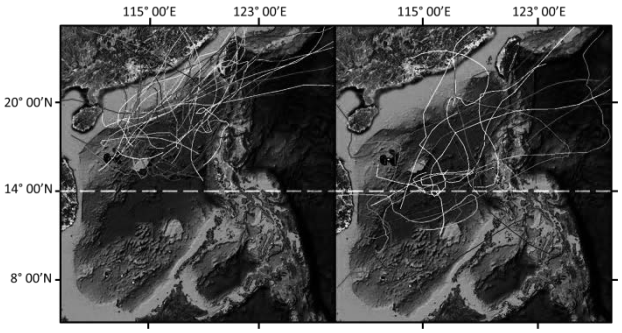


Figure 2.1 East-tracking SCS TCs generated above 14°N (left) and below 14°N (right)

## 2.2 Southwest Monsoon Component

A straightforward calculation by adding the zonal (*u*) and meridional (*v*) wind components of SWM winds in Manila Bay with those of a tropical cyclone used as total wind input into a storm surge model was considered to roughly estimate the southwest monsoon-tropical cyclone synthesis. To perform this, the National Center for Environmental Prediction Final Operational Model Global Tropospheric Analyses (NCEP FNL, 2016) data for *u*- and *v*-components of wind height above sea surface from 2001-2014 in the southwest monsoon months (June to September) were extracted (Figure 2.2). The reliability of NCEP FNL data as input wind to simulate the storm surge in Manila Bay was evaluated using Delft3D Flow and verified accordingly.

The 6-hourly wind data information on days without any occurrence of typhoon were obtained (hereby referred to as no-TC days). It was found that the velocities were fluctuating in each month of the 14-year data and exhibited no significant trend. Results also showed that the four-month average wind speed on no-TC days was 5.4 m/s (9.8 knots) with a *u*-component of 3.7 m/s (7.2 knots) and a *v*-component of 3.4 m/s (6.6 knots). Additionally, it was discovered that the daily maximum monsoon wind strength based on the NCEP-FNL data could rise as high as 14.1 m/s (27.4 knots).

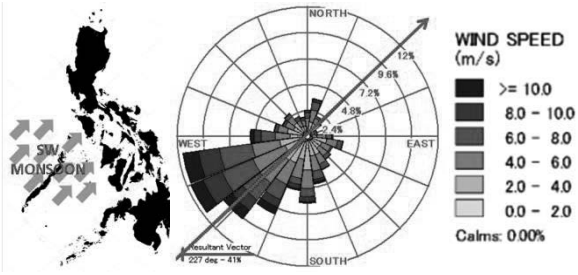


Figure 2.2. Off-Manila Bay wind rose diagram from 2001-2014 shows the prevailing wind coming from the southwest

## 2.3 Tide Component

The tide analysis was achieved using predicted tide data produced from WXTide32 at two tidal stations. Hourly tide values from 2001-2015 (15 years) were gathered during the SWM months (June to September). Days that exhibited the highest tide level for each station were selected for each month for each year and were plotted. Since the tide peak time for the months of June, July and September all aligned within a 2-hour range, it was deemed reasonable to compute for the average high water level of these months to obtain the representative maximum tide value (Figure 2.3). The mean

high water values in these months ranged from 1.43-1.46m with a peak time generally between 10:00-11:00h.

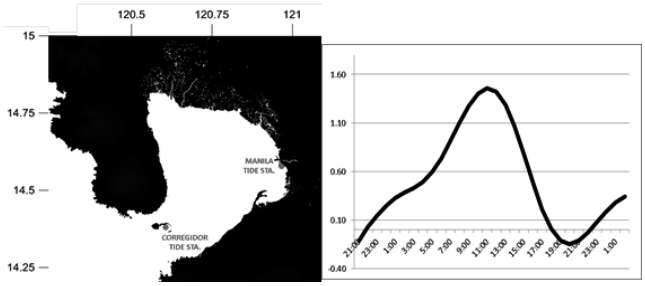


Figure 2.3. (*Left*) Manila Port and Corregidor tidal stations and (*Right*) their derived hypothetical maximum tide time series (unit: meter)

# 3 Storm Surge Simulation

Two SCS TCs, TD W28 (1993) and TY Halong (2008), which exhibited an east-tracking characteristic from the South China Sea were selected in the analysis (Figure 3).

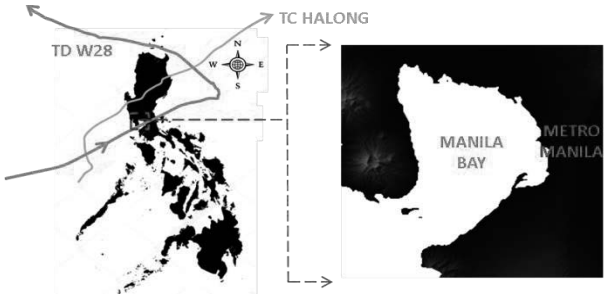


Fig 3. Paths of TD W28 and TC Halong

A model that generates an improved estimation of wind and pressure distribution particularly for typhoons that exhibit a central pressure of 935 hPa or lower was utilized (Takagi and Wu, 2016). The characteristics of TD W28 and TY Halong were adopted from those of Typhoon Haiyan (with a minimum sea level pressure of 895 hPa) to forecast extreme events in Manila Bay. The maximum sustained wind, translation speed, central pressure and radius of 50-knot wind of the two tropical cyclones were patterned from that of Typhoon Haiyan and thereby produced hypothetically extreme versions of TD W28 and TY Halong. The determined values of SWM wind based on NCEP data analysis were directly added to the *u*- and *v*- wind components produced by the typhoon model to roughly estimate the total wind surge attribute. The non-wind surge attribute from the tidal component was inputted in time series form at the open boundary of the computational domain. The simulation was run using Delft3D-Flow which is based on non-linear shallow water equations.

# 4 Simulation Results

Four locations were under observation throughout the simulation to represent four highly-populated communities along the coastline of Manila Bay: Navotas, Roxas Boulevard, Baseco and Cavite City. . It should be emphasized that the typhoon model used to generate the preliminary wind speed did not consider the change of topography.

## 4.1 TD W28 with SWM

For the case of TD W28, Navotas Sta. exhibited the largest water level with peak surges of 5.5m (With-Tide Case) and 2.9m (Without-Tide Case) as compared to the other three stations (Figure 4.1)**.**

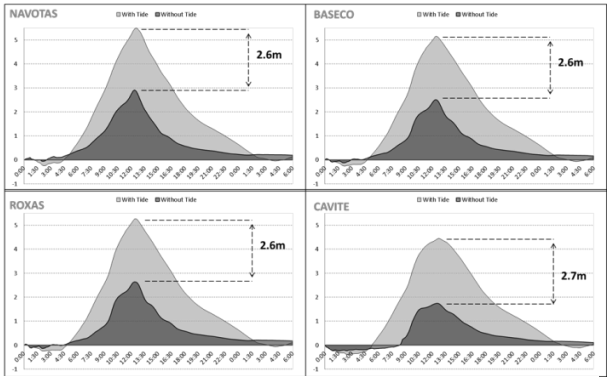


Figure 4.1 Time series of the water level (in meters) at each station for TD W28

The value of 2.9-m peak surge for the Without-Tide Case was not expected mainly due to the fact that Haiyan's exceptional characteristics were included in the reproduced tropical cyclone. This water level was found to be rather low given the extremely high wind speed and extremely low pressure of Haiyan. It should be clarified that the input wind for the Without-Tide Case was exactly the same as that of the With-Tide Case, and therefore, the only difference between the two was the tide input at the boundary condition.

### 4.2 TY Halong with SWM

The results of the numerical simulation of TY Halong were generally similar to the trend of the results of that of TD W28. Although both cases for TD W28 and TY Halong employed a 30-hour simulation run, the biggest difference between the two was the angle of approach of the wind and the time interval before landfall in which the input wind and pressure time series of TY Halong was 6 hours longer than those of TD W28. This result ascertained the sensitivity of the hydrodynamic model to both the input wind and pressure.

Another main difference in the analysis was that the latitude coordinates of TY Halong's original track were adjusted (lowered) to render the storm eye closer to Manila Bay. Several trial simulations were performed to determine by how much the latitude should be adjusted such that the largest storm surge would be generated. It was later discovered that a reduction factor range of 2.1-2.2° onto the latitude coordinates would induce the highest water level at the four observation points (Figure 4.2).

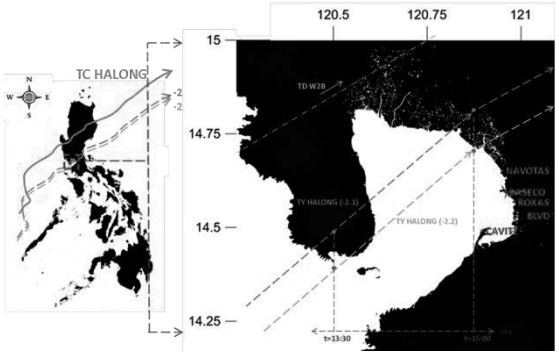


Figure 4.2. TY Halong track adjustment

### 4.3 TY Halong without SWM

The additional 5.4 m/s average monsoon increased the surge height by ~40cm (7% relative change) whereas the additional 14.1 m/s maximum monsoon prompted a ~70cm-rise in water level (13% relative change). It should be noted that only extreme tropical cyclone scenarios were utilized in this study. The increase of surge from SWM which reached up to 13% may seem insubstantial to surges brought about by extreme tropical cyclones but this may be significant enough in the case of lower category tropical systems, most especially for low-lying regions around the coastline of Manila Bay.

## 5 Conclusion

Despite the rarity of SCS-generated TCs, a TC-SWM interaction is potentially catastrophic particularly for Manila Bay which is surrounded by a densely-populated metropolitan area. This may be further exacerbated by the lack of awareness of the people regarding the existence of such unusual SCS TCs.

Irrespective of Typhoon Haiyan's extreme characteristics that ultimately claimed lives of 6,300 people in 2013, one of the contributing reasons for such a great number of casualties was the lack of understanding of the concept of storm surge in the Philippines. In the same logic as what had transpired in the case of Haiyan, thorough understanding of the mechanism of tropical cyclone-southwest monsoon interaction ushers a more pertinent disaster mitigation scheme. Before successful strategies could be formulated and policies be operationalized towards an effective integrated coastal resource management, awareness is the first measure that must be undertaken in order to prevent yet another Haiyan tragedy.

## References

Morin, V. M., Warnitchai, P., & Weesakul, S. (2016). Storm surge hazard in Manila Bay: Typhoon Nesat (Pedring) and the SW monsoon. Natural Hazards, 81(3), 1569-1588.

Takagi, H., & Wu, W. (2016). Maximum wind radius estimated by the 50 kt radius: improvement of storm surge forecasting over the western North Pacific. Natural Hazards and Earth System Sciences, 16(3), 705-717.

National Centers for Environmental Prediction/National Weather Service / NOAA / U.S. Dept. of Commerce. 2000, updated daily. NCEP FNL Operational Model Global Tropospheric Analyses, continuing from July 1999.https://doi.org/10.5065/D6M043C6.

# Utilization of Indonesia Natural Bentonite for Dye Removal

## インドネシア産天然ベントナイトの染料除去への有効利用

15M18285 Harish Reza Septiano Warsono Supervisor: Hirofumi HINODE

本研究ではインドネシア産ベントナイトの有効利用を目的とし、キャラクテリゼーション、ピラリング処理、及び染料除去能の評価を行った。インドネシア産ベントナイトはスメクタイト族の結晶相を含むことが確認され、陽イオン交換容量及び比表面積を測定した。ピラリング処理により、ベントナイトの特性を改善することに成功した。また、インドネシア産ベントナイトの未処理及び、処理後の染料除去能を検証した。

## 1. INTRODUCTION

Bentonite is clay mineral with many applications such as adsorbent, ion exchanger or catalyst support. It exists naturally in area within the volcanic region, and is very abundant in Indonesia. However, its utilization in Indonesia is still not yet fully maximized. Indonesia still imports 20% of its bentonite requirements [1].

This condition occurred mainly due to two reasons: firstly from the demand side, consumers avoid the use of local bentonite due to its unknown characteristics which often lead to substandard performance. Secondly, from the supply side, there are only limited ways of use known for local bentonite, because almost all bentonite consumption in Indonesia is for palm oil purification process. Efforts to overcome these challenges in order to improve local bentonite use, such as characterization and the proposal of other usage of local bentonite, have to be conducted.

Additionally, as a natural clay, bentonite still has a potential to be processed and improved. Many researches have been conducted to improve bentonite utility such as acid treatment, thermal treatment, organobentonite and pillaring. The first three modification treatments already have credibility as robust treatments due to their clear mechanisms. As for the pillaring treatment, despite many studies having reported its ability to improve many of bentonite's capability, it still contains a black box regarding its mechanism and other treatment conditions which are very challenging to be identified.

Therefore, addressing those problems and potentials, the aims of this study are as follow: to characterize the properties of Indonesian natural bentonite; to conduct pillaring treatments as efforts to improve the properties of bentonite as well as to elucidate the effects of the pillaring treatment itself; to evaluate the capability of bentonite and its modified form in removing dye pollutants as an alternative application of Indonesian natural bentonite.

## 2. MATERIALS AND METHODS

### 2.1. Material

The material used as the main target sample is natural bentonite（NB）taken from Bogor Indonesia. The clay was grinded and mixed in one batch in the industrial grinder prior the usage in the laboratory. No additional treatment conducted before experiment.

### 2.2. Characterization

Characterization of NB was conducted using the following methods: x-ray diffraction analysis（XRD）to analyse the crystalline structure of NB; thermogravimetry and differential thermal analysis（TG-DTA）to investigate the thermal stability of NB; Fourier transform infrared spectroscopy（FTIR）to investigate the functional groups in NB; nitrogen adsorption desorption analysis to measure the specific surface area（SSA）and pore size; cation exchange capacity（CEC）analysis using Chapman method [2]; and chemical composition analysis measured by inductively coupled plasma atomic emission spectroscopy（ICP-AES）.

### 2.3. Pillaring Treatment

Pillaring treatments were conducted using Al, Cu, Mn and Ti metal precursors. The technique used in

the Mn and Cu pillaring experiment refers to the method used in Drljalca et al. [3] which is also known as the Base-Acid method. Al pillaring method used in this research is the widely used method for Al referring to the experiment conducted by Bertella et al. [4]. A simple method for intercalating and pillaring bentonite with Ti by directly mixing bentonite with Ti precursor inside ethanol was proposed. For comparison, thermal treatment was also conducted. All the details of the procedure used in this research are shown in Figure 1. The bentonite treated using Mn, Cu, Ti, Al and thermal treatment henceforth are called HMnB, HCuB, HTiB, HAlB and HB, respectively.

All the modified bentonites were also characterized using the same analyses and methods used in the NB characterization experiments. In addition, experiment to determine the exchangeable cation amount of each sample was conducted. 0.1 g of sample was mixed to 12 mL sodium acetate 1.0 M for 5 minutes, and was separated using centrifugation, followed by collection of the supernatant. This procedure was repeated for three times, and the collected liquids were measured using ICP-AES for cation other than Na.

## 2.4. Dye Removal Evaluation

In this study, the effect of time, the effect of initial dye concentration and the effect of pH to the dye removal capability of bentonite and its treated form were investigated. Methylene blue (MB), methyl orange (MO) and naphthol green b (NG) were used as the target dyes.

The effect of time was investigated by mixing 0.05 g of bentonite to 50 mL of dye solution with known concentration (Table 1). Samples were taken at regular intervals and analysed using ultraviolet-visible spectrometer (UV-VIS).

**Table 1 Experiment Condition**

| Dye | Concentration | Bentonite |
|---|---|---|
| MB | 300 mg/L | NB |
| MO | 200 mg/L | NB |
| NG | 200 mg/L | HMnB |

The study of the effect of initial dye concentration to the dye removal performance was conducted by the mixing constant amount of bentonite (0.05 g) to 50 mL solution of dyes with varying concentrations. The concentration range for MB, MO and NG were 50-500 mg/L, 25-300 mg/L and 25-300 mg/L, respectively. The mixing was conducted in room temperature and in natural pH of each dye.

The effect of pH was studied by mixing 0.05 g of bentonite to 50 mL of dye solutions with known concentration, whose pH already adjusted to 3,5,7,9 or 11. The pH of the solutions were adjusted using 0.1M $HNO_3$ and 0.1M NaOH. The dye concentration and bentonite used in this experiment were the same with the effect of time investigation experiment as shown in Table 1.

The wavelength used in the UV-Vis measurement of MB, MO and NG concentration in each experiment were 663 nm, 464 nm and 714 nm, respectively.

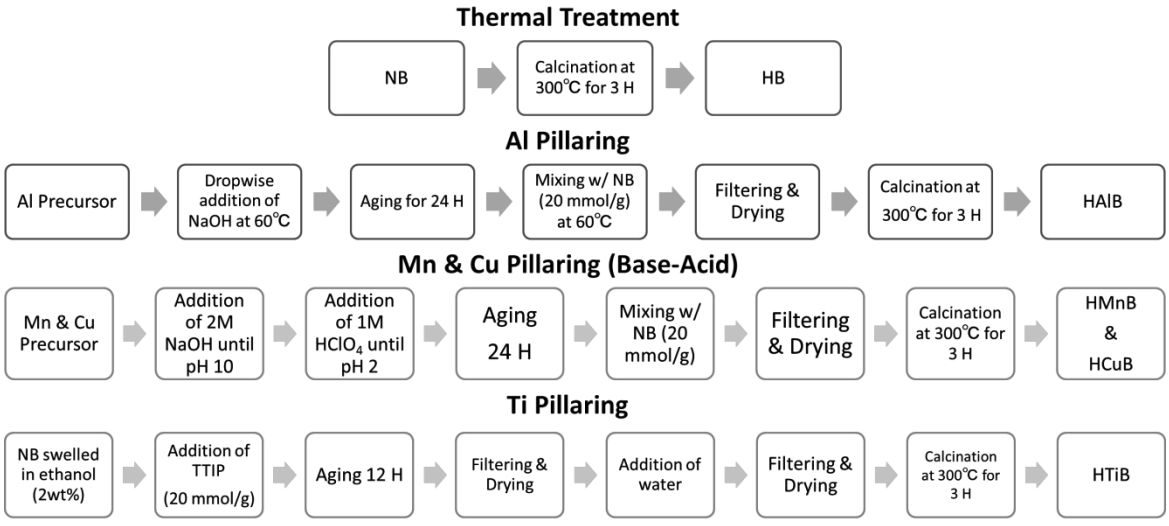


**Figure 1 Details of Procedures**

# 3. RESULTS AND DISCUSSION

## 3.1. Characterization

XRD pattern of NB shows that it contains smectite mineral structure, which may be a mixture of montmorillonite and nontronite with the interlayer spacing around 1.5 nm. This result was in good agreement with the data from chemical composition analysis that shows there are significant percentage of Mg and Fe exist as the structural cation in the clay. The existence of tridymite impurity was also detected through the XRD and FTIR analysis.

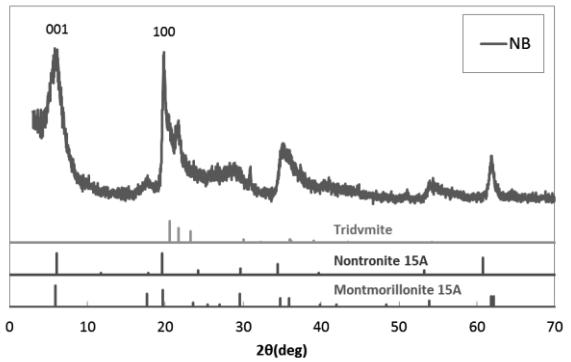


**Figure 2 XRD pattern of NB**

NB was also found to have a relatively high cation exchange capacity (CEC) and specific surface area (SSA) which were determined to be 98 meq/100 g and 70.8 $m^2/g$, respectively.

## 3.2. Pillaring Modification

The intercalation of pillaring agent that is shown by the increase of basal spacing was observed in some of the pillaring treatment (Al and Mn). However, Only AlB could maintain the basal spacing due to the newly made structure bonds after heating. The decrease in basal spacing in other pillaring treatments after calcination was caused by the loss of coordinated water inside the basal spacing. Details of the basal spacing data and peak intensities are shown in Table 2.

Despite the inability to maintain the basal spacing, the intercalation of metal was confirmed in the chemical composition analysis. Moreover, the addition of 5.61 wt% of Al, 1.57 wt% of Mn, 2.01 wt% for Cu and 13.33 wt% of Ti were found to have remained in bentonite bulk, not as exchangeable cation.

**Table 2 Basal Spacing and Intensity**

| | Before Calcination | | After Calcination | |
|---|---|---|---|---|
| | $d_{001}$(nm) | $I^*$ (%) | $d_{001}$(nm) | $I^*$ (%) |
| NB | 1.57 | 102 | 1.00 | 41 |
| AlB | 1.81 | 100 | 1.60 | 67 |
| MnB | 1.57 | 110 | 0.98 | 49 |
| CuB | 1.48 | 78 | 0.99 | 60 |
| TiB | 1.51 | 112 | 1.01 | 48 |

$I^*$ = Intensity of $d_{001}$/ intensity of $d_{100}$

All the conducted pillaring treatment also successfully increased the CEC and SSA of NB. However, each pillaring agent caused different results in terms of average pore size of the bentonite bulk. The result of CEC, SSA values and average pore size values of the samples are shown in Table 3.

**Table 3 CEC, SSA and Average Pore Size**

| | CEC (meq/100g) | SSA ($m^2/g$) | AVG. Pore Size (nm) |
|---|---|---|---|
| NB | 98 | 70.7 | 8.25 |
| HB | 83.2 | 69.8 | 8.32 |
| HAlB | 107.5 | 151.3 | 5.18 |
| HMnB | 107.4 | 92.4 | 7.08 |
| HCuB | 91.2 | 82.8 | 6.35 |
| HTiB | 125.3 | 113.9 | 4.96 |

## 3.3. Dye Removal Evaluation

### 3.3.1. Equilibrium Time Study

In the equilibrium time study, almost 48% of the total amount removal was achieved for all 3 target dyes in the first 5 minutes. Equilibrium was also achieved in around 2 hours after mixing. This equilibrium time was used to determine the period for the study of initial dye concentration effect.

### 3.3.2. Effect of Concentration

All of NB and its modified forms showed capability of MB and MO removal. However, in NG removal test, only HMnB showed the removal capability. The removal increased as the initial dye concentration increased until the adsorbent maximum capacity was reached. This means that the removal occurred due to the existence of limited removal sites in the bentonite.

In MB removal test, HMnB showed the highest removal capability, followed by NB, HB, HCuB, HAlB and HTiB, respectively. The removal process is suggested to be highly influenced by the synergistic effect of the overall negative charge of bentonite structure shown by CEC values and the average pore size which determines the likelihood of MB to enter the bentonite bulk. HMnB has one of the highest CEC values and a sufficiently large average pore size which enable a high amount of MB removal.

In MO removal test, NB achieved the highest removal amount, continued by HB, HTiB, HCuB, HAlB and HMnB, respectively. The removal of MO is believed to be affected by the number of locally positive-charged edge of bentonite platelet. The thermal and pillaring treatment conducted in this study bonded the edges with each other and decreased the positive charge of the bentonite, causing a drop in the MO removal capability in the treated bentonite.

Only HMnB showed capability in removing NG from the solution due to the size of NG which is too big to enter the bentonite bulk. However, only Mn had the capability to attack Fe in the NG structure and degrade it to smaller compounds which are removable.

### 3.3.3. Effect of pH

From the study of pH, it is observed that the process of dye removal by bentonite was significantly affected by the pH condition of the solution and the different characteristics of each dye pollutant.

For cationic dye such as MB, the removal process competes with positive charge from proton so the amount of removal is reduced in lower pH and increase in higher pH. Reversely, for anionic MO and NG dyes, in the removal shows higher removal in lower pH than in the higher pH due to the competition with hydroxide ion in the solution.

## 4. CONCLUSIONS

Characterization of Indonesian natural bentonite was successfully conducted and the result shows it has adequate properties to be utilized. The conducted pillaring treatment also managed to intercalate the metal pillaring agent to the bentonite bulk. NB and its modified form were able to remove some dye pollutants from aqueous water system.

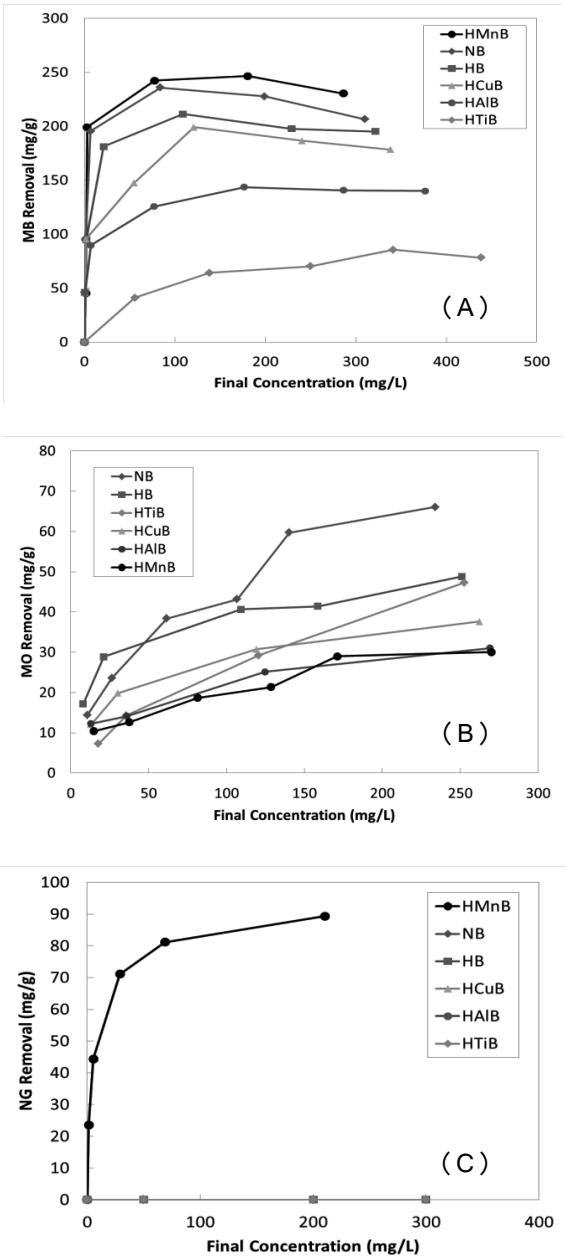


**Figure 3 MB Removal Test (A), MO Removal Test (B), NG Removal Test (C)**

## 5. REFERENCES


1. **Panjaitan, Rumintang Ruslinda.** *The Usage of Bentonite in Industry.* Surabaya : Surabaya Research and Standardization Center, 2010.

2. *Cation-Exchange Capacity.* **H.D.CHAPMAN.** s.l. : Agonomy Mnograph, Methods of Soil Analysis, 1965.

3. *A new method for generating chromium(III) intercalated clays.* **A. Drljaca, J.R. Anderson, L. Spiccia, T.W. Turney.** s.l. : Inorganica Chimica Acta, 1997, Vol. 256.

4. *Pillaring of bentonite clay with Al and Co.* **Francine Bertella, Sibele B.C. Pergher.** s.l. : Microporous and Mesoporous Materials, 2015, Vol. 201.

# SYNTHESIS OF N-DOPED MESOPOROUS $TiO_2$ BY FACILE ONE-STEP SOLVOTHERMAL PROCESS FOR VISIBLE LIGHT PHOTOCATALYSIS

Student Number: 15M51800 Name: Erlandy Dwinanto TOE Supervisor: Hirofumi HINODE

Abstract

In this study synthesis of modified $TiO_2$ by non-metal N-dopant was done with one-step solvothermal method. Under this process, both N-dopant and CTAB could be introduced thus creating N-doped mesoporous $TiO_2$ after template removal using calcination. Several characterizations were done in order to determine the properties of the as-synthesized photocatalyst and also explaining the possible band-gap reduction mechanism. Settling test was done to give qualitative description in the easiness of separation process. Performance of the as-synthesized photocatalysts were tested under visible light (λ>400 nm) and was compared to other commercially available $TiO_2$ photocatalyst.

## 1. Introduction

Water is one of the essential needs to support human life, and as the population is projected to keep on increasing, not to mention the decreasing effective amount of clean water due to contaminant and pollution from industrialization, the needs for effective and efficient waste water treatment is imminent. Since most pollutant is in the form of organic type, advanced oxidation process is deemed good solution with the help of photocatalyst. $TiO_2$ is one of the well-known material for photocatalyst because of good thermal and chemical stability and the fact that it is relatively inexpensive. However, its band-gap of around 3.0 – 3.2 eV means $TiO_2$ only active in the UV region wavelength. Whereas, most of the solar radiation consist of visible light with up to more than 40% and UV light is consisted of only 3 – 5 % from total radiation spectrum.

As a result, in this study band-gap modification of $TiO_2$ was done using nitrogen as non-metal doping to extend the workability range. The material was synthesized under one-step solvothermal method in order to get mesoporous structure. Porous structure is intended to have larger specific surface area without the need for small particle size, thus help easing the photocatalyst separation and recovery process. In addition, characterization was done to give explanation regarding the synthesis condition and mechanism of the visible light photocatalysis.

## 2. Experimental Method

### 2.1. N-doped porous $TiO_2$

In a typical synthesis, 1ml of TTIP ($Ti\{OCH(CH_3)_2\}_4$, Kanto Chemical co., inc.) is inserted into 10 ml of ethanol (99.5% Wako pure chemical industries ltd.) and mixed together with 0.185 g CTAB ($(C_{16}H_{33})N(CH_3)_3Br$, Kanto Chemical co., inc.) and 1 ml of 10x diluted HCl (35-37% Wako pure chemical industries ltd.). CTAB is used here as the template to create porous $TiO_2$. The mixture is stirred in magnetic stirrer for 30 minutes. After that, certain amount of ethylenediamine ($C_2H_4(NH_2)_2$, Wako pure chemical industries ltd.) are introduced as nitrogen source (Table 1), and the mixture further stirred for 60 min.

After that, the solution is transferred into teflon-lined stainless-steel autoclave for solvothermal process at 200 ˚C for 16 h. The obtained precipitate was then filtered and washed after that dried overnight at 80 ˚C. Afterwards, the powder form sample was calcined in tube furnace under air flow with flowrate of 350 ml/h at 400˚C for 3 h. The ramp rate of the calcination is being controlled at a low rate of 1 ˚C/min.

### 2.2. Settling Test

Settling test was done so as to determine the rate of sedimentation of each used photocatalyst (as-synthesized NTi1, Degussa P25, Wako anatase)

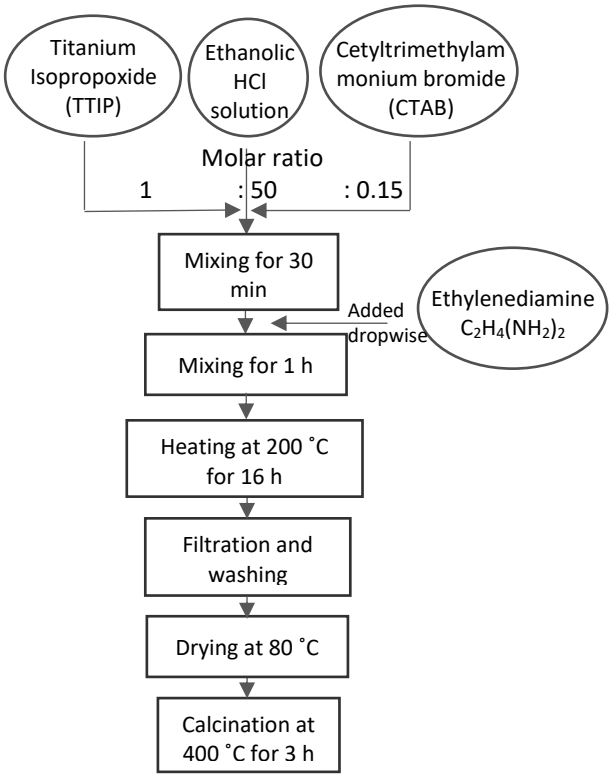


*Figure 1. Flowchart of synthesis process.*

therefore easiness of separation and retrieval process for each catalyst can be relatively compared with each other. In this test, condition similar to the actual photocatalytic test was used, where 100 ml of deionized water with 0.5 g/l catalyst concentration were stirred for 3 h after which each were placed in graduated cylinder and left observed for 1 h, 2 h, 4 h and lastly 24 h.

### 2.3. Photocatalytic Activity Test

Activity of the as-synthesized photocatalyst was tested using Heraeus UV immersion lamp TQ 150, with the distance between light source and solution being kept at 10 cm. During the experiment cooling jacket was used to maintain the temperature constant and film filter was used so as to cut out the UV part (λ < 400 nm) of the spectrum. Methylene blue (MB) (Kanto Chemical Co., Inc) and methyl orange (MO) (Wako pure chemical industries ltd.) were used as model pollutant with initial concentration of 10 ppm and catalyst amount of 0.5 g/l. Prior to each activity test, dark adsorption was done by stirring the solution with catalyst for 60 min without any light source. Next, photocatalytic activity was sampled periodically. Afterwards the concentration was checked by measuring the absorption using Shimadzu UV-1800 UV-vis spectroscopy.

*Table 1. Variation of starting N:Ti molar ratio.*

| Sample | N : Ti molar ratio |
|---|---|
| Undoped | - |
| NTi0.5 | 1:2 |
| NTi1 | 1:1 |
| NTi1.5 | 3:2 |
| NTi2 | 2:1 |

## 3. Results and Discussion

First, by comparing the XRD pattern of the samples to a standard reference, all of the as-synthesized photocatalysts has been synthesized into the photocatalytically active form of anatase phase $TiO_2$ with peak at 2θ angle of 25.4°, 37.8°, 48.3° all conforming to the standard JCPDS card #84-1286 for anatase $TiO_2$.

Moreover, the effect of solvothermal temperature was also observed by varying the oven temperature from 150 °C, 175 °C and 200 °C. It can be seen that at solvothermal temperature of 150 °C, Ostawld-ripening process was just started and that crystallization of $TiO_2$ has not been achieved. In the solvothermal process there will be breaking of metal alkoxide bond in titanium tetraisopropoxide (TTIP) reactant. After that some nucleation will take place, and further excess heat will be used for transformation from the amorphous phase into crystallization and crystal growth. At the same time, solvothermal was also intended so as to make the micelles of CTAB, which act as the pore forming template, to undergo self-assembled and attached on the $TiO_2$ surface before later removed by thermal treatment during calcination.

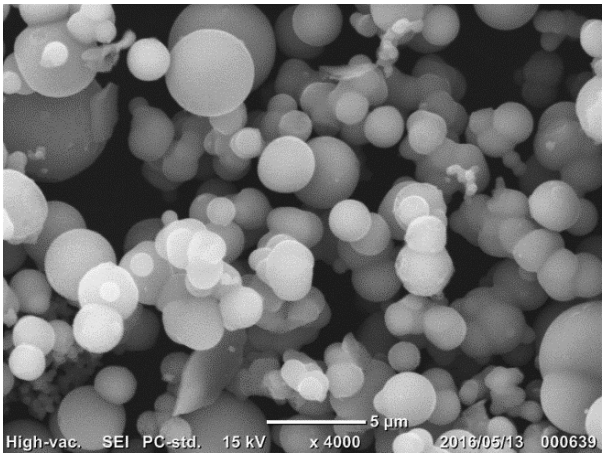


*Figure 2. SEM images at x4000 magnification.*

Based on SEM images, the as-synthesized powder form $TiO_2$ had a spherical morphology with relatively

narrow particle size distribution as shown in Fig.2 and average particle size of around 3 μm. FTIR spectrum for all the synthesized samples were shown. Broad peak at 3400 $cm^{-1}$ indicated the surface hydroxyl and absorbed water. In addition, peak present at 1630 $cm^{-1}$ for all samples indicated the vibrations of O-H bonds, while the deep peak observed at 700 $cm^{-1}$ stands for Ti-O stretching. The difference between undoped and all other N-doped $TiO_2$ samples can be well observed between the region of 1000 – 1550 $cm^{-1}$ which is shown in more detail on Fig.3. The presence of peaks showed some indication that N-doping had been successfully inserted into $TiO_2$, although further verification is needed and will be done by XPS spectroscopy.

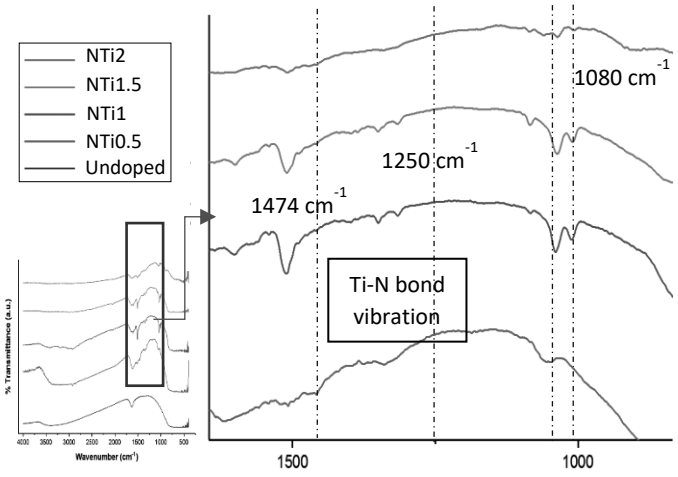


*Figure 3. FTIR spectrum*

Referring to the XPS survey result in Fig. 4, using pass energy of 187.85 eV major peaks such as that of O 1s at 532 eV, Ti $2p_{1/2}$ and Ti $2p_{3/2}$ chemical state at 465 eV and 461 eV, respectively can be observed. Moreover, peak of C 1s which act as the reference for calibration position is also seen at around 285 eV and N 1s is seen for energy level of 400 eV. For purpose of detailed analysis, narrow scans of each observed major peaks were given under the smallest pass energy of 23.5 eV. In this respect, for the case of N 1s chemical state, it was seen that only a single peak at around 400 eV is present. According to reference on several possible N 1s spectrum, N 1s peak in $TiO_2$ at 400 eV is indicating a Ti-O-N bonds, whereas peak at lower energy of 397 eV indicated Ti-N bonds. This means that it can be said that N-dopants has been successfully inserted through the solvothermal synthesis route, and that in this case the nitrogen atom would only act in interstitial doping type in the form of Ti-O-N. Next, in DRS characterization it was shown that NTi1 sample slightly red-shifted to longer wavelength resulting in ~0.1 eV band-gap reduction compared to the undoped $TiO_2$.

Average pore size and specific surface area were calculated using BET method. Both the $N_2$ physisorption characterization results of undoped and NTi1 showed relatively large surface area, that is of 87.82 $m^2/g$ and 69.18 $m^2/g$, respectively. The porous size of the as-synthesized catalyst is around 15 nm which suggest that it is in the mesoporous region.

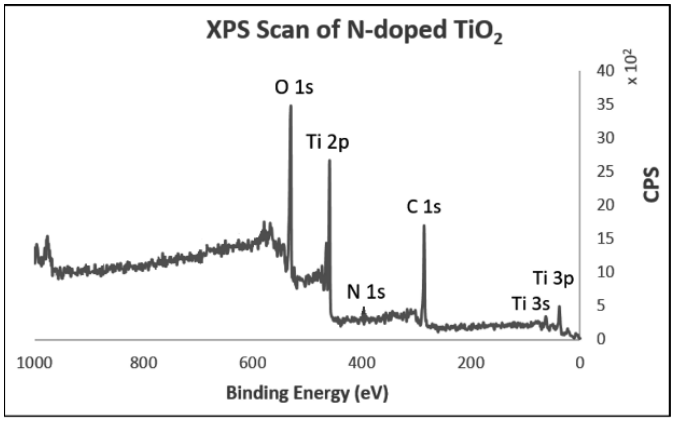


*Figure 4. XPS survey scan of NTi1.*

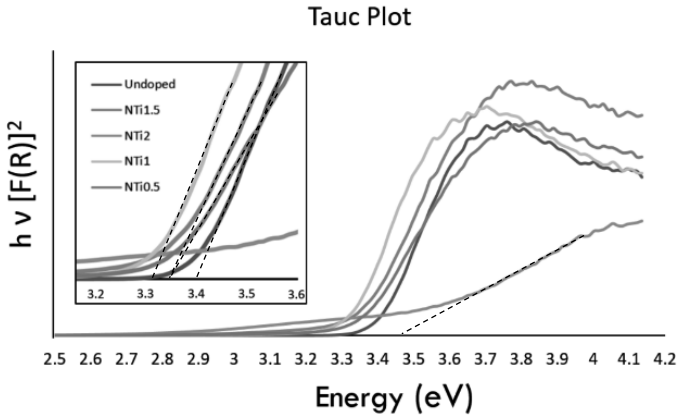


*Figure 5. Tauc plot comparison of all samples.*

NTi1 catalyst have faster settling time, compared to the other two photocatalyst of Degussa P25 (middle) and Wako anatase (right), which means easier separation and recovery process with properties summarized in Table 2.

The photocatalytic activity of methylene blue degradation went according to the following order: NTi1 > Undoped > Degussa P25 > Wako anatase > blank. The photocatalytic activity of NTi1 under the visible light irradiation (λ>400 nm) showing the highest MB degradation rate with the methylene blue fully decolorized under the NTi1 after 5 h of light irradiation, whereas Degussa P25, Wako anatase or undoped $TiO_2$

photocatalyst only show slight degradation, with MB concentration still more than 50% even after 5 h of irradiation while blank test condition showed very small MB degradation. The same can be noticed for methyl orange degradation, however with faster degradation rate. After 2 h of visible light irradiation the 10 ppm MO was showing complete photocatalytic degradation. Based on both photocatalytic performance of NTi1, it is can be said that the presence of N-doping in the form of interstitial doping of Ti-O-N, is able to extend the workability range of $TiO_2$ and induce the visible light responsive of $TiO_2$. This idea is supported by Nakamura, et al [1] which also found that vis light activity not caused by Ti-N bond which come from the notion of substitutional doping or oxygen vacancies previously stated by many studies [2-3].

*Table 2. Properties of NTi1 compared with other photocatalyst.*

| | **NTi1** | **Degussa, P25** | **Wako,** |
|---|---|---|---|
| Chemical; Form | N-doped $TiO_2$; Anatase | $TiO_2$; Mixed Anatase and | $TiO_2$; Anatase |
| Avg. Particle Size | ~ 3 µm | ~ 25 nm | ~ 125 nm |
| Specific Surface Area | ~ 70-80 $m^2/g$ | ~ 50 $m^2/g$ | n/a |

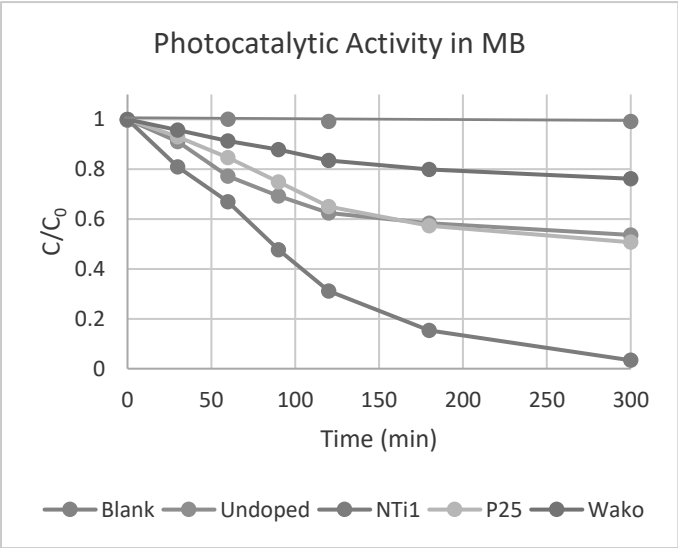


*Figure 6. MB degradation in vis light photocatalysis.*

The mesoporous pore channel in as-synthesized N-doped mesoporous $TiO_2$ might not only enhance the separation of photogenerated electron-hole pairs and decrease their recombination rate, but also in this case increase the effectiveness of interfacial electron transfer. The notion of increased electron transfer in porous structure, especially in the mesoporous channel, is actually given before in multiwalled carbon nanotubes [4] as well as $Co_3O_4$-$CeO_2$/C as highly active electrocatalyst in oxygen reduction reaction [5]. This would mean that $e^-$ photoreduction reaction especially of multi-electron reduction (+0.68 V) which will result in $H_2O_2$ is the dominant degradation path-way:

$$O_2 + 2\,H^+ + 2\,e^- \rightarrow H_2O_2 \qquad (1)$$

This $H_2O_2$ is a strong oxidizing agent which could degrade MO more easily due to the cleavage of azo bond. This was proven in further experimental test using only $H_2O_2$ as oxidizing agent, with MO degradation rate is found to be 36.6% compared to MB of 22.7%. In addition, measurement of MB and MO solutions pH, both are in the range of 6.0. Considering the point of zero charge of $TiO_2$ is at 6.80, there might be some positive surface charge build up on the surface of $TiO_2$ in the solution which will favour the adsorption of anionic dye of MO, whereas MB as cationic dye will have lower adsorption due to charge repulsion.

## 4. Conclusion

The synthesis process of N-doped mesoporous $TiO_2$ has been successfully done by using facile one-step solvothermal method. This synthesis method enabled successful introduction of N-doping into the crystal lattice of $TiO_2$ as well to use CTAB as porous template. The as-synthesized N-doped $TiO_2$ managed relatively large surface area of more than 70 $m^2/g$, although the average particle size is around 3 µm. This is due to the presence of mesoporous structure with average pore size of ~15 nm. NTi1 also had faster settling performance as well as higher photocatalytic performance under visible light source as compared with Degussa P25 and Wako anatase. Based on the characterization this photosensitization towards longer wavelength was caused by the Ti-O-N interstitial doping that had the effect on extending the workability range by providing band-gap reduction by introduction of $N_{2p}$ energy band level just above the $O_{2p}$ valence band level.

## References


[1] Nakamura, R., et al. (2004). *The Journal of Physical Chemistry B*, *108*(30), 10617-10620.
[2] Asahi, Ryoji, et al. *science* 293.5528 (2001): 269-271.
[3] Ghicov, Andrei, et al. *Nano Letters* 6.5 (2006): 1080-1082.
[4] Nugent, J. M., et al. *Nano letters* 1.2 (2001): 87-91.
[5] Liu, Kun, et al. *ACS applied materials & interfaces* 8.50 (2016): 34422-34430.

# DEVELOPMENT OF GPSDO-SYNCHRONIZED CHANNEL SOUNDER USING SOFTWARE DEFINED RADIO

Student Number: 15M51740 Name: DEEPAK Gautam Supervisor: TAKADA Jun-ichi

**Abstract**

In this thesis, time and phase synchronization using GPS Disciplined Oscillator(GPSDO) in low cost Software Defined Radio (SDR) based channel sounder is presented as an alternative to existing synchronization techniques. Phase stability of carrier signals generated in Transmitter (Tx) and Receiver(Rx) using reference signals of GPSDO output in indoor environment is studied thoroughly. Finally, two path channel is measured with developed GPSDO-synchronized channel sounder and result is evaluated by comparing with the result of reference sounder.

## 1 Introduction

Performance of wireless communication system is heavily dependent on the environment between transmitter and receiver known as propagation channel. The directional and delay characteristics of the propagation channel are of great importance for designing such systems. Channel properties need to be measured in order to characterize wireless propagation channel. Measurement system used for channel measurement is known as channel sounder and process of measuring channel response is called channel sounding.

Channel sounder detects the electromagnetic waves transmitted via particular communication channel to determine the statistics of either channels time variance impulse response or time variant frequency response [1] .From early literature to till date, channel sounders are implemented either using off-the-self devices like Vector Network Analyser (VNA) [2], Spectrum analyser or they are designed using dedicated hardware components [3, 4]. Designing channel sounder using dedicated hardware is being popular as off-the-self devices does not offer flexibility to customize for measurement in more complex environment. For example, VNA where transmitter and receiver are in the same device is not suitable for large distance channel measurement due to significant loss in coaxial cable extended from transmit and receive port of VNA. Thus, in this study, we use SDR platform with GPSDO to increase measurement range, reduce cost and for convenience to carry due to its compact size.

### 1.1 Channel sounding methodology

In channel sounding as shown in Fig.1, known sounding signal $x(t)$ is sent from the transmitter at the desired RF frequency. After being propagated through channel, signal is received as $y(t)$ in the receiver and is stored in memory. From the information of the received signal, channel impulse response $h(t)$ of the propagation channel is obtained

$$y(t) = x(t) * h(t) + n(t)$$

where, $n(t)$ is the noise introuduced by the channel. In actual procedure to obtain channel impulse response, computation is done in frequency domain. If $Y(f)$ is the fourier tansform of $y(t)$ and $X(f)$ is fourier transform of $x(t)$, then channel transfer function $H(f)$ is obtained as

$$H(f) = Y(f)/X(f)$$

Inverse Fourier Transform(ifft) of the channel transform function gives the channel impulse response $h(t)$

$$H(f) \underset{\text{ifft}}{\longrightarrow} h(t)$$

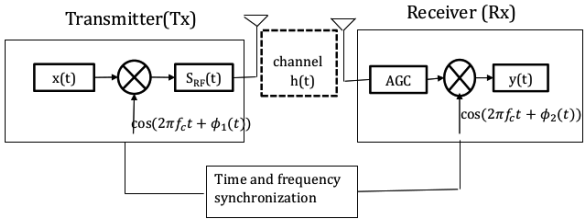


Figure 1: Principle of channel sounding

### 1.2 Methods of Synchronization in channel sounding

Accuracy of the estimated parameters from the measured data in delay and angular domain depends on the precision of the time, frequency and phase synchronization between Tx and Rx. In channel sounding system, phase synchronization depends on the performance of the local oscillator and Phase Locked Loop (PLL) system used to synthesize the carrier frequency.Phase noise affected channel transfer function can be represented as:

$$H_{\text{pn}}(f) = H(f)\exp(\text{j}(\phi_1(t) - \phi_2(t))) \quad (1)$$

Here, $\phi_1(t)$ and $\phi_2(t)$ are phase noise introduced by local oscillator at Tx and Rx respectively.Phase noise is one of the major source of directional characteristic estimation error [5]. $\exp(\text{j}(\phi_1(t) - \phi_2(t)))$ in this work is represented as the phase difference between carrier signals generated in Tx and Rx. Tx and Rx are said to be phase synchronized when phase difference approaches to 0. Phase synchronization is necessary for accurate measurement of directional characteristics.

Highly accurate phase synchronization is achieved in VNA based channel sounding where carrier signal from same local oscilaltor is shared in both Tx and Rx. For frequency and phase synchronization in conventional channel sounder, highly stable 10 MHz reference signal from Rubidium and cesium oscillators are used to synthesize local signal. Either 10MHz signal from one frequency reference source is shared between Tx and Rx or separate signals from two or more than two frequency reference sources are used separately. Later case which is used in distributed channel measurement, frequency offset between Tx and Rx exists due to free running mode.Rubidium and cesium oscillators cost very high and extra synchronization affort is required in distributed channel measurement. So, we are interested to investigate the use of GPSDO as synchronization unit with Software Defined Radio (SDR) based channel sounder. Motivation of selecting GPSDO is due to its low cost and also better phase synchronization between spatially separated Tx and Rx is expected as GPSDOs are phase locked with highly accurate 1 PPS GPS signal.

## 2 SDR based sounder structure

Universal Software Radio Peripheral(USRP), low cost and flexible hardware peripheral hosted in the general purpose computer is used with free and open source software, GNU Radio to make software radio. Structure of USRP and GNU Radio platform is shown in Fig.2. In transmit chain, complex signals generated from eq.(2) are sent from host PC to USRP through gigabit ethernet cable at complex sampling rate of 25MS/s. After digital processing in motherboard, signals are upconverted to desired RF signal in analog quadrature modulator of daughterboard. Finally, RF signal is sent through antenna. In receiver chain, RF signal received is downconverted in RF front end into baseband signal. Then that signal is digitized by ADC and is sent to field-programmable gate array(FPGA). Finally the data is sent to host PC through gigabit ethernet cable.

$$x(t) = \frac{1}{N} \sum_{k=-N/2}^{N/2-1} \exp(\mathrm{j}2k\pi \triangle_F t + \mathrm{j}\phi_k) \qquad (2)$$

Here, $\phi_k = \pi \frac{k^2}{N}$ , Newman phase is added to reduce crest factor of multitone signal, $\triangle_F$ is frequency spacing between tones and $N$ is total number of tones.

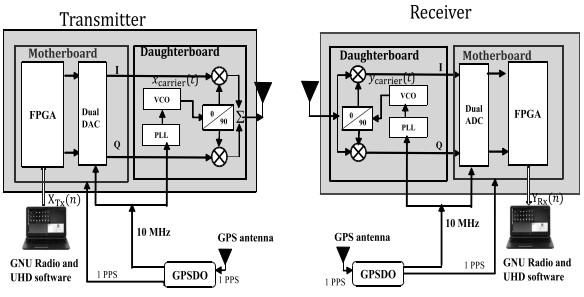


Figure 2: Structure of GPSDO-synchronized USRP and GNU Radio based channel sounder

For time synchronization between Tx and Rx, 1PPS signal generated by reference clock is utilized to trigger the start of transmitting and receiving. For phase synchronization, highly stable 10 MHz signal generated by commercial oscillator is utilized in Tx and Rx chain to generate carrier signal. Three modes of synchronizations are supported in USRP. In default mode, Temperature Compensated Crystal Oscillator(TCXO) generates master clock and reference to carrier signals. Secondly,in external reference mode, USRP accepts 1PPS and 10 MHz signals from any external oscillator. Finally in GPSDO mode, 1PPS and 10 MHz signal of GPSDO is utilized in which GPS information can be tracked and GPS time can be used for time synchronization.

## 3 Description of GPSDO experiment setup

GPS Disciplined Oscillator (GPSDO) utilize GPS signal received from satellites to generate stable frequency of 10 MHz.GPSDO connected to GPS antenna has to be locked with satellites in clear line of sight condition for at least 48 hours to perform at its best [6]. In order to use GPSDO under required condition, GPS antenna is installed in rooftop of 4 stories building at south 6, Ookayama campus, Tokyo Institute of Technology and the signal is carried to ground floor with low loss cable,3D-FB as shown in Fig.3

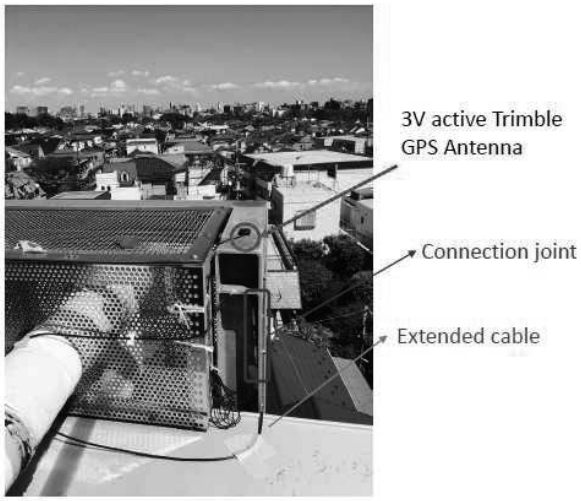


Figure 3: GPS antenna installed in rooftop

## 4 Experiment: Phase synchronization

Before utilizing output of GPSDOs directly to synthesize carrier signals. Phase synchronization between 10 MHz signals of two GPSDOs is presented in Section 4.1 both in free running mode and GPS locked mode. After the information of phase synchronization of reference signals, phase synchronization of 4.85 GHz carrier signals is presented in Section 4.2.

### 4.1 Between 10 MHz reference signals of GPSDOs

Performance of phase synchronization between output of two GPSDOs in free running mode and GPS locked mode is examined from the experiment setup as shown in Fig. 4 and 5 respectively.

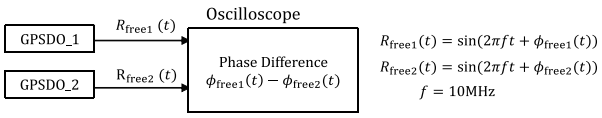


Figure 4: Phase synchronization measurement setup for free running GPSDOs

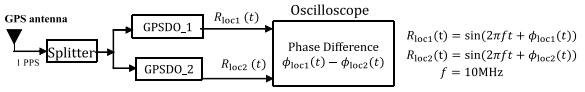


Figure 5: Phase synchronization measurement setup for GPS locked GPSDOs

Phase coherency between two GPSDO reference signals is much improved when they are locked with GPS signal. Fig.6 shows that the phase difference between two 10 MHz reference signals measured over 72 seconds has standard deviation of phase difference of $101.1706^o$ when they are free running. After being locked with GPS antenna, phase difference deviation reduces to $2.5354^o$. From this result, it can be said that oscillators can be phase synchronized with GPS signal in indoor environment.

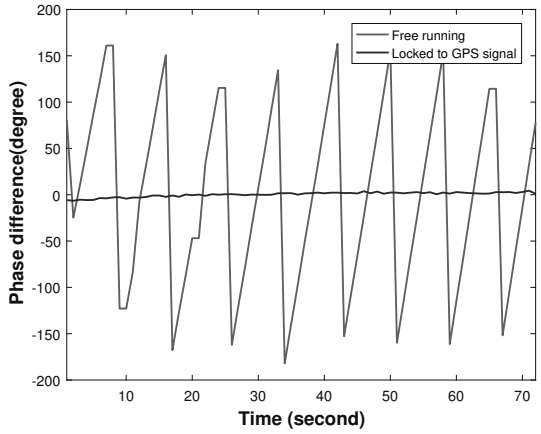


Figure 6: Phase synchronization between 10 MHz signals of two GPSDOs

### 4.2 Between 4.85 GHz signals of Tx and Rx synthesized from separate GPSDO

To examine the phase difference between Tx and Rx at 4.85 GHz synthesized from 10 MHz frequency references of separate GPSDOs, back to back connection between Tx and Rx is made. In this connection, Tx and Rx are directly connected with 1m cable and 30dB attenuator as shown in Fig.7. Complex sinusoid signal,$x[n]$ of 10 Hz is sent from Tx with complex sampling rate of 12.5MSps at 4.85GHz and received as $y[n]$ at Rx.

$$x[n] = a \cdot \exp(2\pi f_b n) \tag{3}$$

If $\delta\phi$ is phase difference introduced due to Tx and Rx chain, receives signal is represented as

$$y[n] = b \cdot \exp(2\pi f_b n + \delta\phi) \tag{4}$$

Here, $a$ and $b$ are amplitude of baseband signal at transmitter and receiver respectively.

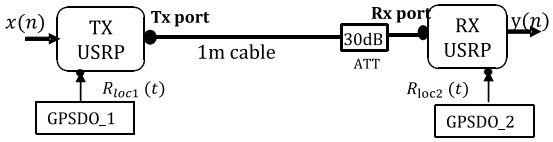


Figure 7: Back to back connection between Tx and Rx

Phase difference from measured data is plotted over time in Fig.8. From the result , it is found that phase is rotated by $478^o$ within 8 seconds and phase difference between Tx and Rx signals seems to be increased linearly over time. From this graph, it can be said that there is possibility of prediction of phase rotation between Tx and Rx while using two GPSDOs.

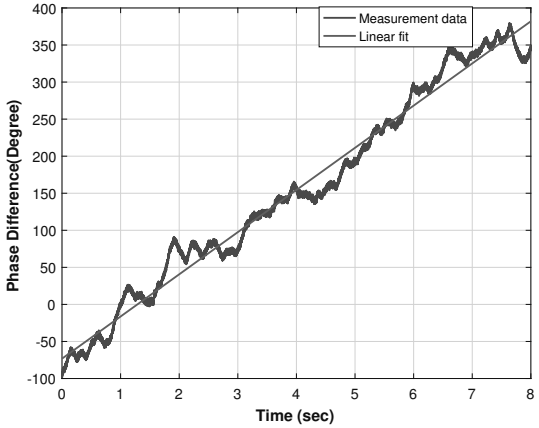


Figure 8: Phase synchronization between 4.85 GHz signals synthesized from separate GPSDOs

### 4.3 Discussion on Coherency between 4.85 GHz carrier signals

Temporal correlation of phase is used as a mean to examine the phase coherency between transmitted and received signal in this work. Higher the value of correlation between samples in time domain, higher the degree of coherency between them. Data received from back to back connection, $y[n]$ is used for this purpose. Autocorrelation is calculated from received data with the resolution of $0.8$ ms over the period of 4 second using eq. (5). Result presented in Fig.9 shows that phase of received signal has high correlation over the period of 4 second.From this result, it can be said that two GPSDOs configuration can be used for the directional measurement with duration of 4 second

$$R(\tau) = \frac{\sum_{i=1,j=\tau}^{N/2} y(i).y^*(i+j)}{\sum_{i=1}^{N/2} y(i).y^*(i)} \tag{5}$$

Where, $N$ is total number of received samples and $\tau \in [0\ \ N/2]$

## 5 Evaluation of channel sounder

To validate the operation of the developed channel sounder, two path channel is measured using this channel

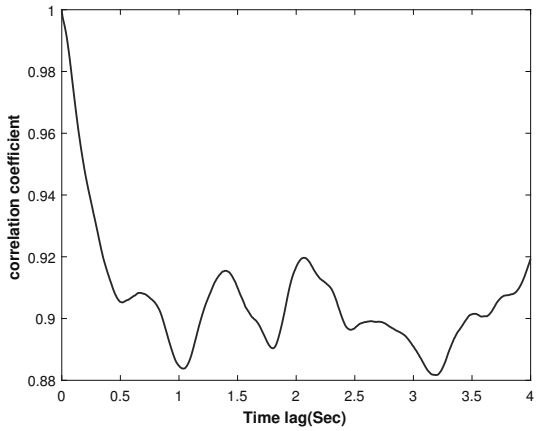


Figure 9: Autocorrelation of received signals

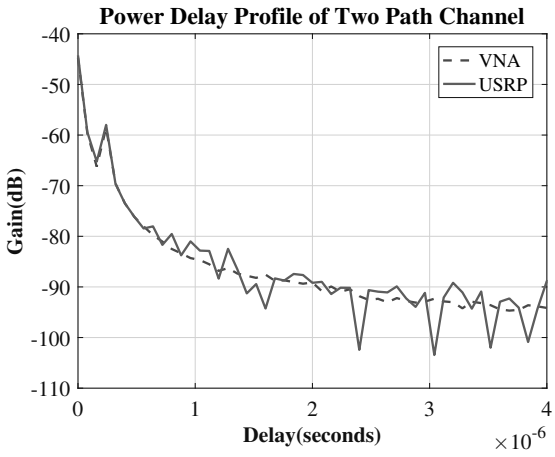


Figure 11: Power Delay Profile of two path channel

sounder and also using Vector Network Analyzer as a reference for comparison. T-junction channel as in Fig.10 is used as two path channel . Multitone signal is sent from Tx and received at Rx .Signal propagating through T junction has two paths. One is direct path from terminal A to terminal B and another path is from C.This channel is measured using developed sounder and VNA in similar setup whose measurement parameters are tabulated in table 1. Power delay profile of this channel measured using both GPSDO synchronized channel sounder and VNA is compared.

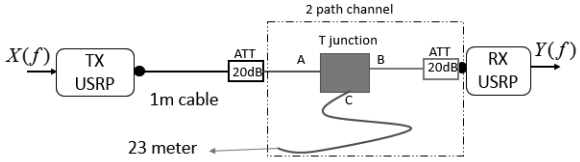


Figure 10: Two path simulator setup

Table 1: Measurement parameters for two path channel

| | |
|---|---|
| Center frequency | 4.85 GHz |
| Bandwidth | 12.5 MHz |
| Sampling frequency | 25 MSps |
| Number of tones | 128 |
| sounding signal | Multitone signal with Newman phase |
| Transmit power | 0 dBm |
| Frequency reference | GPSDO (Separate) |

Cable used in this setup is HUBER+SHUNER SYUCOFLEX100. Propagation speed in cable is 77% of speed of light. Length of cable connected at terminal C is 23 m. Distance of second path is 46 m

$$d_{\text{secondpath}} = \frac{46}{2.9 \cdot 10^8 \cdot 0.77} = 206 \text{ ns}.$$

Where, $d_{\text{secondpath}}$ is time taken to propagate through second path. From our calculation, delay of second path is found to be 240 ns. This is almost equal to the calculated value of delay time. This result validates the operation of channel sounder to be correct. Also power delay profile of two path measured with GPSDO-synchronized channel sounder and VNA as presented in Fig.11 shows good aggreement.

## 6 Conclusions and Future Research

In this work, GPSDO-synchronized channel sounder using commercially available USRP and free and open source tool, GNU Radio is presented for low cost channel sounding. Operation of developed channel sounder is validated by comparing with VNA in two path channel at 4.85 GHz. Coherency of carrier signals at 4.85 GHz synthesized from separate GPSDO in Tx and Rx is confirmed for 4 second duration.

In future, phase coherency of carrier signals using separate GPSDOs for longer duration will be examined. This GPSDO-synchronized channel sounder is expected to be extended in directional channel measurement at 4.85 GHz

## References

[1] S. Salous, *Radio propagation measurement and channel modelling*. John Wiley & Sons, 2013.

[2] S. S. Ghassemzadeh, R. Jana, C. W. Rice, W. Turin, and V. Tarokh, "Measurement and modeling of an ultra-wide bandwidth indoor channel," *IEEE Transactions on Communications*, vol. 52, no. 10, pp. 1786–1796, 2004.

[3] Y. Konishi, Y. Chang, M. Kim, and J.-i. Takada, "Versatile radio channel sounder for double directional and multi-link mimo channel measurements at 11 ghz," *IEICE Transactions on Electronics*, vol. 97, no. 10, pp. 994–1004, 2014.

[4] M. Kim, K. Wangchuk, S. Sasaki, K. Fukawa, and J.-i. Takada, "Development of low cost mm-wave radio channel sounder and phase noise calibration scheme," *COST Action IC1004 (EU), TD (15)*, vol. 12036, 2015.

[5] M. Landmann, *Limitations of Experimental Channel Characterisation*. PhD thesis, 2007.

[6] "Manual FireFly-1A." Available: http://www.jacksonlabs.com/assets/uploads/main/firefly_1A_manual.pdf.

# Estimation of National Logistics Cost Using Macro Economic Data

Student Number: 15M51733 Name: Shidong FENG Supervisor: Shinya HANAOKA

The measurement and comparison of national logistics cost are the focus of this study. By three criteria, Transportation, Inventory and Administration Cost are found to be most appropriate components for national logistics cost measurement and comparison. Cost elements of components are found similar across countries but differences still exist, according to the literature review. Linear model and linear-log models are built for Transportation and Inventory Cost using macro economic data. With concern of multicollinearity, all feasible models are kept. All independent variables have expected signs and are consistent across models. Transportation and Inventory Cost have a trade-off with urban population and GDP per capita, are significantly affected by industry share as % to GDP and urban population respectively, and are negatively related to fuel price.

## 1 Introduction

Logistics cost can take up a high percentage in national economy. Reduction of national logistics cost can benefit national economy. Cost information is needed for the cost reduction and can be obtained by national logistics cost measurement and comparison. Because of the trade-off between many components in logistics, not only should the measurement and comparison should be conducted for the whole national logistics cost, but also for the costs of individual logistics components.

According to Bowersox et al. (2005), the national logistics cost measurement is hard to carry for most developing countries, as the rollup summation method which is proposed by Heskett, Glaskowsky and Nicholas in 1973 asks for too much data. Though Bowersox et al. (2005) managed to solve this by using widely available macro economic data like GDP, Population, Territory Area, etc. and cost data from Heskett Method, they only estimated national logistics cost as a whole without cost estimates of individual logistics components and the Artificial Neural Network model they built is a black box for interpretation. Despite the above, the use of macro economic data for cost estimation of individual logistics component on national level looks feasible.

For the countries that can measure national logistics costs using Heskett Method, there are various logistics components they use to report national logistics cost, which reduces comparability of their reports, a set of components for national logistics cost measurement and comparison is needed for unification of components. As cost for each component is a rollup summation of corresponding cost elements, cost elements also affect comparability of components. A review of cost elements in countries is needed.

Rantasila (2013) tried to unify components by categorizing them into 4 categories. However, after application, some categories indicate no expense for some countries which is logically not likely. Also, as the categories have never been used in any of the studies to the best of my knowledge, the results it generates by the categories may not be so referential and suggestive.

Other studies on logistics component and cost element seldom solve problems for cross country comparison.

In the light of the foregoing discussion, there is thus a need to (1) Identify the logistics components for national logistics cost measurement and comparison and review the cost elements in components and (2) Estimate the cost for logistics component on national level using macro economic data.

## 2 Logistics component & cost elements

### 2.1 Logistics components for national logistics cost measurement & comparison

A set of components for national logistics cost measurement and comparison is desired for components unification. To identify the components, a few criteria are identified.

For the measurement, logistics components should cover entire logistics-related costs. As there are trade-offs between components like a lower inventory may be at the cost of more expensive transportation, the measurement of national logistics should cover entire logistics-related costs to achieve global optimization of national logistics cost.

For comparison, first, the most used components should be used. Naturally, these components have highest comparability. Second, there should be a balance between number of components and comparability. Because the more components to keep, the less possible a comparison of national logistics cost is. If the more disaggregated components are used for comparison, one should expect it is more likely some components used in one country should be broken down to be in line with the more disaggregated component. However, in many cases there seem to be no publication of detailed national logistics cost estimation method or proper data sources to make the breakdown possible. In contrast, if more aggregated components are used for comparison, it is easier for countries to add up their disaggregated components to be the aggregated components. But this aggregation makes the comparison less informative about logistics activities, so a level of disaggregation that provides possibly more detail with a reasonable comparability is desirable.

Components that meet the above three criteria are identified as components for national logistics cost measurement and comparison.

Rantasila (2013) identified the times each component is used in national logistics cost studies by literature review. According to the 23 studies about macro logistics cost with well-established model, components are listed from most used to least used.

The total cost concept of logistics developed by Lambert et al. (2006) identified 5 necessary logistics cost groups and basically they all can be included in the top 4 components in Table 1.

The Warehousing and Inventory Carrying Costs are referred to as storage cost and inventory related cost respectively like in Brazil, Finland, while Japan, USA only use Warehousing for both, which makes it hard to

compare. Also as the storage cost and inventory related cost are closely positively related. A combination of Warehousing and Inventory Carrying Costs to be Inventory Cost promotes comparability without reducing the information out of comparison too much.

According to above, components for national logistics cost comparison and measurement are identified to be Transportation, Inventory and Administration. Various logistics components will be adjusted to fit into these three components according to their characteristics.

**Table 1 Most often used components in macro logistics cost studies**

| Component | Count |
|---|---|
| Transportation | 19 |
| Administration | 16 |
| Warehousing | 15 |
| Inventory carrying | 11 |
| Other cost | 6 |
| Transport pack | 5 |
| Customer service | 4 |
| Obselescence | 3 |
| … | … |

## 2.2 Cost elements in components

For the cost reports found, Japan, USA, Korea and South Africa give most details about how the national logistics cost is obtained, and what the cost elements are, so the reports of these countries are reviewed.

Findings are (1) cost coverage of cost elements is similar across countries and (2) differences in cost coverage do exist. (3) It is hard to make sure how different one component is between two countries when how disaggregated the cost elements are is different in the two countries and (4) it is also hard to make sure whether two elements refer to different coverage of costs when they are not disaggregated in the same way.

Discussions are (1) the differences in disaggregation may be a result of data source, so data availability appears to be a decisive factor for the unification of cost elements. (2) Basic comparability of logistics cost exists between the four countries.

# 3 National logistics cost estimation

## 3.1 Cost estimation method

Among the cost estimation techniques in the review of by Niazi, et al. (2006), the Regression Analysis Models are preferred for this study, as it is applicable and allows interpretation of results, which makes possible the use of previous knowledge to examine the results.

## 3.2 Dependent variables and data collection

Previously identified logistics components Transportation, Inventory and Administration for national logistics cost measurement and comparison are intended to be the dependent variables. The data sources are previous studies on national logistics cost.

National logistics costs are measured as absolute value, % to GDP or % to turn over. This study chooses the metrics of logistics cost measured as percentage to GDP, because this term is widely used and comparable between countries. National logistics costs as absolute value are converted to % to GDP by dividing the country's corresponding year's GDP. National logistics costs as % to turnover cannot be converted, because turnover includes intermediate inputs, but GDP only refers to added value, and there is no data on intermediate inputs on national level.

For some countries where there are available cost data for multiple years, 3 years that are not next to each other are picked out to alleviate the bias of using continuous years which may lead to a higher-than-real $R^2$ and significance and also to provide enough degree of freedom for independent variables. Given some independent variables have available data only after 2005, the 3 years are after 2005. Now, 14 Countries with 29 years are considered as suitable data sources for model building.

**Table 2 National logistics cost measured as % to GDP**

| Country | Year | Transportation Costs | Inventory Costs |
|---|---|---|---|
| Indonesia | 2005 | 12.81 | 9.92 |
| | 2008 | 11.04 | 9.64 |
| | 2011 | 11.63 | 8.73 |
| Thailand | 2005 | 8.50 | 8.10 |
| | 2007 | 8.90 | 8.20 |
| | 2010 | 8.70 | 7.60 |
| China | 2005 | 10.20 | 5.80 |
| | 2008 | 10.00 | 5.90 |
| | 2010 | 9.60 | 6.00 |
| Japan | 2005 | 5.30 | 2.70 |
| | 2007 | 5.50 | 3.00 |
| | 2009 | 5.20 | 3.00 |
| USA | 2005 | 5.90 | 3.20 |
| | 2007 | 6.20 | 3.50 |
| | 2009 | 5.00 | 2.60 |
| South Africa | 2005 | 7.69 | 4.01 |
| | 2008 | 7.55 | 4.89 |
| | 2011 | 7.69 | 3.41 |
| Korea | 2005 | 8.90 | 2.00 |
| | 2008 | 8.80 | 2.80 |
| Sweden | 2005 | 2.94 | 3.68 |
| India | 2005 | 6.70 | 0.10 |
| | 2008 | 6.60 | 0.10 |
| | 2011 | 6.60 | 0.10 |
| Netherland | 2007 | 3.34 | 3.46 |
| Finland | 2013 | 3.74 | 6.05 |
| Brazil | 2008 | 6.90 | 4.20 |
| Norway | 2007 | 6.69 | 5.66 |
| Germany | 2014 | 3.83 | 4.16 |

All 14 countries included Transportation Cost, Inventory Cost or/and Warehousing Cost and Administration Cost in their national logistics cost studies. It is just that some countries included more components like Order Processing, Insurance, etc.

These extra components are usually part of Transportation Cost, Inventory Cost or Administration Cost according to both practices in other countries and the total cost concept of logistics developed by Lambert et al. (2006). With easy summation, these extra components can be aggregated with the Transportation Cost, Inventory Cost and Administration Cost making a unified set of components. An example is Norway uses components of Transportation, Warehousing, Cost of capital, Obsoleteness and wastage, Insurance, Packaging, and Administration. For unification, Transportation and Packaging are added up to be Transportation Cost, the Warehousing, Cost of capital, Obsoleteness and wastage, Insurance are added up to be Inventory Cost and Administration remains unchanged.

It is found there is no well-established method for measuring Administration Cost in previous studies. Not like Transportation Cost and Inventory Cost for which the cost elements are added up to measure the cost, the Administration Cost is measured often as a ratio to

Transportation Cost and Inventory Cost, and the decision of the ratio though fully decides the Administration Cost is usually not explained. So the regression model will only be built for Transportation, Inventory.

Inventory Cost data of India is considered as outliers, and taken out. It is too low compared to all the other countries, even when developing countries often have a higher Inventory Cost, and adding Inventory Cost data of India into the model results in a worse $R^2$ and significance. It seems India fails to consider some necessary costs in Inventory.

### 3.3 Independent variables and data collection

Many studies discuss factors about logistics cost on the micro level. The data drivers can hardly find available data for countries. So the studies about macro logistics cost are referred to in the search of possible cost drivers on the national level.

According to Rantasila (2013), all the factors in logistics cost are affective directly or indirectly to all logistics components. So all the possible cost drivers found in literatures will be used for building Transportation Cost and Inventory Cost model. In total 14 independent variables for each model.

DataBank of World Bank is chosen as the data source of independent variables for its wide coverage of items, years and countries as well as the consistence, reliability and comparability of World Bank data. Independent variables use data that are corresponding to the year of dependent variables' data.

**Table 3 Independent variables and data source**

| Variable | Unit | Variable | Unit | Variable | Unit |
|---|---|---|---|---|---|
| **GDP per capita, PPP** | current international $ | **Urban population** | % of population | **Air transport** | million ton-km |
| **Agriculture, value added** | % of GDP | **Individuals using Internet** | % of population | **Container traffic** | TEU |
| **Industry, value added** | % of GDP | **Real interest rate** | % | **Railways** | million ton-km |
| **Services, value added** | % of GDP | **Cost to build a warehouse** | % of income per capita | **Mortality caused by road traffic injury** | per 100,000 people |
| **Trade openness** (Import + Export) | % of GDP | **Pump price for diesel fuel** | US$ per liter | | |

### 3.4 Multicollinearity

Multicollinearity is certainly an issue in regression model building. There are several ways to solve it as reviewed by Dormann et al. (2013). To take out the multicollinear variable is one of the methods and is chosen to be used in this study for its easiness of interpretation of the results.

To use this method, it is necessary to find the cost drivers, so that the multicollinear variables can be taken out. However, as there is no firm ground on what the cost drivers are on national level, all feasible models are to be discussed as a footstone for future studies.

### 3.5 Transportation/Inventory cost linear model

All feasible models are with high $R^2$ and adjusted $R^2$ and all significant independent variables at 0.01 level. Coefficients in models are consistent and can be properly interpreted.

It should be noted that though Urban Population (% of Total) shows a positive sign in Transportation Cost, which may be a result of more transportation activities in cities, it has a negative sign in Inventory Cost, which may be because of more aggregated demands that are cheaper for inventory to server in cities. The above indicates a trade-off between Transportation Cost and Inventory Cost with Urban Population (% of Total). The sum of Urban Population's coefficients in Transportation and Inventory Cost is negative, which means higher urbanization lowers national logistics cost. This is in line with previous studies, though they only discuss the total effect without knowing the individual effect on Inventory and Transportation Cost.

**Table 4 Transportation cost linear models**

Dependent variable: Transportation cost as % to GDP, ** Significant at 0.01, * Significant at 0.05

| Term | Unit | Coef | SE Coef | T-Value |
|---|---|---|---|---|
| Constant | | -2.79 | 1.22 | -2.29* |
| Industry, value added | % of GDP | 0.2631 | 0.022 | 11.94** |
| Air transport, freight | million ton-km | 0.000157 | 0.00003 | 5.17** |
| Railways, goods transported | million ton-km | -0.000001 | 0.00000 | -3.51** |
| Individuals using Internet | % of population | -0.06462 | 0.009 | -7.18** |
| Urban population | % of population | 0.0554 | 0.0156 | 3.56** |
| **$R^2$ = 92.71%, $R^2$(adj) = 91.13%** | | | | |

| Term | Unit | Coef | SE Coef | T-Value |
|---|---|---|---|---|
| Constant | | 0.6 | 1.07 | 0.56 |
| Industry, value added | % of GDP | 0.2364 | 0.0265 | 8.94** |
| Air transport, freight | million ton-km | 0.000192 | 0.000039 | 4.94** |
| Railways, goods transported | million ton-km | -0.000001 | 0.00000 | -3.54** |
| GDP per capita, PPP | current international $ | -0.000084 | 0.000014 | -5.82** |
| **$R^2$ = 88.46%, $R^2$(adj) = 86.54%** | | | | |

| Term | Unit | Coef | SE Coef | T-Value |
|---|---|---|---|---|
| Constant | | 3.11 | 1.19 | 2.62* |
| Industry, value added | % of GDP | 0.1995 | 0.0255 | 7.83** |
| Pump price for diesel fuel | US$ per liter | -2.519 | 0.54 | -4.67** |
| **$R^2$ = 82.76%, $R^2$(adj) = 81.44%** | | | | |

**Table 5 Inventory cost linear models**

Dependent variable: Inventory cost as % to GDP, ** Significant at 0.01, * Significant at 0.05

| Term | Unit | Coef | SE Coef | T-Value |
|---|---|---|---|---|
| Constant | | 5.59 | 1.47 | 3.79** |
| Urban population | % of total population | -0.063 | 0.0186 | -3.39** |
| Agriculture, value added | % of GDP | 0.4315 | 0.0689 | 6.26** |
| GDP per capita, PPP | current international $ | 0.000075 | 0.000017 | 4.42** |
| Railways, goods transported | million ton-km | -0.000001 | 0.0000 | -3.98** |
| **$R^2$ = 90.85%, $R^2$(adj) = 88.79%** | | | | |

| Term | Unit | Coef | SE Coef | T-Value |
|---|---|---|---|---|
| Constant | | 12.72 | 1.87 | 6.79** |
| Urban population | % of population | -0.0989 | 0.0197 | -5.01** |
| Agriculture, value added | % of GDP | 0.3441 | 0.0605 | 5.69** |
| Mortality caused by road traffic injury | per 100,000 people | -0.1208 | 0.023 | -5.26** |
| Container port traffic | TEU | -0.0000 | 0.0000 | -3.72** |
| Cost to build a warehouse | % of income per capita | -0.1444 | 0.0387 | -3.74** |
| **$R^2$ = 94.28%, $R^2$(adj) = 92.85%** | | | | |

GDP per capita also has the similar case as Urban Population. It has negative sign on Transportation Cost, which seems to owe to more efficient transportation realized by better infrastructure and facility when GDP per capita is high. GDP per capita has positive sign on Inventory Cost, which can be because of high percentage of labor cost in inventory cost when GDP per capita is high. The above indicates a trade-off between Transportation Cost and Inventory Cost with GDP per capita. The sum of the coefficients shows a higher GDP per capita reduces national logistics cost, which agrees with previous study, though they did not go into this detail. Of course, full view of the effects on logistics cost should come after inclusion of Administration Cost, but till now, it is a good sign.

Fuel price is found negatively correlated to Transportation Cost. This can be explained, as it was found with the increase in fuel price, there can be more

decrease in fuel consumption of transportation than transportation activities, which means a more efficient transportation that generates GDP with less cost.

### 3.6 Transportation/Inventory cost linear-log model

The linear models measure whether one factor explains the dependent variable, but it does not measure how strong the explanatory power is, because all the factors are having different units. Linear-log model and log-log model can measure how strong the power is because they measure the effect of 1% change in independent variables. This study uses linear-log model to measure the explanatory power as the log-log model is found to have too different independent variables from the linear models. In this study, linear-log models can tell us how strong explanatory power the variables have, and linear models add confidence to the results when the significance and signs of variables are in line with linear-log models, which can also be referred to as being consistent.

**Table 6 Transportation cost linear-log models**

Dependent variable: Transportation cost as % to GDP, ** Significant at 0.01, * Significant at 0.05

| Term | Unit | Coef | SE Coef | T-Value |
|---|---|---|---|---|
| Constant | | -14.53 | 3.11 | -4.68 |
| Industry, value added | % of GDP | 6.204 | 0.893 | 6.95** |
| Pump price for diesel fuel | US$ per liter | -2.292 | 0.47 | -4.87** |
| **$R^2$ = 81.53%, $R^2$(adj) = 80.11%** | | | | |
| **Term** | **Unit** | **Coef** | **SE Coef** | **T-Value** |
| Constant | | -35.11 | 5.73 | -6.13** |
| Industry, value added | % of GDP | 7.35 | 0.868 | 8.47** |
| Urban population | % of population | 3.83 | 1.05 | 3.64** |
| Air transport, freight | million ton-km | 0.28 | 0.113 | 2.48* |
| Individuals using the Internet | % of population | -1.228 | 0.356 | -3.45** |
| Mortality caused by road traffic injury | per 100,000 people | 1.167 | 0.398 | 2.93** |
| **$R^2$ = 87.81%, $R^2$(adj) = 85.16%** | | | | |
| **Term** | **Unit** | **Coef** | **SE Coef** | **T-Value** |
| Constant | | -17.79 | 2.74 | -6.5** |
| Industry, value added | % of GDP | 7.609 | 0.975 | 7.8** |
| Mortality caused by road traffic injury | per 100,000 people | 1.392 | 0.315 | 4.41** |
| Trade openness | % of GDP | -1.255 | 0.433 | -2.9** |
| **$R^2$ = 84.39%, $R^2$(adj) = 82.52%** | | | | |

**Table 7 Inventory cost linear-log models**

Dependent variable: Inventory cost as % to GDP, ** Significant at 0.01, * Significant at 0.05

| Term | Unit | Coef | SE Coef | T-Value |
|---|---|---|---|---|
| Constant | | 52.44 | 5.74 | 9.13** |
| Urban population | % of population | -10.34 | 1.18 | -8.8** |
| Mortality caused by road traffic injury | per 100,000 people | -2.051 | 0.442 | -4.64** |
| Real interest rate | % | 0.91 | 0.264 | 3.45** |
| **$R^2$ = 84.68%, $R^2$(adj) = 82.13%** | | | | |
| **Term** | **Unit** | **Coef** | **SE Coef** | **T-Value** |
| Constant | | 28.6 | 4.66 | 6.13** |
| Urban population | % of population | -3.657 | 0.941 | -3.89** |
| Mortality caused by road traffic injury | per 100,000 people | -1.659 | 0.262 | -6.32** |
| Cost to build a warehouse | % of income per capita | -0.281 | 0.101 | -2.78* |
| Container port traffic | TEU | -0.3649 | 0.0954 | -3.82** |
| Agriculture, value added | % of GDP | 1.531 | 0.288 | 5.31** |
| Pump price for diesel fuel | US$ per liter | -1.478 | 0.313 | -4.72** |
| **$R^2$ = 94.84%, $R^2$(adj) = 93.21%** | | | | |

All feasible models are with high $R^2$ and adjusted $R^2$ and all significant independent variables at 0.05 level. Most independent variables are the same as those in the linear models. All same variables are consistent in all modes of both kinds and can be properly interpreted.

Transportation Cost is found to have a strong positive correlation on the value added share of industry sector, which can result from more demand of transportation in industry sector. Inventory Cost was found strongly negatively correlated to urban population. Fuel price shows negative relation with Inventory Cost, which may also be because of the more efficient use of fuel like the interpretation in Transportation cost linear model.

## 4 Conclusion

A unified set of logistics components is good for comparison across countries. With three criteria, Transportation, Inventory and Administration are selected to be the components for national logistics cost comparison and measurement.

This guarantees as many countries to do cost comparison as possible which gives countries more reference to evaluate their logistics performance more accurately.

As the costs for components are measured by summing up cost elements, cost elements also affect comparability. A review of cost elements in 4 countries is done. It is found (1) cost coverage of cost elements is similar across countries and (2) differences in cost coverage do exist. (3) It is hard to make sure how different one component is between two countries when how disaggregated the cost elements are is different in the two countries and (4) it is also hard to make sure whether two elements refer to different coverage of costs when they are not disaggregated in the same way.

The lack of data keeps countries from knowing and reducing their national logistics cost. An effort to estimate national logistics cost by components is necessary. Data from previous studies about national logistics cost and macro economic data from World Bank are used to build linear and linear-log models for Transportation Cost and Inventory Cost. With concern of multicollinearity, multiple feasible models are found for discussion. All models can be properly interpreted and are consistent.

Industry share in economy is found to have a trade-off between Transportation Cost and Inventory Cost, as it is positively related to Transportation Cost while negatively to Inventory Cost.

Also a trade-off between Transportation and Inventory Cost is found on urbanization. Urban population as % to total has negative relation with Inventory Cost and positive relation with Transportation.

Fuel price is found to be negatively correlated with Transportation and Inventory Cost.

Industry share as % to GDP is found to have strong positive correlation with Transportation Cost while urban population as % to total has strong negative correlation with Inventory Cost.

Limitation for this study is national logistics cost data are not enough for the models to extrapolate to countries that cannot measure their logistics costs.

## Reference


1 Rantasila (2013). Measuring logistics costs-designing a generic model for assessing macro logistics costs in a global context with empirical evidence from the manufacturing and trading industries.

2 Bowersox, D. – Rodrigues, A. – Calantone, R. (2005) Estimation of Global and National Logistics Expenditures: 2002 Data Update. Journal of Business Logistics, Vol. 26 (2), 1–16.

3 Lambert, D. – Grant, D. – Stock, J. – Ellram, L. (2006) Fundamentals of Logistics Management. European edition. McGraw-Hill, Maidenhead, Berkshire, UK.

4 Niazi, A., Dai, J. S., Balabani, S., & Seneviratne, L. (2006). Product cost estimation: Technique classification and methodology review. Journal of manufacturing science and engineering, 128(2), 563-575.

5 Dormann, C. F., Elith, J., Bacher, S., Buchmann, C., Carl, G., Carré, G. & Münkemüller, T. (2013). Collinearity: a review of methods to deal with it and a simulation study evaluating their performance. Ecography, 36(1), 27-46.

# PASSENGER'S AIRPORT AND AIRLINE CHOICE IN A MULTIPLE AIRPORT REGION: THE CASE OF GREATER JAKARTA

Student Number: 15M51785 Name: Fajar Fauzie RAKHMAN Supervisor: Shinya HANAOKA

Presently, passengers in Greater Jakarta are having varied flight options due to two airports, Soekarno-Hatta and Halim Perdanakusuma, operated in a multiple airport region together with service that offered by two major airlines, Garuda and Lion group, performed in the both airports. This study aims to estimate choice of passenger in the same region by investigating significant factors of airport and airline choice, including the case when passengers are undertaking departure and arrival flight using multinomial logit model. The investigation, furthermore, resulted that airfare, frequency, access time, and airport queue were identified as significant factors. From segmentation estimation of departure and arrival, it resulted that the differences in access cost, airport queue and number of frequency become major differences.

## 1. INTRODUCTION

Greater Jakarta becomes region with the most numerous air traveler passenger in Indonesia. In 2009, the number of passengers that flew in Jakarta airport reached 37 million and it grown significantly to 56 million passengers five years later by 51%. Initially, Greater Jakarta operated solely one main airport, called Soekarno-Hatta International Airport as main hub of all airlines in Indonesia. With the high number of passengers using Soekarno-Hatta airport, however, the condition exceeded more than double from the airport proper capacity and lead to congestion problem. To confront the situation, another existing airport which located in city center of Jakarta, Halim Perdanakusuma airport, a smaller airport located near city center which previously used for military airport. Along with that, major airline groups in Indonesia, Garuda and Lion group operated in both airports and served several dense routes for the passenger through their full-service and low-cost carrier, Garuda Indonesia and Citilink for Garuda group; Batik Air and Lion Air for Lion group. The situation, therefore, leads passenger to choose airport and airline which give them better utility as their flight point compared to the other alternative provided.


**Figure 1 Location of airport in the Greater Jakarta**

Since passengers in Greater Jakarta are provided with two airports and several airlines which operated in both airports, this study aims to estimate choice of passenger's in the same region by investigating significant factors of airport and airline choice in the case of departure and arrival when undertaking a flight. The inventive investigation is being examined in this study by comparing significant factors in an opposing scenario between departure and arrival activity as part of the choice model. The prospective result is expected to give Indonesia's air transportation stakeholder insight about airport and airline choice model, for instance for the government whether Halim airport is still need to be opened as contingency action after congestion in Soekarno-Hatta..

Competition between Soekarno-Hatta and Halim airport and also the airline that operated in both airports occurred quite intense. For instance, Surabaya and Solo as one of the competitive route due to high frequency and competitive capacity production in both airports. From the graphic below we could see that from full-service airlines to low-cost carrier operated with average variation fare that can cover all segmentation of passenger.

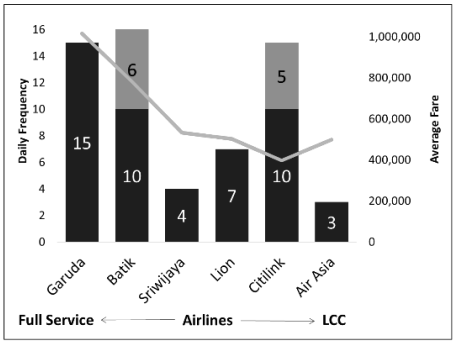


**Daily Frequency and Fare to Surabaya**

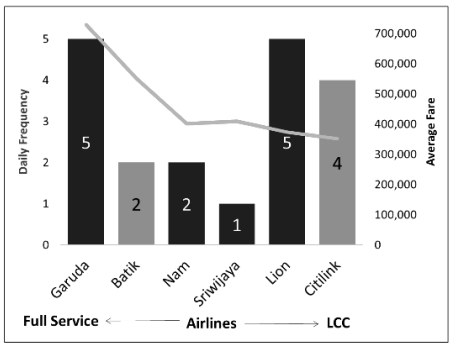


**Daily Frequency and Fare to Solo**


**Figure 2 Flight schedule between Jakarta and other cities**

The discrete choice model is a group of procedures that explains decision maker, alternatives, attributes, and decision rule. In general, consumer decision will be derived by choosing an option which has greater utility function compared to the other alternative. In this research, we analyzed about which airport and airline that will be chosen by passenger in Greater Jakarta.

Loo (2008) investigated passenger choice in the multi-airport region in Hong-Kong with stated preference method and analyzed by multinomial logit model. The result showed that airfare, access time, flight frequency, and the number of airlines operated as significant factors as the most important level-of-service attributes. Jiang-tao (2008) used multinomial logit model as a method to focus on the prediction of airport choice in a multiple-airport region and estimation using passenger data in Chinese metropolitan area. For the airline choice, Hess and Polak (2005) conducted airport, airline, and access mode choice in the San Francisco Bay area with the main discussion of passenger choice was simultaneously determined in that area with airfare and aircraft size become attractiveness attributes as significant factors. Hopefully, this research also can add another insight towards airport airline choice model that has been conducted previously.

## 2. METHODOLOGY

For this research, the survey to airport passengers was conducted during 8th to 17th March 2017 in Jakarta's airports, Soekarno-Hatta and Halim Perdanakusuma, which can covers all segmentation of passengers in Indonesia domestic market. It obtained total 671 answers from respondents of both airports, with specification 317 respondents from Soekarno-Hatta airport and 354 answers from Halim airport. There are two major purposes of the passenger from survey obtained, with 56% traveled for business purpose, and 44% went for non-business purposes such as holiday or leisure, visit relatives or friends, and going back to their hometown. Since the survey used the stratified method, the survey divided by respondents from several major airlines which dominate in Indonesia aviation and belong to the major competitive group, Garuda Indonesia and Citilink from Garuda Group, and Lion Air and Batik Air from Lion Group.

Variables that generated during the survey is mostly represented important and significant factors that affect passenger decision in choosing the flight. Since this research used four alternatives of choice for passenger which combination of airport and airline choice called; Soekarno-Hatta – Garuda Group, Soekarno-Hatta – Lion Group, Halim – Garuda Group, and Halim – Lion Group, therefore, the model estimation that built in this research was established by using multinomial logit model. Airport attributes consist of airport access time, airport access cost, and airport queue. On the contrary, airline attributes consist with airfare, delay probability, airline service (dummy), and daily frequency which can be seen the detail in the table below as follow:

**Table 1 Alternative and attribute setting for model estimation**

| Attribute | Description | Parameter | Data Source |
|---|---|---|---|
| Airline fare | Ticket price | Indonesia Rupiah (IDR) | Respondent data |
| Delay probability | Airline on time performance (OTP) | % | Airline OTP report |
| Airline service (dummy) | Airline type of service | Full service (1), LCC (0) – dummy | |
| Access time | Travel time to airport | Hour | Respondent data |
| Access cost | Travel cost to airport | Indonesia Rupiah (IDR) | Respondent data |
| Airport queue | Queuing time (check-in or baggage delivery) | Minutes | Respondent data |

According to economic theory, consumer or passenger will choose alternative that has greater utility function; where $U$ is utility function; $i$ is alternative; $\beta$ is parameter to be measure; $X$ is attribute explained; $\varepsilon$ is the disturbance term.

$$U_i = \beta_0 + \beta_1 X_1 + \beta_2 X_2 + \cdots + \beta_n X_n + \varepsilon = \sum_n \beta_n X_n + \varepsilon \quad (1)$$

Logistic regression or logit model is one of the most popular practical methods to analyze passenger choice by assuming the choice of probabilities among alternative provided; where $P$ is probability of passenger choice; $i$ is alternative provided; $U_i$ is utility function; $k$ is choice alternative.

$$P_i = \frac{\exp(U_i)}{\sum_k \exp(U_i)} \quad (2)$$

This study exercised logistic regression to conducted significant factors that determined passenger preference in for airport and airline choice. To conduct whether passenger decision is determined by airport or airline attribute, the level nested model conducted to solve the problem.

## 3. RESULTS

### 3.1. Survey Results

Passenger background was examined to know characteristic of passenger in both airports. The majority of respondent dominated by an active production age between 26 to 55 years old. From the survey, Most of them are employee from public and private institution in Indonesia, where the higher income (>20 million IDR) tend to choose Halim rather than Soekarno-Hatta airport. For Garuda passenger, it distributed in low-income (1-3.9 million IDR) and high income (10-19.9 million IDR), while Lion passenger spread in medium income (3-9.9 million IDR).

It revealed that passengers in Halim airport are more familiar to fly from both airports, while passengers in Soekarno-Hatta airport was not familiar fly as passenger in Halim airport. It shows that only 39% of passenger of

Soekarno-Hatta had ever flew from Halim airports. However, almost all respondents from Soekarno-Hatta airport already know if Halim airport now operated again in Jakarta, as 90% of respondent knowing that currently there are two airports carried on in Jakarta.

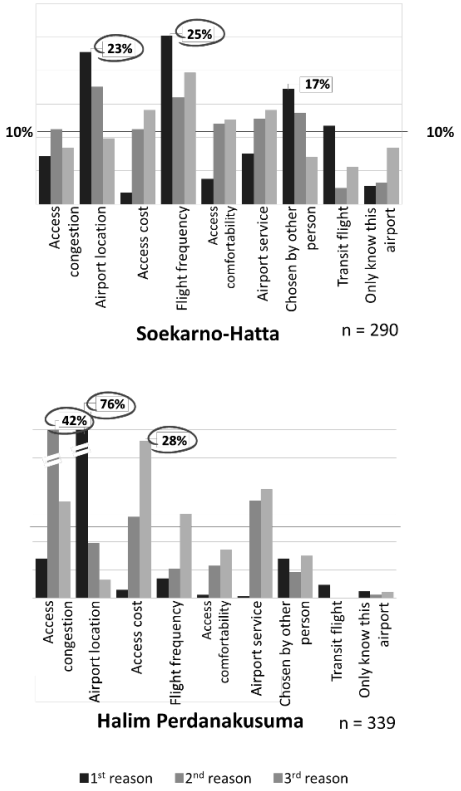


**Figure 3 Reason to choose airport**

For respondents who chose Soekarno-Hatta airport, flight frequency and airport location become important reasons why they choose the airport. It is known that since Soekarno-Hatta capacity is larger compared to Halim, the airport offers more schedule frequency rather than Halim. Therefore, passengers who are sensitive to schedule time, especially the frequency of flights tends to choose Soekarno-Hatta rather than Halim airport. Halim passengers revealed that airport location, access congestion, and access cost to the airport became important reasons for the passenger in Halim to choose the airport. Because of Soekarno-Hatta airport is 27 km away from business district center and located in west part of Jakarta, while Halim airport located 12 km in the east, the location of the airport can be one of advantage to be chosen by respondent.

We analyzed segmentation between departure and arrival passenger and asked them reasons to choose airport and airline in Greater Jakarta. It revealed that, there are no significant different factors between departure and arrival passengers when choose the airport. For the airline choice, departure and arrival passengers valued airfare ticket, fit-in schedule as significant factors, and good service and good safety become the difference factors between both of them.

All in all, from preference survey that had been conducted in both airports, the passenger in Soekarno-Hatta choose their flight because of airline factor and Halim passenger chooses their flight because of airport factor. It revealed that greater schedule that leads airline to offer more frequency of flight create Soekarno-Hatta Airport advantage point to attract the passengers. Moreover, for passengers who are sensitive to level of service and not too considered ticket price, such as Garuda Indonesia passengers, choose the airport Soekarno-Hatta Airport since the airline only operates at this particular airport. On the contrary, Halim airport is very reliable with its location as the main attraction of passenger to choose the airport to reduce access time and access cost to the airport.

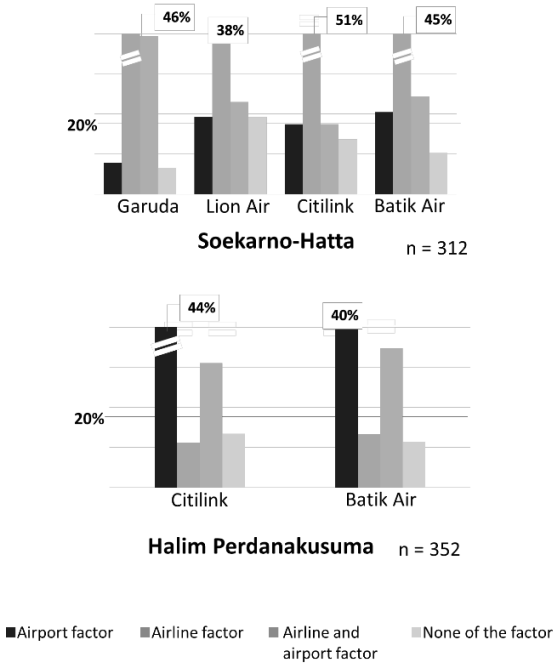


**Figure 4 Reason to choose flight**

## 3.2. Model Estimation

Endogenous data sampling method used in this research to follow actual condition of Indonesia's air transportation and minimize bias of the result. Soekarno-Hatta passenger picked more than Halim passenger to follow actual condition based on current capacity production in each airport. Number of Lion group passengers are greater than Garuda group's passenger according to current market share of seats in Indonesia's domestic market. Furthermore, respondents who don't know their airfare and two airports operated in Jakarta are excluded in the model estimation. Several attributes introduced to be estimated in the model including both alternative factors namely; airline service (ALSVC), airport cost (APCOST), airport queue (APQUEUE), airport access time (APTIME), airline fare (FARE), and airline number of frequency (FREQ). Alternative specific constant (ASC) was observed and estimated in the model to represent the utility of respondent that is not captured by introduced attributes but well known as respondents consideration. Total number of observations is calculated based on market share seats capacity of airline in Indonesia

domestic market.

In the full model estimation, airport queue (value = -10.3) and airport access time (value = -0.982) have negative utility value which explains that respondents in Greater Jakarta are happier with shorter time to access the airport, quicker check-in queuing time before boarding to the aircraft, and faster baggage delivery after they landed in destination airport. Airline fare (value = -3.40) and airport access cost (value = -2.85) also show negative estimation, indicate that passenger valued lower ticket price and total trip cost to or from the airport. On the contrary, airline service (value = 0.890) and the number of frequency (value = 1.44) have positive utility value which means that passenger in Greater Jakarta is the more valued full-service carrier in choosing an airline and greater number of frequency to be picked as their flight choice. In this model estimation, airport queue (p-value = 0.00), airline fare (p-value = 0.00), and number of frequency (p-value = 0.00), and airport access time (p-value = 0.01) were identified as significant factors at level of 5%.

**Table 2 Multinomial logit (full model estimation)**

| Name | Unit | Value | Std err | t-value |
|---|---|---|---|---|
| ASC_CGKGA | | 0.00 | Fixed | |
| ASC_CGKLION | | 0.0605 | 0.546 | 0.11 |
| ASC_HLPGA | | -1.61 | 0.672 | -2.39** |
| ASC_HLPLION | | -0.565 | 0.546 | -1.03 |
| b_ALSVC | FSNC (1)/ LCC (0) | 0.890 | 0.647 | 1.38 |
| b_APCOST | IDR | -2.85 | 5.09 | -0.56 |
| b_APQUEUE | Minutes | -10.3 | 1.10 | -9.34** |
| b_APTIME | Hours | -0.982 | 0.390 | -2.52** |
| b_FARE | IDR | -3.40 | 0.772 | -4.40** |
| b_FREQ | Number | 1.44 | 0.490 | 2.94** |
| Number of observations | | | 218 | |
| Adjusted rho square | | | 0.593 | |

** Significance at level 5%, * Significance at level 10%

To conduct deeper investigation, segmentation analysis for departure and arrival passengers was observed. From the result, there are different motives of choice between departure and arrival passenger. Access cost, airport queue, and the number of airline frequency become differentiator factors between both of segmentation. Number of frequency (p-value = 0.01) become significant factor at 5% for departure passenger, but it did not reflect in arrival passenger result (p-value = 0.25). We assume that departure passenger is more valued number of frequency so that they tend to find an alternative which offers them more flight frequencies. Furthermore, access cost become significant factor for departure passenger (p-value = 0.01), while the result did not led to departure passenger (p-value = 0.32), and airport queue is significant for departure passenger with (p-value = 0.02), while for arrival passenger is tend not to be significance with (p-value = 0.49).

**Table 3 Multinomial logit (departure and arrival)**

| Name | Unit | Departure | | Arrival | |
|---|---|---|---|---|---|
| | | Value | t-value | Value | t-value |
| ASC_CGKGA | | 0.00 | | 0.00 | |
| ASC_CGKLION | | -0.267 | -0.42 | -0.593 | -1.22 |
| ASC_HLPGA | | -1.21 | -1.33 | -3.83 | -3.74** |
| ASC_HLPLION | | -1.71 | -2.21** | -5.29 | -5.03** |
| b_ALSVC | FSNC (1)/ LCC (0) | 1.37 | 2.21** | 2.49 | 3.06** |
| b_APCOST | IDR | -22.5 | -2.74** | -9.84 | -0.99 |
| b_APQUEUE | Minutes | -2.61 | -2.29** | -0.896 | -0.69 |
| b_APTIME | Hours | -1.08 | -2.11** | -3.15 | -4.52** |
| b_FARE | IDR | -3.81 | -5.47** | -5.27 | -5.33** |
| b_FREQ | Number | 1.48 | 2.62** | -0.580 | -1.14 |
| Number of observations | | 115 | | 103 | |
| Adjusted rho square | | 0.431 | | 0.439 | |

** Significance at level 5%, * Significance at level 10%

Moreover, a nested logit model, was estimated to observe which factor that majorly considered by the passenger when undertaken a flight. Airline service, airline fare, and the number of frequencies belong to airline nest, and the other; airport cost, airport queue, and airport access time are included in airport nest. After the simulation had been run, however, the program diagnosed that model estimation does not fit because diagnostic of the model resulted that maximum number of iterations reached, which fails to maintain random maximized utility. We assumed that the error caused by the number of samples that observed in the model was not enough to be estimated, thus larger samples required in the future.

## 4. CONCLUSION

From the study, it can be concluded that airport choice in Greater Jakarta is determined by airport location and access congestion for Halim respondent, and for Soekarno-Hatta's passengers, number of frequency and airport location become the main reason in choosing the airport. For the airline choice, good service and good safety become the difference factors between both of them departure and arrival passengers. The choice of Halim airport is based on airport factor and Soekarno-Hatta is based on airline factor. In multinomial logit, full model estimation resulted that airfare, frequency, access time, and airport queue as significant factors and segmentation estimation resulted the differences in access cost, airport queue and number of frequency for passenger when undertaking departure and arrival flight. From nested logit experiment, the result showed that structure doesn't fit this result because radius of the trust region is too small.

**REFERENCES**


[1] Hess, S and Polak, J. W. (2005). Mixed logit modelling of airport choice in multi-airport regions. Journal of Air Transport Management. 11, p59-68.

[2] Jiang-tao, L. (2008). Airport Choice in Multi-airport Regions: An Empirical Study for Chinese Metropolitan Area. *International Conference on Intelligent Computation Technology and Automation*. p329-332.

[3] Loo, B.P.Y.. (2008). Passengers' airport choice within multi-airport regions (MARs): some insights from a stated preference survey at Hong Kong International Airport. *Journal of Transport Geography*. 16 (1), p117-125.

# Operational sustainability of rural electrification program through an effective fee collection strategy: Case study of the Philippines

Student Number: 15M51779 Name: Keshav Raj POKHREL Supervisor: Naoya ABE

Rural electrification in remote areas of developing countries with renewable energy sources has been a major phenomenon for the past few decades. Operational sustainability is a fundamental concern amid the rapid diffusion of renewable energy technologies in the developing countries. This research assessed the present status and problems being faced by the Solar Home System (SHS) users in a rural and remote island of the Philippines. It has been found that more than 90% of the users have already stopped paying their monthly tariff despite the ability and willingness of payment. Observation of the income and expenditure pattern of those users revealed a major strategical difference between the payment for SHS and the payment for other daily basic utilities. This study suggests a fee collection system for electricity on a daily basis rather than on a monthly basis to ensure the operational sustainability of SHS projects.

Keywords: Rural electrification program, Operational sustainability, Fee collection strategy

## 1. Introduction

Rural electrification is a process of electrifying rural and remote households. Renewable energy sources have been playing a vital role to address the energy scarcity problem of the developing countries. Over the past five years, the market for basic solar powered lights and small home systems with multiple lights, and basic appliances have grown rapidly in developing countries, with more than 24 million units sold [1]. Approximately 1.2 billion people are still without access to clean energy in 2016 [2]. Rural electrification plays a significant role in poverty reduction and economic improvement of these people. However, the implemented projects in rural areas are facing financial and technical challenges, which complicates the long-term operation of these systems. The story does not end with installation of new technologies, and thus operational sustainability has been a major concern.

The major problems faced in the operation of rural electrification programs in developing countries are related to financial ones, such as: (a) users' inability to pay the usage fee because of unaffordability, (b) users' unwillingness to pay the usage fee which might result from low satisfaction with the electricity provision or unfeasible payment strategy, and (c) budget deficiency for maintenance of the project due to stoppage of subsidy from national and international entities and lack of collected tariff [3,4]. Williams et al. and Hong and Abe also highlighted the negative impacts of poor payment morality and budget deficiency, which challenges the sustainability of rural electrification projects [5,6].

This research is a field survey based study. First, literature review was conducted to identify the prospects of off-grid electrification in developing countries and to explore the existing challenges. A field visit was made to the study area to find out the obstacles faced by the program through interviews and questionnaire surveys. Data analysis was performed with the collected primary and secondary data. At last, an effective solution is proposed that would help to ensure the operational sustainability of rural electrification program in the study area.

## 2. Objectives and Significance

### 2.1 Research Question

Why do rural electrification programs face budget deficiency?

### 2.2 Objectives

1. To investigate the present status and the problems in a case of rural electrification program
2. To analyze the income pattern and the expenditure pattern of users for basic daily utilities
3. To propose an effective fee collection strategy that ensures the operational sustainability

### 2.3 Significance

By analyzing a real case scenario, this study proposes an effective strategy to address the underlying problems for sustainable operation. It aims to contribute to the national and international bodies to make rural electrification program more robust and sustainable. Moreover, this study will support the researchers and academicians working on sustainability of renewable energy projects by shedding a light on the practical aspects of sustainable development.

## 3. Study Area

The study area is "Alumar Island", which is a small rural island located at 3-hrs boat ride from Cebu Island, Philippines. It has a population of about 1160 (228 households) with fishing, seaweed and stores as major occupations. In 2008, the Philippine Department of Energy (DOE) in partnership with Japan International Cooperation Agency (JICA) provided solar home systems (SHS) to 50 households of this island [7]. This project was under the Philippine government's program titled as "Sustainability Improvement of Renewable Energy Development in Village Electrification". Each of the 50 households were provided with a complete SHS that is composed of solar panel (50-75 Wp), a charge controller, a lead-acid battery, and a few lightning bulbs. Users paid 1,500 pesos as an initial fee to receive the system. Barangay Alumar Power Association (BAPA) was established as an electric cooperative responsible for monitoring and maintenance of the solar units. Each household is required to pay 200 pesos as a monthly tariff, which is used as savings for the replacement of damaged battery, panel or controller and an honorarium for fee collector and technicians.(1$= 50 pesos)

## 4. Methodology

### 4.1 Case Investigation

Interviews were conducted with the electric cooperative BAPA to understand the overall scenario of the project and to find out the problems that challenges the sustainability of the program. The interview revealed the existence of

poor payment morality among the SHS users. Because of this, BAPA was undergoing a serious financial crisis and could not respond to users' request for the replacement of the batteries and other support.

### 4.2 Data Collection

Face-to-face interviews were made with 48 users of SHS of Alumar island using questionnaire survey to obtain the primary data of the categories as mentioned in Table 1.

Table 1: Variables of data collection.

| Category | Details |
|---|---|
| Present Status of SHS | Components of SHS, Appliances being operated, Record of repair or replacement |
| Training and Maintenance | Things learnt during training program, Types of maintenance services, Satisfaction levels |
| Additional Sources of Energy | Types of additional sources of energy being used, Expenses for them |
| Satisfaction levels with SHS | Capacity of SHS, Availability of electricity, Monthly tariff |
| Personal Information | Gender, Age, Occupation, Education, Income, Number of family members |
| Income and expenditure pattern | Sources of income, Methods of earnings, Expenses for other basic utilities, Methods of expenditure |
| Priorities Ranking | Rank the priorities among the basic needs |
| Miscellaneous | Renewable Energy Knowledge, Willingness to pay (WTP) |

### 4.3 Data Analysis

#### 4.3.1 Descriptive Analysis

The descriptive analysis was performed on the demographic data of the users like gender, education, age, income level and satisfaction ratings of the users to understand the proportions of users in different categories and to understand the percentage of users who were satisfied or not satisfied with the current SHS.

#### 4.3.2 Chi-square Test of Independence

It is used to determine a significant association between the two categorical variables. In this study, the price satisfaction data is used as Variable A with two categories (Satisfied and Not Satisfied) and 13 other categorical variables as Variable $B_m$ (m = 1,2,……,13). This test is used to identify the association of price satisfaction with other users' responses and attributes.

At first, a contingency table is created using Variable A and Variable $B_1$. The expected value for each cell of the contingency table is calculated using eq. 1. Using eq. 2 and eq. 3, the Chi-square value ($\chi^2$) for the table is calculated. Using this $\chi^2$ value and degrees of freedom (df) (eq. 4), p-value is obtained from Chi-square table of significances.

$$E_{AB1} = \frac{M_R * M_C}{N} \quad \text{(eq. 1)}$$

Where:
$E_{AB1}$ = Expected value of that particular cell
$M_R$ = Sum of row values for that cell
$M_C$ = Sum of column values for that cell
N = Total sample size

$$\chi^2_{AB1} = \frac{(O_{AB1} - E_{AB1})^2}{E_{AB1}} \quad \text{(eq. 2)}$$

$$\chi^2 = \sum_{B1=1}^{C} \sum_{A=1}^{R} \chi^2_{AB1} \quad \text{(eq. 3)}$$

df = (Number of rows - 1) * (Number of columns - 1) (eq. 4)

Where:
$O_{AB1}$ = Observed value (actual value)
$\chi^2_{AB1}$= Chi-square value of each cell
$\chi^2$= Sum of Chi-square values of all cells
If the p-value of the table is less than 0.05 (significance level), it indicates that there is a significant association between the two categorical variables.

#### 4.3.3 Cluster Analysis

This study uses cluster analysis, an exploratory data-analysis technique, to classify the SHS users' data into various clusters in order to obtain the similarities and dissimilarities of responses among the users. This study uses hierarchical agglomerative method in which the algorithm joins together similar observations one level at a time until all observations are categorized as one group.

Similarity and dissimilarity is a term to depict the distance measure among groups whose criterion is termed as linkage method. There are three major linkage methods to join the observations: single-linkage (closest pair between two clusters), complete-linkage (farthest pair), and average-linkage (average distance between all data points). This study adopted complete linkage method in which the distance between the farthest pair of observations in two clusters is measured and the two clusters that have the smallest complete linkage distance are combined.

The output of the analysis gives a cluster dendrogram which shows the tree of clusters formed. In this study, 4 different clusters were considered and peculiar characteristics of the users in each cluster were analyzed.

#### 4.3.4 Income and Expenditure Distribution

Since the major occupations of people in Alumar island were fishing, collecting shells, owning a store, the income depended on the factors such as number of working days, amount of catch of fish, types of fish, market price of the day etc. Thus, the residents responded their monthly income in intervals like less than 3k pesos, 3k-6k pesos, 6k-9k pesos and so on. Using this data, the mean and standard deviation of the income were calculated. Lognormal distribution was used to make a good approximation of income distribution for daily and monthly pattern taking reference from [8]. For the expenditure pattern, 2 major studies were taken as references. Secondary data were mostly used for this analysis, household final consumption expenditure data from Philippines Statistics Authority and expenditure pattern for poor households in Metro Manila of Philippines from [9]. Adjustments were made according to the scenario directly observed in Alumar island and an expenditure distribution was created.

### 4.4 Solution Proposal Criteria

An effective solution to the existing problem of non-payment has been proposed. Here "effective" is defined in terms of 3 criteria:

a) **Affordable:** The amount of tariff must be less than users' WTP for electricity which in turn should be a realistic response in comparison with their income amount.
b) **Feasible:** The payment method for electricity should be compatible with users' expenditure strategy for other basic utilities

c) **Sustainable:** The collected tariff should provide enough revenue for BAPA to replace the damaged batteries, panels or controllers and provide an honorarium to fee collectors and technicians.

# 5. Analysis and Discussion

## 5.1 Descriptive Analysis

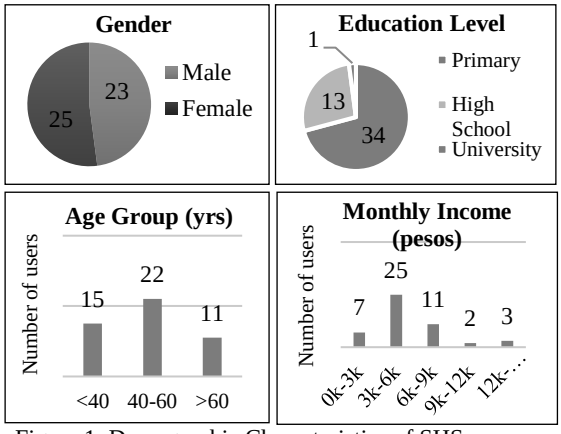


Figure 1: Demographic Characteristics of SHS users.

Figure 1 reflects the basic demographic characteristics of SHS users in Alumar island. Alumar, being a rural and remote island, most of the users' education level was primary and monthly income was quite lower (mostly in the 3k-9k range) than national average (22k pesos/household).

Approximately 90% of the users have already stopped their monthly payment of 200 pesos for more than a year. The general assumption is that users were either dissatisfied with the electricity provision or price or services from BAPA. The satisfaction rating from Figure 2 shows that users were quite satisfied with all the services they were receiving from BAPA (maintenance and trainings) and with the solar home system itself (capacity and availability of electricity). However, half of the users were not satisfied with the price. To understand the reasons behind this price satisfaction/dissatisfaction, chi-square test was performed.

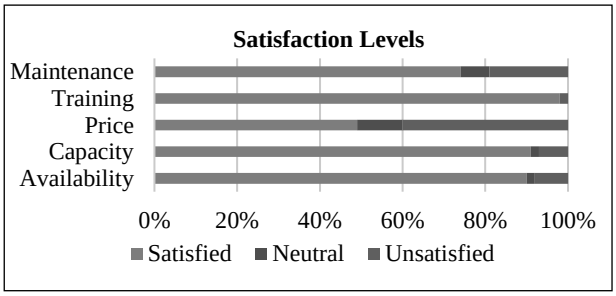


Figure 2: Satisfaction Levels of SHS users.

## 5.2 Chi-square Test of Independence

Chi-square test was performed using price satisfaction as variable A and all other 13 variables mentioned in Table 2 below as variable $B_m$ (m ranges from 1,2,…., 13). It reveals that price satisfaction has no dependency on monthly income, demographics, electricity provision and services from BAPA. Users having renewable knowledge and higher WTP were found to be satisfied with the price. To understand the spread of WTP data among the users (measured by stated preference open ended WTP method) and find the similarities and dissimilarities by classifying them as groups, cluster analysis was performed next.

Table 2: p-values for association with Price Satisfaction.

| Variables ($B_m$) | p-value | Variables ($B_m$) | p-value |
|---|---|---|---|
| Availability | 0.2 | Family Size | 0.26 |
| Capacity | 0.2 | Keep Solar | 0.11 |
| Maintenance | 0.94 | Knowledge | 0.04* |
| Training | 0.43 | Available Hours | 0.07 |
| Gender | 0.08 | WTP | 0.01* |
| Age | 0.17 | Income | 0.17 |
| Education | 0.34 | * means significant at 0.05 level | |

## 5.3 Cluster Analysis

Four clusters were selected from 25 users for the observation. Table 3 summarizes the major properties of each cluster. Users were making significant payment for alternative fuels and their WTP for electricity was significantly high in each group despite having low price satisfaction. The average WTP was 334 pesos while only 10 users responded less than 200 pesos. Thus, amount of tariff being expensive was not a problem. However, users were not making payment for SHS. To explore the reasons behind this, income and expenditure pattern were analyzed.

Table 3: Average data of 4 clusters.

| Factor | Group 1 | Group 2 | Group 3 | Group 4 |
|---|---|---|---|---|
| **Number** | 9 | 9 | 1 | 6 |
| **Age (yrs)** | 53 | 39 | 35 | 47 |
| **Price Satisfaction** | 3 | 3.7 | 2 | 1.8 |
| **Alternative fuels payment(pesos)** | 138 | 590 | 200 | 132 |
| **WTP (pesos)** | 192 | 578 | 1200 | 258 |
| **Available hours** | 4 | 4 | 3 | 1 |

## 5.4 Income and Expenditure Distribution

The earnings from fishing, seashell collections and stores is on a daily basis and is uncertain and vulnerable to many factors. The average number of working days for a fisherman varied from 18 to 22 days with daily income ranging from 200 to 400 pesos (Figure 4). With the calculated mean and the standard deviation of the monthly income as 5,600 pesos and 3,000 pesos respectively, a lognormal distribution of monthly income has been generated using exponential of normal distribution function in EXCEL software and is shown in Figure 3. The income varies each day and each month for all households.

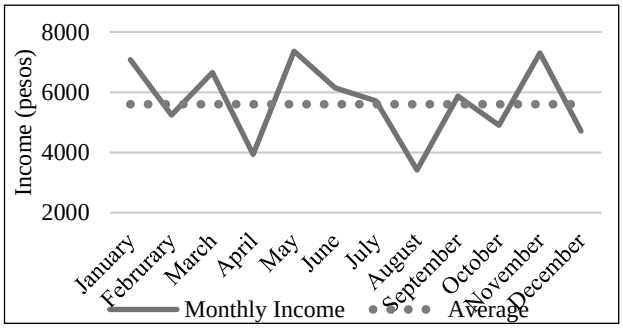


Figure 3: Monthly income distribution pattern

The expenses for the daily basic utilities close to 200 pesos are summarized in Table 4. With the data available for clean water and fuels expenses as shown in Table 5, expenditure pattern for these utilities were analyzed. For clean water, an average household consumed 6-7 containers per month. However, they bought only 1-2 containers at once. Water stands were visible where people could buy 300 ml of drinking water with 1 peso. For

telecommunications, people were using re-loader from 5 pesos despite having recharge cards of 100/200/500 pesos. For alternative fuels like diesel, kerosene, they were buying 1-2 liters at once even though they consumed in higher quantities when accumulated together for a month (Table 5). Thus, people were habitual in making payments on a unit-by-unit pattern.

Table 4: Expenditure amount (pesos)

| Item | Expenses |
|---|---|
| Electricity | 200 |
| Clean Water | 240 |
| Other Fuel Sources | 210 |
| Health | 151 |
| Education | 221 |
| Housing | 194 |
| Clothing and Personal Care | 237 |
| Recreation and Culture | 151 |

Source: [9], Philippines Statistics Authority and modified by author for the scenario of Alumar.

Table 5: Expenses pattern for water and fuels

| Type | Quantity | Price /unit |
|---|---|---|
| Clean water | 6 containers | 40 pesos |
| Water stand | 300 ml | 1 peso |
| Diesel | 4-5 liters | 30 pesos |
| Flashlights | 3-4 batteries | 10 pesos |
| Butane | 3-4 containers | 14 pesos |

Source: Interviews and household surveys

### 5.5 Proposal of Solution

A fee collection strategy of 10 pesos on a daily basis rather than 200 pesos on a monthly basis is proposed as an affordable, feasible and sustainable solution to payment morality problem in the scenario of Alumar island as explained below:

a) **Affordable**: The average WTP was 334 pesos (>200 pesos) and SHS users' income amount also represents the validity of these responses. Since the earnings are on a daily basis (Figure 4) and low income households lack saving habits which is barely 1% of their income [10], 200 pesos at once was not affordable even though 200 pesos per month was affordable. Thus, 10 pesos per day is an affordable option.

b) **Feasible:** Despite having higher WTP, the reasons behind the poor payment morality was the unfeasibility of monthly based payment procedure. As seen from Figure 4, 200 pesos occupies a major portion of their daily income and there are days when the earnings are even lesser than 200 pesos. The expenditure pattern also shows that the residents of Alumar island were making payments in smaller units for their basic necessities like clean water, fuels, recharge cards for cellphones etc. despite the monthly consumption being high. Thus, cooperating with similar strategy, 10 pesos/day is considered a feasible strategy.

c) **Sustainable:** A successful collection of 10 pesos per day will give BAPA 200 pesos a month. From 200 pesos, BAPA is depositing 86 pesos for the replacement of defective batteries, 87 pesos for the replacement of either panel or controller and the remaining as payment for fee collector and technicians. Daily basis collection will increase the operation cost because of addition of fee collectors. However, centralized deposits such as collection in teashops and school can be introduced to make the collection cost effective and to sustain the activities of BAPA.

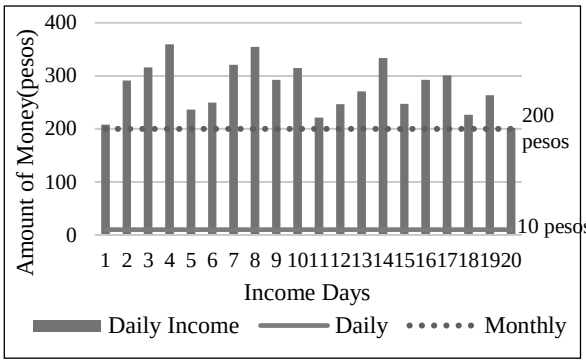


Figure 4: Monthly and daily payment strategies in proportion to daily income.

## 6. Conclusions

1. Poor payment morality was found among SHS users in Alumar island, Philippines
   - Price satisfaction had no significant association with monthly income and electricity provision.
   - Contrary to common hypothesis, amount of tariff was not a problem because users' average WTP was significantly higher than payment for SHS.
2. Earnings were found to be made on a daily basis and expenses for basic utilities were preferable in smaller units rather than purchasing for a whole month at once.
3. A fee collection on a daily basis has been proposed as an effective strategy to ensure the operational sustainability of rural electrification program in Alumar island.

For further studies, it is recommended to propose this strategy to the electric cooperative BAPA and observe the change in users' payment behavior after the application of this strategy in Alumar island and explore similar scenarios in other developing countries as well.

## References

[1] BNEF (2017), Global Trends in Renewable Energy Investment 2017 by UNEP and Bloomberg New Energy Finance

[2] WEO (2016), World Energy Outlook 2016 by International Energy Agency

[3] Nieuwenhout, F. D. J., Van Dijk, A., Lasschuit, P. E., Van Roekel, G., Van Dijk, V. A. P., Hirsch, D., … Wade, H. (2001). Experience with solar home systems in developing countries: A review. *Progress in Photovoltaics: Research and Applications*, *9*(6), 455–474.

[4] Tamir, K., Urmee, T., & Pryor, T. (2015). Issues of small scale renewable energy systems installed in rural Soum centres in Mongolia. *Energy for Sustainable Development*, *27*, 1–9.

[5] Williams, N. J., Jaramillo, P., Taneja, J., & Ustun, T. S. (2015). Enabling private sector investment in microgrid-based rural electrification in developing countries: A review. *Renewable and Sustainable Energy Reviews*, *52*, 1268–1281.

[6] Hong, G. W., & Abe, N. (2012). Sustainability assessment of renewable energy projects for off-grid rural electrification: The Pangan-an Island case in the Philippines. *Renewable and Sustainable Energy Reviews*, *16*(1), 54–64.

[7] Hong, G. W., Abe, N., Baclay, M., & Arciaga, L. (2015). Assessing users' performance to sustain off-grid renewable energy systems: The capacity and willingness approach. *Energy for Sustainable Development*, *28*, 102–114.

[8] Bartošová, J. (2007). Probability models of income distribution, 2–6.

[9] Rufino, C. C. (2013). Consumption Pattern of Poor Households in Metro Manila – A Microeconometric Evaluation, 1, 10–24.

[10] Joseph, A. B. J. (2015). The Quality of Life of Fishermen Community A micro level study Final Report of the Minor Research Project.

# Adsorption Equilibrium of Metal Cations of Acid Mine Drainage Treatment using Indonesian Natural Zeolite

Student Number: 14M51641 Name: Hironobu HASEGAWA Supervisor: Ryuichi EGASHIRA

# インドネシア産天然ゼオライトによる酸性炭鉱廃水の処理における金属陽イオンの吸着平衡

長谷川　博信

インドネシア・ボゴール産の天然ゼオライトを用いて，モデル酸性廃水中の重金属イオン(Mn, Zn, Cu, Fe)の吸着平衡を実測した。ゼオライトおよびモデル酸性廃水を接触させることによりNa，Mg，K，Caイオンが溶出した。初期*p*H(2～5)は，平衡時において7～8に上昇した。*p*Hの上昇により金属水酸化物が析出したと考えられ，Zn，Cu，Feの水溶液中濃度は大きく減少した。Mnは主としてゼオライトによる吸着により濃度が減少した。拡張Langmuir式は実験結果を良好に推算することができた。

## 1. Introduction

Indonesia is a country that has large quantity of mineral resources, especially huge reserves of coal, and this country has been a great exporter of coal. Thus mining industry in Indonesia is expected to further develop in the future[1]. On the other hand, Indonesia has been suffered from acid mine drainage (AMD) caused by mining activities. The AMD is acidic wastewater containing heavy metals sulfate, generated through the oxidization of metal sulfide at the surface of mineral deposit with water or air, and polluting the ecological systems[2]. The AMD is mostly drained from abandoned mining sites where no one has duty to treat AMD, and therefore economical and simple treatment to mitigate the high acidity and remove the heavy metal ions is required[2].

For treatment of AMD, neutralization method is most commonly used. Although the method is effective to remove the heavy metal ions in the AMD, large amount of sledges should be generated and the treatment of the sledges also is necessary. On the other hand, the deposits of Indonesian natural zeolite were found abundantly in West Java Province and the utilization of the natural zeolite for the treatment of AMD has been studied. The base components of the zeolites are mainly clinoptilolite and mordenite. Although the previous studies of our research group reported that the natural zeolite from Bogor deposit was effective for removal of heavy metals from real AMD of coal mine and mitigation of acidity in the solution[3], the effects of precipitation of heavy metals and other cations in the solution on the mechanism of heavy metal removal were still necessary to study.

In this dissertation, the characterization of the zeolite samples and batch treatment of the model AMD solutions containing single and binary heavy metal using Indonesian natural zeolite were carried out to study the effects of *p*H and concentration of metal cations on the adsorption equilibrium in order to clarify the mechanisms of the AMD treatment.

## 2. Experimental

### 2.1 Materials

Natural zeolite sample was obtained from Bogor deposit, Indonesia. According to XRD result of previous study[3], the major components of the zeolite were clinoptilolite-Ca and mordenite. In addition, the sample contained albite, cristobalite, and calcite as non-zeolitic material. Before the experiment, the zeolite sample was crushed (Wonder Blender, WB-1, Osaka Chemical Co., Ltd.), and screened (Testing Sieve, aperture $150 \times 10^{-6}$ m, wire diameter $100 \times 10^{-6}$ m, Tokyo Screen Co., Ltd.) Then obtained powder was washed with deionized water and dried to remove water.

In the cases of adsorption equilibrium measurements, four kinds of heavy metal ions, such as $Mn^{2+}$, $Zn^{2+}$, $Cu^{2+}$ and $Fe^{3+}$, were selected as the model heavy metal ions contained in AMD, and $MnSO_4 \cdot 5H_2O$, $ZnSO_4 \cdot 7H_2O$, $CuSO_4 \cdot 5H_2O$, and $Fe_2(SO_4)_3 \cdot nH_2O$ were used as source of heavy metal ions to prepare the model AMD. The *p*H of the feed solution was adjusted using $H_2SO_4$. All reagents used here were in analytical grade and purchased from Wako Pure Chemical Ind., Ltd.

### 2.2 Characterization of the zeolite sample

The cation exchange capacity (CEC) of the natural zeolite sample also was measured with Method-9081 by the US Environmental Protection Agency. In order to quantify exchangeable cations in the zeolite, leaching of the zeolite using ammonium acetate ($NH_4OAc$) solution were also carried out. The 4g of natural zeolite sample was contacted with 30mL of 1 mol/L aqueous $NH_4OAc$ solution and shaken for 5 minutes. After phase separation using centrifuge, fresh 30mL $NH_4OAc$ solution was added to the solid and this operation was repeated 10 times. The liquid phase obtained from each operation was analysed to determine metal concentrations.

### 2.3 Batch AMD treatment

The experimental conditions of batch adsorption are summarized in **Table1**. Single metal solutions and 3 types of binary metal solutions (Mn-Zn, Zn-Fe, and Mn-Fe) were used as feed solutions. The initial metal

concentrations were varied from $1.0 \times 10^{-3}$ to $1.9 \times 10^{-2}$ mol/L. In the cases of binary metal solutions, summation of initial metal concentrations of both metal ions were varied from $1.0 \times 10^{-3}$ to $1.9 \times 10^{-2}$ mol/L and mass concentration ratio of both metals was set as unity. All experiments were carried out as follows. The specified volume of feed solution $V_0$, and amount of natural zeolite sample $S_0$ were put in a 100mL volume plastic bottles with screw cap and shaken at 300K for 240 hours to be equilibrated. After reaching equilibrium the mixture was filtrated with paper filter. The feed solution and the obtained liquid phases were analysed to determine metal concentrations and *p*H values.

### 2.4 Analysis

The liquid phases were analysed to determine metal concentrations in the solutions by ICP-AES (SPS7800, SII Nano Technology). The *p*H values of the solutions were measured by digital *p*H meter (F-51, HORIBA).

**Table1** Experimental conditions of batch adsorption

| | | |
|---|---|---|
| Solute | | $MnSO_4\ 5H_2O$, $ZnSO_4\ 7H_2O$, $CuSO_4\ 5H_2O$, $Fe_2(SO_4)_3\ nH_2O$ |
| Adsorbent | | Natural zeolite sample from Bogor deposit |
| Volume of solution, $V_0$ | [$m^3$] | $50 \times 10^{-6}$ |
| Initial metal concentration, $C_{i,0}$ | [kmol $m^{-3}$] | $1 \times 10^{-3}$-$1.9 \times 10^{-2}$ |
| Initial *p*H of solution, $pH_0$ | [-] | 2, 3, 5(Mn, Zn, Cu)<br>2 (Fe, binary metals) |
| Mass of zeolite, $S_0$ | [kg] | $2.5 \times 10^{-3}$ |

## 3 Results and discussion

### 3.1 Characterization of the zeolite sample

Based on the method-9081, the CEC of the zeolite sample was determined as 8.42 x $10^{-4}$ eq/g. This value was lower than the theoretical CECs of pure Clinoptilolite-Ca (2.44 x $10^{-3}$ eq/g) and Mordenite (2.24 x $10^{-3}$ eq/g)[4]. Total equivalent of metal ion *i* leached from unit mass of the zeolite sample until the *k* time contacts, $E_{i,k}$, was defined as follows,

$$E_{i,k} = \sum_j^k m_i C_{i,j} V_j / S_0 \qquad (1)$$

where $C_{i,k}$ and $V_k$ ($10 \geqq k \geqq 1$) represent the concentration of metal ion *i* at the *k*-th contact and added volume of solution at the *k*-th contact, respectively.

**Figure 1** shows the plots of $E_{i,k}$ against the total volume of $NH_4OAc$ contacted with the zeolite samples, and the CEC of the zeolite sample measured above was shown as the dashed line. The metal ions of Ca, Na, Mg, and K dissolved into the $NH_4OAc$ solution, and $E_{i,k}$ of Ca was the largest, followed by those of Na, K, and Mg. The $E_{i,k}$ of Na, Mg, and K increased until $k$=2 and kept almost constant in the range of $k$>2. On the other hand, $E_{i,k}$ of Ca kept increasing until 10 time contacts and $E_{i,k}$ of Ca at $k$=10 was almost twice as much as the CEC. According to the previous study, the zeolite sample contained $CaCO_3$ [3] and most of Ca ions in the solution should be derived not from the ion exchange sites of the zeolite, but from $CaCO_3$. Although the amount of $CaCO_3$ leaching were larger, the effects of the leaching on the CEC measurement should be negligible. The concentration of Ca ion at each shaking steps were much lower than the concentration of Na in the sodium acetate solutions which were used for the CEC measurement. Then, the obtained CEC was considered to be reasonable.

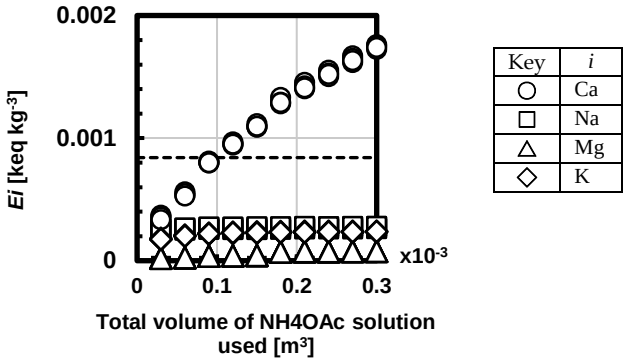


**Fig.1** Accumulated equivalent of leached cations in the NH4OAc solution(equivalent based)

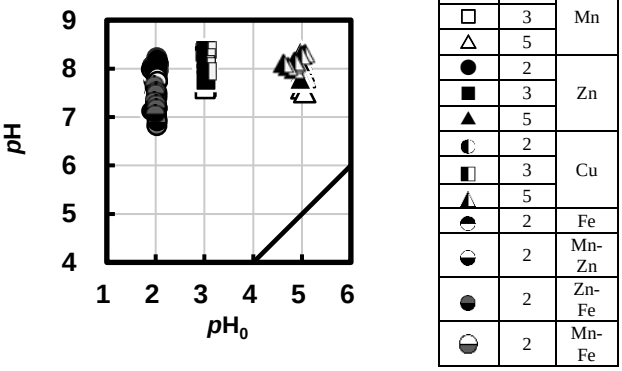


**Fig.2** *p*H changes in the equilibrium solution

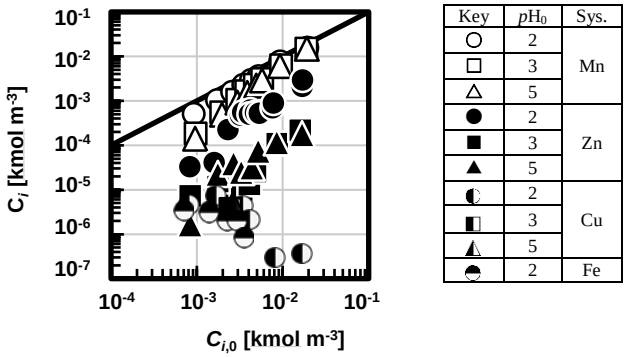


**Fig.3** Concentration changes of heavy metals in equilibrium solution

### 3.2 Batch AMD treatment

**Figure 2** shows *p*H changes of the single and binary heavy metal solution between initial and equilibrium. The *p*Hs in all model AMD solutions at equilibrium increased from the initial ones and settled from 7 to 8, in spite that their initial *p*Hs were varied from 2 to 5. The *p*H increased as the initial concentration of the metal ion decreased. Although this increment of *p*H might be caused by adsorption of hydrogen by the zeolite,

dissolution of $CaCO_3$, from the zeolite, and so on, the substantial contributions of these reasons to the *p*H increment were unclear.

**Figure 3** shows the comparison of initial and equilibrium concentrations of heavy metals in the model AMD with the single heavy metal systems. All metal concentrations in the solution were lowered by contacting with the natural zeolite. Especially the equilibrium concentrations of Zn($pH_0$=3, 5), Cu, and Fe in the single heavy metal systems. In the cases of binary metal systems, the concentrations of all metals also decreased and that of were almost zero.

**Figure 4** shows the relationship of the metal cation concentrations and *p*H in the equilibrium solution in the cases of the single heavy metal systems. The concentrations of leached cations and heavy metal ions increased as *p*H decreased. The cation most leached from the zeolite sample was Ca and its concentration at equilibrium increased as the initial heavy metal concentrations increased in all cases. In the binary heavy metal systems, Ca was most leached and its concentrations increased with the increment of initial heavy metal concentrations, as same as in the single heavy metal systems.

**Figure 5** shows the relationship between the equilibrium *p*H and concentrations of the metal ions at equilibrium, in which the solubility curves of respective metal hydroxides estimated from their solubility products also were indicated as solid lines. The curves represent solubilities of their metal ions at corresponding *p*H, and the solubility products were cited from the previous studies [3] and used as the reference solubilities. In all conditions, the concentrations of $Mn^{2+}$ at equilibrium were smaller than the solubility, and the concentrations of the other metal ions were close to or larger than the estimated solubility curves. Since concentration of $Mn^{2+}$ was larger than estimated solubility curve, $Mn^{2+}$ was removed by adsorption onto zeolite. The concentrations of $Zn^{2+}$ were close to the estimated solubility of $Zn(OH)_2$ and some part of $Zn^{2+}$ might be precipitated to be removed from the solution. The concentrations of $Cu^{2+}$ and $Fe^{3+}$ at equilibrium were larger than solubility of $Cu(OH)_2$ or $Fe(OH)_3$ estimated at each equilibrium *p*H. The concentrations were low enough to be negligible compared to other heavy metal. Thus most of Cu and Fe might be removed by precipitation of hydroxide form in all conditions. The concentration of Ca was the largest among metal ions dissolved from the zeolite sample and the concentration at equilibrium increased as initial heavy metals concentrations increased.

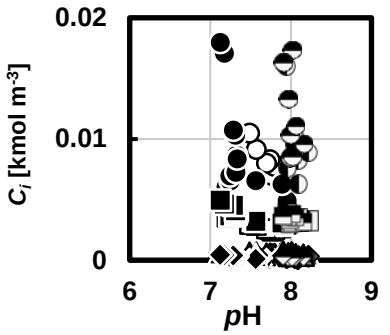


| Key | *i* | Sys. |
|---|---|---|
| ○ | Ca | Mn |
| □ | Na | |
| △ | Mg | |
| ◇ | K | |
| ● | Ca | Zn |
| ■ | Na | |
| ▲ | Mg | |
| ◆ | K | |
| ◐ | Ca | Cu |
| ▮ | Na | |
| ◭ | Mg | |
| ◆ | K | |
| ◓ | Ca | Fe |
| ▬ | Na | |
| △ | Mg | |
| ◆ | K | |

**Fig.4** Equilibrium concentrations of eluted cations form the zeolite into the solution at $pH_0$=2

Finally, we tried to predict adsorption isotherm of heavy metals by Langmuir model. The adsorbed amount of heavy metal cation *i* was calculated from material balance equation and was expressed as,

$$q_i = (C_i - C_{i,0})V_0/S_0 \quad (2)$$

In this experiment we assumed that initial heavy metal concentrations in solid phase were zero ($q_{i,0}$=0) and volume of the solution and mass of the zeolite were same before and after equilibrium ($V_0$=*V* and $S_0$=*S*). The extended Langmuir equation was expressed as,

$$q_i = q^* K_i C_i/(1 + K_{\mathrm{Ca}}C_{\mathrm{Ca}} + K_{\mathrm{Mg}}C_{\mathrm{Mg}} + K_i C_i) \quad (3)$$

where $q_i$* and $K_i$ were the saturated amount of metal ion *i* on the zeolite and the Langmuir parameter of metal ion *i*, respectively. Then it was assumed that only divalent cations were adsorbed; adsorption of $Ca^{2+}$, $Mg^{2+}$ and $Mn^{2+}$ or $Zn^{2+}$ were considered, and the saturated amount of adsorption, $q_i^*$, was decided based on the CEC measured here as 4.21x10$^{-4}$ mol/g, and *K*s of Ca and Mg were same as that of $Mn^{2+}$which had no precipitation of hydroxides.

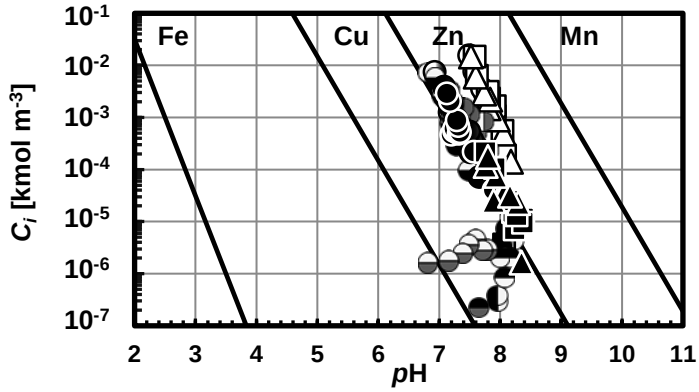


| Key | $pH_0$ | *i* | Sys. | Key | $pH_0$ | *i* | Sys. |
|---|---|---|---|---|---|---|---|
| ○ | 2 | Mn | Mn | ◑ | 2 | Mn | Mn-Zn |
| □ | 3 | | | ◒ | | Zn | |
| △ | 5 | | | ◐ | 2 | Zn | Zn-Fe |
| ● | 2 | Zn | Zn | ◒ | | Fe | |
| ■ | 3 | | | ◑ | 2 | Mn | Mn-Fe |
| ▲ | 5 | | | ◒ | | Fe | |
| ◐ | 2 | Cu | Cu | | | | |
| ◧ | 3 | | | | | | |
| ◭ | 5 | | | | | | |
| ◓ | 2 | Fe | Fe | | | | |

**Fig.5** Estimated solubility curves of the metal hydroxides and the relations between the metal concentrations and *p*H values at equilibrium

**Figure 6** shows the adsorption isotherms of various kinds of metal ions in the single heavy metal solutions. The natural zeolite could remove most of Zn at $pH_0$=3 or 5, Cu and Fe, and their concentrations in the solutions were almost zero. These ions should be removed as the forms of their hydroxides by elevation of *p*H. The obtained parameters were shown in **Table 2** and the estimation results by Eq. (3) were shown in **Fig.6** as lines. The *K* of Mn under the condition of $pH_0$=2 was lower than those of $pH_0$=3 or 5. The *K* of Zn was much larger than those of Mn adsorption because $q_i$ included the effects of precipitation.

The adsorption isotherms of heavy metal ions in the binary heavy metal solutions are shown in **Figure 7**. The concentrations of Fe were almost zero and the $q_{Zn}$s in binary metal systems were lower than those in single Zn system at same equilibrium concentrations of Zn. Since the divalent cations were major among all cations in the solutions at equilibrium, the effects of divalent cations on the removal of heavy metals were considered. Then, the extended Langmuir model was used to predict the adsorption isotherm of the metal ions in the binary system as same as the single system, and prediction results are shown in **Fig. 7** by lines. The *K*s determined here are listed in **Table 3**, where *K*s of divalent cations, Ca and Mg, were set as same as that of Mn. The *K*s of Mn were the same as those measured in single Mn system. Whereas *K* of Zn was higher than that of Mn in the binary metal ion system, it was much smaller than *K* obtained in the single metal ion system. The amount of precipitated $Zn(OH)_2$ in the binary system might be smaller than those in the single system because the concentration of $Zn^{2+}$ in the binary system lied in wider range than that in the single system.

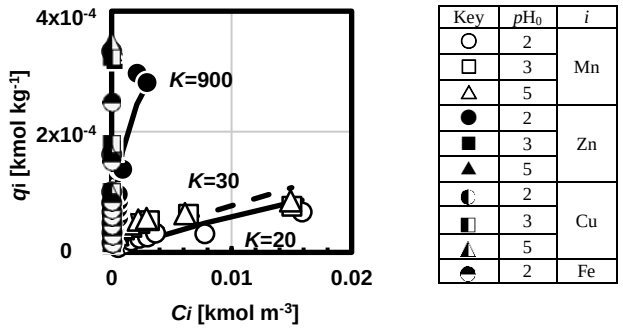


**Fig.6** Adsorption isotherm of heavy metals onto zeolite in single heavy metal solutions

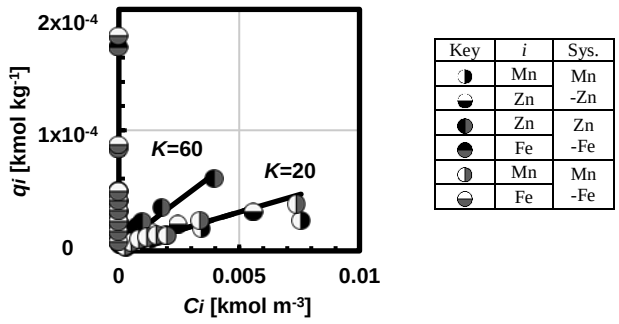


**Fig.7** Adsorption isotherm of heavy metals onto zeolite in binary heavy metal solutions

**Table2** Determined Langmuir parameters of Mn and Zn in adsorption experiment

| System | Metal | $pH_0$ | $K_i$ [$m^3$ $kmol^{-1}$] | $q^*$ [kmol $kg^{-1}$] |
|---|---|---|---|---|
| Mn | Mn | 2 | 20 | $4.21x10^{-4}$ |
| | | 3 | 30 | |
| | | 5 | 30 | |
| Zn | Zn | 2 | 900 | |

**Table3** Determined Langmuir parameters of Mn and Zn in adsorption experiment

| System | Metal | $pH_0$ | $K_i$ [$m^3$ $kmol^{-1}$] | $q^*$ [kmol $kg^{-1}$] |
|---|---|---|---|---|
| Mn -Zn | Mn | 2 | 20 | $4.21x10^{-4}$ |
| | Zn | 2 | 20 | |
| Zn -Fe | Zn | 2 | 60 | |
| Mn -Fe | Mn | 2 | 20 | |

## 4. Conclusions

The natural zeolite sample from Bogor deposit was used as an adsorbent to study the treatment of the model AMD. CEC of the zeolite sample was determined to $8.42x10^{-4}$ mol/g by US-EPA method 9081. Part of eluted Ca ions were not derived from exchangeable sites.

The zeolite sample could increase *p*H of the model AMD solutions to appropriate level (*p*H=7-8). In addition, the natural zeolite could remove heavy metal $Mn^{2+}$, $Zn^{2+}$, $Cu^{2+}$, and $Fe^{2+}$ in model AMD. $Zn^{2+}$, $Cu^{2+}$, and $Fe^{2+}$ were removed not only by the adsorption with the zeolite, but also by precipitation to form metal hydroxides. The $Mn^{2+}$ was mainly removed by adsorption onto the zeolite samples. The extended Langmuir model was used to organize the adsorption of Mn and Zn considering the effects of other metal ions dissolved from the zeolite sample, and favorably predicted the adsorption behavior

.

**Nomenclature**

| | | |
|---|---|---|
| *C* | -concentration in liquid phase | [kmol $m^{-3}$] |
| *q* | -concentration in solid phase | [kmol $kg^{-1}$] |
| *q** | -saturated amount of adsorption | [kmol $kg^{-1}$] |
| *V* | -volume of liquid phase | [$m^3$] |
| *S* | -mass of zeolite | [kg] |
| *E* | -total equivalent of metal leached | [keq $kg^{-1}$] |
| *K* | -Langmuir constant | [$m^3$ $kmol^{-1}$] |
| *m* | -valency of ion | [-] |

**Subscript**

| | |
|---|---|
| 0 | -at initial state |
| *i* | -component *i* |
| *k* | -at *k*-th contact |

## Reference


[1]一般財団法人石油エネルギーセンター, コールデータバンク
[2]JOGMEC 酸性炭鉱廃水問題の対処動向について http://mric.jogmec.go.jp/public/current/03_03.html
[3]Fernando, 東京工業大学大学院 2015年修士論文
[4]https://www.mineralienatlas.de/lexikon/index.php/MineralData

# A MARS ROLLING-ROVER INTEGRATED WITH ENTRY, DESCENT AND LANDING SYSTEM

Student Number: 15M51704 Name: Masaaki ICHIMURA Supervisor: Daisuke AKITA

大気突入機をかねた転がり型火星探査機の可能性

市村 優明

本論文では極めて軽量かつ簡易な構造を持つ, 単独で火星大気突入から着陸, 表面探査までを行うような転がり移動型の火星表面探査機を提案する. 探査ミッションの各フェーズにおいて、満たすべき条件について考察し、実現可能な機体構成を見積もる. 探査機に対する全ての要求について考察した後、機体構成とミッションの一例を示すことで探査機の実現可能性について論じる

## 1. Introduction

Although a number of Mars exploration had been conducted, in-situ explorations are very effective in understanding Mars' environment. However, Mars surface exploration mission is difficult because Mars' atmosphere is very thin despite heavy entry probes.[1] So atmospheric braking tends to insufficient, and then probes collide with Mars' surface at very high speed. It results in 2/3 failure of Mars surface exploration mission. This study proposes extremely lightweight probe as shown in Figure 1.

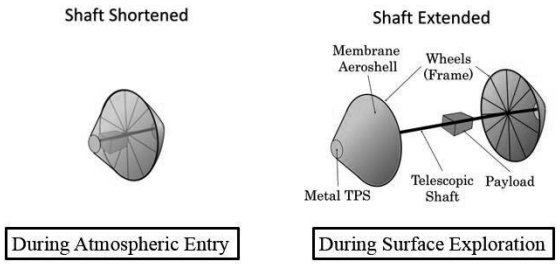


Fig 1. The concept of the rover

This probe takes two types of configurations; aeroshell and rover. The aeroshell, which works for atmospheric braking and heat shielding, has a shape like a cone. The rover is a mobile probe exploring the planets or asteroids surface. This probe uses frames of the aeroshell as wheels. The two aeroshells are connected with a shaft, which can be extended and shortened like a telescope. This system enables the probe to roll down the slope on Mars. Wheels are made of super elastic alloy, to avoid plastic deformation caused by collision with rocks. The aeroshells are made of Zylon® or alumina fiber cloth membrane. All materials of the probe is available on market currently. Furthermore, this probe does not need additional landing systems such as parachutes or airbags. The probe proposed in this study is an all-in –one system which contains the functions of decending, landing and roving. This study investigates the possibility of this all-in-one system. The mission scenario of the probe is shown in Figure 2.

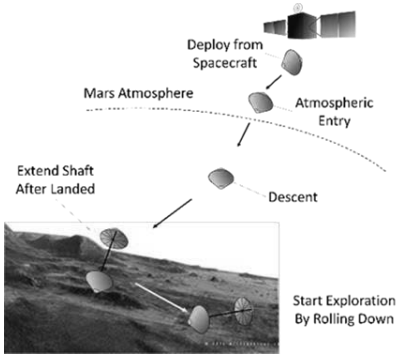


Fig 2. Mission scenario

At first, the probe is deployed from mother spacecraft, and then enters into Mars atmosphere. During contained in the spacecraft and atmospheric entry, the shaft of the probe is shortened. Before touchdown to Mars surface, the probe descends and decelerates by using atmospheric braking. After sufficiently decelerated, the probe lands on Mars surface. By using impact of touchdown, the shaft can be extended by spring just like a knock-type pen. Finally, the probe plays a role as rover, rolling down the slope on Mars surface. During surface exploration, this probe is intended to take some pictures of Mars surface. The data of the pictures will be sent to mother spacecraft by communication device.

To achieve Mars surface exploration mission, four requirements below are need to be satisfied.

(1) To endure aerodynamic heating

(2) To avoid twist buckling of wheels caused by aerodynamic force
(3) To endure impact of landing on Mars surface
(4) To roll down a gentle slope and run over obstacles

This study investigates the possibility of the probe by considering the configurations of the probe to satisfy the four requirements.

# 2. Mars Atmospheric Entry

To calculate the trajectory from the orbit of the mother spacecraft to Mars' surface, this study considers two cases of initial condition. The first one is a direct entry at initial height of 125[km] and initial velocity of 5.6[km/s] (Condition A). The other one is initial Mars orbit 27,000[km] × 3,700[km] (Condition B). The orbit of the probe is determined by a ballistic coefficient, expressed by the equation below.

$$\beta = \frac{m}{C_D S} \tag{1}$$

($m$: mass[kg], $C_D$: Drag coefficient, S: Projected area[m$^2$])

## 2.1. Aerodynamic Heating

The aerodynamic heating had been estimated by the trajectory calculation. Figure 3. shows the estimated result of the max temperature of the probe surface varying with the ballistic coefficient β.

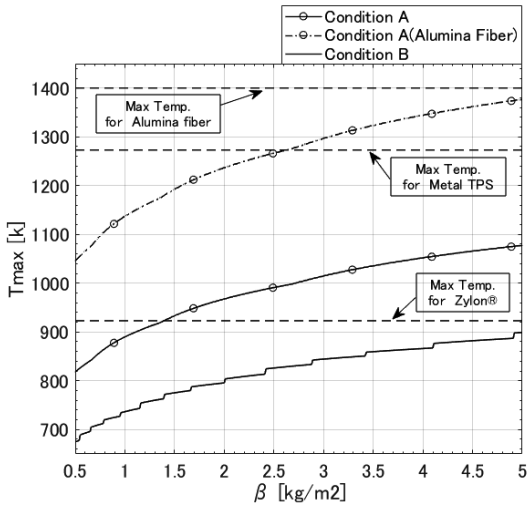


Fig 3. Ballistic Coefficient vs. Max Temp

The local curvature of the probe is set to be 1.0 (m) and emissivity is set to be 0.8. The max temperature on Zylon® membrane surface is set to be the same as that at the stagnation point. The max temperature increases as β increases. Lower β is derived by larger area of membrane, thus larger wheel radius. The dashed line represents the max temperature on the membrane in the case of alumina fiber cloth. The alumina fiber have a characteristic that emissivity depends on its temperature. In some cases, the surface temperature of the probe at Condition A exceeds its heatproof temperature. On the other hand, it does not exceed the heatproof temperature at Condition B. Thus, in order to endure aerodynamic heating, Condition B seems to be more desirable.

## 2.2. Aerodynamic Force

The aerodynamic force yields a tensile force on the membrane of the aeroshell. This tensile force possibly causes out-of-plane buckling of the frames. Out-of-plane buckling load of a ring is expressed by an equation below.[2]

$$p_{cr} = \frac{9\alpha}{1+4\alpha}\frac{EI}{R^3} \tag{2}$$

($p_{cr}$: buckling load[N/m], $E$: modulus of elasticity[Pa], I: moment of inertia of area[m$^4$], R: ring radius[m])

From this equation, a required thickness of the frame can be calculated. To examine the validity of this equation, a hypersonic wind tunnel test had been conducted. The test was conducted at Hypersonic Wind Tunnel at University of Tokyo Kashiwa Campus.[3] Mach number of the wind tunnel is M=7. At this Mach number, the dominating parameter of the flow is Mach number. Thus, the wind tunnel test is goodly reproduced despite Reynolds number of the wind tunnel is different from actual case. The probe model used at the test is shown in Figure 4.

Fig 4. Probe Model

The model is made of Zylon® membrane and Ni-Ti shape memory alloy. The diameter of the model projected area is 30[mm]. To examine the validity of eq. (2), the effect of the ring thickness was investigated. From eq. (2) estimates, the ring thickness of d=0.454[mm] where the out of plane buckling occurs. Then, preparing the ring of 0.35, 0.4, 0.5[mm] thickness, the deformation of the ring is observed. Figure 5 shows the appearance of the wind tunnel test.

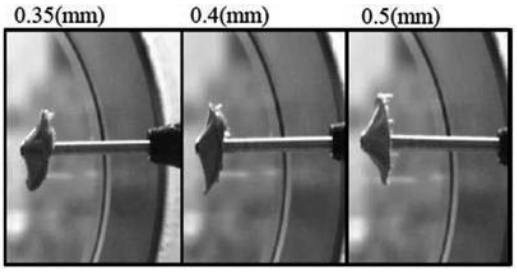


Fig 5. Wind Tunnel Test

The out of plane buckling occurs at ring thick of 0.35, 0.4[mm]. At the ring thick of 0.5[mm], deformation of the frame was not observed. Thus, the validity of eq. (2) had been proven.

Fig 6. shows the requirement for ring thickness to endure the aerodynamic force by using eq. (2). For 1 to 5 [m] ring diameter, the ballistic coefficient varies 2.2 to 5 [kg/m$^2$]. Furthermore, Condition B requires smaller ballistic coefficient. Thus, Condition B is also desirable in terms of to endure the aerodynamic force. So the following discussion is focused on Condition B.

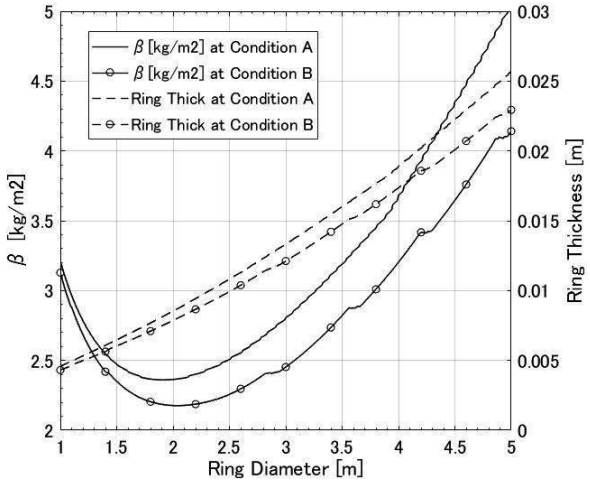


Fig 6. Ring Diameter vs. β and Ring Thickness

## 3. Landing

When the probe reaches in the vicinity of Mars surface, the probe generally have a velocity of 30 to 55 [m/s]. Without any shock absorber, the probe must be broken. A shock absorber using aluminum honeycomb is considered. Aluminum honeycomb is made of laminar sheets of aluminum as shown in Figure 7.

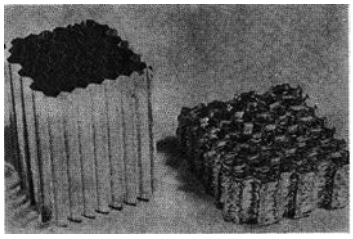

Fig 7. Aluminum honeycomb

This structure is lightweight and have significant shock absorption performance. The energy absorption is estimated by equation as follows.

$$E_C = \sigma_{cr} \cdot T_C \cdot A \quad (3)$$

($E_C$: absorbed energy [J], $\sigma_{cr}$: crush strength[Pa], $T_C$: crush stroke[m], $A$: cross section area[m$^2$])

For example, if we consider a case at $\beta = 5$[kg/m$^2$] and m=5[kg], the touchdown speed would be 55[km/s]. The honeycomb's crush strength and, density is assumed to be 8[MPa] and 110[kg/m$^3$], respectively. The cross section has a circular shape of 0.1[m] diameter. If the speed of the probe is 6[m/s] after the shock absorption, the crush stroke of 0.12[m] is needed. Since the crush stroke is 3/4 of the honeycomb full stroke, honeycomb weight would be 138[g]. Figure 8 depicts an example of the shock absorbing system.

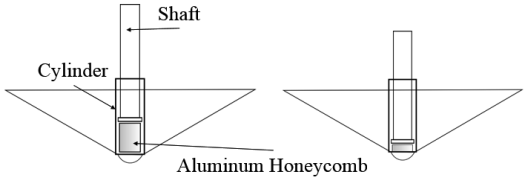


Fig 8. An Example of Shock Absorbing System

## 4. Mars Surface Exploration

The probe moves on Mars surface by rolling down the slope. The wheels of the probe are affected by rolling resistance effect, where prevents the rolling motion of wheels. The effect is expressed by the rolling resistance coefficient, $C_{rr}$. The slope which the probe can start roll down is determined as follows.

$$\tan^{-1}(C_{rr}) > \theta \quad (4)$$

($C_{rr}$: rolling resistance coefficient, θ: slope [deg.])

To start rolling down at 10[deg.] slope, $C_{rr} < 0.17$ is needed to be satisfied.

The relationships between the wheel distortion caused by self-weight and the rolling resistance coefficient is modeled by NASA.[5] The assumption is following

$$C_{rr} = [p_\delta(1 - p_\delta)]^{1/2} \quad (5)$$

($p_\delta$: wheel deformation [m])

From this equation, requirement for wheel thickness can be estimated.

Consider to explore 10 [deg.] slope, thus the requirement is $C_{rr} < 0.17$. And assume the ballistic coefficient should be less than 5[kg/m$^2$]. If $\beta < 5$

[kg/m$^2$], the probe can endure the aerodynamic heating and aerodynamic force. Note that the shape of cross section of the wheels are set to rectangular.
Figure 9. shows the result of estimation of requirements. For the wheels diameter of 1 to 5 [m], any size can be selected. The thinner wheels would be favorable because the mass of the probe needs to be small for the sake of reduction in the cost of mission and the landing impact.

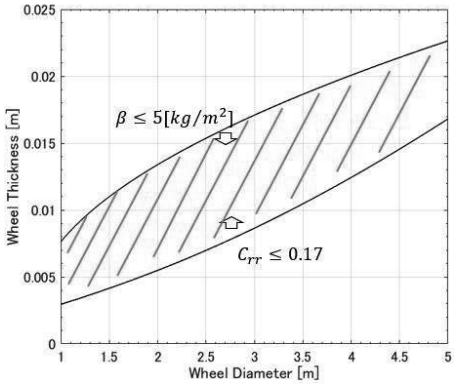


Fig 9. Requirements for Wheel's Size and Thickness

To roll over the rock is important matter because there are many rocks. To roll over rocks on Mars surface. It is modeled like in Figure 10.

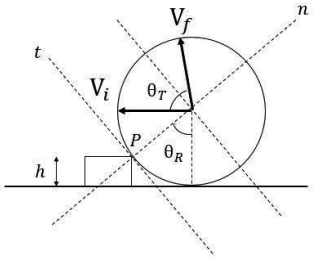


Fig 10. Model of the Rolling Over the Rocks

This model considers rover's collision with a rock. After the collision with the rock, rover have a velocity vector normal to Mars surface. Then, if the kinetic energy of the normal to surface component exceeds the potential energy at the rock height, rover can roll over the rock.

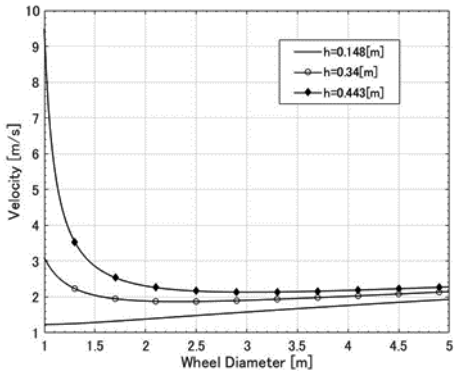


Fig 11. Requirement for rolling speed

Figure 11 shows the result of estimation of requirements for rover's size and initial rolling speed. In the case of the initial speed of 3[m/s], about 90% of Martian rocks can be rolled over.

## 5. Rover and Mission Example

An example of probe configuration is shown in Fig 11. This rover can endure the aerodynamic heating and aerodynamic force, land on Mars surface successfully, and start rolling down at 10[deg.] slope. If the initial rolling speed exceed 3[m/s], 90% of Martian rocks can be rolled over. Valles Marineris, Martian extremely huge canyon that has 4,000 [km] length, 200 [km] width and 7 [km] depth could be one of the most hopeful exploration sites.

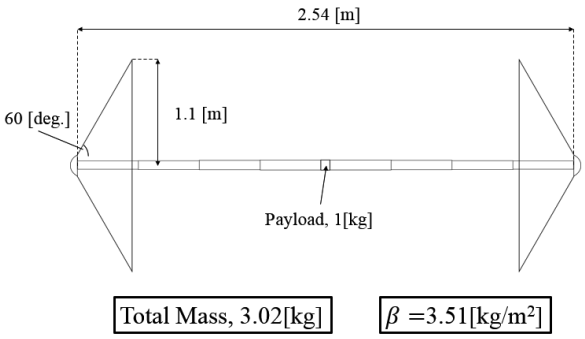


Fig 11. An Example of probe

## 6. Conclusion

By examining the requirements to achieve the mission, a feasible configuration of the proposed probe is illustrated. The all-in-one probe must be very cost effective and robust system for Mars surface exploration.

## References


[1] R. D. Braun and R. M. Manning, "Mars Exploration Entry, Descent, and Landing Challenges", Journal of Spacecraft and Rockets, vol. 44, no. 2, 2007.

[2] Thein Wah, "Buckling of Thin Circular Rings under Uniform Pressure", Int. J. of Solids Structure, vol.3, pp. 967-974, 1967.

[3] http://daedalus.k.u-tokyo.ac.jp/wt/, accessed Aug. 25, 2017

[4] 小田 周平・野口 元,"ハニカムの衝撃エネルギー吸収性について", 圧力技術, Vol.15 No.1 p41-49, 1977

[5] J. Antol, et al, "Low Cost Mars Surface Exploration: The Mars Tumbleweed", NASA TM-2003-212411, 2003.

# DEVELOPMENT OF A MULTI-BEAM STRUCTURE BY STACKING COMB-SHAPED RUBBERS

Student Number:15M51710 Name: Mikhail SALYUKOV Supervisor: Kunio TAKAHASHI

# くし状構造の積層による側面接触型弾性梁集合体の試作

サリュコフ ミハイル

本研究では、マニピュレーション用デバイスとしての利用可能性が示唆される斜め梁構造の梁集合梁の試作と把持脱離の容易性の評価を行うため、梁の取り付け角が任意に調整可能な梁集合体の手法を提案して梁集合体の試作を行い、その凝着力の水平力依存性を実験的に測定した。その結果、提案した手法で試作可能な取り付け角が小さい梁集合体は水平力による把持脱離操作が容易に可能であり、マニピュレーション用デバイスとしての利用可能性が高いことが示された。

## 1 Introduction

In recent years, automation and speed enhancing of the manipulation process has been carried out on various production sites. Although, conventional devices for manipulation have difficulties operating the objects that have surface with unevenness and roughness, which hinders the progress of automation and speed enhancing. In order to solve this problem, a concept of a gecko-inspired manipulation device (GIMD) has been introduced. Gecko has a remarkable ability to grip on uneven and rough surfaces, which is thought to have application possibility to achieve the manipulation of objects that conventional devices have difficulty operating.

It is known that gecko's ability is made possible by the microscopic oblique hairs existing on their toes[1]. Analytical and experimental results suggest that the oblique structure of the hairs contributes to the increase and tangential force dependency of the adhesion force, which are both important properties for easy grip and release of the surface[2,3]. Thus, it is suggested that GIMD could be realized by mimicking gecko's fibrillar structure in a form of multi-beam structure with beams mounted obliquely. On the contrary, conventional methods commonly used to develop the multi-beam structures have difficulties in achieving an oblique mounting angle of beams due to the technical constraints, thus not suitable for developing the GIMD[5,6,7,8].

In this paper, an improved method of developing the multi-beam structure with oblique mounting angles of beams is proposed to achieve the GIMD with improved sufficiency. The development of multi-beam structure was done for evaluation of the proposed method. Developed multi-beam structure was tested for tangential force dependency of the adhesion force, to consider the ability of easy grip and release operations which is a highly important aspect in manipulation.

## 2 Method of developing the multi-beam structure

The molding process of a multi-beam structure is shown in Figure 1. In the beginning of the process, blocks with beams at the bottom arranged in a row (i.e. comb-shaped rubbers) are molded. Two kinds of flat molds are used in the process. One has single rectangular hole in the middle and an opening on the top of it. The other mold has additional multiple rectangular slits for the formation of beams. Two molds are mutually fixed between two plates to form a disassemblable mold and filled with curable liquid material. After curing, mold is disassembled and the comb-shaped rubber is removed. Molded comb shaped rubbers are then stacked vertically with fixed intervals in a horizontal direction. Finally, stacked comb-shaped rubbers are put into a container filled with curable liquid material for a fixation. Using the method described above, it is possible to develop a multi-beam structure with oblique mounting angles of beams. By changing the length of fixed intervals in a horizontal direction, mounting angle of beams $\theta$ can be arbitrarily set within an adjustment range of $0 < \theta \leq 90°$.

In this study, flat molds were made from sheets of SUS304 by metal etching. Height, width and length of the slits for the formation of beams were each set to $H = 100, W = 300, L = 1000\mu m$. For formation of the disassemblable mold, mold with the multiple slits was placed over the glass plate, in order to transfer the smooth glass surface to the contact face of the beams. Mold without the slits was placed over the thin metal sheet coated with mold release agent (DAIKIN, DAIFREE GW-250), for easy disassembling of the mold after material curing. PDMS (sylgard®184 SILICONE ELASTOMER KIT, Dow Corning) that has high mold releasability and transferability, was used as a curable liquid material for molding the comb-shaped rubbers. PDMS was filled into disassemblable mold in low vacuum atmosphere and cured at a temperature of

65℃ on a hotplate. Stacking of the comb-shaped rubbers was done using stepwise jig, designed to achieve the mounting angle of $\theta = 20°$ which has not yet been achieved by conventional methods.

## 3 Measurement method of tangential force dependency of adhesion force of the developed multi-beam structure

To evaluate the easiness of grip and release operations of the GIMD that uses multi-beam structure developed by the method proposed in this study, the tangential force dependency of the adhesion force of the developed multi-beam structure was measured experimentally using the set-up shown in Figure 2. A 5mm-thin flat glass plate (Matsunami Glass, Blue-board glass plate) was mounted on x-axis motorized linear stage (Suruga Seiki, K101-20MS-M) and z-axis motorized linear stage (Suruga Seiki, KS322-8N) along with angle regulation stages. The test sample of developed multi-beam structure was mounted on a 3-axis force sensor. After the horizontal adjusting, the test sample was first pressed vertically against the glass plate(i.e. loading process), then pulled off at a fixed angle of $\varphi$ until the beams of the sample had completely detached(i.e. unloading process). The amount of displacement of the beam from the moment of the contact with the plate until the end of the loading process was set to $327\mu m$ to avoid the contact between beams. In order to change the direction and magnitude of the tangential force during the unloading process, experiments were conducted for 11 different values of pull off angle $\varphi$. Both normal and tangential forces working on the test sample were simultaneously measured during the loading-unloading process using the 3-axis force sensor (KYOWA, LSM-B-10N). The deformation state of the beams during the experiment were observed using the images captured by the digital microscope (Saitoh Kougaku, SKM-3000B-PC).

## 4 Results and discussions

### 4.1 Observation of the developed multi-beam structure

Developed multi-beam structure shown in Figure 4 was observed with digital microscope (RH2000, HiROX). Photo images of the contact side of the beams suggested that shape of the mold was successfully transferred to the beams. Additionally, the surface of the beams on the contact side transmitting light without scattering suggested low roughness on the contact side of the beams. Mounting angle of beams $\theta$ was confirmed to be approximately the same to the target value of $20°$ by visual observation. Deducing from these results, the method proposed in this study is suitable for developing a multi-beam structure with beams in submillimeter scale, with smooth contact surfaces and adjustable mounting angles.

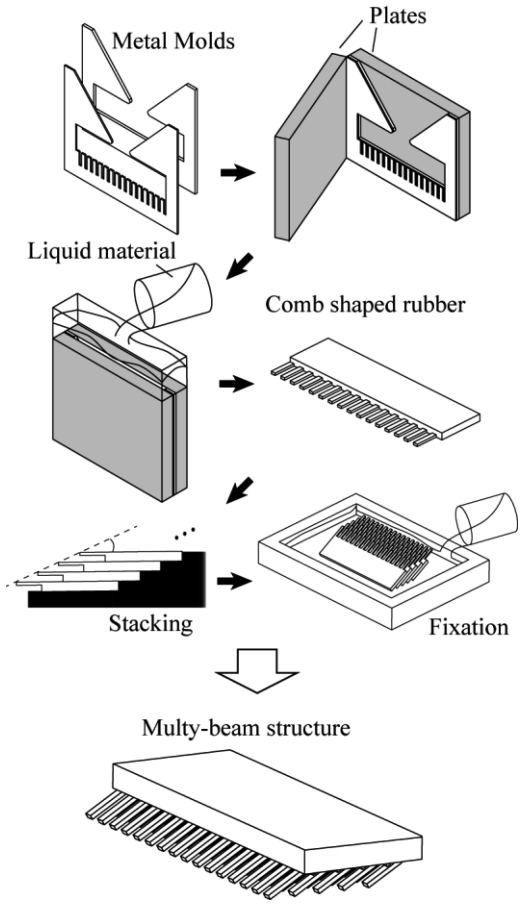


**Figure 1.** Schematic illustration of developing process of a multi beam structure by stacking comb-shaped rubbers

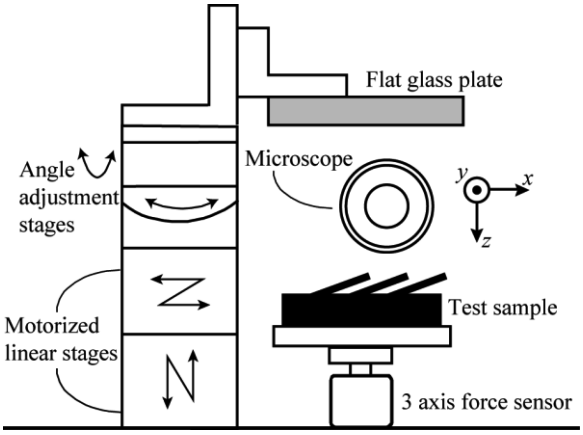


**Figure 2.** Schematic illustration of experimental set-up for loading-unloading experiment

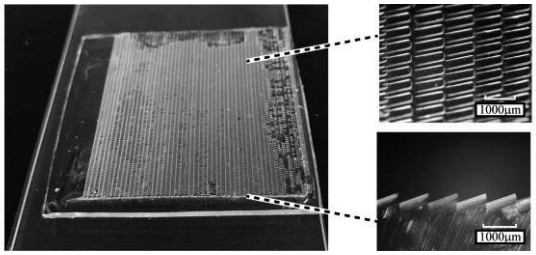


**Figure 3.** Photo images of developed multi-beam structure

### 4.2 Experimental results of the measurement of tangential force dependency of adhesion force of the developed multi-beam structure

The results of the experiments measuring the tangential force dependency of adhesion force of the developed multi-beam structure at pull of angle of $\varphi = 45°$ and $\varphi = 135°$ are shown in Figure 5 (a) and Figure 5 (b), respectively.

When pull of angle was $\varphi = 45°$, negative normal force $F_n$ (i.e. adhesion force) working on the multi-beam structure was observed during the unloading process. Tangential force $F_t$ took a negative value during the loading but increased during the unloading process and stayed positive while adhesion force was observed. The beams of the developed multi-beam structure were deformed by bending as they formed a side contact with the plate during the loading process. The magnitude of deformation of the beams by bending kept decreasing during the unloading process while the magnitude of deformation by elongation in the axial direction increased. Immediately after adhesion force became maximum, "Stick-slip" phenomenon was observed around the contact area of the beams causing the value of the tangential force $F_t$ to decrease gradually, followed by the detachment of the beams.

In contrast to the results described above, when the pull off angle was set to $\varphi = 135°$, tangential force $F_t$ took a negative value during both loading and unloading processes and adhesion force was not observed.

The magnitude of deformation of the beams by bending kept increasing during the unloading process, causing a large deformation. During the increase of bending deformation, a shift of a contact state from side contact to tip contact and to line contact was observed.

The experimental results of forces working on the multi-beam structure during loading-unloading processes for all 11 different values of pull off angle $\varphi$ are shown in Figure 6. For $18° \leq \varphi \leq 90°$, the changes in the forces working on the multi-beam the contact were similar to those of $\varphi = 45°$, as long as the changes in contact state of the beams. Larger maximum adhesion force at a larger $F_t$ was observed at smaller values of $\varphi$. For $108° \leq \varphi \leq 162°$, he changes in the forces working on the multi-beam the contact were similar to those of $\varphi = 135°$, as long as the changes in contact state of the beams. Larger maximum repulsive force at a smaller $F_t$ was observed at larger values of $\varphi$.

As is evident from the results described above, multi-beam structure with oblique beams has a tangential force dependency of adhesion force that allows the easy grip and release operations by changing the direction of tangential force working on it. Results suggest that this tangential force dependency occurs due to the difference in deformation state of beams owing to a difference in direction of applied tangential force, which affects the energy state of the beams. The total energy of a beam $U_{total}$ that adheres with rigid surface could be described as

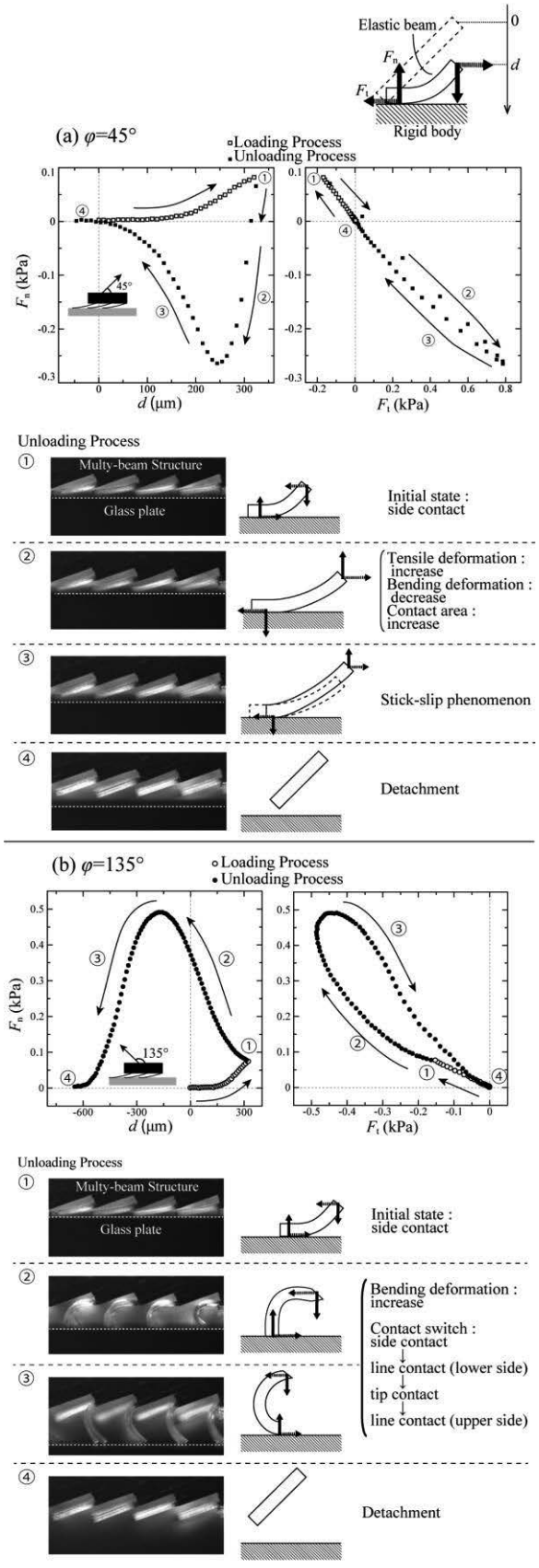


**Figure 5.** Experimental results during the unloading process at the unloading angle of (a) 45° and (b) 135°

$$U_{\text{total}} = U_{\text{elastic}} + U_{\text{surface}}$$

, where $U_{\text{elastic}}$ is the elastic energy attributable to the deformation of the beam and $U_{\text{surface}}$ is the energy attributable to the work of adhesion. When tangential force was applied to the positive direction, a decrease of $U_{\text{elastic}}$ is estimated to cause the shift of energy minimum of $U_{\text{total}}$ causing the decrease of $U_{\text{surface}}$. This resulted in beams adhering to the surface at a stable energy state with low $U_{\text{total}}$, generating the adhesion force. On the contrary, when tangential force was applied to the negative direction, an increase of $U_{\text{elastic}}$ is assumed to cause an unstable energy state with high $U_{\text{total}}$, generating the repulsive force against the contact surface.

The obvious difference in beam deformation during the unloading process that is suggested to cause the tangential force dependency of the adhesion force is achieved by the highly directional geometry of the beams that have a mounting angle of $\theta = 20°$. Thus, it could be suggested that multi-beam structure for easy grip and release operations should have the oblique beams with small mounting angles.

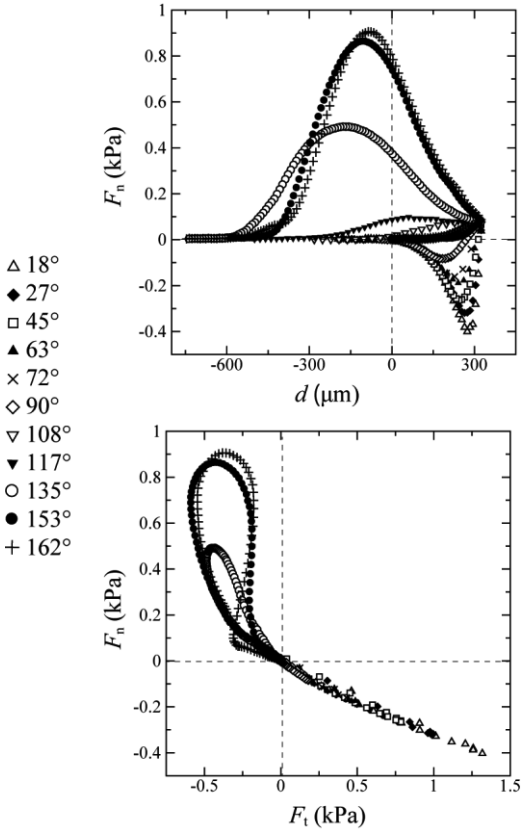


**Figure 6.** Experimental results of measured normal and tangential forces for different pull-off angles

## 5 Conclusions

In this paper, we proposed a new method of developing the multi-beam structure that allows to adjust mounting angle of the beams to an arbitrary value. The validity of the method was confirmed by analyzing the experimental results of observation of the developed multi-beam structure. From the experimental results of loading-unloading test with multiple pull-off angles, we suggested that the multi-beam structure with small mounting angles shows tangential force dependency of the adhesion force, thus is applicable to develop the device for manipulation with easy grip and release operation ability.

Methods for designing a beam with the geometry and determining an optimal pull off angle that maximize tangential force dependency of the adhesion force need to be confirmed in further studies for achieving an optimal manipulation process, along with testing the ability of a multi-beam structure with inclined beams to manipulate objects with uneven surfaces.

## 6 References


[1] Autumn, K., et al., "Frictional adhesion: a new angle on gecko attachment", *The Journal of Experimental Biology*, Vol. **209**, pp. 3569–3579, 2006

[2] Sekiguchi, Y., et al., "Adhesion between side surface of an elastic beam and flat surface of a rigid body" *Journal of Adhesion Science and Technology*, Vol. **26**, No. **23**, pp. 2615–2626, 2012

[3] Shimahara, M., "Effect of tangential force on adhesion between an elastic beam and a rigid body", Master thesis of Tokyo Institute of Technology, 2016

[4] Parness, A., et al.,"A microfabricated wedge-shaped adhesive array displaying gecko-like dynamic adhesion, directionality and long lifetime", *Journal of The Royal Society Interface*, vol.**6**, pp.1223–1231, 2009

[5] Day, P., et al., "Microwedge machining for the manufacture of directional dry adhesives", *Journal of Micro Nano-Manufacturing*, **1(1)**, pp. 011001–011001-10, 2013

[6] Murphy, M., et al., "Gecko-inspired directional and controllable adhesion" *Small* **5**, pp.170–175. 2008

[7] Aksak, B., et al., "Adhesion of Biologically Inspired Vertical and Angled Polymer Microfiber Arrays", *Langmuir*, Vol.**23**, pp.3322–3332, 2007

[8] Qu, L., et al.,"Carbon Nanotube Arrays with Strong Shear Binding-On and Easy Normal Lifting-Off", *Science*, Vol. **322**, Issue**5899**, pp.238–242, 2008

# A Huge and High Resolution Large Eddy Simulation Coupling with Energy Balance Model in Urban Area

Student Number: 15M18090 Name: Takafumi SUEISHI Supervisor: Manabu KANDA

# 街区のエネルギー収支を考慮した都市の大規模高解像度 LES 数値解析

居石貴史

本研究では、LES (Large Eddy Simulation) Model と Energy Balance Model のオフラインカップリングを行い、2m の高解像度で、都市街区の 3 次元的な空間構造を考慮した気象場の解析を実施した。RCP (Representative Concentration Pathways)シナリオと SSP (Shared Socio-economic Pathways)シナリオを用いて、インドネシアのジャカルタにおいて、現在と将来の気象状況を再現・予測し、都市街区内の温熱環境を評価した。

## 1. Introduction

Global temperature is increasing at a rate of 0.64℃/100 years [1]. In urban areas, this condition is exacerbated by the urban heat island (UHI) effect, phenomenon wherein urban areas have higher temperatures than urban areas. UHI is also detected to affect temperature trends in cities (e.g. annual average temperature in Tokyo increased about 3.2℃/100 years, a rate higher than the global temperature rise [2].) On the other hand, Asian megacities are projected to expand rapidly resulting to serious in the future atmospheric environment. Thus, detailed analysis of urban meteorology for Asian megacities is needed to prescribe optimum countermeasure for these issues.

Future mesoscale can be downscaled using PGW (Pseudo Global Warming) Method developed by Kimura et al (2007) [3]. Through PGW, Varquez et al (2017) succeeded to simulate future mesoscale weather condition including global warming effects and UHI effects by using RCP (Representative Concentration Pathways) and SSP (Shared Socio-economic Pathways) scenarios [4].

Mesoscale models cannot consider very fine resolution which includes detailed, realistic roughness effects such as actual buildings and vegetation. Recently, LES (Large Eddy Simulation) has been developed to calculate weather condition inside urban area with a few meter resolution. For example, Keck et al (2014) conducted LES simulation for real city with 2m resolution, and investigated characteristics of urban flow [5]. At the surface of LES, thermal comforts at the pedestrian level can be estimated.

Thermal comfort at pedestrian level is largely dependent on heat balance within the city. An energy balance model developed by Ashie et al (2011) successfully calculates energy balance of sun radiation and evapotranspiration from vegetation [6]. Bakkali et al (2015) simulated weather condition inside real city by using coupling of LES and energy balance model [7].

In this study, a building-resolving large eddy simulation coupled with an energy balance model is conducted for a highly urbanized district in central Jakarta (Figure 2) on typical daytime hours. Six cases were considered; two cases which utilizes present urban scenario and four cases represent different urban configurations in 2050s. Meteorological inputs were acquired from mesoscale simulation by Varquez et al (2017).

## 2. Simulation Outline

### 2.1. Simulation Methods

Figure 1 shows the simulation flow of this study. The results from GCM (General Circulation Model) were downscaled using WRF (Weather Research and Forecasting) Model through PGW. The simulation results were then further downscaled using an energy balance model and LES.

Future scenarios are based on RCP (future climate) and SSP (urbanization) scenarios. RCP2.6 and SSP1 represents best scenario for 2050s and RCP8.5 and SSP3 represents worst scenario for 2050s. Based on these scenarios, PGW Method was applied to WRF Model, and future urbanization and AHE (Anthropogenic Heat Emission) were determined.

LOCALS-UCSS developed by Ashie et al (2011) was the energy balance model used. It calculates energy balance of sun radiation and evapotranspiration from vegetation, and outputted sensible and latent heat flux from ground surfaces for thermal boundary condition of LES. AHE from buildings and roads were added to sensible heat flux. AHE was acquired from a global database by Dong et al (2016) [8].

PALM (PArallelized LES Model) developed by Raasch et al (2001) was the LES used. It simulates weather condition inside a city at 2m resolution. Simulated parameters were then used to evaluate thermal comfort at pedestrian level through SET* (Standard new Effective Temperature) [9]. SET* can evaluate thermal

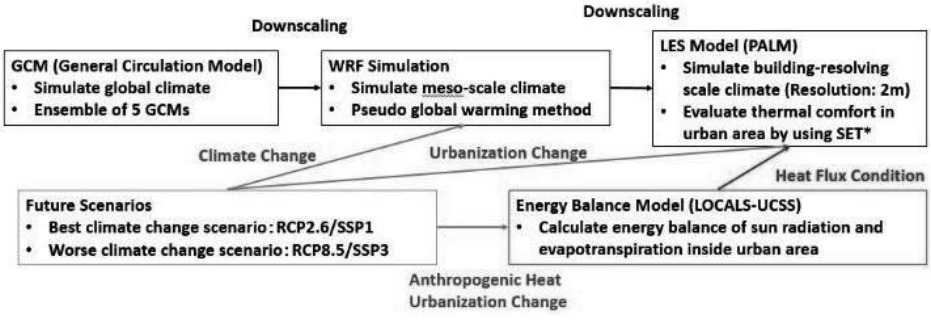


Figure 1. Simulation Flow

comfort based on the effects from temperature, humidity, wind speed, radiation, clothing and metabolism.

## 2.2. Simulation Settings and Objectives

Table 1 shows 6 cases of this study. Figure 2 shows simulation domain (inside red rectangle) and observation route (orange line). Table 2 shows initial conditions used in PALM taken from Varquez et al (2017). Table 3 shows its simulation settings. Figure 3 shows the building height map and land use map for 6 cases.

Moving observation was conducted around 14:00 on August 13, 2016. *Case Observation* reproduced this observation condition for validation of simulation results. Initial condition of *Case Current* was based on August 2006~2015 results of the WRF, which utilized present climate condition. Building height map and land use map in *Case Observation* and *Case Current* were created by combining the data acquired by Emporis and satellite imageries.

Initial condition of *Case Best Scenario*, *Case Worst Scenario*, *Case Complex City* and *Case Green City* were based on August 2046~2055 results of WRF Model by using PGW Method. RCP2.6 and SSP1 scenarios were used for *Case Best Scenario*, which represents best scenario for 2050s. On the other hand, RCP8.5 and SSP3 scenarios were used for *Case Worst Scenario*, which represents worst scenario for 2050s. Homogeneous building array was applied to the central area of *Case Best Scenario* and *Case Worst Scenario* to increase total building volume because of increasing population inside city in the future.

Objective of *Case Complex City* and *Case Green City* was to investigate how urbanization change weather condition inside a city. More complex urbanization was applied to *Case Complex City* and added more green area in *Case Green City* with keeping total building volume. RCP8.5 and SSP3 scenarios were used for *Case Complex City* and *Case Green City* to compare the results from *Case Worst Scenario*.

Table 1. Simulation Cases

| Case Name | Target Day & Time | RCP/SSP | Urbanization |
|---|---|---|---|
| Observation | 2016/08/13, 14:00 | Current | Current |
| Current | August 2006-2015, 14:00 | Current | Current |
| Best Scenario | August 2046-2055, 14:00 | RCP2.6/SSP1 | Homogeneous |
| Worse Scenario | August 2046-2055, 14:00 | RCP8.5/SSP3 | Homogeneous |
| Complex City | August 2046-2055, 14:00 | RCP8.5/SSP3 | Complex City |
| Green City | August 2046-2055, 14:00 | RCP8.5/SSP3 | Green City |

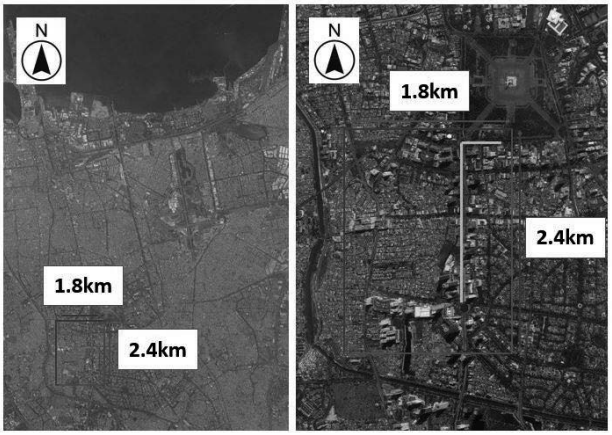


Figure 2. Simulation Domain

Table 2. Initial Condition of LES from WRF Model

| | Case Observation | Case Current | Case Best Scenario | Case Worst Scenario<br>Case Complex City<br>Case Green City |
|---|---|---|---|---|
| RCP/SSP | - | - | RCP2.6/SSP1 | RCP8.5/SSP3 |
| Potential Temperature | 30.183 ℃ | 34.367 ℃ | 34.768 ℃ | 35.572 ℃ |
| Wind Speed | 1.39 m/s | 3.3928 m/s | 2.7885 m/s | 2.8950 m/s |
| Wind Direction | 0˚ | 72.325˚ | 73.456˚ | 72.288˚ |
| Specific Humidity | 17.04 g/kg | 13.318 g/kg | 13.693 g/kg | 14.332 g/kg |

Table 3. Simulation Settings for LES

| Setting | Value |
|---|---|
| Target Area | Jakarta, Indonesia |
| Domain Size | 1800m x 2400m x 3378m |
| Grid Points | 900 x 1200 x 400 |
| Resolution | 2m (z<680m)<br>Stretched (Factor:1.08, z>680m) |
| Simulation Time | 3600s |
| Disturbance Energy | 0.01m$^2$/s$^2$ every 150s |
| Boundary Condition | Top: Slip<br>Bottom: No Slip<br>Lateral: Cyclic |

# 3. Simulation Results

## 3.1. Validation of Simulation Results

To validate simulation results, moving observation along an orange line in Figure 2 was conducted around 14:00 on August 13, 2016. From this observation, WBGT (Wet Bulb Globe Temperature) was calculated to evaluate thermal comfort.

Figure 4 compares simulation results of *Case Observation* (left) and moving observation results (right). Both area A and C in simulation results and those in observation show relatively lower WBGT, because vegetation interrupted sun radiation. On the other hand, both area B and D in simulation results and those in observation show

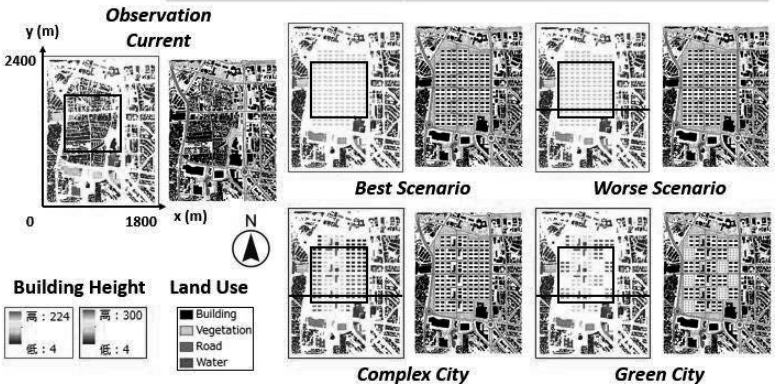


Figure 3. Building height map and land use map

relatively higher WBGT, because there was no obstacle to interrupts sun radiation. The distribution of WBGT in simulation results and observation results corresponded well with each other such as in the circled regions. Some areas don't match because of vegetation area mismatch and the sun radiation change during observation. We concluded that our model performs relatively well to estimate actual thermal comfort at pedestrian level.

## 3.2. Thermal Comfort at Pedestrian Level

Figure 5 shows sensible heat flux three dimensionally from south-east direction by Energy Balance Model. North and west surface and roof had higher sensible heat flux because sun radiation came directly. But south and east surface and shade of buildings and vegetation had lower sensible heat flux because sun radiation was interrupted. Road had also high sensible heat flux because of AHE from road.

Figure 6 shows SET* contours at 1m height by LES Model. Radiation affected SET* results significantly, SET* at shadowed areas by buildings and vegetation was lower and SET* at area with direct sun radiation was higher. So, central area of *Case Best Scenario*, *Case Worst Scenario*, *Case Complex City* and *Case Green City* (black rectangle in Figure 6) had lower SET* because added high-rise buildings interrupted sun radiation.

Table 4 shows averaged potential temperature, humidity, wind speed, MRT (Mean Radiant Temperature), SET* at 1m height inside central area (black rectangle in Figure 3). Potential temperature in *Case Current* was higher than *Case Best Scenario*, but lower than other cases. However, *Case Current* had the highest SET* of 5 cases because there was no high-rise buildings in central area of *Case Current* and it resulted to increase MRT and SET*. *Case Best Scenario* had lower potential temperature than *Case Current* though initial potential temperature was higher in *Case Best Scenario*. This is because there were higher sensible heat flux near the surface and air near the surface was heated in *Case Current*.

## 3.3. Urbanization Effects

Figure 7 shows profiles of wind speed, potential temperature and heat flux. In *Case Best Scenario* and *Case Worst Scenario*, the profiles changed significantly at the shear level of homogeneous buildings (80m). Within the canopies, wind speed was weak and potential temperature was high in these cases. On the other hand, above building height, wind speed increased rapidly and temperature decreased rapidly. Heat flux also decreased rapidly near building height. It means that homogeneous buildings separated the air below building height and above building height, and heat flux from surface was kept below building height. As a result, potential temperature below building height in *Case Worst* was higher than those of *Case Complex*

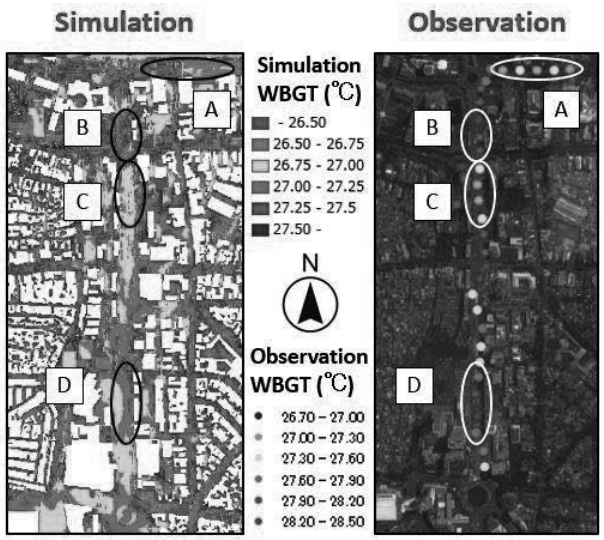


Figure 4. WBGT distribution comparison for simulation and observation

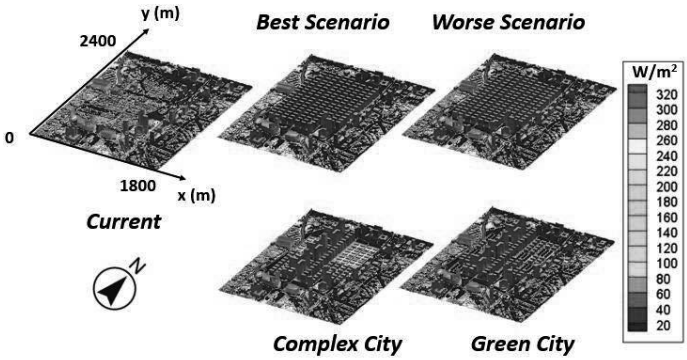


Figure 5. Sensible heat flux from surfaces

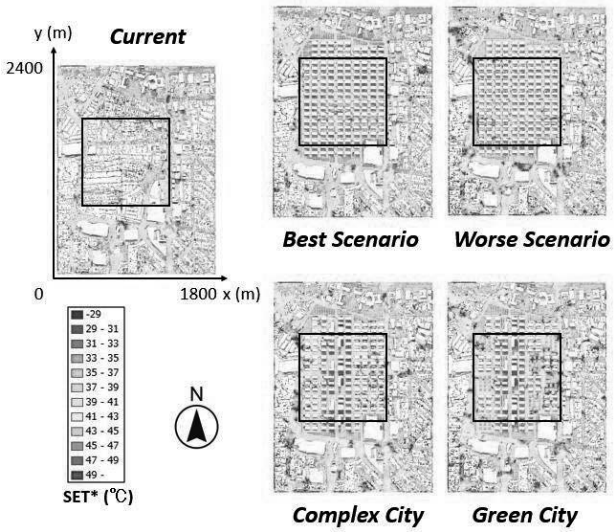


Figure 6. SET* contours at 1m height

Table 4. Averaged parameters inside central area

| | Case Current | Case Best Scenario | Case Worst Scenario | Case Complex City | Case Green City |
|---|---|---|---|---|---|
| Potential Temperature (℃) | 36.37 | 36.11 | 37.04 | 37.23 | 37.19 |
| Specific Humidity (g/kg) | 13.48 | 13.72 | 14.39 | 14.38 | 14.43 |
| Wind Speed (m/s) | 0.496 | 0.628 | 0.555 | 0.609 | 0.726 |
| MRT (℃) | 73.74 | 65.62 | 68.38 | 74.05 | 71.06 |
| SET* (℃) | 40.89 | 38.67 | 39.46 | 39.78 | 39.64 |

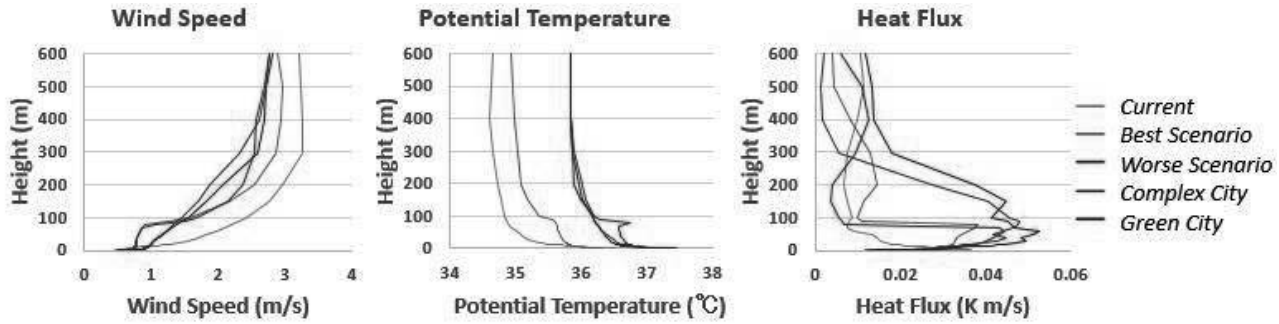


Figure 7. Profile data inside central area

*City* and *Case Green City*.

Figure 8 shows potential temperature contours at y=1000m (black line in Figure 3). The vectors depict wind speed velocity for *Case Worst Scenario*, *Case Complex City* and *Case Green City*. In *Case Worst Scenario*, wind above the building height was almost horizontal and clear potential temperature difference below building height and above building height can be seen. On the other hand, extremely high rise building (300m) generates updrafts in *Case Complex City* and it generates downdrafts in *Case Green City*. These high rise buildings promote mixing of air between high altitudes and near-ground level.

# 4. Conclusion

In the future, average temperature in Jakarta will increase by 0.4 ~ 1.2℃ because of global warming (from mesoscale model). But there will also have high rise buildings inside a city with an increase of population density. These high rise buildings will interrupt sun radiation. As a result, future SET* averaged over central area was 1~2℃ lower than current SET* at pedestrian level. Vegetation also interrupts sun radiation and makes cooler environment at pedestrian level. Homogeneous buildings kept heat flux within the canopies and it makes higher temperature inside canopies. There are little mixing of air between high altitudes and near-ground level. It may prevent to reduce temperature if cooler air comes to this area. On the other hand, height distribution of buildings inside city generates updrafts and downdrafts and it promotes mixing of air between high altitudes and near-ground level. Therefore, optimum urbanization is high rise buildings with height distribution and adding vegetation reduces SET* by interrupting sun radiation.

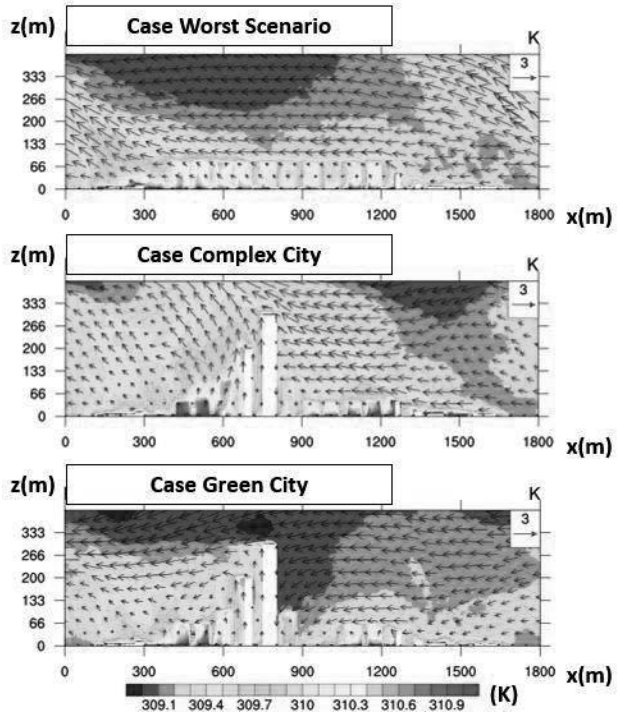


Figure 8. Potential temperature contour at y=1000m with speed vectors

# References

[1] IPCC (Intergovernmental Panel on Climate Change), AR5 (Assessment Report 5), WG I (Working Group 1), SPM (Summary for Policymakers), 2013

[2] Web site of Japan Meteorological Agency

[3] Kimura F. and Kitoh A., "Downscaling by pseudo global warming method", In The Final Report of ICCAP, Research Institute for Humanity and Nature (RIHN), 2007

[4] Varquez A.C.G., Darmanto N., Kawano N., Takakuwa S., Kanda M. and Xin Z., "Representative urban growing scenarios for future climate models", Journal of Hydraulic Engineering, Vol 73. I_103-I_108, 2017

[5] Keck M., Raasch S., Letzel M. O. and Ng E., "First results of high resolution large-eddy simulation of the atmospheric boundary layer", Journal of Heat Island International, Vol 9-2, 39-43, 2014

[6] Ashie Y. and Kono T., "Urban scale CFD analysis in support of a climate-sensitive design for the Tokyo Bay area", International Journal of Climatology, Int. J. Climatol, Vol 31, Issue 2, 174-188, 2011

[7] Bakkali M., Inagaki A., Ashie Y., Yoshida Y., Kanda K. and Raasch S., "Thermal large eddy simulation with sensible heat flux distribution from 3D building geometries", Journal of Hydraulic Engineering, Vol 71, I_433-I_438, 2015

[8] Dong Y., Varquez A.C.G. and Kanda M., "Global anthropogenic heat flux database with high spatial resolution", Atmospheric Environment, Vol 150, 276-294, 2017

[9] Raasch S. and Schroeter M., "PALM-A large-eddy simulation model performing on massively parallel computers", Meteorol. Z., Vol 10, No 5, 363-372, 2001

# Studies on Human Motion Recognition through Wireless Sensing with Communication Devices

Student Number: 15M51762 Student Name: Haitao PANG Supervisor:Jun-ichi TAKADA

**Abstract**

This research studies using electromagnetic (EM) signals from wireless communication systems for human motion recognition (HMR) via radio frequency (RF) sensing. Modern high data-rate RF communication systems have inherent sensing capabilities for moving objects. Contact-less, device-less, camera-less HMR by ordinary radio signals is very advantageous compared with traditional method by computer vision or wearables. However, the physical phenomena of RF scattering from biological bodies are complicated and dependent on many factors such as shape, material properties, polarization, geometry, etc. To demonstrate this, the author focus on the characteristics of time variant scattering from a human body performing various kinds of motions, in a data-centric manner. Using inputs of measured motion data, generative human models in various postures, and a numerical EM simulator based on a high frequency asymptotic method of physical optics (PO), large datasets can be generated. This can be used for better and more comprehensive understanding of the RF interaction with human body, and for development and comparison of future robust recognition RF algorithms and joint communication and radar (RAdio Detection And Ranging) devices.

## 1 Introduction

Radar and wireless communication use the same medium of EM waves as information carrier. Potentially the two classes of technologies can converge, so that the same RF devices could allow double use. Recent advancements in miniaturized, high frequency, high performance devices, advanced communication technologies and computing power have made RF sensing possible with ordinary communication devices. To list a few examples, mobile networks could be used for vehicular radar, and IEEE 802.11 series Wireless LAN signals used for human behaviour recognition [1]. Human motion recognition has many important applications such as human computer interface, smart home, etc. In 5G era, an exploding number of RF devices will operate at higher frequencies and wider bandwidth, equipped with directional massive MIMO (Multiple Input Multiple Output) which can exploit spatial diversity, and other advanced technologies. These advancements will bring about higher resolution and better sensing performance. This 5G perspective may provide a ubiquitous and more powerful distributed radar sensing service for wireless recognition of human activities.

However, most of the past researches are built on empirical data from site-specific, target-specific, scenario-specific measurement campaigns, sometimes conducted with specific unmodifiable commercial-grade devices with specification partially unknown. Consequently, these results are sometimes not fully reproducible, with limited generality, considering the complicated different propagation channel and other important factors. Also these results are usually not openly, easily available for other researchers' usage or comparison. Therefore, the author turns to fundamental theories and physically sound EM simulations. This will allow us to better understand the potentials and fundamental limitations, and to study the characteristics of the complicated time variant scattering problem with modifiable parameters. These factors include various motions, human body shape, EM properties of clothing, carrier frequencies, transmitter-target-receiver geometry, channel characteristics, etc. Also, a large amount of data can be generated. This is crucial for development of data-driven methods/algorithms, whereas it is difficult, time-consuming and costly to acquire by actual measurements.

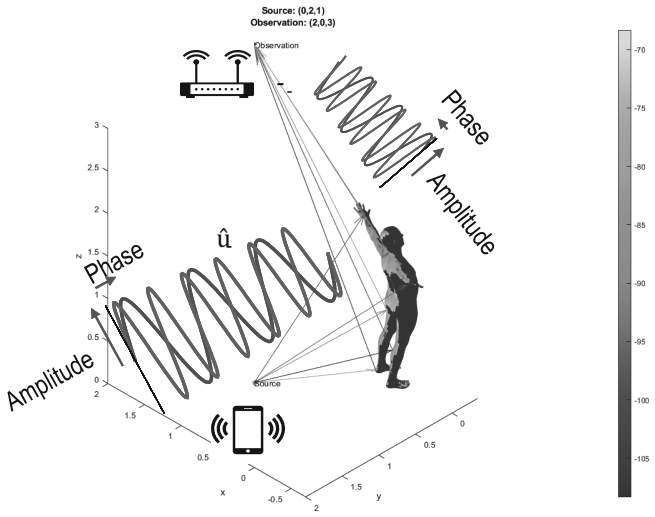


Figure 1: Ubiquitous RF sensing of human body

## 2 Radar principles and the recognition problem

Relevant radar principles is shortly introduced in this section and detailed explanation can be found in [2]. Fundamentals of RF sensing is illustrated as in Figure 1. RF signal is emitted by the transmitter and scattered by target of interest, and then the scattered signal reaches the receiver antenna. A moving target performing certain motion, which models a part of human body in motion in our case, will modulate the signals in terms of three parameters:

- **Time delay**

$$\tau_h = 2\frac{R_{t,h} + R_{r,h}}{c_0}, \tag{1}$$

where $c_0$ is the speed of EM wave in air, $R_{\mathrm{t},h}$ and $R_{\mathrm{r},h}$ are the distances from target to the transmitter and to the receiver, respectively.

- **Doppler frequency** is

$$f_{D,h} = 2\frac{v_{\mathrm{rel},h}}{c_0} f_c, \tag{2}$$

where $v_{\mathrm{rel},h}$ is the relative radial velocity of the target and $f_c$ the carrier frequency.

- **Complex amplitude** $\alpha_h$, which is related to the shape and EM properties of the target and can be modelled as

$$\alpha_h = \sqrt{\frac{\sigma_h c_o^2}{(4\pi)^3 R_{t,h}^2 R_{r,h}^2 f_c^2}} \tag{3}$$

Equation 3 assumes a point target model in free space using radar cross section (RCS) $\sigma_h$. $h$ is the index number of the target.

These parameters are true values related to the targets and describe the state of the targets. Hence they are the source of information in radar systems. RF sensing hardware processes the modulated receive signals to extract these parameters. Finally, these estimated parameters $\sum(\hat{\tau}_h, \hat{f}_{D,h}, \hat{\alpha}_h)$ in snapshots collected from a period of observation are used to recognize the state of the target of human body motion. Mathematically, the recognition process is a mapping from a set of the estimated parameters to a set of labels.

Estimation performance of these parameters are fundamentally limited by specifications of the whole RF system, such as the waveform in use and hardware. Targets are considered distinguishable by a radar system, only if the differences of their parameters are larger than the system resolution. In most modern high data-rate communication systems, Orthogonal Frequency Division Multiplexing (OFDM) is used and its resolution is given by [3] as:

- **Range resolution**, or the smallest resolvable unit in distance measurement, is

$$\triangle R = \frac{c_0}{2B}, \tag{4}$$

where $B$ is the bandwidth. For example in 802.11ac with maximum bandwidth of 160MHz this is just 0.94 m.

- **Velocity resolution**

$$\triangle v = \frac{c_0}{2 f_c M T_{\mathrm{OFDM}}}, \tag{5}$$

where $T_{\mathrm{OFDM}}$ is the time duration of one OFDM symbol and $M$ is the number of symbols used in coherent signal processing for extraction of Doppler frequency. For 802.11ac WLAN, integration of 60 ms of OFDM symbols means a velocity resolution of 0.5 m/s

Low resolution means only coarse estimation of whole body posture in one single snapshot, which may not be enough for imaging or localization of body parts. However, combining data from more snapshots where estimated parameters are different, recognition of motion could be possible. Human body parts are inherently constraint, so that exhibit different but interrelated velocity profile while performing certain kinds of motions. Scattering from each type of motion can be represented by a set of these parameters with innate eigen characteristics. In later sections, the author generates receive signals to show this.

# 3 Methodology

Figure 2 shows the overall methodology in this research.

- **Step 1** Human motion data is recorded using motion capture technology (MOCAP). Here data from an open adataset [4] is used, in which key points of human body are captured at 120 Hz.
- **Step 2** A skeleton form constructed by 17 points is extracted from motion data in each snapshot.
- **Step 3** Transform skeleton form data in each snapshot to a proper 3D human model suitable for EM simulation.
- **Step 4** Execute EM simulation to model received signal using 3D models in each snapshot.
- **Step 5** Apply time-frequency analysis to the received signals.

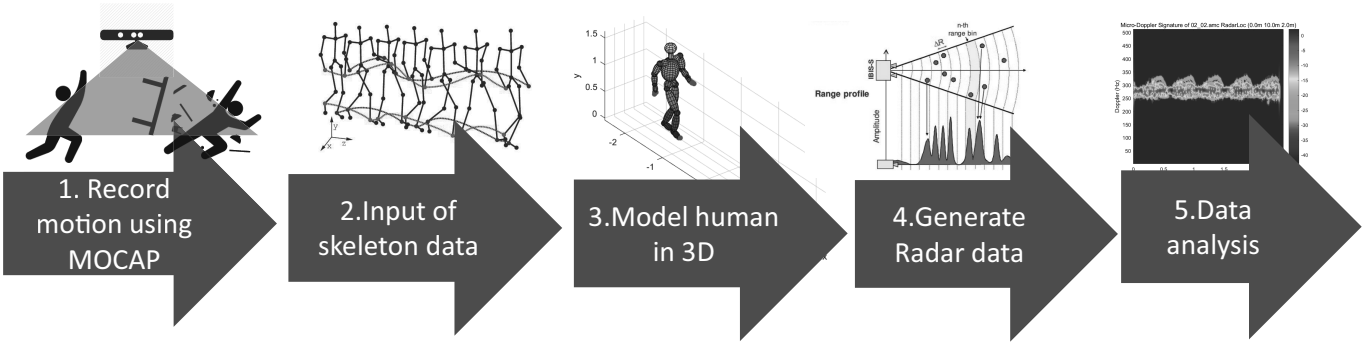


Figure 2: Overview of research methodology

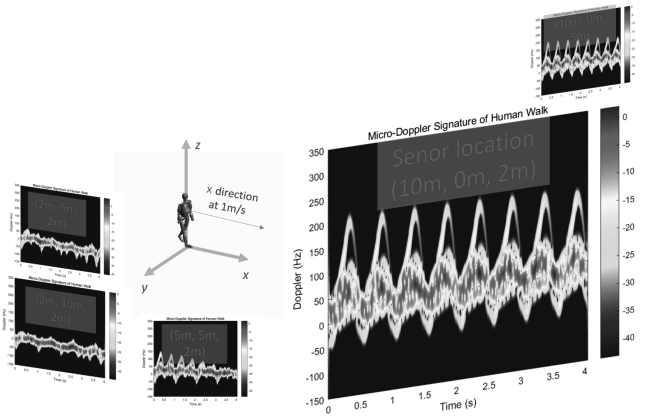


Figure 3: Spectrogram patterns from a walking human

# 4 EM simulation with ellipsoidal model

For fast calculation and without loss of generality, in this section human body is modelled as a combination of 19 ellipsoids similar to [5]. The modelled human body is as illustrated in step 3 in Figure 2. With this model, patterns of micro Doppler due to different velocity of body parts can be identified.

## 4.1 Signal model

Consider single carrier RF signals in frequency $f_c$, in every snapshot the receive signal is modulated by each moving ellipsoid $h$, which can be parametrized as $(\tau_h, \alpha_h)$. Receive signal at the antenna consists of reflected signals from all 19 ellipsoids, superimposed during one snapshot. The energy at the receiver $E_{\text{rx}}$ then has a relationship to the transmitted signal in each snapshot as

$$E_{\text{rx}} = E_{\text{tx}} \sum_{h=0}^{18} \alpha_h e^{j2\pi f_c (t-\tau_h)} \tag{6}$$

Without loss of generality, $\sqrt{\sigma_h}$ is used as $\alpha_h$ for later simulation, omitting propagation attenuation. And an approximate bistatic RCS solutions for perfect electric conductor (PEC) ellipsoid from [6] is used for calculation of $\sigma_h$, which is represented as Equation 7.

where $\phi_i, \theta_i$ are the incidence angle and azimuth angle of incident wave to the ellipsoid, and $\phi, \theta$ are observation angles, respectively.

Once the data in each snapshot is calculated, time sequence received data is available for joint time-Doppler analysis.

## 4.2 Time frequency analysis

Spectrogram represented by short time Fourier transform (STFT) is used for the analysis of the time variant change of Doppler frequencies in the receive signals due to the modulations by target's complex movements.

$$\text{Spectrogram}(t, \omega) = |\text{STFT}(t, \omega)|^2 \tag{8}$$

$$\text{STFT}_{x,w}[n, \omega] = \sum_{m=-\infty}^{\infty} x[n+m] w[m] e^{-j\omega m} \tag{9}$$

Gaussian windows is used as window function $w[m]$ in STFT. For the radar signal sampled at 1200 snapshots per second, FFT size and window size of $w[m]$ is set to 512. And overlap is used with a hopsize of 1/8 of the window size.

## 4.3 Results for Doppler signature

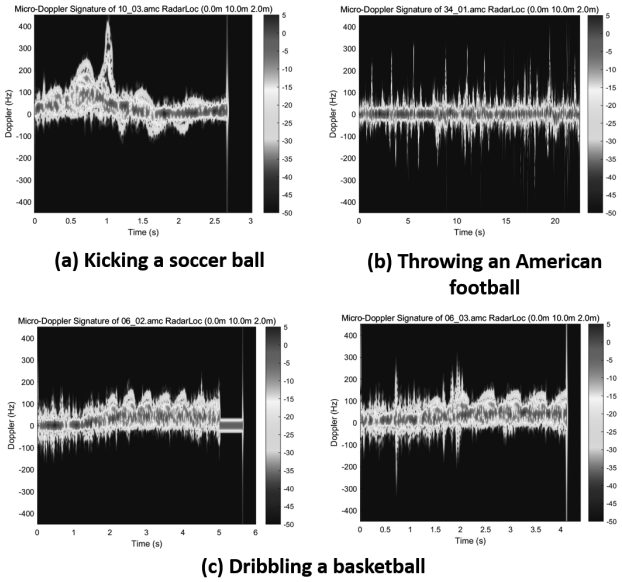


Figure 4: Spectrogram patterns from some sports activities

Simulation is conducted at frequency of 5 GHz, with transmitter and receiver located in the same position (monostatic) at different locations. Figure 3 shows the results of monostatic backscattering from a walking human at speed of 1 m/s towards the $+x$ axis direction. An enlarged version is in Figure 6. And Figure 4 shows the spectrogram from several sports activities.

First, the patterns of spectrogram are clearly and visually recognizable and classifiable. Some activities do have an innate Doppler signature, which can be used in classification algorithm. Second, sensors at some locations (e.g. at (2m, 5m, 2m)) cannot generate recognizable pattern. This is because radial velocity is angle dependent and given the antenna location, it is not detectable. Third, sensors at several locations show different but similar patterns, due to the fact that the radial velocity is different

$$\sigma_h = \frac{4\pi a^2 b^2 c^2 \left[\left(1 + \cos\vartheta^i \cos\vartheta\right)\cos\left(\phi - \phi^{\text{i}}\right) + \sin\vartheta^{\text{i}} \sin\vartheta\right]^2}{\left[a^2 \left(\sin\vartheta\cos\phi + \sin\vartheta^{\text{i}}\cos\phi^{\text{i}}\right)^2 + b^2\left(\sin\vartheta\sin\phi + \sin\vartheta^{\text{i}}\sin\phi^{\text{i}}\right)^2 + c^2\left(\cos\vartheta + \cos\vartheta^{\text{i}}\right)^2\right]^2} \tag{7}$$

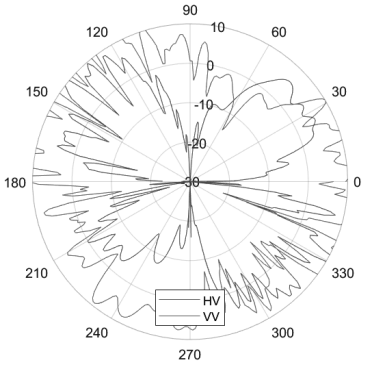


Figure 5: Example of polarimetric RCS from a PEC human body in Figure 1 with vertically polarized incident wave from top

from different observers. This also suggests that a multi-static configuration with multiple measurement link could possible provide extra spatial diversity to increase sensing performance.

# 5 Polarimetric signature by PO simulation

In section 4, electromagnetic polarization was ignored. To solve the polarimetric EM scattering problems, a high frequency asymptotic method of Physical optics (PO)[7] is applied to meshed human models.

## 5.1 Physical optics approximation

PO is based on the field equivalence principle so that only surface equivalent currents on the surface illuminated by the incident wave, are considered in the calculation of scattered field at the observation point. It is a common method for calculation of RCS of complex shaped objects, known for its good balance between fast calculation, less computation resources and good accuracy for backscattering region with relatively small bistatic angle. In this simulation, only first order PO currents are taken into account and Ludwig's method [8] [9] is used for fast calculation of the PO integrals for triangular meshes.

## 5.2 Human mesh model

To create realistic, highly accurate, configurable 3D meshed human models, a generative algorithm of Skinned Multi-Person Linear Model (SMPL) [10] is used. SMPL can represent a wide variety of body shapes in natural human poses. One example of a generated meshed model is showed in Figure 1. To fulfil the small size mesh requirements for highly accurate PO simulation, surfaces of generated models are subdivided until the length of all triangular meshes are smaller than 1/10 of the wavelength.

## 5.3 Result for polarimetric signature

Figure 5 shows a result for polarimetric RCS from a PEC human body in posture as illustrated in Figure 1. The incident wave is vertically polarized, with incidence angle of zero from top. Result shows that the co-polarization and cross-polarization scattering from the complex-shaped human body is different and this suggests the use of a pair of orthogonally polarized antenna could help improve the sensing performance by exploiting this polarimetric diversity.

# 6 Conclusion and future work

This research proposes the general idea of ubiquitous RF sensing for human motion recognition, and simulation approaches are taken to demonstrate useful characteristics. Using these approaches, large datasets can be generated for development of actual hardware system and recognition algorithms, also for their verification and comparison. Still, better modelling techniques that could model the different dialectic clothing components with different EM properties, and better simulation techniques such as iterative PO could help improve accuracy.

The relevant algorithms used in this research would be put on GitHub to encourage open research. As a preliminary trial classification, a mini VGG Convolutional Neural Network was used with inputs of noisy spectrogram figures as in Figure 4 to classify sports activity. And the result accuracy is between 65% ~80%.

# References

[1] S. Yousefi, et al. "A Survey on Behavior Recognition Using WiFi Channel State Information," in IEEE Communications Magazine, vol. 55, no. 10, pp. 98-104, Oct. 2017.

[2] M. I. Skolnik, Introduction to Radar Systems, 3rd Edition, McGraw-Hill, New York, 2001.

[3] K. M. Braun. "OFDM Radar Algorithms in Mobile Communication Networks." PhD thesis, Karlsruher Institute of Technology, 2014.

[4] http://mocap.cs.cmu.edu/

[5] V. C. Chen, "Doppler signatures of radar backscattering from objects with micro-motions," in IET Signal Processing, vol. 2, no. 3, pp. 291-300, September 2008.

[6] K. D. Trott, "Stationary Phase Derivation for RCS of an Ellipsoid," in IEEE Antennas and Wireless Propagation Letters, vol. 6, pp. 240-243, 2007.

[7] C.A. Balanis. Advanced Engineering Electromagnetics, 2nd Edition. Wiley, 2012.

[8] A. Ludwig. Computation of radiation patterns involving numerical double integration. IEEE Transactions on Antennas and Propagation, 16(6):767-769, 1968.

[9] Tokio Miyake. Numerical simulation of scattering from random rough surface by using physical optics. 2018.

[10] M. Loper, et al. SMPL : A Skinned Multi-Person Linear Model. ACM Trans. Graphics (Proc. SIGGRAPH Asia), 34(6):248:1|-248:16, 2015.